Evaluation of high-strength concrete interior beam-column joints under simulated seismic loading

Leong, Chee Lai

2012

Leong, C. L. (2012). Evaluation of high-strength concrete interior beam-column joints under simulated seismic loading. Doctoral thesis, Nanyang Technological University, Singapore.

https://hdl.handle.net/10356/50867

https://doi.org/10.32657/10356/50867

NANYANG TECHNOLOGICAL UNIVERSITY

EVALUATION OF HIGH STRENGTH CONCRETE INTERIOR BEAM-COLUMN JOINTS UNDER SIMULATED SEISMIC LOADING

Leong Chee Lai

School of Civil & Environmental Engineering

Nanyang Technological University

2012

Evaluation of High-Strength Concrete Interior Beam-Column Joints under Simulated Seismic Loading

Leong Chee Lai

School of Civil & Environmental Engineering

A thesis submitted to the Nanyang Technological University in partial fulfilment of the requirements for the degree of Doctor of Philosophy

2012

ACKNOWLEDGEMENTS

The research reported in this thesis was undertaken at the School of Civil and Environmental Engineering of Nanyang Technological University, Singapore under the supervision of Assoc. Prof. Li Bing.

First of all the author would like to express his highest gratitude to his supervisor, Assoc Prof. Li Bing, for his professional guidance, invaluable advice and continuous encouragement throughout the duration of this research. The patience and tolerance of Assoc Prof Li with author is highly appreciated. The author also would like to thank the technicians from the Protective Technology Lab of the School of Civil and Environmental Engineering for their helpful assistance in the experimental work.

This acknowledgement would not be complete without mentioning the contributions of these researchers in NTU for their assistance and support. They are Mr. Yap Sim Lim, Mr. Cao Thanh Ngoc Tran and Ms. Grace Chua. Their constructive suggestions, fruitful discussion, as well as technical support had made this project a most memorable one. The author also would like to appreciate his company Det Norske Veritas for their understanding to allow the author to be absent from work during the preparation of test and execution of test.

Without the love from the family, the author could not undertake the research. Thus, the author would like to thank his beloved wife Wen Chi for her constant encouragement throughout the research. Her understanding and love enabled the research study to run smoothly. Lastly, the author would like to share the joy of this piece of work with his dearest daughter Zee Tien. Her laughter has been the best encouragement to the author whenever the author faced setbacks in the research.

TABLE OF CONTENTS

ACKNOWLEDGEMENTS ii
TABLE OF CONTENTS iii
LIST OF FIGURES vii
LIST OF TABLES xii
LIST OF NOTATIONS xiii
SUMMARY xvi
Chapter 1 Introduction 1
1.1 Statement of the Problem 1
1.2 Problems of Non-Seismic Detailed Beam-Column Joints 3
1.3 Objectives and Scope 4
1.4 Thesis Organisation 5
Chapter 2 Literature Review 7
2.1 Test Studies on Seismic Behaviour of Beam-Column Joints 7
2.1.1 Research Conducted by Kurose *et al*. (1988) 8
2.1.2 Research Conducted by Pessiki *et al*. (1990) 8
2.1.3 Research Conducted by Xin (1992) 9
2.1.4 Research Conducted by Hakuto *et al*. (1995) 10
2.1.5 Research conducted by Li *et al.* (2002) 11
2.2 Studies on Structural Bahaviour of HSC Beam-Column Joints 12
2.3 Studies on Bond Properties of HSC Beam-Column Joints 14
2.4 Characteristics of Beam-Column Joints 17
2.4.1 Joint Classification 17
2.4.2 Characteristics of Seismic Detailed Beam-Column Joints 18
2.4.3 Characteristics of Non-Seismic Detailed Beam-Column Joints 19
2.4.4 Failure Models of Interior Beam-Column Joints 21
2.5 Seismic Design Codes 24
2.5.1 New Zealand Standard (NZS 3101-2006) 24
2.5.2 American Concrete Institute Code (ACI 318-08) 26
2.5.3 Summary of Design Codes 27
2.6 Conclusions on Literature Review 28

Chapter 3 Experimental Programme.....31
3.1 Experiment Planning..... 31
3.1.1 Test Specimens Details..... 32
3.1.2 Test Specimens Fabrication..... 37
3.2 Test Setup..... 39
3.3 Loading Arrangement..... 40
3.4 Instrumentation..... 40
3.4.1 Observation of Cracking Development..... 41
3.4.2 Measurement of Applied Load..... 41
3.4.3 Measurement of Horizontal Displacement..... 41
3.4.4 Measurement of Rotation of Beam and Column..... 42
3.4.5 Measurement of Curvature of Beam and Column..... 45
3.4.6 Measurement of Shear Strains of Joints and Joint Expension..... 45
3.4.7 Measurement of Strains in Reinforcing Bars..... 46
3.5 Components of Horizontal Displacement..... 47
3.5.1 Displacement Due to Beam Deformations..... 47
3.5.2 Displacement Due to Column Deformations..... 49
3.5.3 Displacement Due to Joint..... 50
3.6 Theoretical Yield Displacements & Initial Stiffness..... 50
3.7 Conclusions..... 53
Chapter 4 Experimental Results.....54
4.1 Test Result of Group One (NS1 and AS1)..... 54
4.1.1 Specimen NS1..... 55
4.1.2 Specimen AS1..... 70
4.2 Test Result of Group Two (NS2 and AS2)..... 83
4.2.1 Specimen NS2..... 83
4.2.2 Specimen AS2..... 98
4.3 Test Result of Group Three (NS3 and AS3)..... 111
4.3.1 Specimen NS3..... 111
4.3.2 Specimen AS3..... 126
4.4 Test Result of Group 4 (NS4 and AS4)..... 139
4.4.1 Specimen NS4..... 139

4.4.2 Specimen AS4 154
4.5 Conclusions 167
Chapter 5 Discussion and Analysis of Test Results 168
5.1 Discussion of Experimental Results 168
5.1.1 Load-Carrying Capacity and Energy Dissipation 169
5.1.2 Comparison of Stiffness Degradation 175
5.1.3 Joint Behaviour 177
5.1.4 Member Contribution to Horizontal Displacement 178
5.1.5 Bond Stress 180
5.1.6 Concrete Strength Effect 181
5.1.7 Effect of Column Axial Compressive Load 182
5.1.8 Effect of Bottom-Reinforcement-to-Top-Reinforcement Ratio, β 184
5.2 Finite Element Modelling 185
5.2.1 Modelling of Concrete 185
5.2.2 Modelling of Reinforcement 188
5.2.3 Bond Slip Law 189
5.2.4 Mesh Generation 190
5.2.5 Boundary Condition and Loading Condition 192
5.2.6 Material Properties 193
5.3 Finite Element Models Results Verification 194
5.3.1 Hysteretic Behaviour 194
5.3.2 Overall Strength and Stress Contours 195
5.3.3 Cracking Patterns 205
5.3.4 Strains in Beam and Column Longitudinal Bars 205
5.3.5 Joint Shear Stres 212
5.4 Summary of Test Results Analysis 213
Chapter 6 Parametric Investigations on High Strength Concrete Beam-Column Joints 215
6.1 Findings on Concrete Beam-Column Joints 215
6.2 Assembly of Database for Parametric Studies 217
6.2.1 Experimental Results of Conventional Beam-Column Joints 217
6.2.2 Finite Element Modelling 220

6.3 Discussion of Database Results 226
6.3.1 Effect of Concrete Compressive Strength..... 226
6.3.2 Effect of Column Axial Load 228
6.3.3 Effect of Beam Reinforcing Ratio and Reinforcing Details 231
6.3.4 Effect of Joint Core Reinforcement 233
6.3.5 Effect of Bond Condition..... 235
6.3.6 Effect of Transverse Beams 237
6.3.7 Summary of Parametric Studies..... 238
6.4 Joint Shear Design of New Zealand Standard NZS 3101 239
6.4.1 Structural Behaviour of Beam-Column Joints..... 241
6.4.2 Bond Deterioration Control Review 244
6.4.3 Parametric Study on Shear Design 254
6.5 Conclusions..... 259
Chapter 7 Summary and Conclusion 261
7.1 Experimental Studies on High Strength Concrete Beam-Column Joint..... 261
7.2 Parametric Studies on Influence of Variables..... 263
7.3 Design Recommendations 265
7.4 Recommendations for Future Work..... 265
REFERENCES 267
Appendix A: Summary of Cracking Pattern of Specimens NS1 to NS4 & AS1 to AS4.....277

LIST OF FIGURES

Figure 1.1 Epicenter Locations of Earthquakes in Sumatra Region [P1].....1
Figure 2.1 External Actions of Internal Beam-Column Joint.....21
Figure 2.2 Definition of Effective Joint Width [P3].....21
Figure 3.1 Details of Specimens NS1 and AS1.....33
Figure 3.2 Details of Specimens NS2 and AS2.....33
Figure 3.3 Details of Specimens NS3 and AS3.....34
Figure 3.4 Details of Specimens NS4 and AS4.....34
Figure 3.5 Reinforcement Cage and Formwork of Specimens Prior to Casting 37
Figure 3.6 Cast Specimens 38
Figure 3.7 Schematic Test Setup.....39
Figure 3.8 Cyclic Loading and Displacement History 40
Figure 3.9 Displacement Transducers for Displacement Measurement.....42
Figure 3.10 Displacement Transducers for Rotation Measurement 43
Figure 3.11 Estimation of Rotation of Beam [H2] 43
Figure 3.12 Measurement of Joint Shear Distortion [H2] 46
Figure 3.13 Strain Gauge Position of Specimen.....47
Figure 3.14 Measurement of Horizontal Displacement Due to Joint [H2].....50
Figure 4.1 Final Crack Pattern of NS1 56
Figure 4.2 Progressive Cracking Development of NS1 57
Figure 4.3 Storey Shear Force versus Horizontal Displacement for NS1 58
Figure 4.4 Decomposition of Horizontal Components of NS1 58
Figure 4.5 Contributions of Horizontal Components of NS1.....59
Figure 4.6 Strain Profiles of Beam Bars of NS1 62
Figure 4.7 Curvature Distribution of Beam of NS1 63
Figure 4.8 Strain Profiles of Column Bars of NS1.....65
Figure 4.9 Curvature Distribution of Column of NS1.....66
Figure 4.10 Bond Stress of Beam Bar of NS1.....68
Figure 4.11 Bond Stress of Column Bar of NS1 69
Figure 4.12 Joint Shear Distortion and Expansion of Specimen NS1 70
Figure 4.13 Final Crack Pattern of AS1 71
Figure 4.14 Progressive Cracking Development of AS1.....72

Figure 4.15 Storey Shear Force versus Horizontal Displacement for AS1 73
Figure 4.16 Decomposition of Horizontal Components of AS1 73
Figure 4.17 Contributions of Horizontal Components of AS1.....74
Figure 4.18 Strain Profiles of Beam Bars of AS1 76
Figure 4.19 Curvature Distribution of Beam of AS1 77
Figure 4.20 Strain Profiles of Column Bars of AS1.....78
Figure 4.21 Curvature Distribution of Column of AS1.....79
Figure 4.22 Bond Stress of Beam Bar of AS1.....80
Figure 4.23 Bond Stress of Column Bar of AS1 81
Figure 4.24 Joint Shear Distortion and Expansion of Specimen AS1 82
Figure 4.25 Final Crack Pattern of NS2 84
Figure 4.26 Progressive Cracking Development of NS2.....85
Figure 4.27 Storey Shear Force versus Horizontal Displacement for NS2 86
Figure 4.28 Decomposition of Horizontal Components of NS2 87
Figure 4.29 Contributions of Horizontal Components of NS2.....88
Figure 4.30 Strain Profiles of Beam Bars of NS2 90
Figure 4.31 Curvature Distribution of Beam of NS2 91
Figure 4.32 Strain Profiles of Column Bars of NS2.....93
Figure 4.33 Curvature Distribution of Column of NS2.....94
Figure 4.34 Bond Stress of Beam Bar of NS2.....96
Figure 4.35 Bond Stress of Column Bar of NS2 97
Figure 4.36 Joint Shear Distortion and Expansion of Specimen NS2.....98
Figure 4.37 Final Crack Pattern of AS2 99
Figure 4.38 Progressive Cracking Development of AS2.....100
Figure 4.39 Storey Shear Force versus Horizontal Displacement for AS2 101
Figure 4.40 Decomposition of Horizontal Components of AS2 101
Figure 4.41 Contributions of Horizontal Components of AS2.....102
Figure 4.42 Strain Profiles of Beam Bars of AS2 104
Figure 4.43 Curvature Distribution of Beam of AS2 105
Figure 4.44 Strain Profiles of Column Bars of AS2.....106
Figure 4.45 Curvature Distribution of Column of AS2.....107
Figure 4.46 Bond Stress of Beam Bar of AS2.....108
Figure 4.47 Bond Stress of Column Bar of AS2 109
Figure 4.48 Joint Shear Distortion and Expansion of Specimen AS2.....110

Figure 4.49 Final Crack Pattern of NS3 112
Figure 4.50 Progressive Cracking Development of NS3.....113
Figure 4.51 Storey Shear Force versus Horizontal Displacement for NS3 114
Figure 4.52 Decomposition of Horizontal Components of NS3 115
Figure 4.53 Contributions of Horizontal Components of NS3.....116
Figure 4.54 Strain Profiles of Beam Bars of NS3 118
Figure 4.55 Curvature Distribution of Beam of NS3 119
Figure 4.56 Strain Profiles of Column Bars of NS3.....121
Figure 4.57 Curvature Distribution of Column of NS3.....122
Figure 4.58 Bond Stress of Beam Bar of NS3.....124
Figure 4.59 Bond Stress of Column Bar of NS3 125
Figure 4.60 Joint Shear Distortion and Expansion of Specimen NS3.....126
Figure 4.61 Final Crack Pattern of AS3 127
Figure 4.62 Progressive Cracking Development of AS3.....128
Figure 4.63 Storey Shear Force versus Horizontal Displacement for AS3 129
Figure 4.64 Decomposition of Horizontal Components of AS3 129
Figure 4.65 Contributions of Horizontal Components of AS3.....130
Figure 4.66 Strain Profiles of Beam Bars of AS3 132
Figure 4.67 Curvature Distribution of Beam of AS3 133
Figure 4.68 Strain Profiles of Column Bars of AS3.....134
Figure 4.69 Curvature Distribution of Column of AS3.....135
Figure 4.70 Bond Stress of Beam Bar of AS3.....136
Figure 4.71 Bond Stress of Column Bar of AS3 137
Figure 4.72 Joint Shear Distortion and Expansion of Specimen AS3.....138
Figure 4.73 Final Crack Pattern of NS4 140
Figure 4.74 Progressive Cracking Development of NS4.....141
Figure 4.75 Storey Shear Force versus Horizontal Displacement for NS4 142
Figure 4.76 Decomposition of Horizontal Components of NS4 143
Figure 4.77 Contributions of Horizontal Components of NS4.....144
Figure 4.78 Strain Profiles of Beam Bars of NS4 146
Figure 4.79 Curvature Distribution of Beam of NS4 147
Figure 4.80 Strain Profiles of Column Bars of NS4.....149
Figure 4.81 Curvature Distribution of Column of NS4.....150
Figure 4.82 Bond Stress of Beam Bar of NS4.....152

Figure 4.83 Bond Stress of Column Bar of NS4 153
Figure 4.84 Joint Shear Distortion and Expansion of Specimen NS4 154
Figure 4.85 Final Crack Pattern of AS4 155
Figure 4.86 Progressive Cracking Development of AS4 156
Figure 4.87 Storey Shear Force versus Horizontal Displacement for AS4 157
Figure 4.88 Decomposition of Horizontal Components of AS4 157
Figure 4.89 Contributions of Horizontal Components of AS4 158
Figure 4.90 Strain Profiles of Beam Bars of AS4 160
Figure 4.91 Curvature Distribution of Beam of AS4 161
Figure 4.92 Strain Profiles of Column Bars of AS4 162
Figure 4.93 Curvature Distribution of Column of AS4 163
Figure 4.94 Bond Stress of Beam Bar of AS4 164
Figure 4.95 Bond Stress of Column Bar of AS4 165
Figure 4.96 Joint Shear Distortion and Expansion of Specimen AS4 166
Figure 5.1 Comparison of Hysteresis Loop of NS1 to NS4 172
Figure 5.2 Comparison of Hysteresis Loop of AS1 to AS4 174
Figure 5.3 Stiffness Degradation of All Specimens 176
Figure 5.4 Decomposition of Lateral Displacement of All Specimens 179
Figure 5.5 Material Modelling [D1] 188
Figure 5.6 Material Modelling of Reinforcement [D1] 189
Figure 5.7 Typical Meshing of Model 192
Figure 5.8 Loading Procedures 193
Figure 5.9 Hysteresis Loop of Specimens NS1 to NS4 197
Figure 5.10 Hysteresis Loop of Specimens AS1 to AS4 199
Figure 5.11 Stress Contour of Specimens NS1 to NS4 201
Figure 5.12 Stress Contour of Specimens AS1 to AS4 203
Figure 5.13 Ratio of Shear Strength Predictions to Test Results 204
Figure 5.14 Comparison of Crack Profiles of NS1 and AS1 206
Figure 5.15 Comparison of Crack Profiles of NS2 and AS2 206
Figure 5.16 Comparison of Crack Profiles of NS3 and AS3 207
Figure 5.17 Comparison of Crack Profiles of NS4 and AS4 207
Figure 5.18 Comparison of Beam Strain Profiles of NS1 to NS4 208
Figure 5.19 Comparison of Beam Strain Profiles of AS1 to AS4 209
Figure 5.20 Comparison of Column Strain Profiles of AS1 to AS4 210

Figure 5.21 Comparison of Column Strain Profiles of AS1 to AS4 211
Figure 6.1 Shear Strength Envelopes for Various Concrete Compressive Strength 223
Figure 6.2 Shear Strength Envelopes for Various Axial Compressive Load 223
Figure 6.3 Shear Strength Envelopes for Various Beam Bottom Bar to Top Bar Ratio 224
Figure 6.4 Joint Shear Strength versus Concrete Compressive Strength Relation via Experimental Approach 227
Figure 6.5 Joint Shear Stress Factor *k* versus Column Axial Compressive Loading Relation via Experimental Approach 229
Figure 6.6 Joint Shear Stress Factor *k* versus Column Axial Compressive Loading Relation via Analytical Approach 230
Figure 6.7 Joint Shear Stress Factor *k* for Concrete C30 and C70 231
Figure 6.8 Joint Shear Stress Factor *k* versus Beam Bar Ratio Relation via Experimental Approach 232
Figure 6.9 Joint Shear Stress Factor *k* versus Joint Core Reinforcement Ratio Relation via Experimental Approach 234
Figure 6.10 Joint Shear Stress Factor *k* versus Bond Index via Experimental Approach 236
Figure 6.11 Shear Resisting Mechanisms in Beam-Column Joints [P3].....239
Figure 6.12 External and Internal Actions of Interior Beam-Column Joints [P3].....242
Figure 6.13 Illustration of Bond in Reinforcement Bar in a Joint 245
Figure 6.14 Bond Development in a Joint 248
Figure 6.15 Relation between Parameters α, β and α_m 249
Figure 6.16 Joint Shear Stress Limits in NZS (1982) and NZS (2006).....253
Figure 6.17 Prediction of Shear Strength versus Experimental Results.....255
Figure 6.18 Normalised Shear Strength versus Control Parameters 256

LIST OF TABLES

Table 3.1 Summary of Specimens Detail 35
Table 3.2 Comparison on Design Limits of NSZ3101 1985 & 2006 36
Table 3.3 Properties of Concrete 38
Table 3.4 Properties of Reinforcement 38
Table 5.1 Comparison of Joint Shear Stress of Test Results 178
Table 5.2 Summary of Measured Maximum Bond Stress 180
Table 5.3 Material Properties of Finite Element Model 193
Table 5.4 Comparison of Test Results and Analysis 204
Table 5.5 Comparison of Joint Shear Stress of Test Results and Analysis 212
Table 6.1 Parameters of Database 218
Table 6.2 Summary of Material Properties of Analytical Studies 221
Table 6.3 Summary of Parameters Investigated in Analytical Studies 221
Table 6.4 Verification of Proposed Equations 251
Table 6.5 Parametric Studies on Shear Design Equations 257

LIST OF NOTATIONS

A_s' = area of longitudinal compression reinforcement of beam

A_s = area of longitudinal tension reinforcement of beam

A_{sc} = total area of longitudinal reinforcement of column

A_c = gross area of column

b = width of beam

b_c = width of column

b_j = effective joint width

d = depth of beam

E_c = modulus of elasticity of concrete,

Es = modulus of elasticity of steel

f = shape factor (taken as 1.2)

f_c' = concrete compressive strength

f_{cu} = concrete cube strength

f_c' = concrete tensile strength

f_t = yield strength of steel reinforcement

h = storey height or vertical distance between the column end pins

h_b = depth of beam

h_c = depth of column

h_i' = distance between left and right transducers in the 1st region in the column

h_i' = distance between left and right transducers in the region *i*

h_i = distance between top and bottom transducers in the region *i*

h_1 = distance between top and bottom transducers in the 1st region in beam

I_e = effective moment of inertia

I_g = moment of inertia of uncracked gross concrete area

l_c' = distance from the beam face to the center of the column end pin

l_b' = distance from the column face to the center of the beam end pin

K_{th} = theoretical initial stiffness

l = beam span or horizontal distance between the beam end pins

l'_b = distance from the column face to the center of the beam end pin

l'_c = distance from the beam face to the center of the column end pin

l_j = initial length of the diagonal in the joint core

N^* = axial compressive load acting on the column

P_{th} = theoretical ideal load strength

s_i = gauge length of the region i in the beam

s'_i = gauge length of the region i in the column

V_b = beam shear force at developing the ideal horizontal load strength

V_c = column shear force at developing the ideal horizontal load strength

x_i = distance from the column faces to the center

y_i = distance from the beam faces to the center of the region i

α_j = angle of the diagonal to the horizontal.

α_f = factor used in Eq 5.2

α_o = factor used in Eq 5.2

β = bottom-reinforcement-to-top-reinforcement ratio

δ_j = changes in the lengths of the diagonals

δ'_j = changes in the lengths of the diagonals

$\delta_{b,fe}$ = fixed end deformations of the beams as defined in Eq. 3.8

$\delta_{b,f}$ = flexural deformations of the beams as defined in Eq. 3.10

$\delta_{b,th}$ = theoretical elastic deformation of beam

${}_l\delta_1$ = left displacements measured over the 1st region in the column

${}_l\delta_i$ = left displacements measured over the region i in the column

${}_r\delta_1$ = right displacements measured over the 1st region in the column

${}_r\delta_i$ = right displacements measured over the region i in the column

${}_t\delta_i$ = top displacements measured over the region i in the beam

$\delta_{c,th}$ = theoretical elastic deformation of column

$\delta_{b,f,th}$ = theoretical flexural deformation of beam

$\delta_{b,s,th}$ = theoretical shear deformation of beam

$\delta_{c,f,th}$ = theoretical flexural deformation of column

$\delta_{c,s,th}$ = theoretical shear deformation of column

$\Delta_{b,th}$ = theoretical displacement contribution of beam

$\Delta_{c,th}$ = theoretical displacement contribution of column

$\Delta_{j,th}$ = theoretical displacement contribution of joint

$\Delta_{j,th}$ = theoretical deformation due to joint shear distortion

ρ = ratio of tension reinforcement (over beam cross-sectional area)

ρ' = ratio of compression reinforcement (over beam cross-sectional area)

ρ_t = ratio of longitudinal reinforcement (over column cross-sectional area)

$\theta_{b,i}$ = beam flexural rotation of the region *i* as defined in Eq. 3.2

$\theta_{b,i}$ = rotation measured over the region *i* in the beam (From Section 3.4.4)

$\theta_{c,i}$ = rotation measured over the region *i* in the column (From Section 3.4.4)

$\theta_{c,fe}$ = column fixed-end rotation as defined in Eq. 3.3

$\theta_{c,i}$ = column flexural rotation as defined in Eq. 3.4

$\theta_{b,fe}$ = beam fixed-end rotation as defined in Eq. 3.1

SUMMARY

With the rapid proliferation of high-rise buildings, the use of high strength concrete in construction is becoming increasingly common. High strength concrete provides many benefits such as a smaller column area as a result of higher compressive strength thereby creating more useable space within the buildings which can lead to higher commercial value. However, the strength, ductility, and energy dissipation capacity of these beam-column joints may not be adequate to sustain earthquake-induced loads due to the inherent brittle characteristics of high strength concrete. In this research program, the behaviour of high strength concrete interior beam-column joints under reversed cyclic loading was investigated through a rigorous test programme, finite element analysis and parametric studies. The research program summarised in this thesis is aimed at investigating the performance of normal strength concrete and high strength concrete beam-column joints subjected to earthquake actions, which are hitherto not addressed in Singapore.

A total of eight high strength concrete beam-column joints were built and tested under reversed cyclic loadings to study the structural behaviour of high strength concrete beam-column joints. All specimens only partially met the seismic detailing requirements in NZS 3101: 2006 and the respective test findings explored the possibility of improving upon the design code NZS3101 to accommodate the use of high strength concrete. Four specimens were tested with zero column axial compressive loading while another four specimens were tested with a column axial compressive loading of $0.3A_cf_c'$. Based on the test results, some relaxation of the bond requirements in beam-column joints is possible as improvement of bond strength was noticed where the bond strength increases with the increase in concrete compressive strength. The congestion of reinforcement in a high strength concrete beam-column joint can be improved when the usage of larger bars are allowed.

In the parametric studies, eighty three interior beam-column joints from test data were summarised to study the influences of parameters such as concrete compressive strength, bond index, column axial load, joint hoop reinforcement ratio

and beam reinforcement ratio on structural behaviour of beam-column joints. Besides that, the maximum joint shear stress of seventy five finite element models were verified to study the influence of column axial load on structural behaviour of beam-column joints. These models were built and analysed using the finite element analysis program DIANA. In general the following parameters have significant effects on the joint shear capacity: concrete compressive strength, bond index, joint hoop reinforcement and beam reinforcement ratio. The column axial compressive load on the other hand has more influence on the deformational behaviour of an interior beam-column joint than on the strength capacity. Column axial compressive load generally has no direct effect on the maximum joint shear strength, but it does affect the joint shear deformation and may lead to different deterioration behaviours after the peak column shear strength was reached, depending on the availability of joint hoops

Design recommendations were proposed based on the findings in the experimental programme and parametric studies. To incorporate the effect of concrete grade, as well as the ratio of total area of bottom beam bars top beam bars and axial compressive load in the bond condition of larger bar in high strength concrete beam-column joint, modified equations on bond development of beam reinforcement was proposed to the current NZS 3101. In the modified equation, the overstrength factor in NSZ 3101 was changed from 1.25 to 1.30. The design equations on bond development of beam reinforcement were verified by test data, which agreed well with the findings. The shear design equations in NSZ 3101 were reviewed where test results of eighty three interior beam-column joints were compared with estimates based on the equation. The study revealed that marginal improvement was found in the calculated ultimate shear strength with modified equation in NSZ3101. The limit of joint shear stress was also modified based on test findings so that it is applicable to both normal strength concrete and high strength concrete beam-column joints.

Chapter 1 Introduction

1.1 Statement of the Problem

The geographical location of Singapore is near to the seismic risk area where the active earthquake belt comprising the Sumatra Fault and the subduction zone lie, which is about 350 km away at the closest point. Figure 1.1 shows the epicenters of earthquakes occurring in this region between 1960 and 1995. In the figure, the large circle centered at Singapore with 500-km radius is included for reference, and the size of small circles indicates the earthquake magnitude. Numerous large earthquakes have been generated along this faultline including the great earthquake in 1833 which was estimated to have had a moment magnitude of around 8.7 and was believed to have caused a 500-km long rupture along the interface.

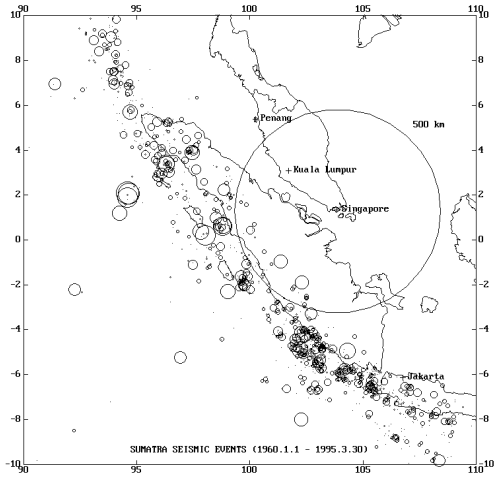

Figure 1.1 Epicenter Locations of Earthquakes in Sumatra Region [P1]

The size, location and timing of earthquakes are generally erratic. The study by Pan and Sun [P1] studied the strongest earthquakes that have been reported in Sumatra in each decade since 1830 and there have been no great earthquakes in the last half-century. The last two greatest earthquakes in Sumatra both occurred in the previous century, when there were practically no high-rise structures or reclaimed land like that in Singapore now. Although there has never been any earthquake damage to

Singapore, ground tremors have been felt in these areas for many times, and the incidents have increased significantly in number over the last three decades. There have been no seismographic stations in Singapore until very recently, and the ground motion reports therefore have been based solely on local newspapers and anecdotal history. Epicenters of the Sumatra earthquakes responsible for the tremors felt in Singapore generally fall around a circle of 500-km radius centered at Singapore.

With the rapid development of high-rise buildings locally and internationally, the use of high strength concrete (HSC) in construction is getting more common. HSC, providing benefits such as a higher strength and a low column area, creates more useable space within the buildings and leads to higher commercial value. However, the strength, ductility, and energy dissipation capacity of these beam-column joints may not be adequate to sustain earthquake-induced loads due to the inherent brittle characteristics of HSC [L2, L3, L4].

By reviewing the previous studies in the area of beam-column joints, the following problems were found [P3, P4, P7]:

- Although beam-column joints have been studied for more than thirty years, less attention was focused on the seismic design of high strength concrete beam-column joints and only recently a few studies conducted on the assessment of seismic performance of high strength concrete beam-column joints.
- In order to simplify the loading arrangement as a result of limitation in test setup, the assessment of seismic performance of high strength concrete beam-column joints were mostly carried out with zero column axial compressive loading. Such a loading arrangement simulated the most critical loading condition in a beam-column joint experiment but it is not realistic to neglect the presence of column axial compressive load in actual practice.
- The absence of column axial compressive load in most of the beam-column joint experiments performed led to a conservative design guide as the beneficial confinement effects due to the presence of column axial compressive load can delay the deterioration of the joint under cyclic loading.

- Due to the inherent complexity of beam-column joint regions, the effects of several parameters on joint behaviour, such as joint transverse reinforcement and axial loads, are still controversial.

Therefore to better understand the seismic behaviour of HSC beam-column joints and the effects of critical parameters on the joints' behaviour; an experimental and analytical study is being undertaken at NTU, Singapore. The investigation results will be useful in identifying the seismic weaknesses of such beam-column joints and establishing the hierarchy of failures. Knowing the deficiencies, it should be possible to improve the survivability of high strength concrete beam-column joints during earthquakes.

1.2 Problems of Non-Seismic Detailed Beam-Column Joints

The beam-column joint has been one of the most essential element in seismic design. In order to prevent beam-column joint failure, seismic design codes [A1, A2, N1, N2] emphasize that joints must be strong enough to withstand the yielding of the connected beams and columns. This can be achieved by the following principles:

- To make sure that a beam failure occurs earlier than a column failure;
- To ensure the integrity of the joint so that the strength and deformation capacity of the connected members can be developed;
- Strength and stiffness degradation of the joint must be prevented to reduce the increase of lateral displacement.

If a beam-column joint is designed to fulfill these criteria, it should be able to transfer the induced forces and achieve the desired performance.

In Singapore, the local design codes such as BS8110 [B5] and Eurocode 2 [E1] have been widely used for most civil engineering and building structures for many years. These codes are based on limit state design principles for the design and construction of reinforced and prestressed concrete structures under gravity loads as well as wind load for a structural frame. Little attention has been paid to seismic detailing since the code was initially developed in non seismically active regions in

Europe. As a result, no special detailing is dedicated to beam-column joints while no joint hoop is provided within the beam-column joints to ease the construction. Large bars have been used extensively in the detailing of beams and columns in order to simplify the construction activities. This is in contrast to typical detailing in seismic design where a smaller bar is preferred as it helps maintain good bond stress in joint core while limiting bond development length.

With reference to the above design criteria and design approaches, beam-column joints in a non-seismic detailed moment resisting frame may lead to a different behaviour from a seismically designed beam-column joint [L2, L3, L4]. In a non-seismically designed reinforced concrete frame, beam-column joints are not confined by the joint transverse reinforcement, therefore the desired truss mechanism will not develop. As a result joint shear forces can only be resisted by the diagonal concrete compression strut. During an earthquake, the contribution of the concrete to the joint shear strength is gradually reduced and the joint shear failure will occur eventually once the diagonal concrete compression strength is reached. The failure mode is undesirable as the building may fail catastrophically and abruptly without giving adequate warning signs for evacuation.

1.3 Objectives and Scope

As far as this project is concerned, the objective is to understand the fundamental mechanism of high strength concrete beam-column joints and how various parameters affect their behaviour under reversed cyclic loadings. The results and conclusions obtained from this study will be dedicated to improving the overall performance of the structures subjected to seismic loadings. Through the experimental findings on high strength concrete beam-column joints which only partially met the seismic detailing, the possible room to improve and relax on the design code NZS3101 is explored. With the use of high strength concrete and various parameters such as beneficial confinement from column axial compressive load, the bond development length within a joint core is reviewed. By reviewing the limiting values from the results of this study, the use of larger beam reinforcement passing through the joint core could be justified.

The scope of this project encompasses two major parts. Firstly, experimental studies involving eight high strength concrete interior beam-column joints under reversed cyclic loadings were carried out at Nanyang Technological University. The research program summarized in this thesis is aimed at investigating the performance of normal strength concrete and high strength concrete beam-column joints subjected to earthquake actions, which are not addressed in Singapore. Secondly, a parametric study was conducted to identify the influence of variables and understand the interactions among various parameters. Based on these works, design recommendations were proposed.

This research consists of the following experimental and analytical components:

- Conducting a series of experiments to study the seismic behaviour of beam-column joints with substandard detailing.
- To perform thorough test analysis to understand the general behaviour, observed crack patterns, the measured load-displacement responses and behaviour of beams, columns and joints from test findings.
- Undertaking a parametric study to provide additional information for understanding of the variable influences of beam-column joints in the reinforced concrete frames designed with out seismic provisions.
- To propose practical detailing which allow use of HSC and bigger bar size by reviewing the bond development length detail in seismic design code eg: NZS 3110 code [N1].

The long-term purpose of this research program is to provide guidelines for practicing structural engineers in evaluating existing reinforced concrete moment resisting frame structures, mitigating seismic hazards, and reducing the risk level to building occupants and owners in Singapore.

1.4 Thesis Organisation

The thesis reports the research findings of experimental studies, finite element analysis and parametric studies on the structural behaviour of high strength concrete beam-column joints. It is organised into seven chapters as below:

- Chapter 1 presents the background and summarises the main objectives of the proposed research.
- Chapter 2 presents a literature review of previous analytical and experimental researches on the subject of interior beam-column joints of normal strength concrete and high strength concrete.
- Chapter 3 describes the experimental program of eight HSC interior beam-column joints subjected to quasi-static cyclic loadings simulating earthquake actions with applied column axial compressive loading.
- Chapter 4 discusses the test results of eight HSC interior beam-column joints in terms of general behaviour, observed crack patterns, the measured load-displacement responses and the decomposition of lateral displacements. The behaviour exhibited by each individual component such as beam, column and joint core is explained.
- Chapter 5 analyses experimental findings on load-carrying capacity and strength degradation, stiffness degradation, joint shear, member contribution to horizontal displacement and energy dissipation. Besides that, the summaries of nonlinear finite element analysis to simulate a laboratory experiment that provides insight understanding structural behaviour of beam-column joints are discussed.
- Chapter 6 explains the findings of parametric studies based on test data from experiment and nonlinear finite element analysis to develop the relationship between various variables and joint shear resistance under lateral loads. The existing shear design equation in New Zealand Standard (NZS 3101) [N1] is reviewed and improvement is proposed.
- The conclusions are drawn from the studies and suggestions for future research are discussed in Chapter 7.
- Lastly, Appendix A summarised the cracking pattern of Specimens NS1 to NS4 & AS1 to AS4 to give readers a clear picture of the structural behaviour of the specimens tested by author.

Chapter 2 Literature Review

Strength and ductility have been the key criteria in designing buildings to withstand earthquake loading. To avoid the collapse of tall reinforced concrete multi-storey frames, structural systems with a strong column and weak beam are required where the input earthquake energy is absorbed and dissipated by the structures through the formation of plastic hinges at beam. To maintain the integrity of the structure, the joints connecting the beams and columns must not be a weak link during seismic loading. The beam-column joints have thus become a major study in seismic design. Even though high strength concrete has been used more widely in construction, less attention was drawn on the seismic design of high strength concrete beam-column joints. Due to the inherent brittle characteristics of HSC, the strength, ductility, and energy dissipation capacity of these beam-column joints may not be adequate to sustain earthquake-induced loads. This chapter summarises the findings of literature reviews on studies on seismic behaviour of beam-column joints, which sheds the light on the direction of this study. The summary of seismic design codes and findings on both non-seismically detailed and seismically detailed beam-column joints are also addressed in this chapter.

2.1 Test Studies on Seismic Behaviour of Beam-Column Joints

Extensive experimental studies have provided a fundamental understanding of many aspects of reinforced concrete beam-column joint behavior for the past thirty over years. Hanson and Connor [H3] performed the very first beam-column joint test and the testing results showed that the performance of beam-column joints was improved by providing joint hoop reinforcement. Then, levels of maximum joint shear stress were established by Meinheit and Jirsa [M3] by designing their specimens to fail by joint shear. Tests conducted by Paulay [P4] showed the importance of limiting bond demand upon bars passing through a joint. The aforesaid studies laid the strong foundation on the formation of current seismic design codes such as ACI 318-08 [A1], NZS 3101:2006 [N1], AIJ guidelines [A5], and EC8 [E2] were established.

To withstand lateral load induced by earthquake, these seismic design codes require that considerable amounts of transverse reinforcement be placed in beam-column joints even though joint shear failure models are different from each other and no unified model or theory of the joint failure has been established. On the other hand, for these non-seismically detailed joints found in older frame structures and frame structures in low seismic hazard zones especially in Singapore, the current design codes do not provide the necessary information to assess their strength and deformation capacity. These frames are mostly constructed without special joint reinforcement. Recently a few researches have been done by Kurose *et al.* [K2, K3], Hakuto *et al.* [H2], and Li *et al.* [L2, L2, L4] to assess the performance of non-seismically detailed joints.

2.1.1 Research Conducted by Kurose *et al*. (1988)

Kurose *et al.* [K3] conducted one throughout and comprehensive analysis of the factors affecting the strength of beam-column joints. The control parameters studied were concrete strength, beam-to-column width ratio, beam-to-column depth ratio, transverse beams, lateral reinforcement, and column axial load. Through the parametric study, the following findings were concluded:

- The joint shear strength was found to increase with the following: increase in concrete strength and beam to column width ratio
- The joint shear strength was observed to decrease as the beam to column depth ratio increased
- There was no clear correlation between masking ratio and joint shear strength when two transverse beams are present
- The increase in lateral reinforcement increased the shear strength of the joints
- The different level of axial force had little influence on joint shear strength.

2.1.2 Research Conducted by Pessiki *et al*. (1990)

A total of ten interior beam-column connection region specimens were tested by

Pessiki *et al.* to identify the reinforcing details of the beam-column joint region, which could prove critical to the safety of a structure during an earthquake [P9].

For specimens with continuous positive beam reinforcement, it was found that:

- For the reinforcing details and specimen geometries considered, the column splices performed adequately. Most of the energy dissipation and stiffness loss that occurred in the columns can be attributed to the region adjacent to the joint.
- A peak joint shear stress of about $1.10\sqrt{f_c'}$ was reached in each continuous beam reinforcement specimen. It is concluded that the benefit of small amounts of joint reinforcement is limited to improving ductility rather than increasing the joint shear strength.
- Each lightly-reinforced specimen displayed little toughness, characterized by limited ability to maintain peak resistance with continued cycling beyond the cycle during which peak resistance was obtained. The stiffness of each specimen decreased rapidly with increasing drift.

For specimens with embedded positive beam reinforcement, it was found that:

- Peak pullout resistance was the same for both specimens; with each size bar pulling out from the joint prior to yielding at a force of about 24 kips.
- Pullout resistance was not affected by the change in axial force level, and fewer cycles of load could be applied at peak resistance in the presence of a smaller axial force.
- The peak pullout resistance may be slightly increased by the presence of transverse confinement.

2.1.3 Research Conducted by Xin (1992)

Xin [X1] performed test of six cruciform internal beam-column joint of various reinforcement detailing and different concrete grade. The research aimed to investigate the behaviour of beam-column joints in reinforced ductile frames with a range of concrete compressive strengths and with Grade 430 steel. The test also helped to investigate the possible of relaxation of code requirement on the beam bar

diameter for ductility design.

The specimens were divided into three groups according concrete strength *i.e.* 20, 40 and 60 MPa respectively. Both symmetric and unsymmetric reinforced sections were designed in each group. The amount of horizontal reinforcement in joint core was only 60% of required in NZS 3101:1982 and vertical shear reinforcement on the hand was only 75% of required in NZS 3101:1982. Only one specimen (Unit 1) complied with design requirement of the longitudinal bar diameter for ductility design as per NZS 3101:1982 while the other five specimens did not satisfy the requirement.

The research revealed the followings:

- The effect of concrete strength on the bond-slip of longitudinal beam bars passing through the joint core was very significant. The requirement for longitudinal bar diameter can be relaxed with the increase in concrete strength.
- The bond condition of top and bottom bar in joint core was changed as the ratio of total area of bottom beam bar to top beam bar was revised. Hence a limitation of beam bar diameter for top and bottom reinforcement could be different.
- Higher strength of steel bar did not lead to serious bond-slip on beam bars when a higher concrete grade was used. Hence it was suggested the lowest grade of 30 MPa usage when high strength steel was used.

2.1.4 Research Conducted by Hakuto *et al.* (1995)

Hakuto *et al.* [H2] had conducted a series of test involving existing reinforced concrete beam column joints, which were designed and built in New Zealand in the late 1950s. The test results indicated that:

- The seismic performance of interior beam-column joints without transverse reinforcement in the joint cores would be poor in a severe earthquake if the nominal horizontal joint shear stress exceeds approximately $0.17 f_c^{'}$.

- If the frame responds in the post-elastic range, the available shear strength of interior beam-column joint cores without transverse reinforcement decreases while there is an increase in the imposed ductility of the adjacent beam plastic hinge regions.
- Based on the test data, it was found that even when joint core hoops was absent in existing one-way interior beam-column joints, no additional joint core hoops are required for shear reinforcement if the existing column is enlarged by jacking so that the horizontal nominal shear stress in the joint core is reduced to less than $0.07 f_c^{'}$.

2.1.5 Research conducted by Li *et al.* (2002)

Li, Wu and Pan [L2, L3, L4] had conducted a series of tests involving four reinforced concrete beam-wide column joints with non-seismic or limited seismic detailing. The two variables in the test specimens were the amount of joint transverse reinforcement and the lap splice details for column and beam reinforcement. The beam to column width ratio of the specimens was about 3. Based on these experimental results, the maximum nominal horizontal shear stress in the joint core was $0.15 f_c^{'}$. The joint without joint horizontal transverse reinforcement failed at a displacement ductility factor of 2, which correlates well with the model proposed by Hakuto *et al* [H2]. This suggests that joint shear failure occurs around a displacement ductility factor of 2, where the joint shear stress is between $0.11 f_c^{'}$ and $0.17 f_c^{'}$. Due to the presence of the joint transverse reinforcement, the modified joint achieved a ductility factor of 3.

Li, Wu and Pan [L2, L3, L4] also conducted parametric studies based on strut-and-tie modeling and finite element analysis program WCOMD-2D [W1] on the behavior of test specimens. Based on the parametric studies, they found that:

- Transverse reinforcement was able to reduce the principal compression stresses within the diagonal compression strut, however it can not prevent the future failures at higher ductility levels due to the increasing tensile strains in the

transverse direction, which reduced the capacity of the diagonal compression strut.

- For an oblong joint, when $N^* / A_g f_c^{'} < 0.4$ the axial compression load was beneficial to the joint, while when $N^* / A_g f_c^{'} > 0.4$ the axial compression load became detrimental to the joint.
- For a deep wall-like column joint, both of the finite element analysis and the strut-and-tie analysis showed that the joint's performance was better when the axial compression load was zero or $0.2 f_c^{'} A_g$. Unlike the oblong joint, the effect of axial compression load was not constant for the behavior of the wall-like column joint. It changed at various axial loading levels.

2.2 Studies on Structural Bahaviour of HSC Beam-Column Joints

El-Nabawy Atta *et al.* [E3] performed test on ten normal strength and high strength concrete beam-column joints. These specimens were edge beam-column joints. The specimens were grouped into three groups to test. Group 1 was three samples made of normal strength and high strength concrete to study the influence of concrete strength on the specimens. The influence of joint hoops was the focus of the test of Group 2, made of high strength concrete. Lastly Group 3 studied the influence of reinforcement in beams, columns and joints. This research revealed that concrete strength was the major parameter that controlled the behaviour of beam-column joints with less cracks appeared in high strength concrete specimens and vice-visas. The reinforcement detailing on the other hand influenced the ultimate capacity. Higher shear reinforcement in joint core yielded the maximum capacity while sample without hoop reinforcement failed with the lowest load in an abrupt manner.

With the available test data, El-Nabawy Atta *et al.* [E4] performed finite element analysis to verify the model built by ANSYS 5.4 package by using eight nodded three dimensional brick element with option to allow concrete to crack and crush when the tensile or compressive strength is reached. With the verification of test data with models, parametric studies were carried out. The main variables in the

analysis were concrete grade, reinforcement area, hoop reinforcement, pre-loading condition and etc. Concrete grade, was the main factor that influenced the behaviour of models. The hoops reinforcement and also longitudinal reinforcement in column controlled the governing trust mechanism and thus influenced the system stiffness, cracking pattern and ultimate capacity. This research explained that the modes of failure and shear behaviour of high strength concrete joints behaved differently from normal strength concrete joint at various axial load levels.

Attaalla *et al.* [A6] conducted experiment on interior beam-column connections cast from high strength concrete and designed to exhibit joint shear mechanism under earthquake simulated loads. The investigation focused on the seismic shear characteristics of the joint core and covered joints reinforced with conventional ties as well as joints reinforced with only steel fibers. Low compression were applied on columns in order to simulate the combined effects of overturning moment, produced by the horizontal acceleration, and the vertical component of earthquake excitation. Test findings indicate that defining the joint shear strength as a function of the square root of the concrete compressive strength as adopted by the current ACI-318 code seems to be unsuitable approach for joints constructed with high strength concrete. Decrease in the range of about 45 percent in the joint deformability was observed due to reinforcing the joint core with steel fibers only.

Mo *et al.* [M6] explained the test results for four prestressed concrete beam-column connections subjected to reversed cyclic loading. The specimens were part of an experimental program designed to investigate the effect of design provisions/specifications and concrete strength on seismic performance behavior of such connections. The major design parameters varied in the specimens were the design code (AASHTO versus New Zealand codes) and the concrete strength (high versus normal strength concrete). From the test results, it was concluded that both the AASHTO and New Zealand codes provide sufficient capacities for earthquake-resistant design, and before spalling of the concrete cover, the stiffness degradation of the specimen with high strength concrete was less serious than that with normal strength concrete. To account accurately for the hysteretic behavior, a new set of

rules for such connections to predict the hysteretic loops is proposed.

Four beam-column joint tests were undertaken by Brooke [B4] to assess the accuracy of New Zealand design rules relating to bond strength in beam-column joints when applied to large diameter, high-strength reinforcement. The ratio of longitudinal beam reinforcement diameter to column depth intentionally did not meet the requirements of the New Zealand design standard for any of the units. The units were subjected to cyclic displacements up to interstory drift angles of 5%. Bond failure occurred in two of the four test units, at drift levels exceeding those allowed by international codes. It is believed that the unexpectedly good bond performance of the remaining two units was due to the large excess of vertical joint shear and column moment capacity.

Over the last 30 years, significant amount of research has been carried out on cyclically loaded exterior beam-column joints. In spite of the cumulated data, there is still no consensus between the research circles regarding the factors affecting the joint shear strength. Bakir and Boduroglu [B1] investigated the influence of different parameters on the joint shear strength. For this purpose, an experimental database consisting of 60 cyclically loaded exterior beam-column joints is used. Several parametric studies are carried out on the experimental database. It is apparent from these parametric studies that the joint shear strength increases as the beam longitudinal reinforcement ratio, and the concrete cylinder strength increase. The joint shear strength decreases when the joint aspect ratio increases.

2.3 Studies on Bond Properties of HSC Beam-Column Joints

An experimental investigation was conducted by Alavi and Marzouk [A3] on high-strength concrete specimens to examine the bond strength characteristics under monotonic loading. The range of compressive strengths tested was between 70 and 95 MPa. The influences of load history, confining reinforcement, bar diameter, concrete strength, reinforcement spacing and rate of pull out were investigated experimentally. The internal concrete strains close to the contact surface as well as the steel strain were measured. The test set-up, load application, instrumentation

and measurement, and test procedure were designed to measure strains and deformations. Several specimens with reinforcement bar diameters of 20, 25 and 35 mm were tested.

The test results revealed that the bond strength of high-strength concrete is higher than the corresponding normal strength concrete. However, the bond behaviour of high-strength concrete is more brittle in comparison with normal strength concrete. The concrete strains were measured around the steel reinforcement. Concrete strain measurements are useful to identify the internal crack pattern and to predict possible failure modes. The area under the curve of the bond stress–slip curve can define the bond energy. The bond energy is related to ductility and can be used along with the bond strength in evaluating the bond behaviour of high-strength concrete.

It is generally accepted that the bond strength increases with the concrete strength. However, due the inherent characteristic the bond failure in HSC is brittle. Research by Mendis and French [M5] revealed the brittle failure mode of HSC was due to the engagement of only few deformations. On the other hand, Pendyala *et al*. concluded that even HSC is brittle in nature, the flexural HSC members can be ductile due to lower neutral axis depth [P8]

To understand the bond slip characteristics of high strength concrete under cyclic loading, Alavi and Marzouk [A4] performed another series of test for the aforesaid objective. The cyclic bond of high strength concrete was investigated under different parameters, including load history, confining reinforcement, bar diameter, concrete strength, and the rate of pull out. The bond strength, cracking, and deformation are highly dependent on the bond slip behavior between the rebar and the concrete under cyclic loading.

The results of cyclic testing indicated that an increase in cyclic displacement will lead to more severe bond damage. The slope of the bond stress – displacement curve can describe the influence of the rate of loading on the bond strength in a cyclic test. Specimens with steel confinement sustained a greater number of cycles

than the specimens without steel confinement. It has been found that the maximum bond strength increases with an increase in concrete strength. Cyclic loading does not affect the bond strength of high strength concrete as long as the cyclic slip is less than the maximum slip for monotonic loading. The behavior of high strength concrete under a cyclic load is slightly different from that of normal strength concrete.

For structural utilisation of high-strength concrete (HSC), a good understanding of the bond and anchorage behaviours of ribbed bars in HSC is essential. An extensive experimental study on the bond and anchorage behaviour in HSC was carried out by Magnusson [M2]. Four types of HSC specimens were tested where replica normal strength concrete specimens of each type were tested for comparison. Both numerical modelling based on schematic bond stress-slip relationships and non-linear finite element modelling were used to complement the experiments.

The study showed that the bond and anchorage behaviours were similar in both concrete types, and governed by the same phenomena. The bond strength in well-confined concrete increased linearly with the concrete compressive strength. Furthermore, high-strength concrete gave a much stiffer local bond stress-slip relationship than normal strength concrete. Once the yield capacity of the reinforcing steel was reached, the local bond resistance decreased substantially, especially in high-strength concrete. Schematic local relationships between bond stress and slip are proposed for anchorage in confined normal strength and high-strength concrete; these take into account the bond deterioration when the yield capacity of the reinforcement steel is reached or exceeded.

Although the anchorage capacity of a high-strength concrete specimen was higher than that of a comparable normal strength one, the increase was not in proportion to the rise in compressive strength, unlike the local bond strength under well-confined conditions. However, the high-strength concrete showed less capacity for stress redistribution, both along anchorage or lap lengths and between bars anchored in

the same region. This can result in premature and brittle failures, unless compensated by a sufficient amount of stirrups. The design method examined usually gave results on the safe side when compared with test results. However, the scatter was large and there was a tendency for the safety to decrease with greater concrete strength.

2.4 Characteristics of Beam-Column Joints

This section summarises the studies on beam-column joints in term of physical characteristics and structural characteristics. The scopes of studies include the joint classifications, seismic detailed beam-column joints, non-seismic detailed beam-column joints and also failure mode or failure criteria of a beam-column joint.

2.4.1 Joint Classification

Shear mechanism and bond resistance within the joint is profoundly affected by the connecting beams and columns. According to Paulay and Priestley [P7] it is recommended to ensure that joints remain essentially in the elastic range throughout the inelastic response of the structure. This type of joint is called an elastic joint. Smaller amount of joint shear reinforcement is generally sufficient if inelastic deformations do not occur in the beams or columns adjacent to the joint.

However, as a general rule, plastic hinges are expected to develop at the ends of beams when a structure is subjected to the design earthquake load. In such cases, it is not possible to prevent some inelastic deformation occurring in the joint. This is due primarily to the penetration of inelastic strains along the reinforcing bars into the joint. These joints are classified as inelastic joints which require larger amount of joint shear reinforcement.

The ACI-ASCE Committee 352 [A2] has similar definitions. The elastic joints are denoted as “type 1 joints” in the code. Any joint designed to resist gravity and normal wind loads would fall into this category. On the other hand, ‘type 2’ is a joint that connects members which are required to dissipate energy through

reversals of deformation into the inelastic range. Joints in moment resisting frame structures designed to resist earthquake motion, strong wind load or blast effect are of this category. Details on the joint classification can be referred at Reference [A2]

Besides the classification based on structural behaviour, the beam-column joints may be classified in terms of differences in the mechanism of beam bar anchorage either interior types or exterior joints [P7]. To illustrate, the beam reinforcement passes through the joint region in an interior joint while for the exterior joint, the reinforcing bars are bent down and terminate into the connecting columns.

2.4.2 Characteristics of Seismic Detailed Beam-Column Joints

Under moderate to strong earthquakes, the beam-column joint region undergoes severe stiffness degradation and strength deterioration. Hence beam-column joint is one of the most critical regions to resist seismic loading during the inelastic response. The seismic detailed beam-column joints are subjected to large shear forces due to lateral earthquake force and also need to provide sufficient anchorage length for longitudinal beam and column bars. The joints need to be strong with good bond characteristics as to function well in a strong column-weak beam structural system. To achieve good bond characteristics, limitation on the main reinforcement size is imposed to achieve sufficient anchorage length. Appropriate amount of transverse reinforcement within the joint panel is provided to avoid excessive shear deformation in the joint region.

In capacity design [H2] the designer chooses the most desirable mechanism for the structure to achieve the required displacement ductility factor in the post-elastic range during a major earthquake, normally by flexural yielding at selected plastic hinge positions. The capacity design procedure aims to provide an appropriate balance of flexural strength between the plastic hinge region and other modes of failure. All other regions of the structure will be made adequately strong to ensure that the plastic hinges will only occur at the selected regions and failures due to shear and loss of bond between concrete and reinforcement are avoided.

The seismic design codes for example, New Zealand Standard (NZS 3101), American Concrete Standard (ACI 318-08) and Japan Standard (AIJ-1994) use the concept of strong column-weak beam to ensure beam hinging mechanism for a moment resisting structure, or at the very least, a mixed side-sway mechanism should be formed during severe earthquake loading. After ensuring strong column-weak beam behaviour, appropriate measures should be taken to avoid excessive shear deformation in the joint region and reinforcement bar slip due to bond deterioration within the joint panel under reversed cyclic loading.

In comparison, columns are considered to be more vulnerable elements than beams. If a number of columns in a moment resisting frame structure achieve their flexural capacity, a column sideway mechanism can form, leading to a very high ductility demand around the plastic hinge regions in the columns. The result can be catastrophic soft story failures which are not the favourable failure modes [H2].

2.4.3 Characteristics of Non-Seismic Detailed Beam-Column Joints

The characteristics of a non-seismic detailed beam-column joint widely used in Singapore construction practice are summarised below through review of the design code BS8110 [B5]:

- Bottom beam bars in the vicinity of joint region are either discontinuous or with very short embedment length into the joint core.
- Within the joint region, the amount of top beam reinforcement is normally twice that of the bottom resulting in premature bottom beam reinforcement yielding during large loading reversals
- No horizontal or vertical transverse reinforcement is provided within the joint panel.
- Beam and column reinforcement passing through the joint has relatively large diameter resulting in poor anchorage condition.
- Columns might be designed weaker than the adjacent beams potentially leading to an undesirable soft story or column sway mechanism under relatively large lateral load.

- Around 2% longitudinal column reinforcement is provided with lap splices all located immediately above floor levels in the zone of maximum lateral load moment.
- Design shear force in columns is relatively very small under gravity loading, much less transverse reinforcement is required resulting in widely spaced column links, particularly in the potential plastic hinge zones.

In general, the local non-seismic detailed beam-column joints are built without joint hoops and it can be termed as lighly reinforced beam-column joints. They are totally different from ductile joints in seismic design where adequate measures are taken to avoid excessive shear deformation in the joint region and reinforcement bar slip due to bond deterioration within the joint panel under reversed cyclic loading.

With the absence of joint core hoops and poor bond development within the joint core, the typical local non-seismic beam-column joint might not perform well under reversed cyclic loading. The past experimental programme undertaken by Li *et-al* on the research of structural behaviour of lightly reinforced concrete beam-column joints under reversed cyclic loading revealed that the overall performance of lightly reinforced concrete beam-column joints were found to be unsatisfactory in terms of lateral load capacity, drift, and displacement ductility. The joints failed at the low displacement ductility level and shear failure formed in the joints [L2, L3, L4].

The research findings by Li *et-al* demonstrated that even limited seismic detailing could improve the seismic behaviour of the joints. However, to build structures under full seismic design guide in Singapore is costly and not practical. As such, the more practical way to improve the performance of local non-seismic beam-column joints is to limit the main reinforcement size to achieve sufficient anchorage length then to provide appropriate amount of transverse reinforcement within the joint panel [L2, L3, L4]. Such practice can help to avoid excessive shear deformation in the joint region and reinforcement bar slip due to bond deterioration within the joint panel under reversed cyclic loading.

2.4.4 Failure Models of Interior Beam-Column Joints

The following sections explain the failure models of interior beam-column joints. The models shown below are referred to past research performed by various researchers as to summarise the failure models developed to-date.

2.4.4.1 Joint Shear Resisting Mechanisms of Interior Beam-Column Joints

Figure 2.1 shows the forces acting on the joint core resulting from the moments and the shear forces generated in the beams and the columns of a building frame. The horizontal shear force acting on the joint core is:

$$V_{jh} = (M_{b1} + M_{b2}) / jd - V_c \qquad (2.1)$$

Joint shear stress can be calculated as following:

$$v_{jh} = \frac{V_{jh}}{b_j h_c} \qquad (2.2)$$

where h_c = column depth

b_j = effective joint width as defined in Figure 2.2.

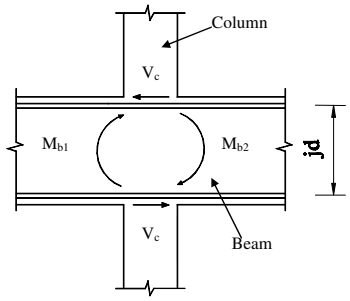

Figure 2.1 External Actions of Internal Beam-Column Joint

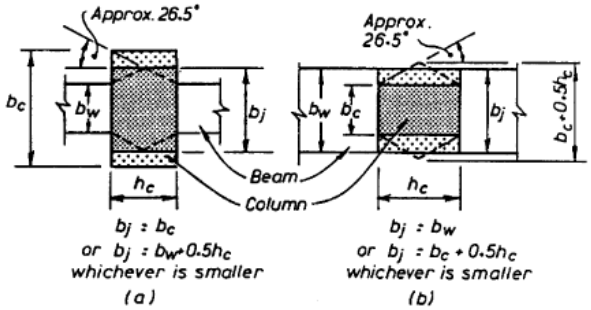

Figure 2.2 Definition of Effective Joint Width [P3]

There are two basic mechanisms in joints [P3] which are the diagonal compression strut and the truss mechanism. The diagonal compression strut sustains the compression forces transferred from the column and beam compression zones, whereas the truss mechanism sustains the forces transferred from the column and beam main bars by the bond mechanism. If the bond condition is sufficiently good, more shear stress will be sustained by the truss mechanism. Otherwise, the diagonal compression strut will sustain more of the stress. Details of joint mechanism are explained in Section 6.4 of Chapter 6

2.4.4.2 Failure Criteria of Interior Beam-Column Joints

According to the definition of CEB [C1, C2], the failure criteria of interior beam-column joints can be summarized into three categories, as follow:

Category 1:

This category deals with lightly reinforced beams, or columns with high axial force levels where the truss mechanism may be too weak for joint cracking to develop. The critical parameter here is the principal tension stress in the joint, rather than the shear stress level. Based on the studies done by Priestley and Calvi [P11], the diagonal tensile strength of the concrete may conservatively be taken as $0.29\sqrt{f_c'}$ MPa ($3.5\sqrt{f_c'}$ psi). Thus

$$f_{dt} = \frac{f_c}{2} - \sqrt{\left(\frac{f_c}{2}\right)^2 + v_{jh}^2} \le 0.29\sqrt{f_c'} \qquad (2.3)$$

Category 2:

This category of failure is dominated by the premature failure of diagonal compression struts. The tests of Pessiki and Beckingsale [P9] showed that the diagonal compression strength of the concrete is limited to $0.5 f_c'$. Thus:

$$f_{dc} = \frac{f_c}{2} + \sqrt{\left(\frac{f_c}{2}\right)^2 + v_{jh}^2} \le 0.5 f_c' \qquad (2.4)$$

Category 3:

For beam-column joints with principal tension stress $f_{dt} > 0.29\sqrt{f_c'}$ MPa ($3.5\sqrt{f_c'}$ psi) and principal compression stress $f_{dc} < 0.5f_c'$, failure may be due to joint shear, bond slip of the reinforcing bars through the joint, or beam flexural ductility.

2.4.4.3 Failure Mode of Lightly Reinforced Beam-Column Joints

Joint shear failure can be detected by two means depending on the joint details. For a ductile joint configuration, failure can normally be defined as joint hoop yielding; whereas for a lightly reinforced beam-column joint, most of the researchers believe in the diagonal compression strut failure mechanism [H2, P4]. In the compression strut failure mechanism, the presence of diagonal tensile strains in the joint core will reduce the diagonal compressive strength of the concrete. When the joint shear stress is large, and transverse reinforcement is not present in the joint core, significant diagonal tension cracking in both directions will occur in the joint core. Under reversed cyclic loading in the inelastic range, these diagonal tension cracks will become large, and disintegration of the concrete will begin because of the repeated opening and closing of the cracks along which shear sliding movements occur. This will be associated with a drastic volumetric increase of the joint core concrete unless adequate confinement is provided. These phenomena will reduce the diagonal compressive strength of the concrete of the joint core. Hence, it is evident that after excessive diagonal tension in the core of the interior beam-column joint without transverse reinforcement, the eventual failure of the joint core will generally occur as a result of compression failure of the diagonal compression strut.

Hakuto *et al* [H2] believed that diagonal compression failure will occur in a lightly reinforced beam-column joint regardless of the degree of bond deterioration along the reinforcing bars passing through the joint core. On one hand, if the bond condition is poor, the diagonal compression strut mechanism will transfer the joint shear since the truss mechanism will not function under poor bond condition. On the other hand, if the bond condition is good, the truss mechanism cannot transfer

the joint shear without shear reinforcement in the joint core. This will force the joint shear to be carried out mainly by the diagonal compression strut mechanism, while bond forces will be transferred to the diagonal compression strut over the width of the compression zone at the end of the strut.

2.5 Seismic Design Codes

Due to the complexity of joint behaviour under cyclic loadings, there is no direct solution to predict the joint shear stress for beam-column joint design. Seismic design codes such as New Zealand Standard (NZS 3101-2006) and American Concrete Institute Code (ACI 318-08) have been referred as the basis of beam-column joint design. These design codes have been developed based on extensive experimental research and the fundamental concepts of these design codes are explained in the following sections:

2.5.1 New Zealand Standard (NZS 3101-2006)

The New Zealand Standard are intended to ensure that a joint core has sufficient strength to cause energy dissipation to happen at the potential plastic hinge regions of the adjoining members and not the joint core itself. The joint core shall also be designed to withstand the forces arising when the overstrength of the framing members is developed. The design actions are obtained by assuming the stresses in the flexural steel at the plastic hinges are 1.25 times of the yield strength of the reinforcement used. The maximum allowable shear stress limits is $0.2f_c'$ MPa.

The design code assumed that two self-equilibrating mechanisms of shear transfer should be mobilised if a joint core is adequately detailed. These mechanisms are namely, diagonal strut mechanism and trust mechanism. The diagonal strut mechanism is initiated at the initial stage of response before the beam yielding starts to penetrate from the adjacent beam-column interface into the joint. After several significant cycles of loading, the beam yield penetration and bond deterioration will start, and full-depth cracking will also be formed. The normal stresses acting on the

concrete compression zones of the framing members will eventually be eliminated. As a result, both the horizontal and vertical member shear forces have to be transferred through bond effect. As the bond has been destroyed by yield penetration, it is suggested that stress transfer moves towards the central region of the joint, causing significant stress redistribution within the joint. It is assumed at this point that the concrete strut mechanism is no longer activated.

On the other hand, a self-equilibrating truss mechanism, formed by both horizontal and vertical shear reinforcement and longitudinal column reinforcement, starts to carry the distributed forces. The concrete core supplies the necessary compression field which is balanced by the tension forces in the reinforcement. To sustain this mechanism, a large amount of horizontal reinforcement and even vertical joint reinforcement are required.

The code neglects the contribution of the main strut mechanism unless significant column axial load greater than $0.1f_c'A_c$ exists, where f_c' is the concrete compressive strength and A_c is the gross column cross-sectional area. The horizontal shear reinforcement is considered to take all the probable horizontal shear forces while the vertical shear reinforcement is considered to take all the probable vertical shear forces. Noteworthy that the vertical reinforcement also includes the intermediate column reinforcement placed in the plane of bending between corner bars. The NZS 3101-2006 code also requires provision of horizontal transverse confinement reinforcement to prevent possible concrete dilation. If a joint is framed at all four column faces, the amount of confinement reinforcement could be reduced by 50%.

The code also recognises the influence of column axial compressive load. The applied column axial compressive load is applicable in the formula for obtaining both the horizontal and the vertical shear reinforcement. It is also proposed that the column axial compression contributes to the compression strut by increasing its steepness towards the vertical plane, therefore the joint shear strength should be increased when significant axial load is present.

To control bond deterioration within the joint volume, NZS 3101-2006 code gives the requirement of the maximum beam bar diameter passing through the joint in terms of concrete compressive strength f_c' and steel yielding strength f_y. The use of bar of larger diameter to pass through the joint core is possible when high strength concrete is used. The detailed discussion of bond deterioration control is explained in Section 6.4.

2.5.2 American Concrete Institute Code (ACI 318-08)

For a proper design of beam-column joint, the concept of strong-column-weak beam must have been ensured, prior to the check on the maximum joint shear stress and anchorage length requirement. The flexural ratio at a joint is defined as the sum of the nominal moment strength of the columns to that of the beams framing at a joint. The ACI 318 committee requires ratio to be greater than 1.2 for nominal values and this ratio is stated to be greater than 1.4 for nominal flexural strength in ACI 352R-91 recommendations.

In ACI Code, the joint core is considered as part of a column. As such, the joint lateral reinforcement is designed as that in any critical column region. The Code assumes a critical horizontal shear force is introduced into the joint while the adjacent beam members are assumed to be able to develop their full flexural resistance with the formation of beam flexural hinging mechanism. Due to such arrangement, this shear force is primarily resisted by the joint core and the longitudinal column reinforcement. The concrete contribution to the overall resistance is limited to maximum $0.29\sqrt{f_c'}$ MPa by considering occurrence of diagonal tension failure in concrete. Transverse reinforcement in the form of hoops or stirrups are provided to resist the difference between the designed shear input and the concrete contribution. Because joint shear can cause dilation of the joint volume, transverse reinforcement especially hoops also help to confine the concrete core.

The allowable shear stress limits to prevent excessive shear deformation of the joint core is summarised as below:

- $1.7\sqrt{f_c'}$ MPa for joint confined in 4-face (interior joint)
- $1.25\sqrt{f_c'}$ MPa for joint confined in 3 or 2-face
- $1.0\sqrt{f_c'}$ MPa for other joints

Lastly, to limit bond deterioration, the size of beam bar diameter passing through the joint is restricted to a fraction of 1/20 of the column dimension in the direction parallel to the beam reinforcement.

2.5.3 Summary of Design Codes

It is generally accepted that the NZS 3101-2006 design code imposes the most stringent requirement on joint shear reinforcement, large amount of both horizontal and vertical reinforcement in the joint core are required. ACI code on the other hand, only rely on horizontal reinforcement in the joint core and ignores the existence of the vertical joint shear stress, which was found inadequate to sustain the truss panel mechanism [P2].

As the joint core is designed as part of column, the presence of high column axial compressive load may demand heavy reinforcement in column design which in return produces a heavily reinforced joint core, and vice versa. Therefore, the ACI requirements were on the unconservative side when small axial loads were present [P6].

The common drawback among the ACI 318-08 and NZS 3101-2006 are as below:

- Not considering the biaxial stress interaction in the joint, which means that for space frames, direction of bending is assessed independently.
- No acceptable joint shear deformation level is stated. A moment-resisting frame structure will not be able to perform well if there is substantial joint

shear deformation, even though the joint might still be able to sustain high joint shear stress. Without this limit, the performance of frame is solely controlled by joint shear stress limit which could be too optimistic.

2.6 Conclusions on Literature Review

- Although interior beam-column joints have been studied worldwide for more than thirty years, more attention was drawn on the seismic design of ductile beam-column joints, and only until recently a few studies have been done on the assessment of seismic performance of non-seismically detailed beam-column joints. The only available experimental study of such joints was conducted by Li, Wu and Pan [L2, L3]. However, the experimental study did not consider the influence of column axial force, which is one of the important parameters on the behavior of beam-column joints.
- Currently, there is only one model proposed by Hakuto *et al.* [H2] to assess the behavior of non-seismically detailed beam-column joints. However, this model did not consider the influence of column axial force, which is one of the important parameter on the behavior of beam-column joints. The model would be a useful tool to assess the behavior of beam-column joints especially for those tested without axial force
- Test on HSC beam-column joint revealed that concrete strength was the major item that controlled the behaviour of beam-column joints with less cracks appeared in high strength concrete specimens and vice-visas. The modes of failure and shear behaviour of high strength concrete joints behaved differently from normal strength concrete joint at various axial load levels. It was concluded that the stiffness degradation of the specimen with high strength concrete was less serious than that with normal strength concrete.
- Past parametric studies carried out on the experimental database demonstrated that the joint shear strength increases as the beam longitudinal reinforcement ratio, and the concrete cylinder strength increase. The joint shear strength decreases when the joint aspect ratio increases.

- Bond test on concrete revealed that the bond strength of high-strength concrete is higher than the corresponding normal strength concrete. However, the bond behaviour of high-strength concrete is more brittle in comparison with normal strength concrete.
- The results of cyclic testing indicated that an increase in cyclic displacement will lead to more severe bond damage. Cyclic loading does not affect the bond strength of high strength concrete as long as the cyclic slip is less than the maximum slip for monotonic loading. The behavior of high strength concrete under a cyclic load is slightly different from that of normal strength concrete.
- Although the anchorage capacity of a high-strength concrete specimen was higher than that of a comparable normal strength one, the increase was not in proportion to the rise in compressive strength, unlike the local bond strength under well-confined conditions. However, the high-strength concrete showed less capacity for stress redistribution, both along anchorage or lap lengths and between bars anchored in the same region. This can result in premature and brittle failures, unless compensated by a sufficient amount of stirrups.
- With the advanced in building technology, it is timely to study the structural behaviour of HSC beam-column joint especially when limited reasech on the effect of high strength concrete (HSC) beam-column joints was available.
- Most experiments assumed no axial load existed in the test, which was albeit the most critical case that led to conservatism in design. However, the presence of axial load is inevitable and the practical way to conduct a test is to have the minimum of axial load to represent the actual condition.
- With the absence of joint core hoops and poor bond development within the joint core, the typical local non-seismic beam-column joint might not perform well under reversed cyclic loading.
- The detailing of beam-column joints based on seismic design codes such as New Zealand Standard (NZS 3101-2006) and American Concrete Institute Code (ACI 318-08) have been discussed.

- It is generally accepted that the NZS 3101-2006 design code imposes the most stringent requirement on joint shear reinforcement, large amount of both horizontal and vertical reinforcement in the joint core are required.
- ACI code on the other hand, only rely on horizontal reinforcement in the joint core and ignores the existence of the vertical joint shear stress, which was found inadequate to sustain the truss panel mechanism

Chapter 3 Experimental Programme

In the design of earthquake resistant structures, the "strong columns-weak beams" structural system is required to ensure good earthquake energy absorption and energy dissipation in order to avoid collapse of buildings. The beam-column joints have been the most critical elements to ensure the integrity of structures during earthquake attack. Due to the inherent less ductile characteristics of high strength concrete (HSC), a series of test was carried out to study the structural behaviour of HSC beam-column joints under reversed cyclic loadings. This chapter explains the experimental programme of eight (8) HSC beam-column joints under reversed cyclic loadings. The test results of each specimen and the test findings are presented in Chapter 4 and Chapter 5 respectively. Meanwhile, the anchorage length requirement in NSZ3101 [N1, N2] was reassessed through the findings of experimental programme and parametric studies on literatures.

3.1 Experiment Planning

To explore the possibility to relax the design requirement in NZS 3101: 1982 for the use of high strength building material such as high strength reinforcement, Xin [X1] performed a series of test on six beam-column joints. These specimens were made of concrete grade varying from 30.9 MPa to 60.7 MPa and beam reinforcement ranging from 12mm diameter to 28mm diameter. Due to the limitation in experiemental setup in the past, the specimens were tested by assuming zero column axial compressive loading. This is the most critical loading condition in earthquake design and a safe yet conservative conclusion has been drawn by neglecting the possible beneficial confinement effects from column axial compressive loading.

In this study, four specimens of Xin were selected as prototype to cast with high strength concrete grade C60 to study the structural behaviour of HSC beam-column joints. For comparison, these specimens namely X1, X2, X3 and X4 was initially made of normal strength concrete ranging 30.9 MPa to 47.2 MPa. The column

axial compressive load was simulated in the test via flat jacks and post tension steel rods which exerted constant compressive stress on the column. In summary, two sets of identical HSC beam-column joint specimens were cast where each set of specimens consists of four beam-column joints based on the details of X1, X2, X3 and X4. The first set of HSC specimens, namely NS1 (X1), NS2 (X2), NS3 (X3) and NS4 (X4) were fabricated to test with zero column axial compressive loading. On the other hand, another set of HSC specimens comprising AS1 (X1), AS2 (X2), AS3 (X3) and AS4 (X4) were cast to test with the presence column axial compressive loading of $0.3A_c f_c'$.

3.1.1 Test Specimens Details

Figure 3.1 to Figure 3.4 show the configuration of reinforcement in each specimen. The beam dimension was 250 x 500mm and column dimension was 450 x 300mm. The overall beam span was designed to be 4800mm while the column height was fixed at 3275mm. Table 3.1 summarises the reinforcement details of each specimen while Table 3.2 summarises the design limits for all specimens based on the design limits in NZS 3101: 1982 and NZS 3101: 2006 for comparison. With the "strong-columns weak-beams" configuration, the plastic hinges of all specimens were designed to take place at the beam adjacent to the column faces and the column should remain elastic during the test [X1].

Specimens NS1 and NS3 had similar beam tension reinforcement area and beam compression reinforcement area. NS1 was made of 7T12 for top and bottom reinforcement while NS3 was made of bigger bar 4T16. The ratio of total area of bottom beam bars to top beam bar, β of NS1 and NS3 was 1.00. On the other hand, NS2 was made of 4T16 and 2T16 for top and bottom reinforcement with β of 0.50. The last specimen NS4 was made of bigger bar 2T20 as top reinforcement and 2T16 as bottom reinforcement with β of 0.64. For comparison, all the specimens were reevaluated based on design limits of older and newer NSZ3101. As explained in Table 3.2, except for X4 (NS4 / AS4), all specimens met the bond development limit for beam reinforcement in NZS 3101: 2006.

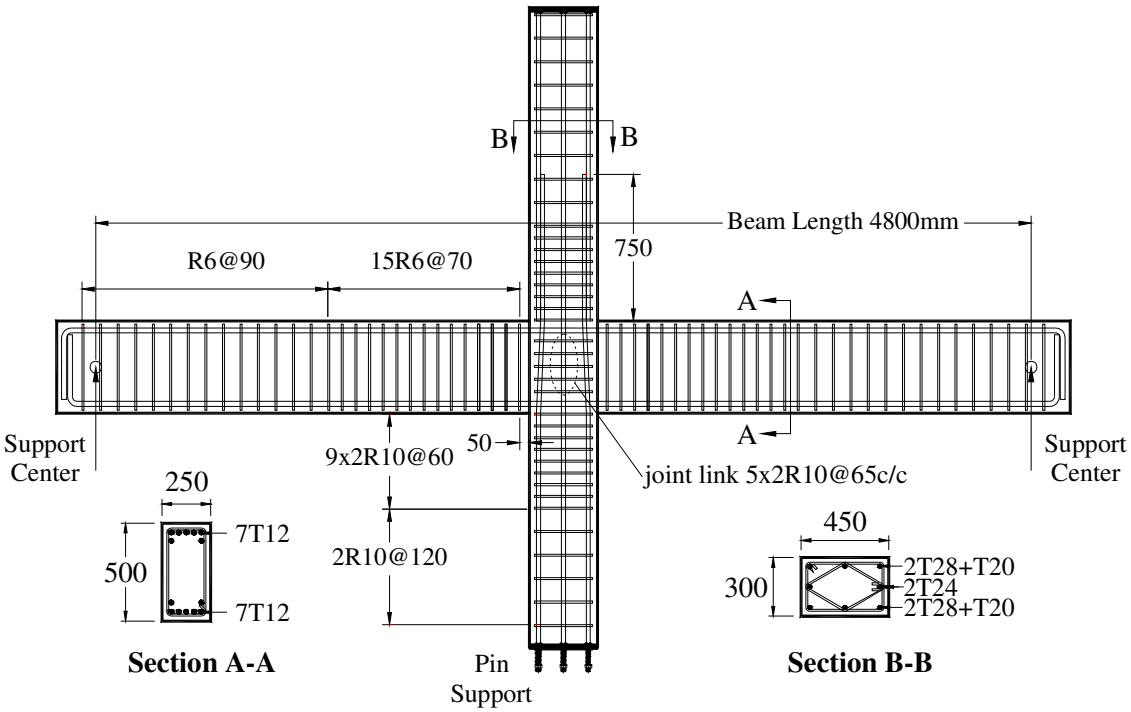

Figure 3.1 Details of Specimens NS1 and AS1

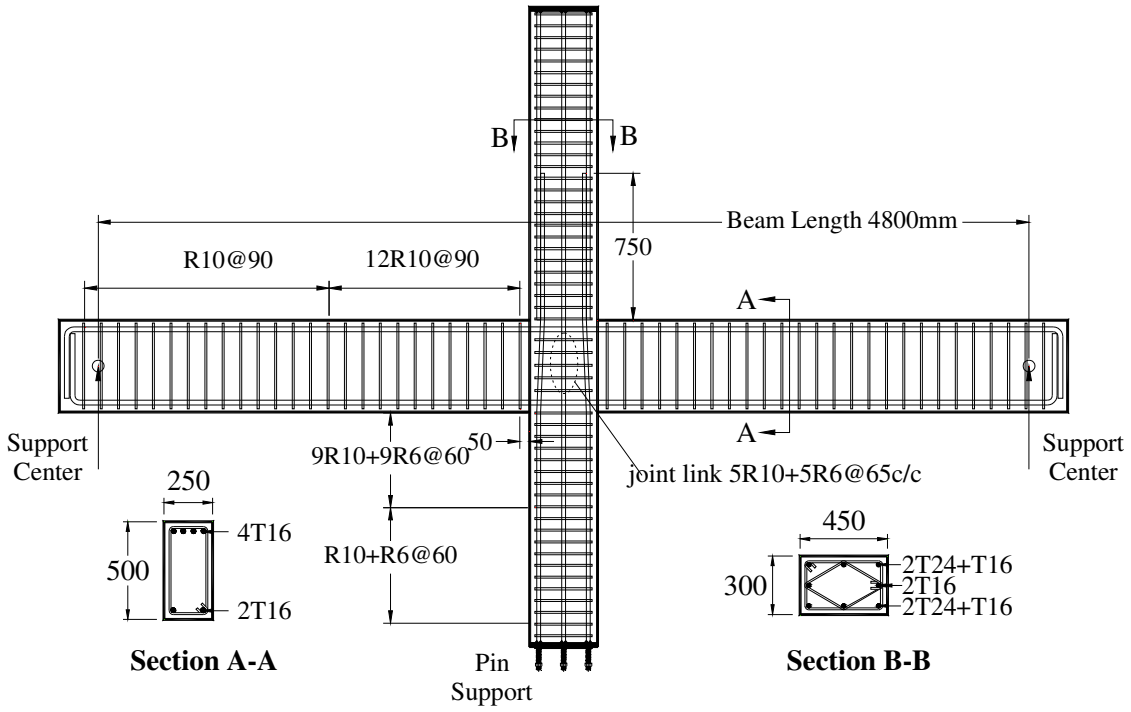

Figure 3.2 Details of Specimens NS2 and AS2

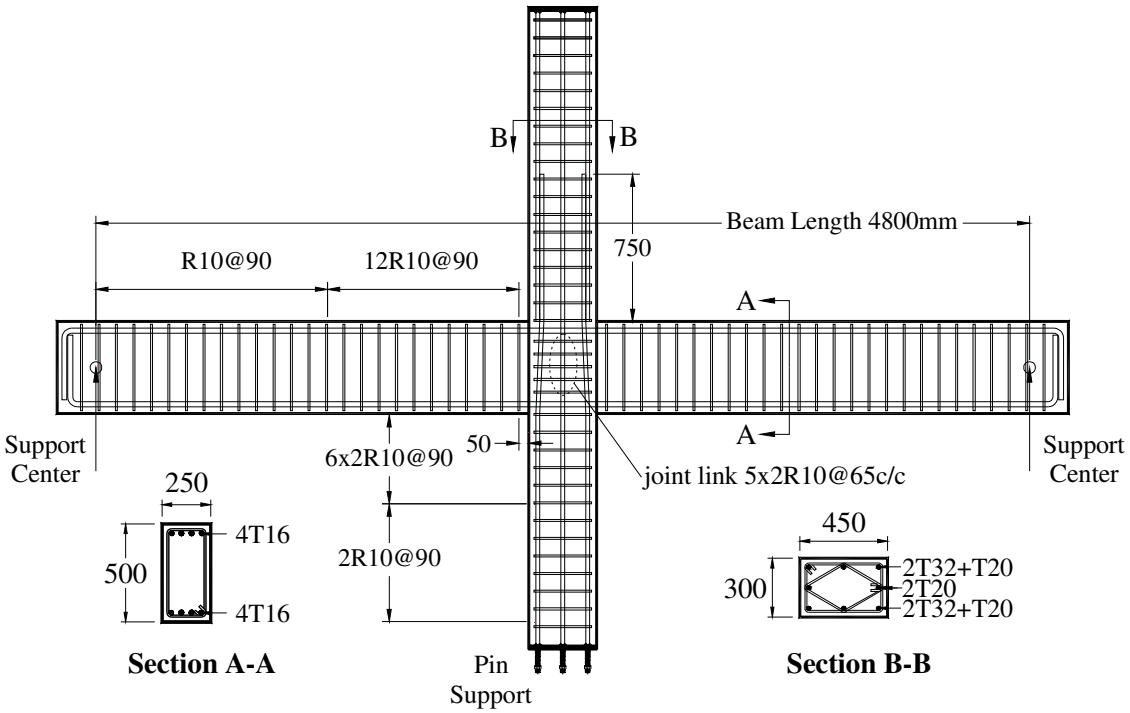

Figure 3.3 Details of Specimens NS3 and AS3

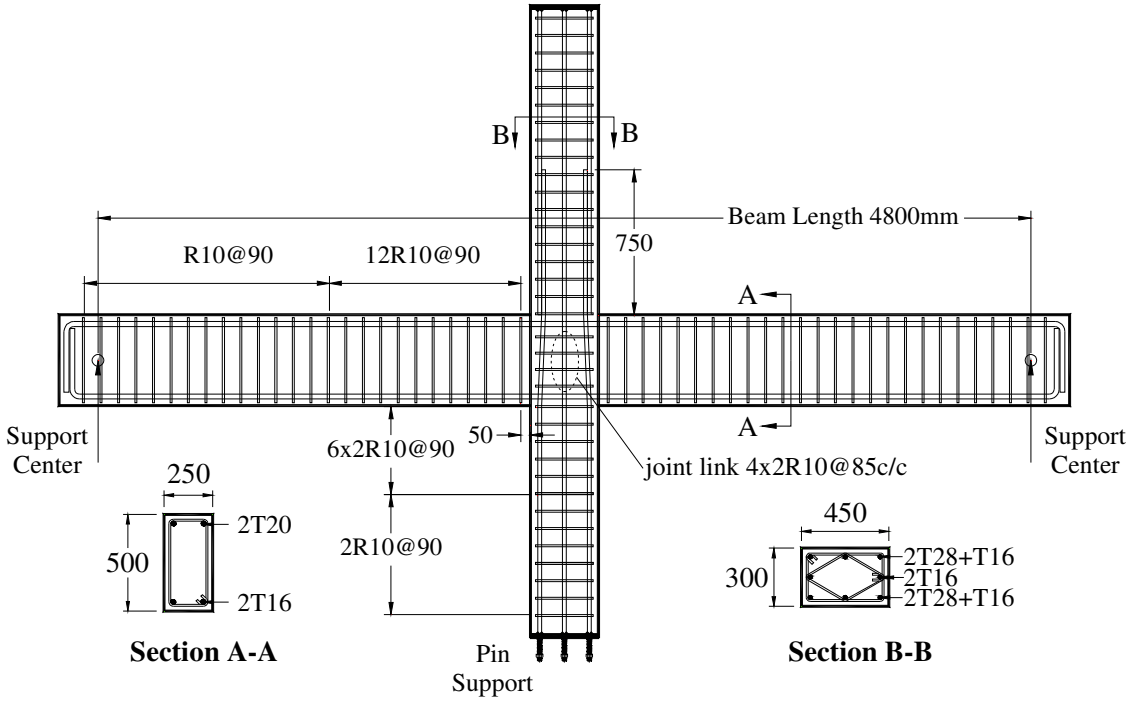

Figure 3.4 Details of Specimens NS4 and AS4

Table 3.1 Summary of Specimens Detail

		NS1 / AS1	NS2 / AS2	NS3 / AS3	NS4 / AS4
Beam	Size	250 x 500			
	Top bar	7T12 (ρ = 0.73%)	4T16 (ρ = 0.71%)	4T16 (ρ = 0.71%)	2T20 (ρ = 0.56%)
	Bottom bar	7T12 (ρ' = 0.73%)	2T16 (ρ' = 0.36%)	4T16 (ρ' = 0.71%)	2T16 (ρ' = 0.36%)
	Stirrups	R6@75 & R6@150	R10@90 & R6@150	R10@90 & R6@150	R10@90 & R6@150
Column	Size	450 x 300			
	Main bar	4T28+2T24+2T20 (ρ_t = 1.40%)	4T24+4T16 (ρ_t = 0.92%)	4T32+4T20 (ρ_t = 1.60%)	4T28+4T16 (ρ_t = 1.29%)
	Hoops	2R10@60 & 2R10@120	(R10+R6)@60 & (R10+R6)@120	2R10@90 & 2R10@120	2R10@90 & 2R10@120
Joint	Hoops	5x2R10@65	(5R10+5R6)@65	5x2R10@65	R10@65

Note: $\rho = A_s / bd$, $\rho' = A_S^{'} / bd$, $\rho_t = A_{sc} / A_c$

where:

ρ = ratio of tension reinforcement (over beam cross-sectional area)

ρ' = ratio of compression reinforcement (over beam cross-sectional area)

ρ_t = ratio of longitudinal reinforcement (over column cross-sectional area)

$A_s^{'}$ = area of longitudinal compression reinforcement of beam

A_s = area of longitudinal tension reinforcement of beam

A_{sc} = total area of longitudinal reinforcement of column

A_c = gross area of column

b = width of beam

d = depth of beam

Table 3.2 Comparison on Design Limits of NSZ3101 1985 & 2006

Specimen X1 (NS1 / AS1)	Actual Details	Limit in NSZ 3101 (1985)	Limit in NSZ 3101 (2006)
Beam Bar	$\frac{d_b}{h_c} = \frac{1}{37.50}$	$\frac{1}{37.75} < \frac{1}{37.50}$ -Not OK	$\frac{1}{30.87} > \frac{1}{37.50}$ -OK
Column Bar	$\frac{d_c}{h_b} = \frac{1}{17.86}$	$\frac{1}{22.65} < \frac{1}{17.86}$ -Not OK	$\frac{1}{20.37} < \frac{1}{17.86}$ -Not OK
Joint Core Bar	65mm c/c spacing	max 100mm c/c spacing > 65mm -OK	max 100mm c/c spacing > 65mm -OK

Specimen X2 (NS2 / AS2)	Actual Details	Limit in NSZ 3101 (1985)	Limit in NSZ 3101 (2006)
Beam Bar	$\frac{d_b}{h_c} = \frac{1}{28.13}$	$\frac{1}{37.08} < \frac{1}{28.13}$ -Not OK	$\frac{1}{26.39} > \frac{1}{28.13}$ -OK
Column Bar	$\frac{d_c}{h_b} = \frac{1}{20.83}$	$\frac{1}{22.25} < \frac{1}{20.83}$ -Not OK	$\frac{1}{17.42} > \frac{1}{20.83}$ -OK
Joint Core Bar	70mm c/c spacing	max 60mm c/c spacing < 65mm -Not OK	max 60mm c/c spacing < 65mm -Not OK

Specimen X3 (NS3 / AS3)	Actual Details	Limit in NSZ 3101 (1985)	Limit in NSZ 3101 (2006)
Beam Bar	$\frac{d_b}{h_c} = \frac{1}{28.13}$	$\frac{1}{37.08} < \frac{1}{28.13}$ -Not OK	$\frac{1}{25.86} > \frac{1}{28.13}$ -OK
Column Bar	$\frac{d_c}{h_b} = \frac{1}{15.63}$	$\frac{1}{22.25} < \frac{1}{15.63}$ -Not OK	$\frac{1}{17.06} < \frac{1}{15.63}$ -Not OK
Joint Core Bar	70mm c/c spacing	max 60mm c/c spacing < 65mm -Not OK	max 60mm c/c spacing < 65mm -Not OK

Specimen X4 (NS4 / AS4)	Actual Details	Limit in NSZ 3101 (1985)	Limit in NSZ 3101 (2006)
Beam Bar	$\frac{d_b}{h_c} = \frac{1}{22.50}$	$\frac{1}{41.00} < \frac{1}{22.50}$ -Not OK	$\frac{1}{27.13} < \frac{1}{22.50}$ -Not OK
Column Bar	$\frac{d_c}{h_b} = \frac{1}{17.86}$	$\frac{1}{24.60} < \frac{1}{17.86}$ -Not OK	$\frac{1}{17.90} < \frac{1}{17.86}$ -Not OK
Joint Core Bar	70mm c/c spacing	max 100mm c/c spacing > 70mm OK	max 100mm c/c spacing > 70mm OK

3.1.2 Test Specimens Fabrication

The specimens were cast in two batches where four specimens NS1 to NS4 were fabricated in first round and followed by four more specimens AS1 to AS4 in batch two. Steel cages were prepared with strain gauge installed for measuring of strain development in test. As shown in Figure 3.5, all the formwork and the moulds were moistened before casting. During casting, compaction was achieved by using a 1-inch poker vibrator to ensure good flow of concrete around the reinforcement. Figure 3.6 depicts the specimens after casting was completed where polythene sheet coverings were used to keep the specimens and all the samples moist. The specimens were demoulded after three days and were left for air curing for at least three weeks before testing.

Figure 3.5 Reinforcement Cage and Formwork of Specimens Prior to Casting

Figure 3.6 Cast Specimens

In order to ascertain the properties of concrete, cylinders of ϕ150 mm x 300 mm (height) were prepared. Strength development of concrete was observed on the 7th and 28th day based on the average strength of three cylinders. Seven types of reinforcement were used and tensile tests were carried out to ascertain the respective yield strength of reinforcement. Material properties of both concrete and steel were recorded in Table 3.3 and Table 3.4 respecitvely.

Table 3.3 Properties of Concrete

$f_c^{'}$ on 7-day (MPa)	43.8
$f_c^{'}$ on 28-day (MPa)	60.2
Average $f_c^{'}$ of 8 specimens (tested on actual test day) (MPa)	61.7

Table 3.4 Properties of Reinforcement

Bar Size	Yield Strain, ε_y	Yield Strength, f_y (MPa)
6	0.001766	362
10	0.001727	354
12	0.002488	510
16	0.002478	508
20	0.002502	513
24	0.002522	517
28	0.002468	506

3.2 Test Setup

A schematic of the loading apparatus is shown in Figure 3.7 where a reversible horizontal load was applied on the column using a double acting 500 kN capacity hydraulic actuator. The column was pinned to a strong floor, and beam ends were connected to the strong floor by steel links. The column axial compressive load was simulated in the test via flat jacks installed at top of column. A displacement transducer with 300mm travel was installed on top of the column to measure the storey horizontal displacement.

To simulate the worst loading arrangment, no axial compressive loading was applied in the test of Specimens NS1 to NS4. On the other hand, constant axial compressive load of magnitude $0.3f_c'A_c$ (approximately 2470kN) was applied on the columns of Specimens AS1 to AS4 throughout the test at top of column prior to the applied cyclic loading. The column axial compressive load was set at $0.3f_c'A_c$ which is the value used in the design code BS8110 [B1].

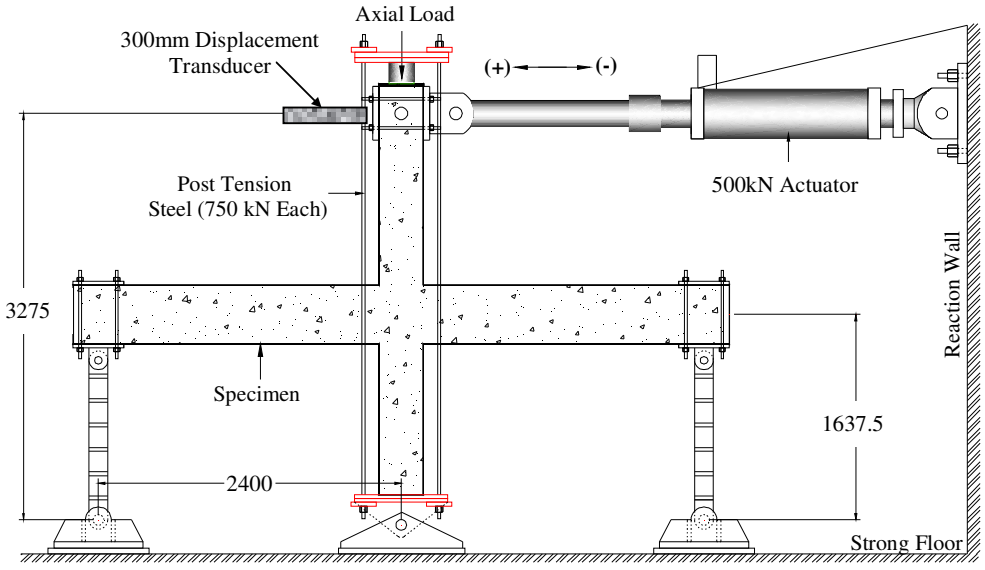

Figure 3.7 Schematic Test Setup

3.3 Loading Arrangement

All test specimens were subjected to cyclic quasi-static loading, as shown in Figure 3.8. During the period of the test, a series of lateral displacements were imposed corresponding to a drift ratio from 0.5% up to 4.0%. The lateral loads were applied in terms of a drift controlled rather than ductility controlled manner which has been used for many years by other researchers [H2] as a significant gap between the measured yield displacement and the predicated value in the later test method [T11]. This might be due to the overestimation of the specimen's capacity as the early damage and incidence of bond slip were overlooked.

The test specimens were subjected to two cycles of loading with displacement equivalent to storey drift ratio (DR) of 0.5%, 1%, 1.5%, 2%, 2.5%, 3%, 3.5% and 4%. The drift ratio (DR) is defined as Δ/h, where Δ as the inter-storey horizontal displacement of the test specimen and h as the storey height or vertical distance between the column end pins (=3275 mm). The test was ended when the second load cycle of DR 4% was completed.

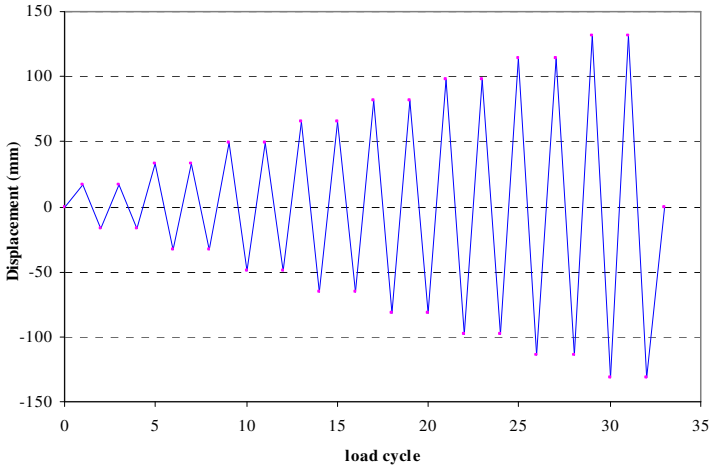

Figure 3.8 Cyclic Loading and Displacement History

3.4 Instrumentation

In order to obtain the test results that explained most of the observation qualitatively, instrumentations such as dynamic actuator, strain gauges, and

displacement transducers were installed in the test setup. The specimens were loaded horizontally using dynamic actuator where the load applied was recorded in the data acquisition system of the actuator. For the joint core area, beam and column, displacement transducers were installed to observe their respective response in test. The behaviour of reinforcement bars in terms of stress level was observed by installing strain gauges in the bars before casting of specimens took place.

3.4.1 Observation of Cracking Development

All cracks observed in each test specimen were marked on the white painted concrete surfaces. In order to capture the development of the cracking, photographs were taken at the peak of each loading cycle and other relevant stages. The crack width in the joint and critical regions of the test specimens was measured by using a crack magnifier with a 0.02 mm division at the peak of each loading cycle.

3.4.2 Measurement of Applied Load

A 500 kN capacity double acting dynamic actuator with built-in load cells was used to measure the horizontal load or storey shear force applied to the specimens (see Figure 3.7). Two full-bridge circuits were installed in the load cell. One circuit was connected to an X-Y recorder to monitor the applied horizontal load during the test. The other circuit was connected to data logger unit to observe and record the applied load.

3.4.3 Measurement of Horizontal Displacement

External deformation of the specimens can be monitored by measuring the displacement. The arrangement of transducers for measuring the displacement was identical for all specimens as shown in Figure 3.9. Two types of displacement transducers of 300mm and 100mm travel distance were used to measure the different displacements. In order to estimate the horizontal displacement at the top column end-pin, one displacement transducer with 300 mm travel was used. Due to the maximum measureable displacement of 150mm in both push and pull cycles,

the test was ended at DR 4%. The horizontal displacement measured at the top face of the column (shown in Figure 3.7) was connected to the X-Y recorder to obtain the applied horizontal displacement. This assisted in controlling the imposed horizontal loading during the displacement controlled cycles.

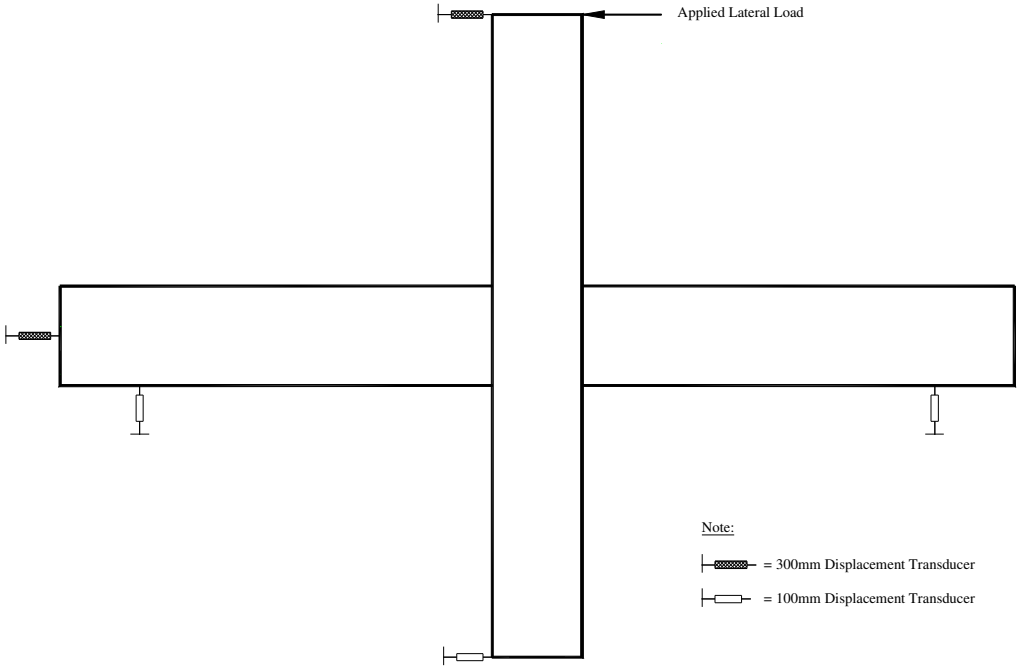

Figure 3.9 Displacement Transducers for Displacement Measurement

To measure rigid body movement, one displacement transducer with 300 mm travel distance was placed at a further end of the beam. Two transducers with a distance capacity being of 100 mm were placed vertically on the bottom of the beams to measure vertical displacement. The positions of this measurement were determined in which the maximum vertical displacement on the beams was expected. One more transducer with a distance capacity of 100 mm was used to measure the lateral displacement on the level of the bottom end of the column

3.4.4 Measurement of Rotation of Beam and Column

The typical location of 50mm displacement transducers installed to monitor the rotation of beam and column is illustared in Figure 3.10. These displacement

transducers were mounted on steel brackets screwed into 10 mm steel rods embedded in the concrete.

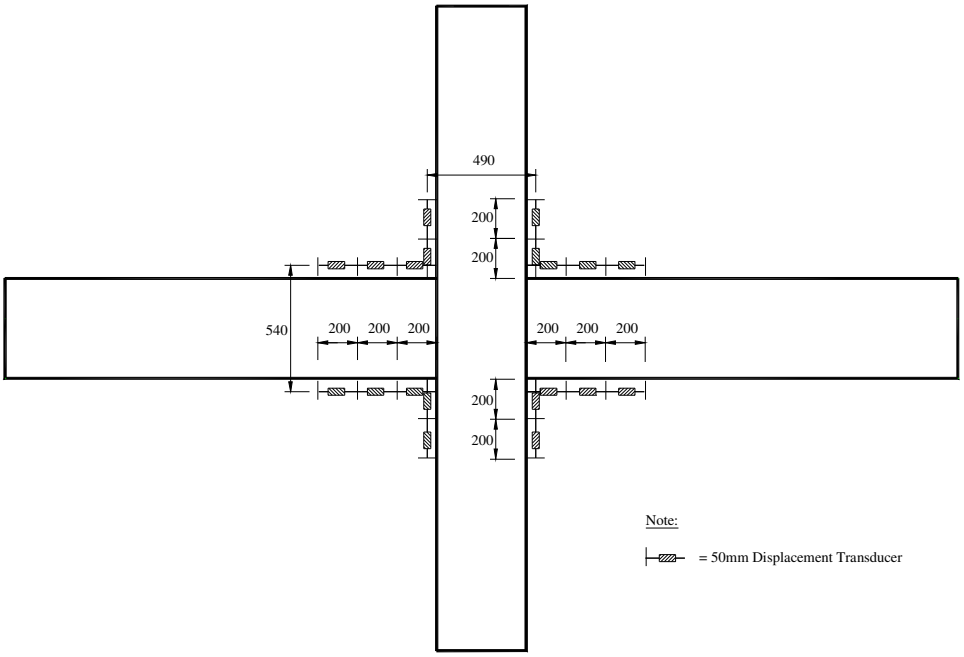

Figure 3.10 Displacement Transducers for Rotation Measurement

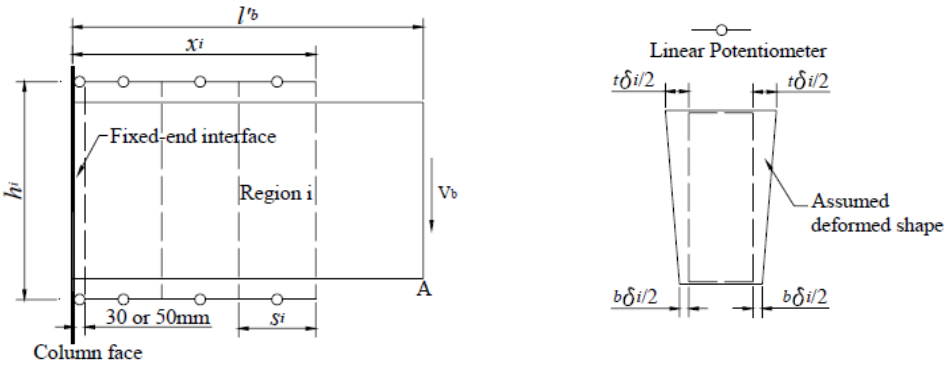

Figure 3.11 Estimation of Rotation of Beam [H2]

Figure 3.11 shows the typical procedures to measure the rotation at beam end "A" over a region in a beam by using a pair of potentiometer / transducers [H2]. In general, the beam rotations namely fixed end rotation and flexural rotation were

obtained by measuring the difference in displacement of top and bottom transducers in respective to the vertical distance of these transducers.

The beam fixed end rotation $\theta_{b,fe}$ is derived as below:

$$\theta_{b,fe} = \frac{{}_t\delta_1 - {}_b\delta_1}{h_1} \tag{3.1}$$

where:

${}_t\delta_1$ = top displacements measured over the 1st region in the beam

${}_b\delta_1$ = bottom displacements measured over the 1st region in the beam

h_1: = distance between top and bottom transducers in the 1st region in the beam

The beam flexural rotation at a particular region $\theta_{b,i}$ is estimated as below:

$$\theta_{b,i} = \frac{{}_t\delta_i - {}_b\delta_i}{h_i} \tag{3.2}$$

where:

${}_t\delta_i$ = top displacements measured over the region i in the beam

${}_b\delta_i$ = bottom displacements measured over the region i in the beam

h_i: = distance between top and bottom transducers in the region i

Similarly, the column rotations due to fixed end rotation $\theta_{c,fe}$ and due to flexure $\theta_{c,i}$ are explained as below by measuring the difference in displacement of left and right transducers in respective to the horizontal distance of these transducers:

$$\theta_{c,fe} = \frac{{}_r\delta_1 - {}_l\delta_1}{h_1'} \tag{3.3}$$

where:

${}_r\delta_1$ = right displacements measured over the 1st region in the column

${}_l\delta_1$ = left displacements measured over the 1st region in the column

h_i' = distance between left and right transducers in the 1st region in the column

$$\theta_{c,i} = \frac{{}_r\delta_i - {}_l\delta_i}{h_i'} \tag{3.4}$$

where:

$_r\delta_i$ = right displacements measured over the region *i* in the column

$_l\delta_i$ = left displacements measured over the region *i* in the column

$h_i^{'}$ = distance between left and right transducers in the region *i*

3.4.5 Measurement of Curvature of Beam and Column

From the estimatation of rotations of beams and columns in Section 3.4.4, the curvatures of the respective beams $\phi_{b,i}$ and columns $\phi_{c,i}$ are obtained as below:

$$\phi_{b,i} = \frac{\theta_{b,i}}{s_i} \tag{3.5}$$

where:

$\theta_{b,i}$ = rotation measured over the region *i* in the beam (From Section 3.4.4)

s_i = gauge length of the region *i* in the beam

$$\phi_{c,i} = \frac{\theta_{c,i}}{s_i^{'}} \tag{3.6}$$

where:

$\theta_{c,i}$ = rotation measured over the region *i* in the column (From Section 3.4.4)

$s_i^{'}$ = gauge length of the region *i* in the column

3.4.6 Measurement of Shear Strains of Joints and Joint Expension

The measurements from the transducers placed diagonally on the joint enabled the average shear strains to be estimated. Joint core expansion was also estimated from the diagonal measurements by the average value of the diagonal displacements. The locations of transducers installed and the calculation of joint shear strain γ_j is explained in Figure 3.12:

$$\gamma_j = \gamma_1 + \gamma_2 = \frac{\delta_j - \delta_j^{'}}{2l_j}(\tan\alpha_j + \frac{1}{\tan\alpha_j}) \tag{3.7}$$

where:

δ_j and $\delta_j^{'}$ = changes in the lengths of the diagonals

l_j = initial length of the diagonal in the joint core

α_j = angle of the diagonal to the horizontal.

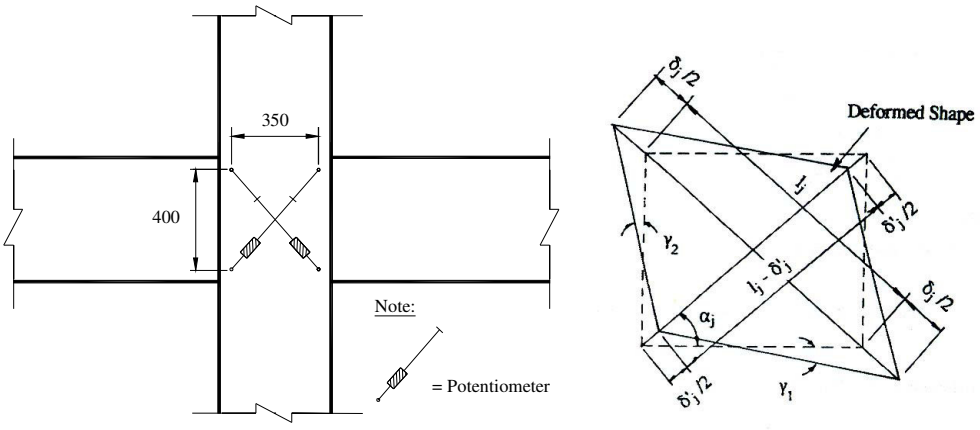

Figure 3.12 Measurement of Joint Shear Distortion [H2]

In this study, joint expansion was defined as the average value of the diagonal displacements i.e. $(\delta_j + \delta_j^{'}) / 2$. The joint expansion so obtained was proportional to the increase in the volume of the joint core concrete. Therefore, the joint expansion can be used as an index to gauge the failure of the joint core concrete.

3.4.7 Measurement of Strains in Reinforcing Bars

The local strains in the reinforcing bars in the beams, columns and joint were measured using electric resistance wire strain gauges (TML FLA-5-11-5LT). The locations of the gauges in each specimen are shown in Figure 3.13. Strain gauges were placed on both the longitudinal and transverse reinforcement at selected locations within and around the concrete beam-column joints. Wires were attached to each strain gauge. To ensure that the concrete-rebar bond was unaltered, these wires were gathered into bundles and run along the center of the reinforcing cage in the beam or column to the closest end where the wires exited the test unit. Precautions were taken to protect the strain gages during the casting process.

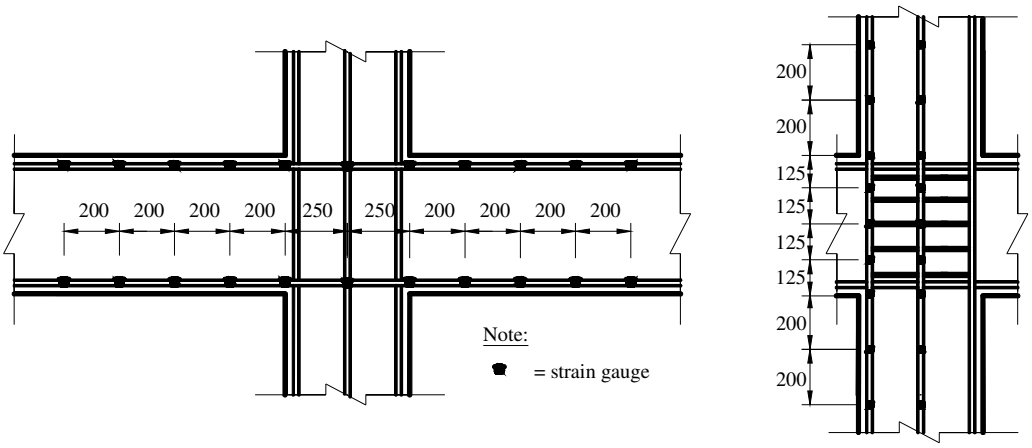

a. Beam **b. Column and Joint Core**

Figure 3.13 Strain Gauge Position of Specimen

3.5 Components of Horizontal Displacement

The horizontal displacements of the test specimens defined in Section 3.4.3 are composed of various deformation contributions from the beams, columns and joints. The measurements mentioned in Section 3.4 enabled the estimation of the different sources of the horizontal displacement to be made. The procedures to estimate those sources of the horizontal displacement are described below.

3.5.1 Displacement Due to Beam Deformations

Two components in beam deformations, namely beam fixed end deformation $\delta_{b,fe}$ and beam flexural deformation $\delta_{b,f}$ contribute to the total horizontal displacement. These beam deformations were then transformed into the respective horizontal displacement through the ratio of column height-to-beam span.

a. Beam Fixed End Deformation and Displacement

The tensile strains or the slippage of the longitudinal bars anchored in the joint core causes the fixed-end rotation of the members adjacent to the joint. The estimation of beam fixed-end rotation was monitored by a pair of transducers located next to

the column faces as explained in Figure 3.11. The beam fixed-end deformation $\delta_{b,fe}$ can be obtained as:

$$\delta_{b,fe} = \theta_{b,fe}\, l_b^{'} \tag{3.8}$$

where:

$\theta_{b,fe}$ = beam fixed-end rotation as defined in Eq. 3.1

$l_b^{'}$ = distance from the column face to the center of the beam end pin

The horizontal displacement at the column top due to beam fixed-end rotation $\Delta_{b,fe}$ can be calculated based on fixed-end deformations of beams $\delta_{b,fe}$ where:

$$\Delta_{b,fe} = \delta_{b,fe}\, \frac{h}{l} \tag{3.9}$$

where:

$\delta_{b,fe}$ = fixed end deformations of the beams as defined in Eq. 3.8

h = storey height or vertical distance between the column end pins (= 3235 mm)

l = beam span or horizontal distance between the beam end pins (= 4800 mm)

b. Beam Flexural Deformations and Displacement

Flexural deformations of the beams $\delta_{b,f}$ were obtained from the flexural rotation of each region in the beam $\theta_{b,i}$ as defined in Section 3.4.5. As shown in Figure 3.11, the flexural deformation of the beam can be derived as follows:

$$\delta_{b,f} = \sum (\theta_{b,i})(l_b^{'} - x_i) \tag{3.10}$$

where:

$\theta_{b,i}$ = beam flexural rotation of the region i as defined in Eq. 3.2

$l_b^{'}$ = distance from the column face to the center of the beam end pin

x_i = distance from the column faces to the center

The horizontal displacement at the column top due to the beam flexural displacement $\Delta_{b,f}$ is estimated based on flexural deformations of beams $\delta_{b,f}$ where:

$$\Delta_{b,f} = \delta_{b,f}\, \frac{h}{l} \tag{3.11}$$

where:

$\delta_{b,f}$ = flexural deformations of the beams as defined in Eq. 3.10

h = storey height or vertical distance between the column end pins(= 3275 mm)

l: = beam span or horizontal distance between the beam end pins (= 4800 mm)

3.5.2 Displacement Due to Column Deformations

Column deformation consist of two components, namely column fixed end deformation $\delta_{c,fe}$ and column flexural deformation $\delta_{c,f}$ contribute to the total horizontal displacement. These column deformations were directly taken as their respective column displacement ($\delta_{c,fe} = \Delta_{c,fe}$ and $\delta_{c,f} = \Delta_{c,f}$).

a. Column Fixed-End Rotation and Displacement

The component of horizontal displacement due to fixed-end rotation of the column, $\Delta_{c,fe}$ can be obtained by using the same way used for the beam in Section 3.5.1 by obtaining the column fixed end deformations $\delta_{c,fe}$ where:

$$\Delta_{c,fe} = \delta_{c,fe} = \theta_{c,fe}\, l_c' \tag{3.12}$$

where:

$\theta_{c,fe}$ = column fixed-end rotation as defined in Eq. 3.3

l_c' = distance from the beam face to the center of the column end pin

b. Column Flexural Deformations and Displacement

The column flexural deformation component $\Delta_{c,f}$ of the horizontal displacement, can be obtained by the same way mentioned in Section 3.5.1 by obtaining the column flexural deformations $\delta_{c,f}$ where:

$$\Delta_{c,f} = \delta_{c,f} = \sum(\theta_{c,i})(l_c' - y_i) \tag{3.13}$$

where:

$\theta_{c,i}$ = column flexural rotation as defined in Eq. 3.4

l_c' = distance from the beam face to the column end pin

y_i = distance from the beam faces to the center of the region i

3.5.3 Displacement Due to Joint

The average shear distortion in the joint core has been defined in Section 3.4.6. The joint shear distortion contributes towards the horizontal displacement of the specimen as explained in Figure 3.14 with the deformed shape of the test specimen due to joint shear distortion when the beam and column ends are not supported. When considering the support conditions of the loading systems used in this study, the horizontal displacement due to joint shear distortion Δ_j can be derived as follows:

$$\Delta_j = \gamma_j (h - h_b - \frac{h}{l} h_c) \tag{3.14}$$

where:

γ_j = joint shear distortion defined in Section 3.4.6

h = storey height or vertical distance between the column end (= 3275 mm)

l = beam span or horizontal distance between the beam end pins (= 4800 mm)

h_b = depth of beam

h_c = overall depth of column

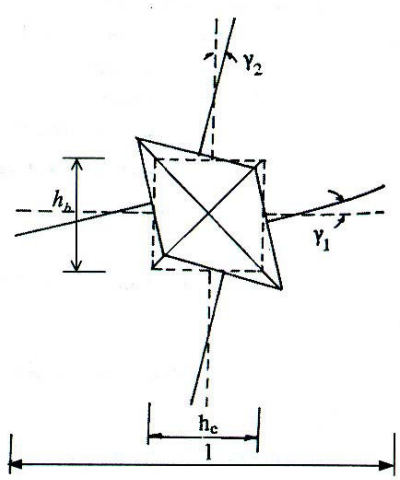

Figure 3.14 Measurement of Horizontal Displacement Due to Joint [H2]

3.6 Theoretical Yield Displacements & Initial Stiffness

The theoretical yield displacements $\Delta_{y,th}$ and the theoretical initial stiffness K_{th} of all test specimens were calculated and this section explains the methods to estimate

these values. In the estimation of $\Delta_{y,th}$ and K_{th}, it was assumed that the theoretical flexural strength M_{th} was reached simultaneously at the critical sections of the members when the theoretical ideal load strength P_{th} of the specimen developed.

The theoretical initial stiffness K_{th} is estimated as:

$$K_{th} = \frac{P_{th}}{\Delta_{y,th}} \tag{3.15}$$

The theoretical yield displacement $\Delta_{y,th}$ consists of theoretical displacement contribution of beam $\Delta_{b,th}$, column $\Delta_{c,th}$ and joint $\Delta_{j,th}$ where:

$$\Delta_{y,th} = \Delta_{b,th} + \Delta_{c,th} + \Delta_{j,th} \tag{3.16}$$

The theoretical displacement contribution of beam $\Delta_{b,th}$ and column $\Delta_{c,th}$ is closely related to the theoretical elastic deformation contributions of beams and columns:

$$\Delta_{b,th} = \frac{h}{l}\delta_{b,th} \tag{3.17}$$

$$\Delta_{c,th} = \delta_{c,th} \tag{3.18}$$

where:

$\delta_{b,th}$ = theoretical elastic deformation of beam

$\delta_{c,th}$ = theoretical elastic deformation of column

h = storey height (= 3275 mm)

l = beam span (= 4800 mm)

The theoretical elastic deformations of the beams $\delta_{b,th}$ and columns $\delta_{c,th}$ during the development of theoretical ideal load strength P_{th} of the specimen were estimated as following:

For beam: $\delta_{b'th} = \delta_{b,f,th} + \delta_{b,s.th}$

$$\delta_{b,th} = \frac{V_b l_b'^3}{3E_c I_e} + \frac{V_b f l_b'}{0.2E_c b h_b} \tag{3.19}$$

where:

$\delta_{b,f,th}$ = theoretical flexural deformation of beam

$\delta_{b,s,th}$ = theoretical shear deformation of beam

V_b = beam shear force at developing the ideal horizontal load strength of specimen

$l_b^{'}$ = distance from the column face to the center of the beam end pin

f = shape factor (taken as 1.2)

E_c = modulus of elasticity of concrete, $4700\sqrt{f_c^{'}}$ MPa

I_e = effective moments of inertia

b = width of beam

h_b = depth of beam

For column: $\delta_{c,th} = \delta_{c,f,th} + \delta_{c,s,th}$

$$\delta_{c,th} = \frac{V_c l_c^{'3}}{3E_c I_e} + \frac{V_c f l_c^{'}}{0.2E_c b_c h_c} \tag{3.20}$$

where:

$\delta_{c,f,th}$ = theoretical flexural deformation of column

$\delta_{c,s,th}$ = theoretical shear deformation of column

V_c = column shear force at developing the ideal horizontal load strength of specimen

$l_c^{'}$ = distance from the beam face to the center of the column end pin

f = shape factor (taken as 1.2)

E_c = modulus of elasticity of concrete, $4700\sqrt{f_c^{'}}$ MPa

I_e = effective moments of inertia

b_c = width of column

h_c = depth of column

In this study the effective moment of inertia I_e was assumed to be half of the moment of inertia based on uncracked gross concrete area I_g :

$$I_e = 0.5I_g \tag{3.21}$$

Due to the complexity of stress in joint, the theoretical deformation due to joint shear distortion was assumed to contribute to the total theoretical horizontal displacement by 20% [C3] where:

$$\Delta_{j,th} = 0.2\Delta_{y,th} \tag{3.22}$$

Based on the assumption made in Eq. 3.22, Eq. 3.16 can be rewriten and simplied as:

$$\Delta_{y,th} = \Delta_{b,th} + \Delta_{c,th} + 0.2\Delta_{y,th}$$

$$\Delta_{y,th} = \frac{\left(\Delta_{b,th} + \Delta_{c,th}\right)}{0.8} \tag{3.16a}$$

3.7 Conclusions

- The experimental programme of eight (8) HSC beam-column joints under reversed cyclic loadings was discussed. Two sets of identical HSC beam-column joint specimens were cast where each set of specimens consists of four beam-column joints based on the details of four specimen by Xin [X1].
- The first set of HSC specimens, namely NS1, NS2, NS3 and NS4 were fabricated to test with zero column axial compressive loading. Another set of HSC specimens comprising AS1, AS2, AS3 and AS4 were cast to test with the presence column axial compressive loading of $0.3A_c f_c'$.
- Based on the NZS 3101: 2006 design limits checking, except for NS4 and AS4, all specimens met the bond development limit for beam reinforcement in NZS 3101: 2006.
- The test set-up with loading arrangement and the measurement of test data was introduced. The test result of each specimen and the test findings are presented in Chapter 4 and Chapter 5 respectively.

Chapter 4 Experimental Results

This chapter gives a comprehensive presentation of the test results for each specimen so as to reflect the behaviour of each joint under reversed cyclic loading. For the ease comparison, the specimens were divided into four groups according to their reinforcement details in the following arrangement:

Group One: NS1 and AS1
Group Two: NS2 and AS2
Group Three: NS3 and AS3
Group Four: NS4 and AS4

The test results were obtained from the readings measured by the strain gauges and the displacement transducers attached on each specimen. The recorded data were converted into the relevant information based on formulae described in Chapter 3. Pictorial results in the graphs and photographs are presented in this chapter to give a clearer interpretation and to better understanding of the test results. The general behaviour of each specimen is identified, essentially based on the observed crack patterns, the measured load-displacement responses and the decomposition of lateral displacements. The behaviour exhibited by each individual component, namely beam, column and joint core is also described separately. The discussion of test results comparison is presented in Chapter 5 to give an insight view of the structural behaviour of high strength concrete beam-column joints.

4.1 Test Result of Group One (NS1 and AS1)

Group one consists of specimens NS1 and AS1 with same dimension and reinforcement details as described in Chapter 3. NS1 was a high strength beam-column joint tested without column axial compressive loading while its counterpart AS1 was tested with column axial compressive loading of $0.3f_c'A_c$.

The typical features of these specimens are summarised as follows:

- smallest beam reinforcement size in top and bottom reinforcement bar (12mm diameter)
- actual maximum beam-bar-to-column-depth = 1/37.5

- actual column-bar-to-beam-depth = 1/17.86
- calculated maximum beam-bar-to-column-depth based on Eq. 7-13 in NZS 3101 :

  NS1 = 1/24.92 AS1= = 1/24.65
- calculated maximum column-bar-to-beam-depth based on clause 7.5.3.4 in NZS 3101:

  NS1 = 1/16.45 AS1= = 1/16.27
- NS1 and AS1 met both the requirement of maximum beam-bar-to-column-depth and maximum column-bar-to-beam-depth set in NZS 3101
- Joint core reinforcement detailing complied with the requirement in clause 7.5.3.4 in NZS 3101 (maximum bar spacing = 65mm, allowable bar spacing = 100mm)

The following sections report the test result of specimens NS1 and AS1

4.1.1 Specimen NS1

In general, specimen NS1 showed a stable energy dissipation capacity with cracks developed all over the specimens and behaved in a ductile manner. The cracks on column were less severe and the column remained elastic. The energy dissipation capacity was good and consistent throughout the test.

4.1.1.1 General Observation

Specimen NS1 was a typical strong column-weak beam which met the bond development limits in NZS 3101. The final crack pattern of NS1 is depicted in Figure 4.1 where NS1 behaved in a ductile manner throughout the test with good energy dissipation capacity. Flexural cracks were observed on the beams top and beam bottom with limited cracks at the column as shown in Figure 4.1. Cracks at joint core spanned across diagonal corners of the joint panel. Bottom reinforcement and top reinforcement yielded at the end of test and column reinforcement remained in elastic range. The energy dissipation capacity was good and consistent throughout the test.

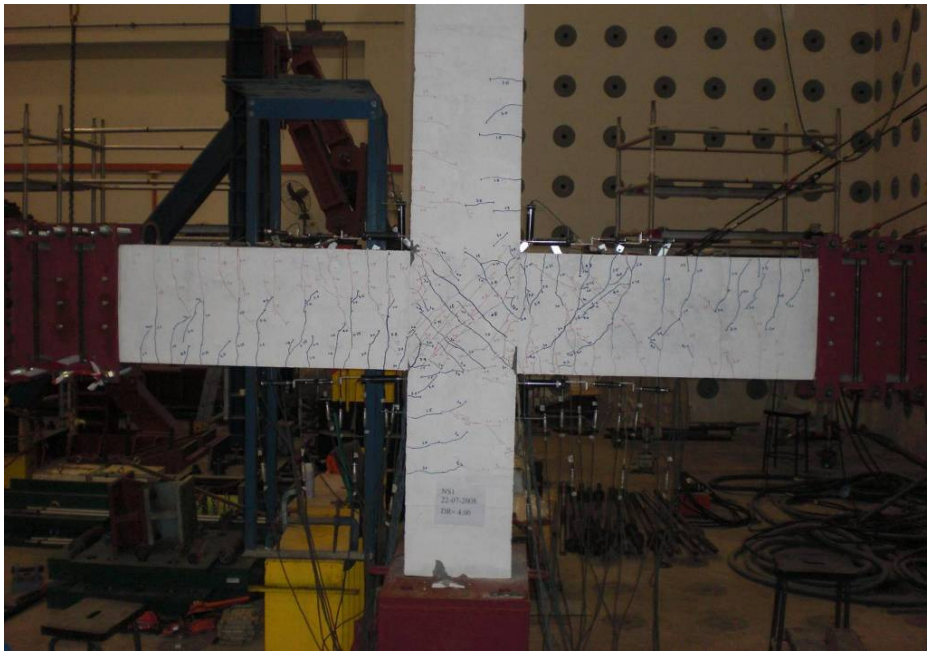

Figure 4.1 Final Crack Pattern of NS1

The crack development of NS1 is illustrated by a series of photographs taken at the peak of storey drift ratio of 1.0% (DR 1%), 2.0% (DR 2%), 3.0% (DR 3%) and 4.0% (DR 4%), as shown in Figure 4.2. It is noticed that the flexural cracks caused by sagging and hogging moment initiated at top and bottom surface of beams when DR 1% was surpassed. Several diagonal cracks were formed at joint core area which initiated the formation of compression strut of the joint core. When DR 2% was attained, cracks were found at column of specimen. More flexural cracks were observed at beam while the formation of compressive strut at joint core was significant with more diagonal shear cracks formed and intersected. Flexural cracks formation was persist till DR 3% where cracks at beam begun to turn inwards to joint core to form shear cracks. Cracks development at column stopped after DR 3%. At DR 4% more shear cracks were found at joint core accompanied with some minor spalling of concrete at joint core. The major cracks at beam were mainly flexural and shear cracks at the end of the test. No major beam bond failure was observed in the end of the test and no joint core failure was observed.

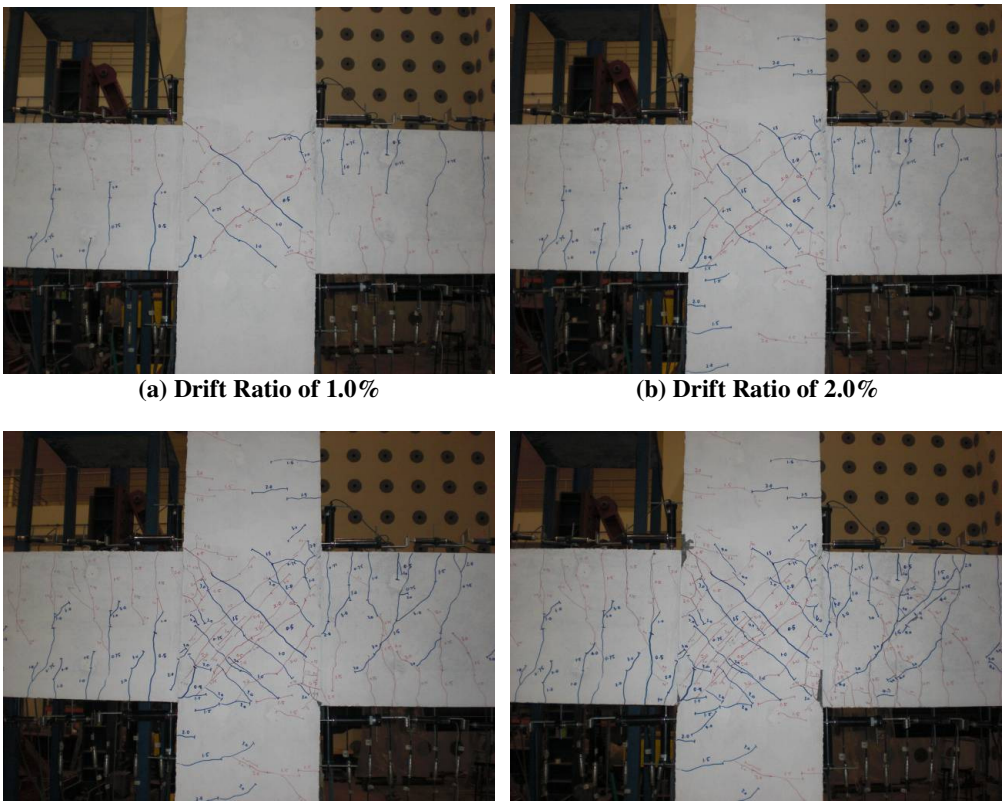

(a) Drift Ratio of 1.0% **(b) Drift Ratio of 2.0%**

(c) Drift Ratio of 3.0% **(d) Drift Ratio of 4.0%**

Figure 4.2 Progressive Cracking Development of NS1

4.1.1.2 Hysteretic Behaviour

The measured horizontal storey shear versus horizontal displacement hysteresis loops is shown in Figure 4.3. In addition, the theoretical ideal storey horizontal load strength P_i when the beam plastic hinges were developed and the theoretical stiffness K based on the assumptions mentioned in Chapter 3 are also shown in Figure 4.3. For specimen NS1, the stiffness and strength increased as the load was applied from beginning until DR 4%. The strength of specimen was maintained at the maximum when the test was halt. Although yielding of beam bars took place in the test, the load remained stable in the test. Pinching was not observed even though cracks were formed in the beams explaining the good energy dissipation of the specimen.

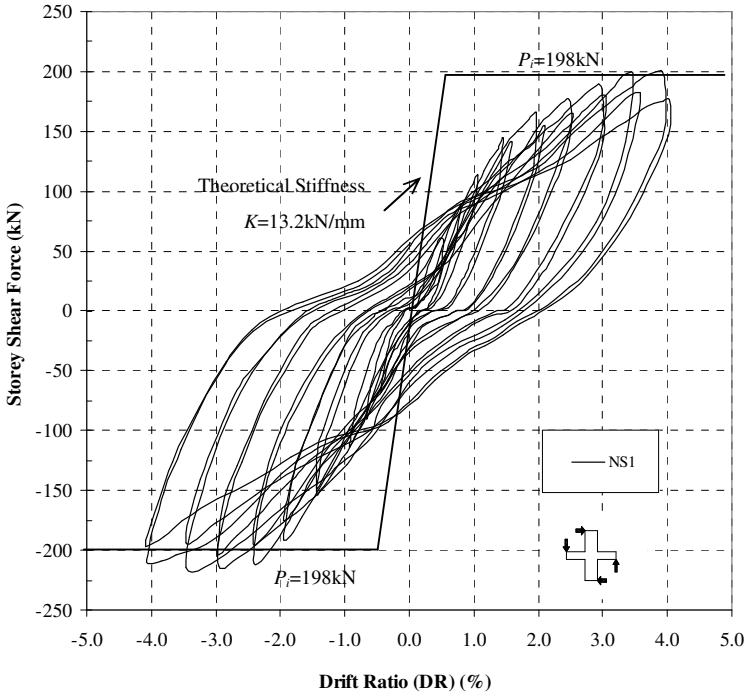

Figure 4.3 Storey Shear Force versus Horizontal Displacement for NS1

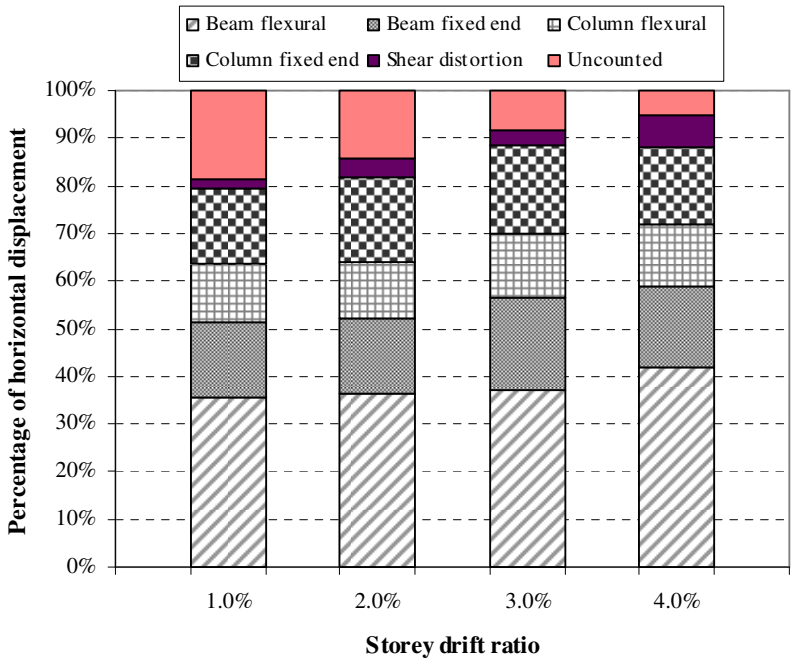

.

Figure 4.4 Decomposition of Horizontal Components of NS1

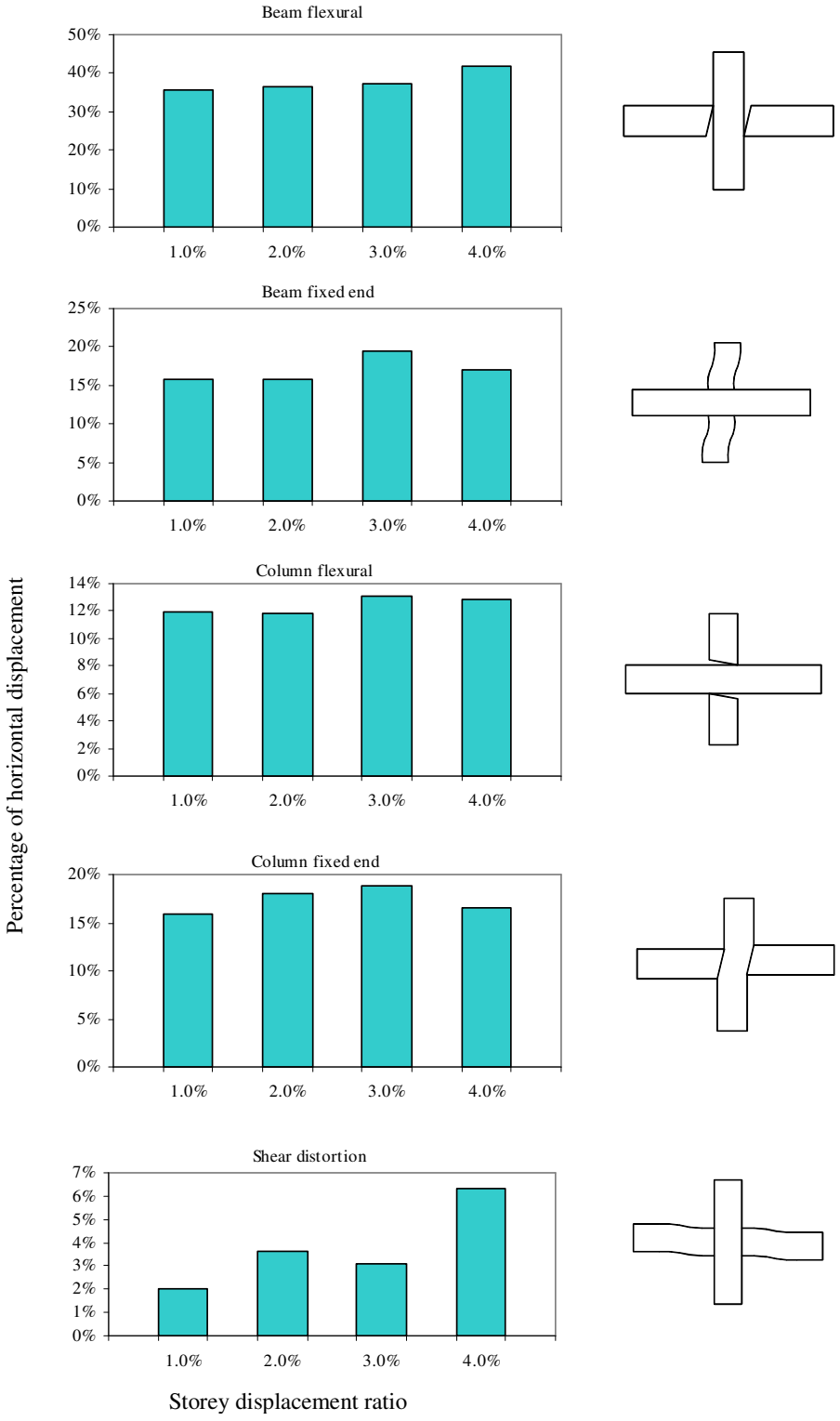

Figure 4.5 Contributions of Horizontal Components of NS1

4.1.1.3 Decomposition of Horizontal Displacement

Figure 4.4 shows the components of the horizontal displacement measured for NS1 at the peak of the selected loading cycles, expressed as a percentage of the horizontal displacement. The definition of each displacement was explained in Chapter 3. The contributions of each components of the horizontal displacement measured for NS1 are explained in Figure 4.5**.** The major source of the storey drift was the beam displacement, indicating a "strong-column-weak-beam" response. The contributions of beam flexure and fixed-end rotation were ranging from 36% to 42% and 16% to 19%, respectively. The contribution to the total drift of column flexure and column fixed-end rotation did not change significantly during the testing. The maximum contributions of column flexure and fixed-end rotation were 13% and 18% respectively. The contribution of the displacement due to joint shear distortion increased gradually in the test while the contribution of uncounted component such as rigid body movement was significant in the early stage of test and eventually reduced in the end of test

4.1.1.4 Beam Behaviour

The evaluation of strains in beam reinforcement and beam curvatures are discussed in the following sections. The strain profiles and curvatures at DR 1% push/pull and DR 3% push/pull cycles are selected to represent the early loading stage and late loading stage.

Beam Reinforcement Strains

The strain profiles of the top and bottom beam reinforcement of NS1 are explained in Figure 4.6. As explained in Figure 4.6, top beam reinforcement and bottom reinforcement of specimen NS1 showed a steady increase in its strain gauge readings when DR 3% was attained where the strain measured near to the column face surpassed the yield strain and penetrated through a certain distance into the joint core. On the other hand, the strain measured however dropped below the yield strain for gauges installed at the middle of the joint core. The bond condition of both top and bottom reinforcement in joint core was good where strain gauges of

beam reinforcement showed significant readings when a positive load cycle was applied and these readings dropped sharply when the load cycle was reversed. Yielding was found in reinforcement demonstrating that stress was sustained by the reinforcement and plastic hinges formed in the beam in the vicinity of the column face. The general behaviour of "strong-column-weak-beam" combinations with the formation of plastic hinges at beams was observed.

Beam curvature

Figure 4.7 shows the beam curvature distributions estimated from the transducer readings. The theoretical yield curvatures of 0.0078 (1/m) for the beam positive moment and 0.0082 (1/m) for the beam negative moment calculated from section analysis are also shown in this figure. With the positive beam moment during DR 1%, the beam curvature measured near the column face reached the theoretical yield curvature. Rapid increase in the curvature was observed in the subsequent loading cycles. This was mainly due to the plastic hinges forming in the beam end. A similar situation was also observed in the negative loading cycles.

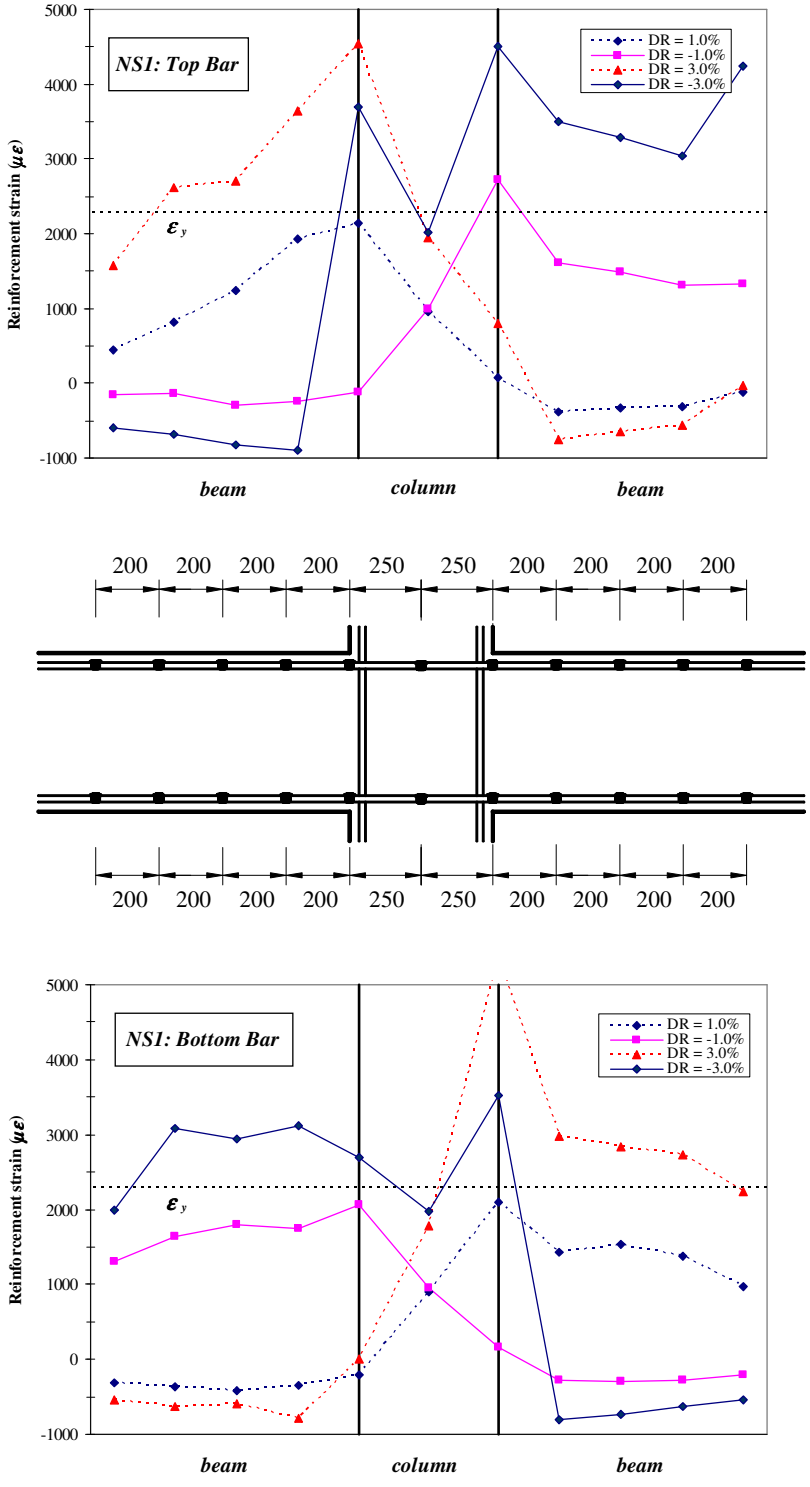

Figure 4.6 Strain Profiles of Beam Bars of NS1

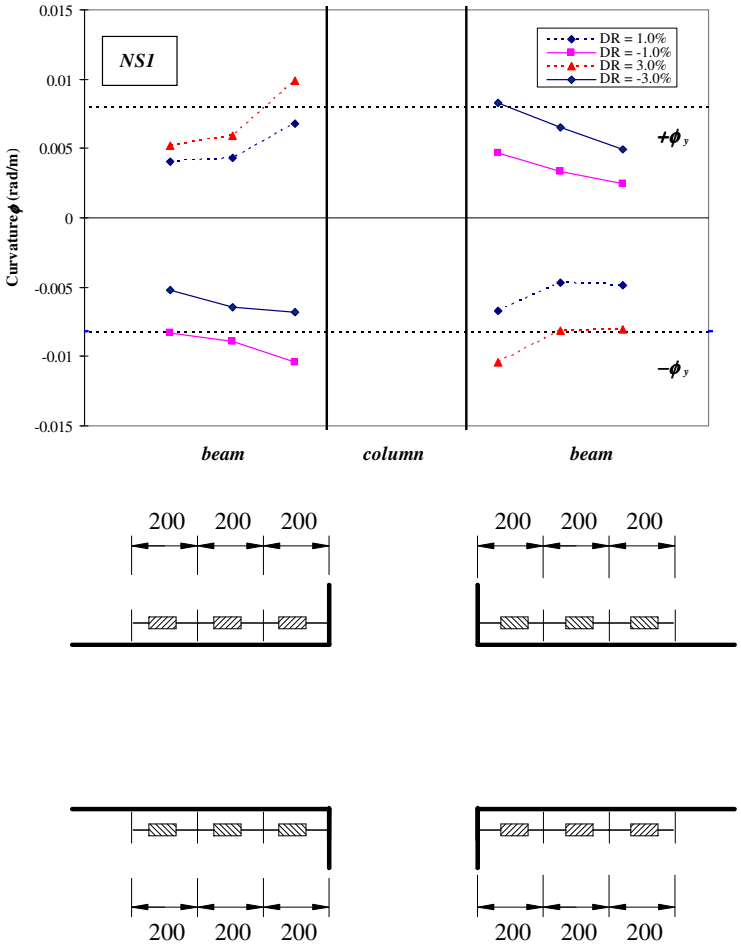

Figure 4.7 Curvature Distribution of Beam of NS1

4.1.1.5 Column Behaviour

The evaluation of strains in column side reinforcement, column middle reinforcement and column curvatures are discussed in the following sections. The strain profiles and curvatures for DR 1% push/pull and DR 3% push/pull cycles are selected to represent the early loading stage and late loading stage.

Column Reinforcement Strain

Figure 4.8 shows the strains of side bar and central bar of column. Generally the strains increased, although they did not reach the yield strain. From the top beam face to the bottom beam face, the column reinforcement was experiencing tension. The central column bars experienced lower stress compared to the side column bars in general. The column remained elastic at the end of test.

Column curvature distributions

Figure 4.9 depicts the column curvature distributions as per instrumented in the test. The curvatures measured at the upper column were slightly larger than those at the lower column. Although the curvatures increased gradually throughout the test, its theoretical yield curvatures were not exceeded. This shows the behaviour of the column was still in its elastic range.

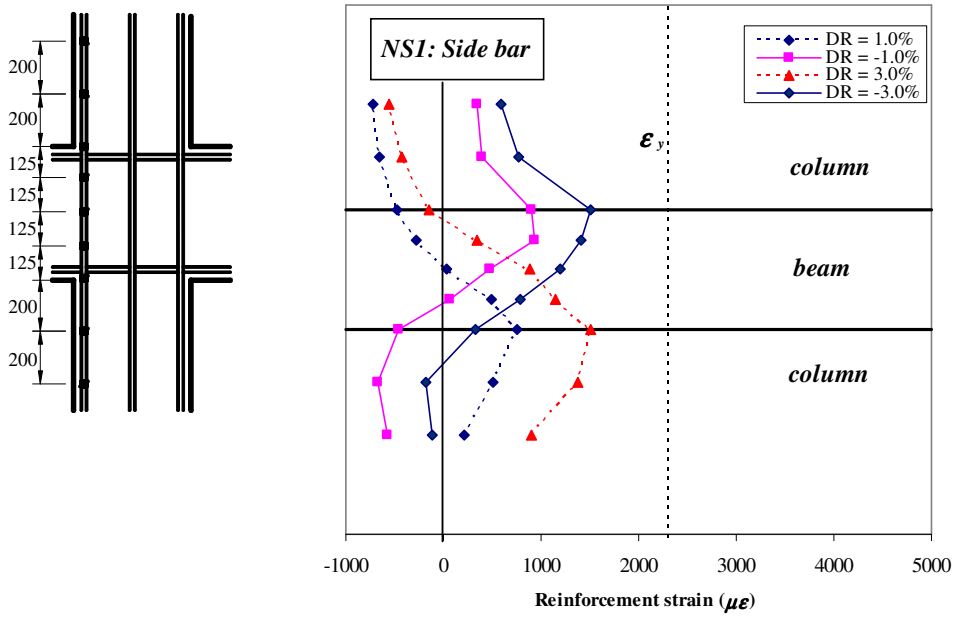

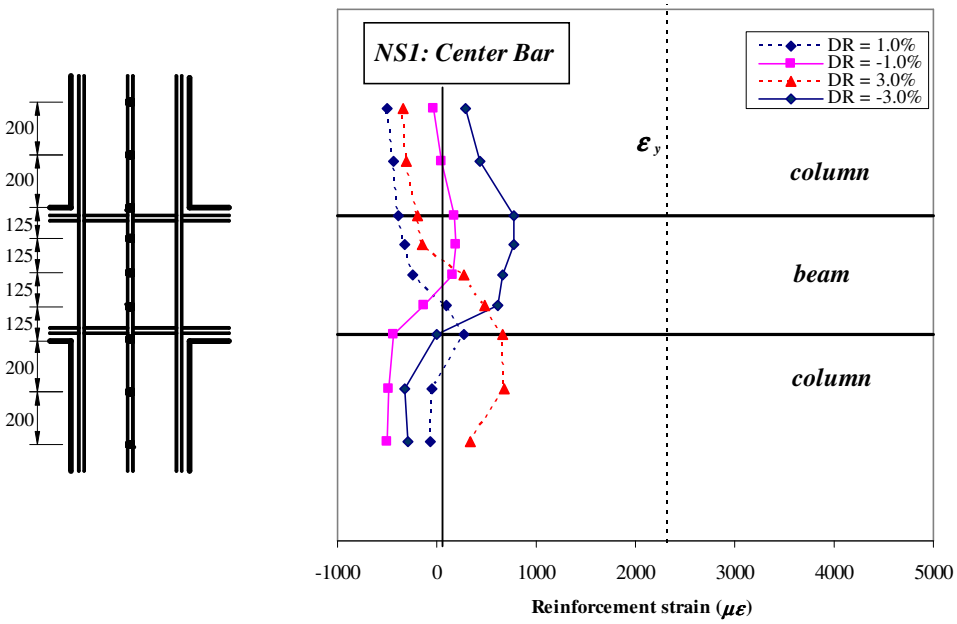

Figure 4.8 Strain Profiles of Column Bars of NS1

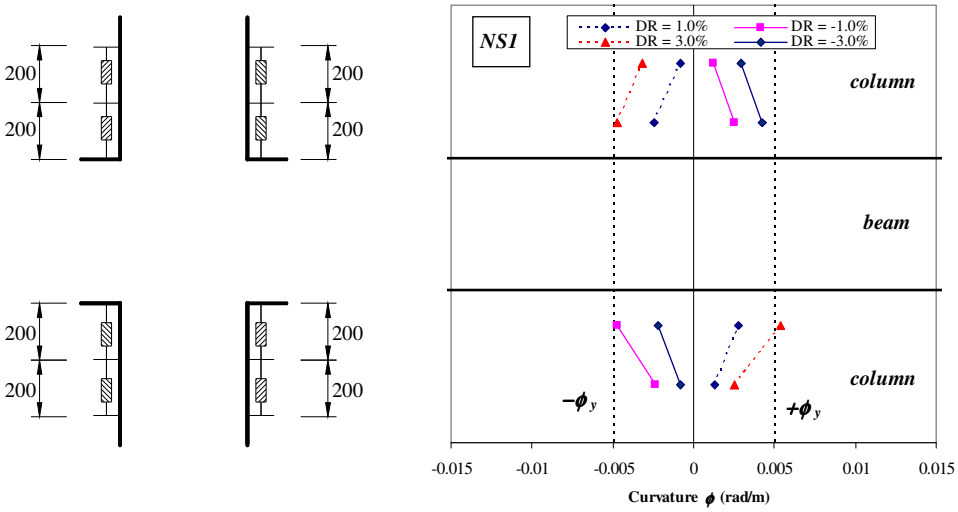

Figure 4.9 Curvature Distribution of Column of NS1

4.1.1.6 Joint Behaviour

The evaluation of joint behaviour on bond stress of beam reinforcement and column reinforcement, joint shear distortion and joint shear expansion are discussed in the following sections:

General Behaviour

Initiation of diagonal tension cracks were observed in the DR 1% (see Figure 4.2a). In the subsequent loading cycles, more cracks appeared on joint core and during DR 3%, the joint diagonal tension cracks opened wide and extended to connect with the bond splitting cracks along the column bars (see Figure 4.2c). A maximum nominal horizontal shear stress in the joint core of 5.87MPa or 0.096 $f_c^{'}$ was observed where $f_c^{'}$ is the measured compressive cylinder strength of concrete. Subsequent loading cycles resulted in strength and stiffness degradation due to joint diagonal tension cracking and bond deterioration along the beam bars.

Bond Stresses of Beam and Column Reinforcement Bars in Joint Core

The average bond stresses for beam bars and column bars are plotted in Figure 4.10 and Figure 4.11 respectively. Only the bond stresses at the peaks of the selected loading cycles are plotted. The average bond stresses measured along the longitudinal beam and column bars in the joint, assumed to be uniformly distributed over the gauge length as shown in Figure 4.10 and Figure 4.11 were calculated using the wire strain gauge readings.

The maximum bond stress obtained along top beam bars was 4.54 MPa (=0.074 $f_c^{'}$) while the maximum bond stress observed along bottom beam bars was 5.34 MPa (=0.088 $f_c^{'}$). Bond deterioration was obvious in bottom beam bars where bond stresses decreased rapidly in the end of test. On the other hand, the column reinforcement remained elastic in the end of the test with maximum bond stress of 5.73 MPa (=0.088 $f_c^{'}$) on side bar and maximum bond stress of 3.72 MPa (=0.061 $f_c^{'}$) on centre bar, respectively.

Joint Shear Distortion and Joint Shear Expension

The measured joint shear distortion and expansion are shown in Figure 4.12. The procedures for estimating the joint shear distortion and expansion were described in Chapter 3 Section 3.4.6 . In the loading to DR 1%, there was a small joint shear distortion and expansion while in the loading to DR 2%, diagonal tension cracks were observed in the joint core. The joint shear distortion and expansion increased rapidly in the subsequent loading stage. In the loading to DR 4%, the joint diagonal tension cracks opened wide with the maximum joint distortion of 0.23% and the maximum joint expansion of 1.79 mm.

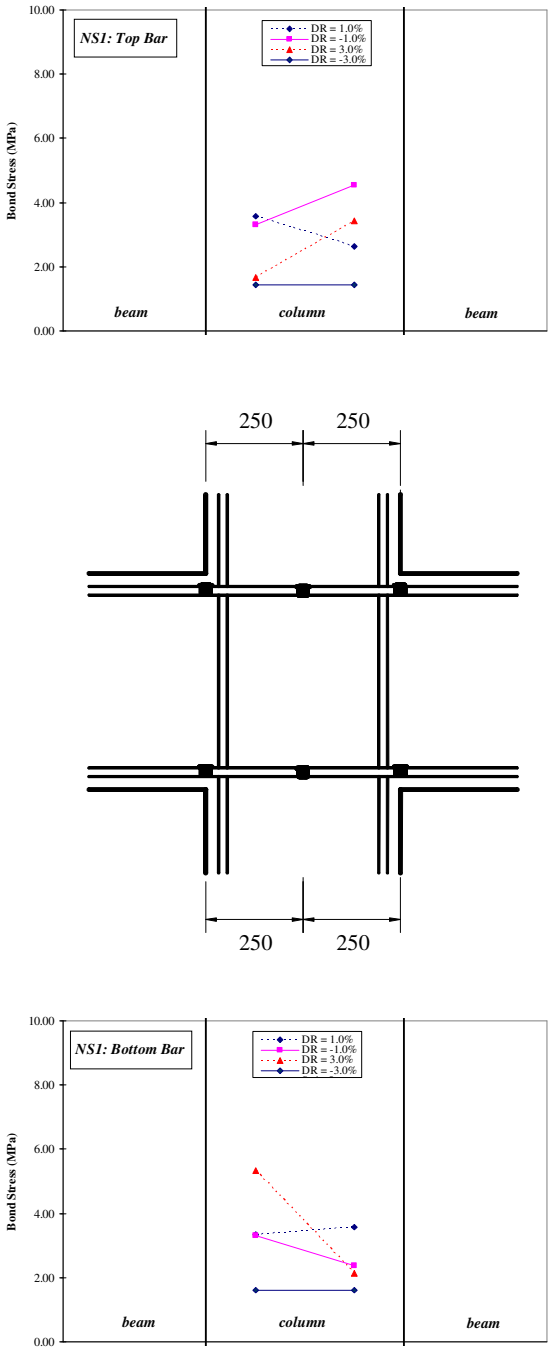

Figure 4.10 Bond Stress of Beam Bar of NS1

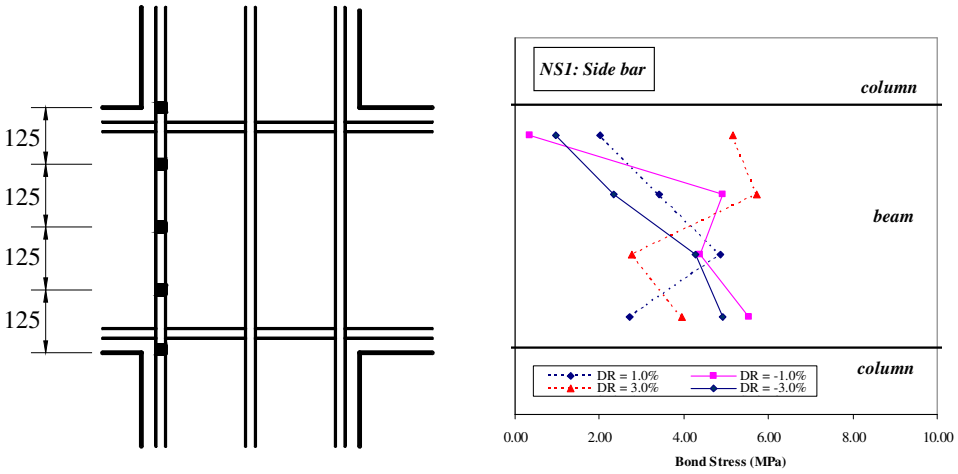

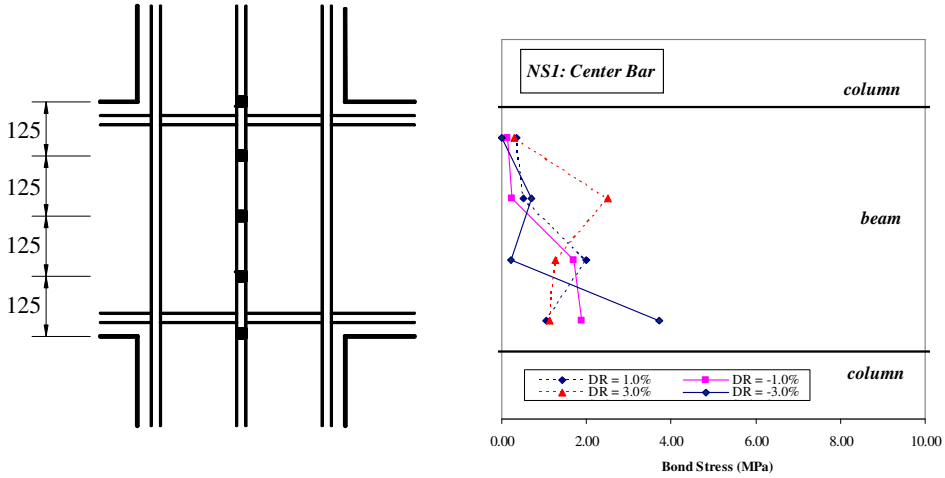

Figure 4.11 Bond Stress of Column Bar of NS1

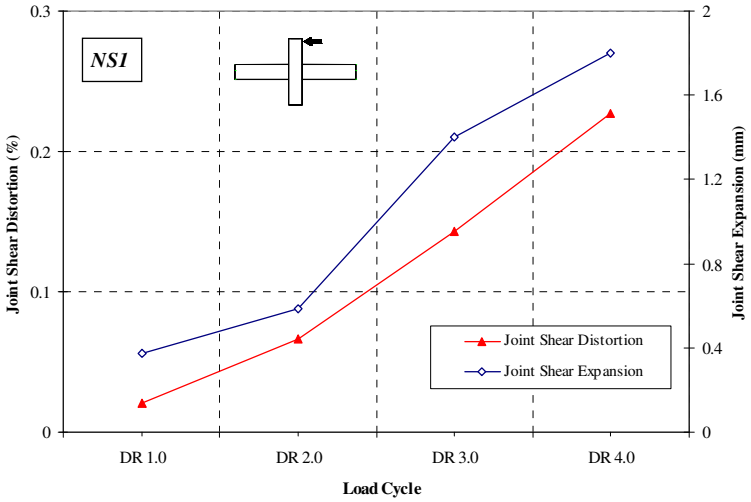

Figure 4.12 Joint Shear Distortion and Expansion of Specimen NS1

4.1.2 Specimen AS1

Due to the beneficial confinement effect of column axial compressive load, no crack was found on the column of AS1 and the column remained elastic throughout the test. Cracks were mainly found on beams and some cracks occurred on joint core panel. The specimen exhibited good energy dissipation capacity and behaved in a ductile manner.

4.1.2.1 General Observation

Specimen AS1 was the counterpart of NS1 with the same dimension and detailing except AS1 was tested with column axial compressive loading of $0.3f_c'A_c$. Figure 4.13 explains the final crack pattern of AS1 in the end of the test. Due to the confinement by column axial compressive load applied, its column remained elastic throughout the test. Some diagonal cracks with steeper inclination angle than its counterpart NS1 tested without column axial compressive load were found on joint core panel. The cracks were mainly formed on beams which explained the energy dissipation contribution were mainly from beams. Both beam top reinforcement and beam bottom reinforcement were found to yield in the end of test. AS1 exhibited good energy dissipation capacity in general.

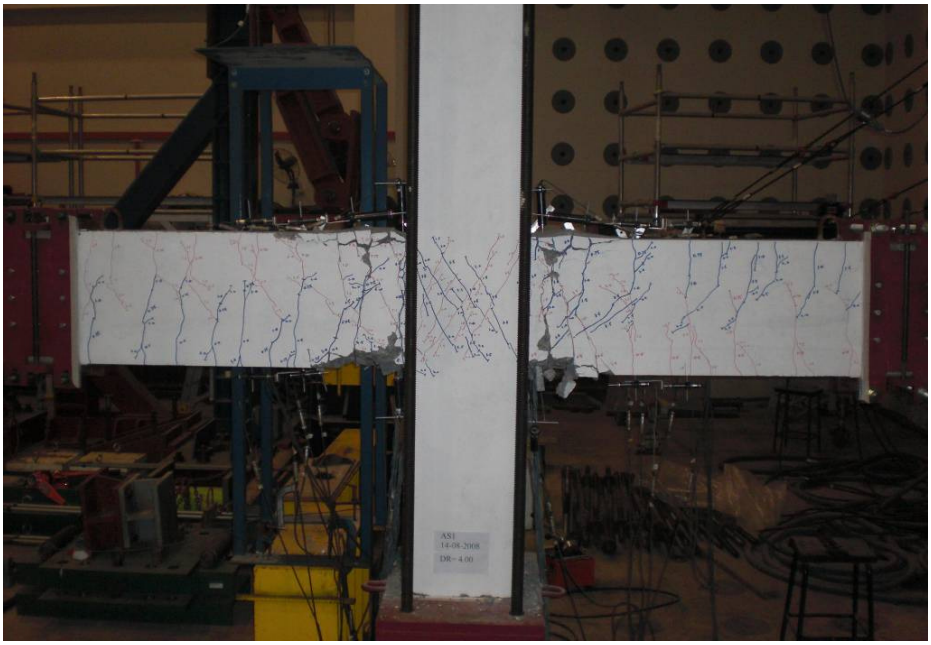

Figure 4.13 Final Crack Pattern of AS1

Figure 4.14 explains the crack development of AS1 at the peak of storey drift ratio of 1.0% (DR 1%), 2.0% (DR 2%), 3.0% (DR 3%) and 4.0% (DR 4%). During DR 1%, initiation of flexural cracks caused by sagging and hogging moment was noticed on beams as shown in Figure 4.14 while limited diagonal cracks were formed at joint core area at this stage. More flexural cracks were observed on beams while the formation of compressive strut at joint core was significant with more diagonal shear cracks formed and intersected, during the subsequent loading stage of DR 2% and DR 3%. Cracks formation was almost stabilised after DR 3% while spalling began to take place at beam ends near to column. At DR 4%, serious spalling of concrete was observed at the top and bottom surfaces of beam ends due to bond deterioration of beam reinforcement. As explained earlier, no crack was found on column throughout the test.

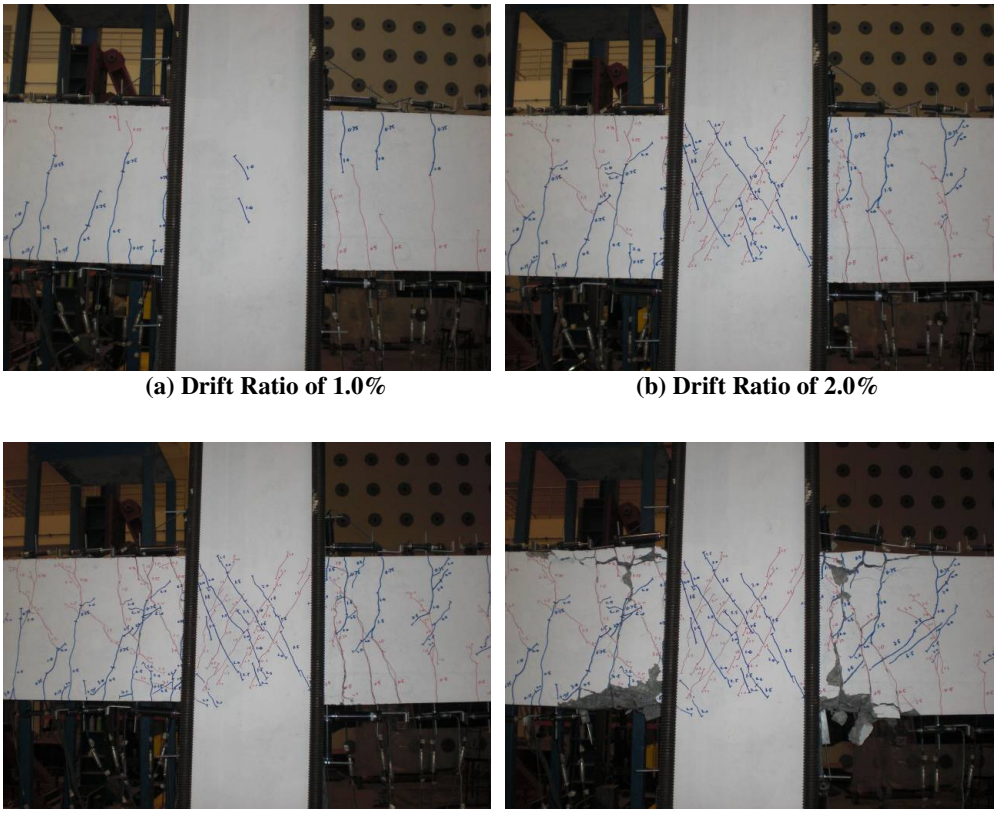

(a) Drift Ratio of 1.0% **(b) Drift Ratio of 2.0%**

(c) Drift Ratio of 3.0% **(d) Drift Ratio of 4.0%**

Figure 4.14 Progressive Cracking Development of AS1

4.1.2.2 Hysteretic Behaviour

Figure 4.15 shows the measured horizontal storey shear versus horizontal displacement hysteresis loops with the theoretical ideal storey horizontal load strength P_i and the theoretical stiffness K. As compared to NS1 tested without column axial compressive load, AS1 exhibited higher initial stiffness which is slightlty closer to its theoretical stiffness. The storey shear force of AS1 increased rapidly in the early loading stage till DR 2% where the maximum storey shear force was attained. The storey shear force begun to drop after DR 3% and at DR 4% a drop of 12.5% of strength was noticed, compared to its maximum shear force at DR 2%. Generally, the energy dissipation of AS1 was good with large area confined in the hysteresis loops and no pinching was observed throughout the test.

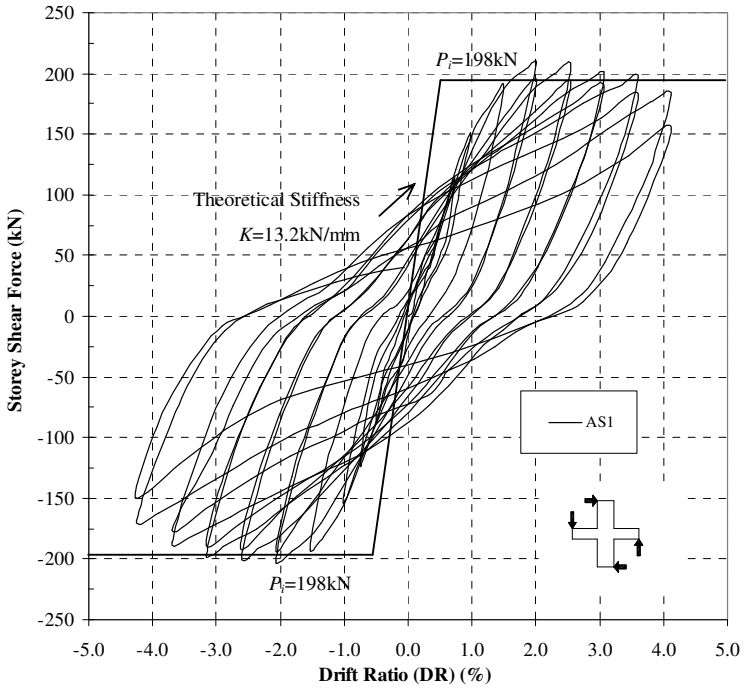

Figure 4.15 Storey Shear Force versus Horizontal Displacement for AS1

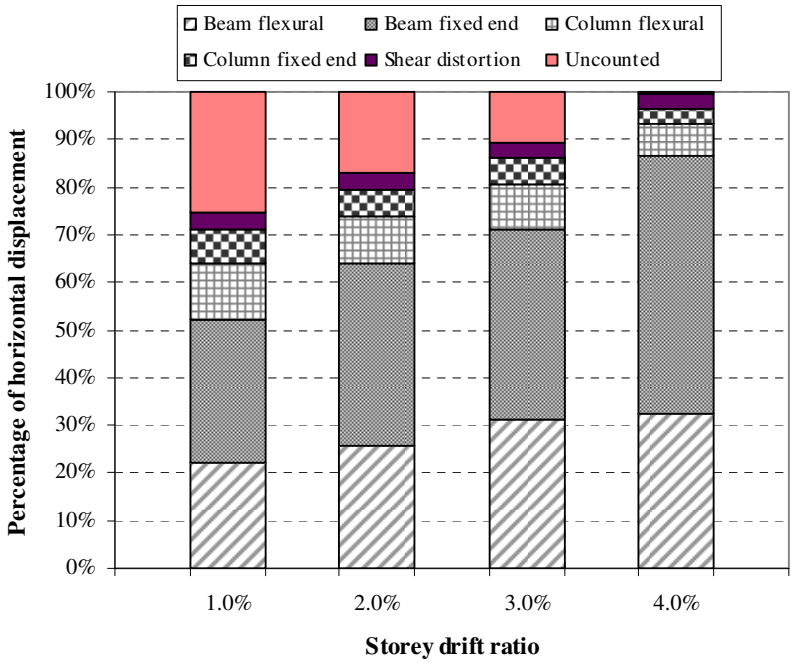

Figure 4.16 Decomposition of Horizontal Components of AS1

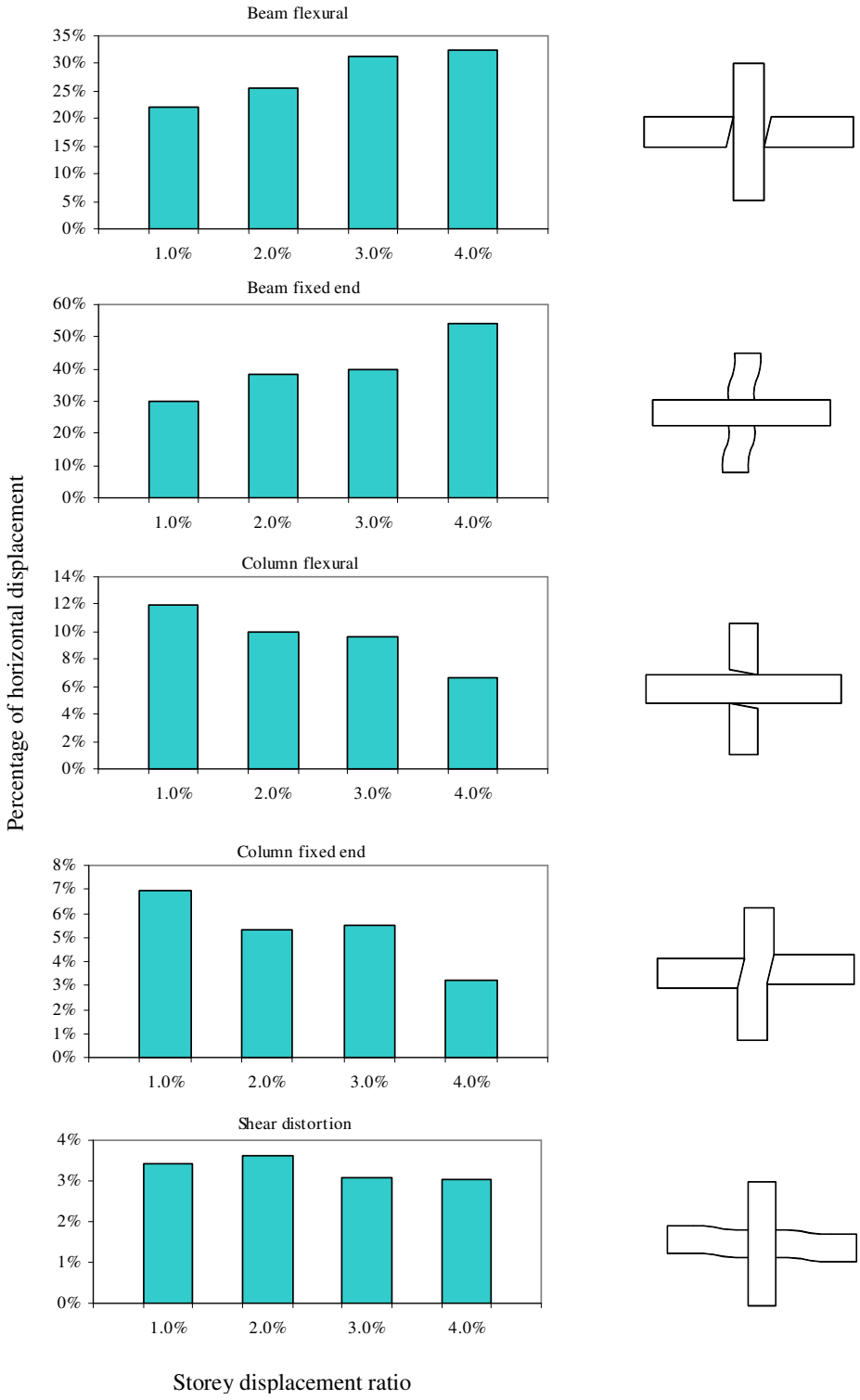

Figure 4.17 Contributions of Horizontal Components of AS1

4.1.2.3 Decomposition of Horizontal Displacement

The components of horizontal displacement measured for AS1 at the peak of the selected loading cycles is depicted in Figure 4.16. The contribution of uncounted component such as rigid body movement was significant in the early stage of test and eventually reduced in the end of test while the contribution from beam component dominated in the end of test. Figure 4.17 explains the contributions breakdown of each components of the horizontal displacement measured for AS1**.** The maximum contributions of beam flexure and fixed-end rotation were 32% and 54% respectively, which formed the main source of the storey drift. The contributions of column flexure and column fixed-end rotation to the total drift were relatively small during the testing. The presence of column axial compressive load has produced a rigid joint where the contribution of joint shear distortion to horizontal displacement was small.

4.1.2.4 Beam Behaviour

The evaluation of strains in beam reinforcement and beam curvatures are discussed in the following sections:

Beam Reinforcement Strains

Figure 4.18 shows the strain profiles of the top and bottom beam reinforcement of AS1 where the beam reinforcement of AS1 showed a steady increase in its strain gauge readings in the initial loading stage of DR 1%. As explained in Figure 4.18, the strain gauges at tension face almost reaching its yield strain while the strain of gauges at compression face was still relatively low. The strain measured along the tension face surpassed the yield strain during DR 3%. Strain gauges of beam reinforcement showed significant readings when a positive load cycle was applied and these readings dropped sharply when the load cycle was reversed. This explained the effective bond strength of joint core which enable the reversal of stress in a bar. The strain measured within the joint was small confirmed the presence of good bond in joint core with the bar size used in both top and bottom reinforcement.

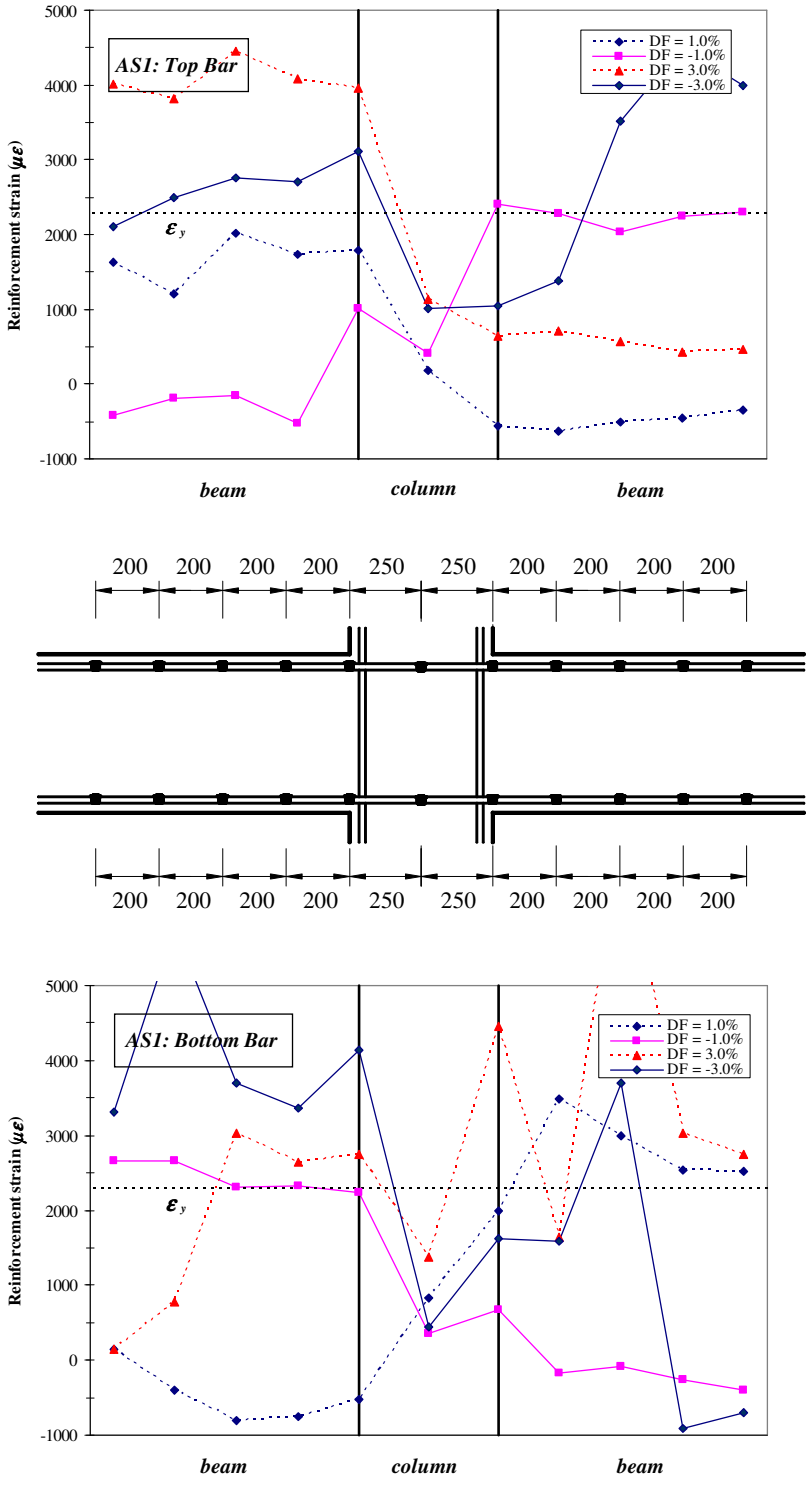

Figure 4.18 Strain Profiles of Beam Bars of AS1

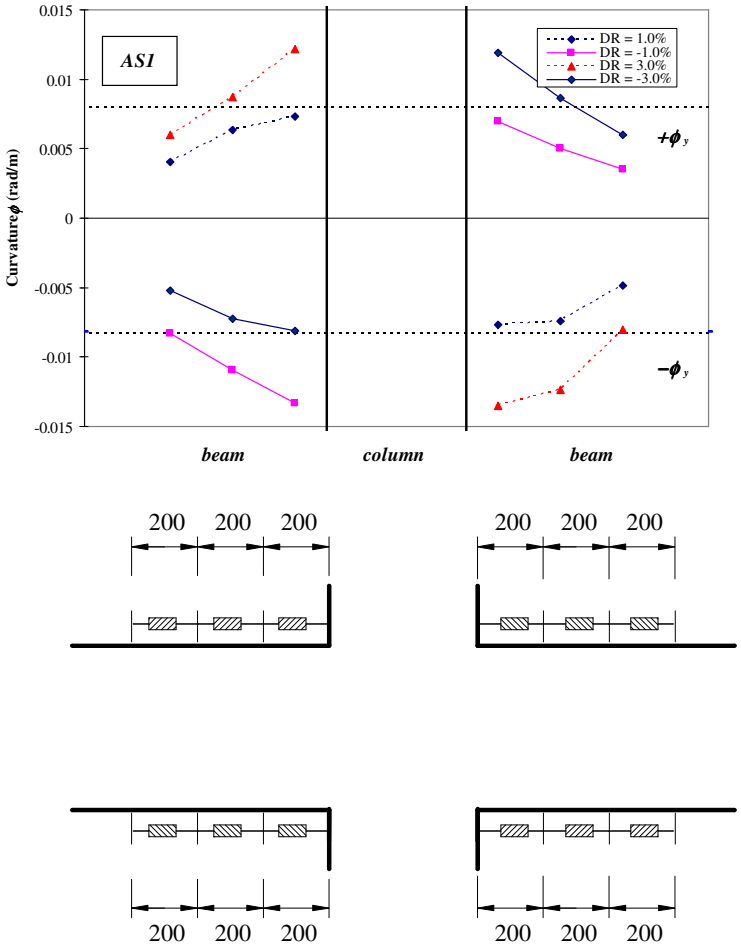

Figure 4.19 Curvature Distribution of Beam of AS1

Beam curvature

Figure 4.19 shows the beam curvature distributions estimated from the transducer readings. The beam curvature measured near the column face almost reached the theoretical yield curvature in the loading stage of DR 1%. In the subsequent loading cycles, increase of the curvature was fast and the curvature of the first two segment measured had surpassed its yield curvature. A similar situation was also observed in the negative loading cycles. Beam curvature increases rapidly after DR 3% with the formation of plastic hinge at beam end.

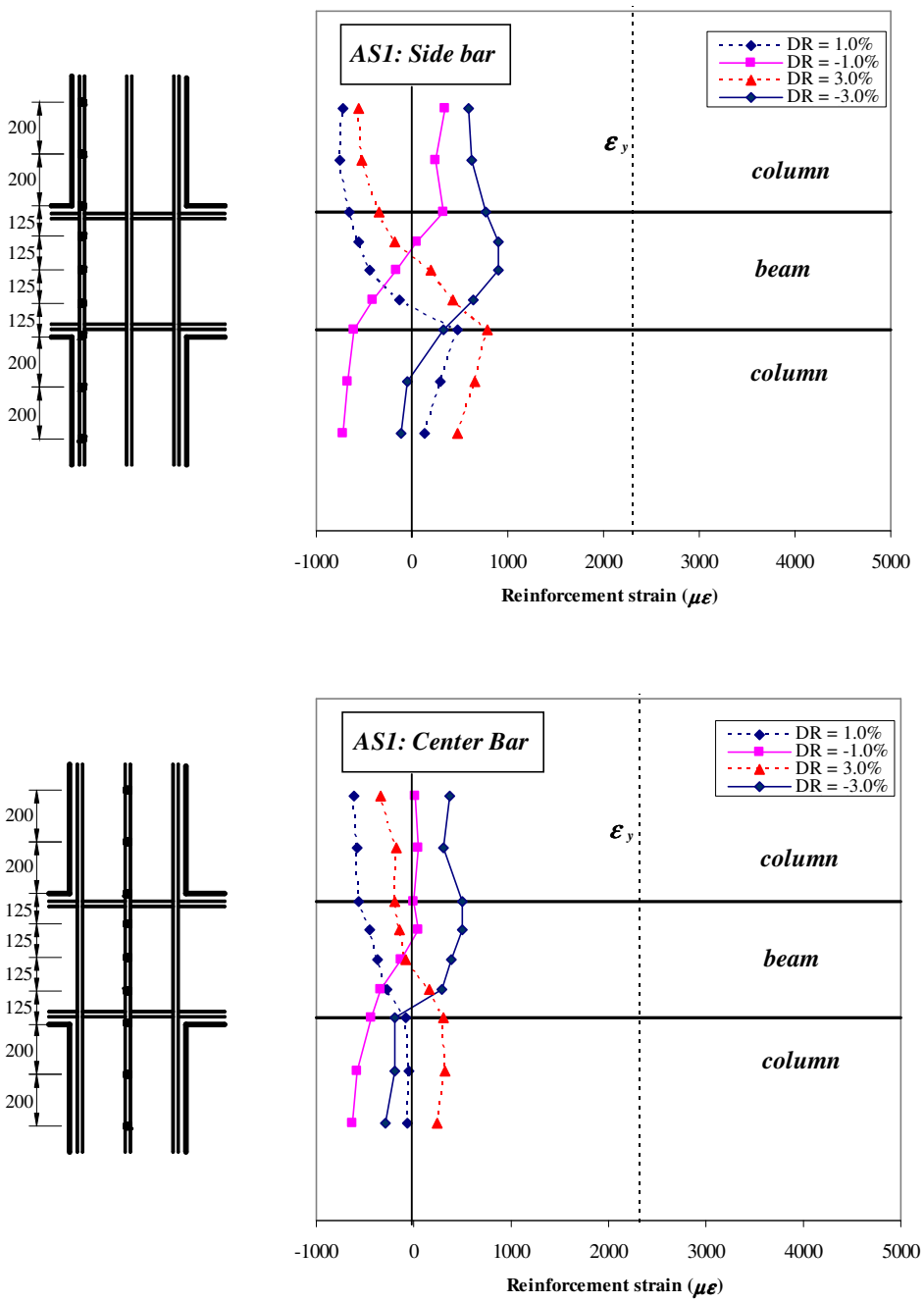

Figure 4.20 Strain Profiles of Column Bars of AS1

4.1.2.5 Column Behaviour

The evaluation of strains in column side reinforcement, column middle reinforcement and column curvatures are discussed in the following sections:

Column Reinforcement Strain

The strains of side bar and central bar of column are explained in Figure 4.20. Due to the confinement from column axial compressive load, the column basically remained elastic throughout the test. Although the strains of column bar increase gradually, they did not reach the yield strain. The central column bars experienced lower stress compared to the side column bars and the respective strain measured were very low compared to the side bars.

Column curvature distributions

Figure 4.21 shows the column curvature distributions as per instrumented in the test. The curvatures measured at the upper column were similar to those at the lower column. As the column was still in its elastic range, the respective curvatures increased gradually but never exceed the theoritical yield curvature limit.

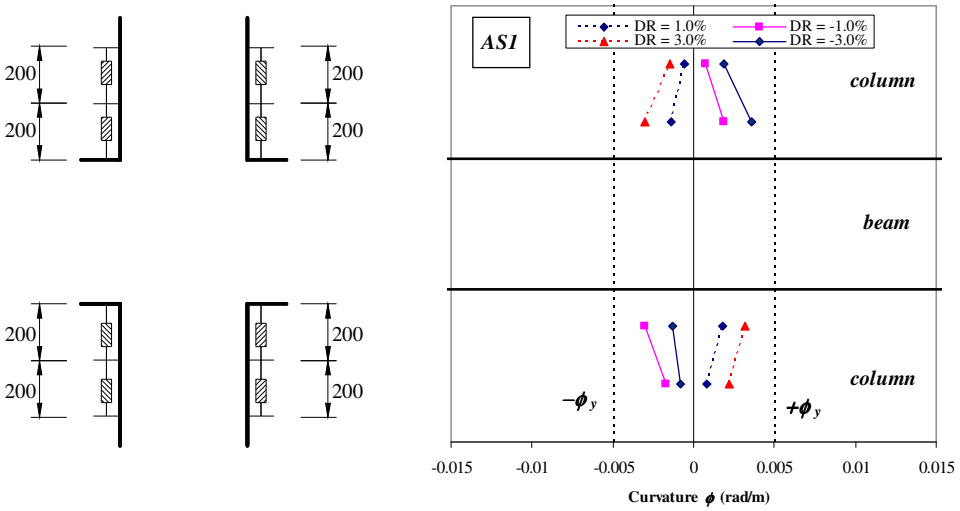

Figure 4.21 Curvature Distribution of Column of AS1

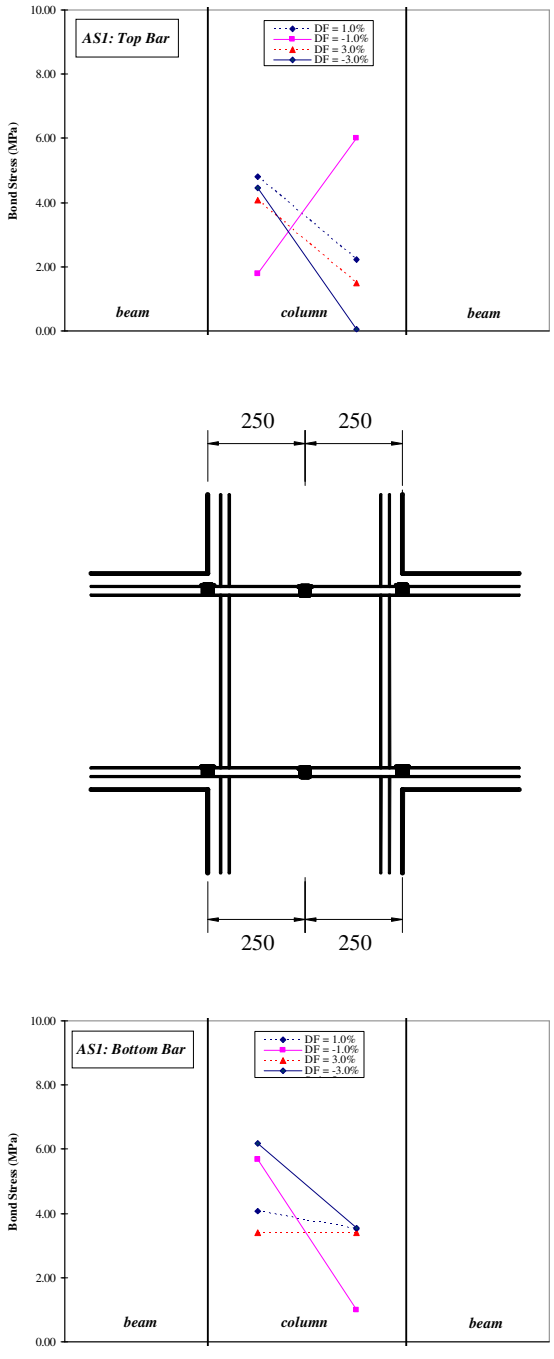

Figure 4.22 Bond Stress of Beam Bar of AS1

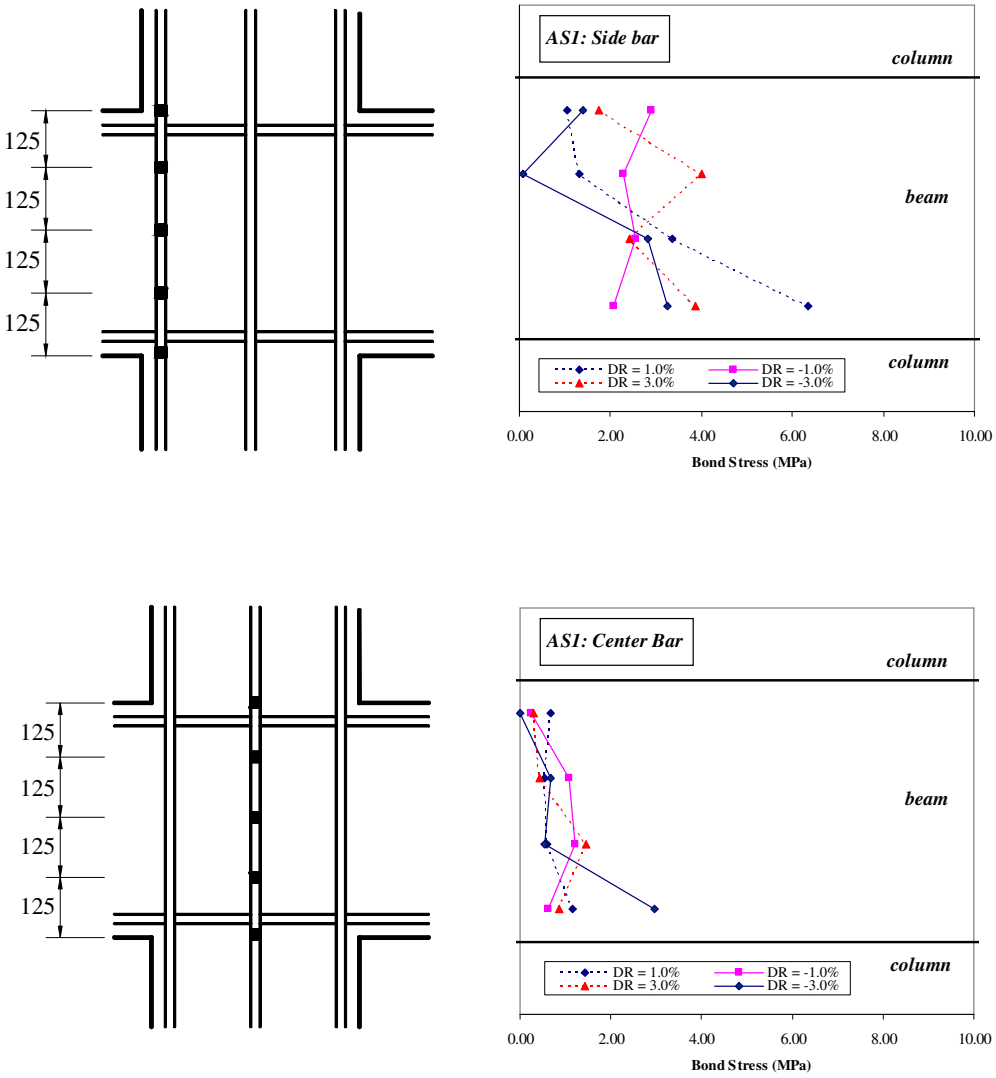

Figure 4.23 Bond Stress of Column Bar of AS1

4.1.2.6 Joint Behaviour

The bond stress of beam reinforcement and column reinforcement, joint shear distortion and joint shear expansion are evaluated in the following sections:

General Behaviour

A maximum nominal horizontal shear stress in the joint core of 5.79 MPa or $0.095 f_c^{'}$ was observed which met the requirement in NZS 3101. The initial diagonal tension cracks formed in the DR 1% (see Figure 4.14a). In the subsequent

loading cycles, more cracks appeared on joint core and during DR 2% (see Figure 4.14b). The joint diagonal tension cracks opened wider and extended till DR 3% was reached and these cracks at joint stabilised after then.

Bond Stresses of Beam and Column Reinforcement Bars in Joint Core

Figure 4.22 and Figure 4.23 show the average bond stresses for beam bars for column bars. The maximum bond stress obtained along top beam bars was 6.01 MPa (=0.096 $f_c^{'}$) while the maximum bond stress observed along bottom beam bars was 6.18 MPa (=0.1013 $f_c^{'}$). Bond deterioration was obvious in bottom beam bars where bond stresses decreased rapidly in the end of test. On the other hand, the column reinforcement remained elastic in the end of the test with maximum bond stress of 6.34 MPa (=0.104 $f_c^{'}$) on side bar and maximum bond stress of 2.96 MPa (=0.049 $f_c^{'}$) on centre bar, respectively.

Joint Shear Distortion and Joint Shear Expension

Figure 4.24 explains the measured joint shear distortion and expansion of AS1. The joint shear distortion and expansion of AS1 is generally small due to the beneficial confinement effects from column axial compressive load. In the loading to DR 4%, the maximum joint distortion was 0.14% and the maximum joint expansion was 1.58 mm.

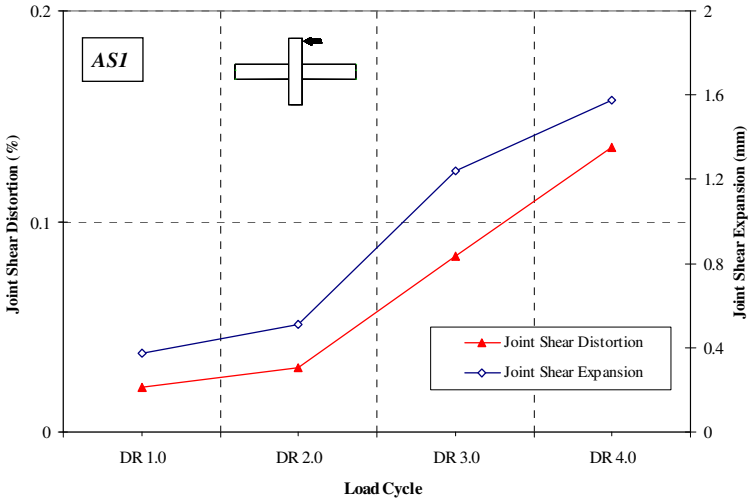

Figure 4.24 Joint Shear Distortion and Expansion of Specimen AS1

4.2 Test Result of Group Two (NS2 and AS2)

Specimens NS2 and AS2 were included in Group Two with details as described in Chapter 3 where NS2 was tested without column axial compressive loading while its counterpart AS2 was tested with column axial compressive loading of $0.3f_c'A_c$. The typical features of these specimens are summarised as follows:

- beam reinforcement size of was 33% larger than specimens NS1 (16mm for NS2 and 12mm for NS1)
- ratio of beam bottom reinforcement to top reinforcement = 0.5
- actual maximum beam-bar-to-column-depth = 1/28.13
- actual column-bar-to-beam-depth = 1/20.83
- calculated maximum beam-bar-to-column-depth based on Eq. 7-13 in NZS 3101 :

  NS2= 1/24.60 AS2= 1/24.68
- calculated maximum column-bar-to-beam-depth based on clause 7.5.3.4 in NZS 3101:

  NS2= 1/16.23 AS2= 1/16.29
- NS2 and AS2 met both the requirement of maximum beam-bar-to-column-depth and maximum column-bar-to-beam-depth set in NZS 3101
- Joint core reinforcement detailing did not comply with the requirement in clause 7.5.3.4 in NZS 3101 (maximum bar spacing = 70mm, allowable bar spacing = 60mm)

The test results of Specimens NS2 and AS2 are summarised in the following sections.

4.2.1 Specimen NS2

Specimen NS2 was detailed with unequal beam reinforcement where the area of bottom reinforcement area was only half of the top reinforcement. Due to such detailing, limited crack was observed at the column while flexural cracks formed at the beam. In joint core region, concrete at both lower corner of the panel spalled and crushed, due to the excessive deformation of beam bottom with lower reinforcement compared to beam top.

4.2.1.1 General Observation

The final crack pattern of NS2 is shown in Figure 4.25. Even though Specimen NS2 was made of larger beam bars, it met all the bond development limits in NZS3101 and the specimen exhibited satisfactory energy dissipation capacity and failed in a ductile manner in the end of test. The major cracks were found to form at joint core with spalling observed at the bottom corner of the joint core diagonal corners of the joint panel. Due to the unequal beam bar area, the bond condition of beam top was better than beam bottom where slip of bottom bars was larger than the top bar. The flexural cracks at beam bottom were fully closed and the concrete was subjected to a large compression force than the concrete at top at the opposite corner. Hence, spalling due to crushing was noticed at the beam bottom of NS2. Flexural cracks were observed on the beams top and beam bottom with limited cracks at the column as shown in Figure 4.25.

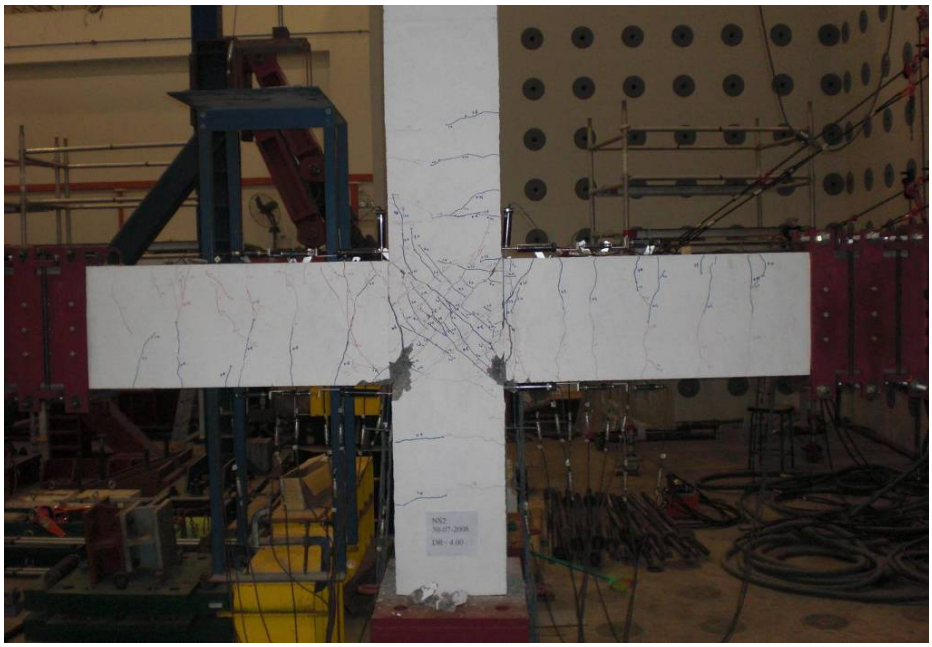

Figure 4.25 Final Crack Pattern of NS2

As explained in Figure 4.26, the crack development of NS2 is illustrated by a series of photographs taken at the peak of storey displacement ratio of 1.0% (DR 1%), 2.0% (DR 2%), 3.0% (DR 3%) and 4.0% (DR 4%). Flexural cracks were first

observed at beam bottom when loading at DR 1% was attained as shown in Figure 4.26. The diagonal crack at the joint core area and column occurred at this loading stage. At loading stage of DR 2%, flexural cracks formed on beams begun to propagate and the cracks at joint core too progress rapidly. Conversely, no new crack was found on column at this stage till the end of test. Noteworthy that beyond DR 3%, cracks were mainly found to take place at joint core region and at the final loading stage of DR 4%, spalling was observed at joint core area as shown in Figure 4.26, due to the excessive fixed-end deflection of beam caused by lower bottom reinforcement that compressed against joint core that eventually crush the joint core to spall.

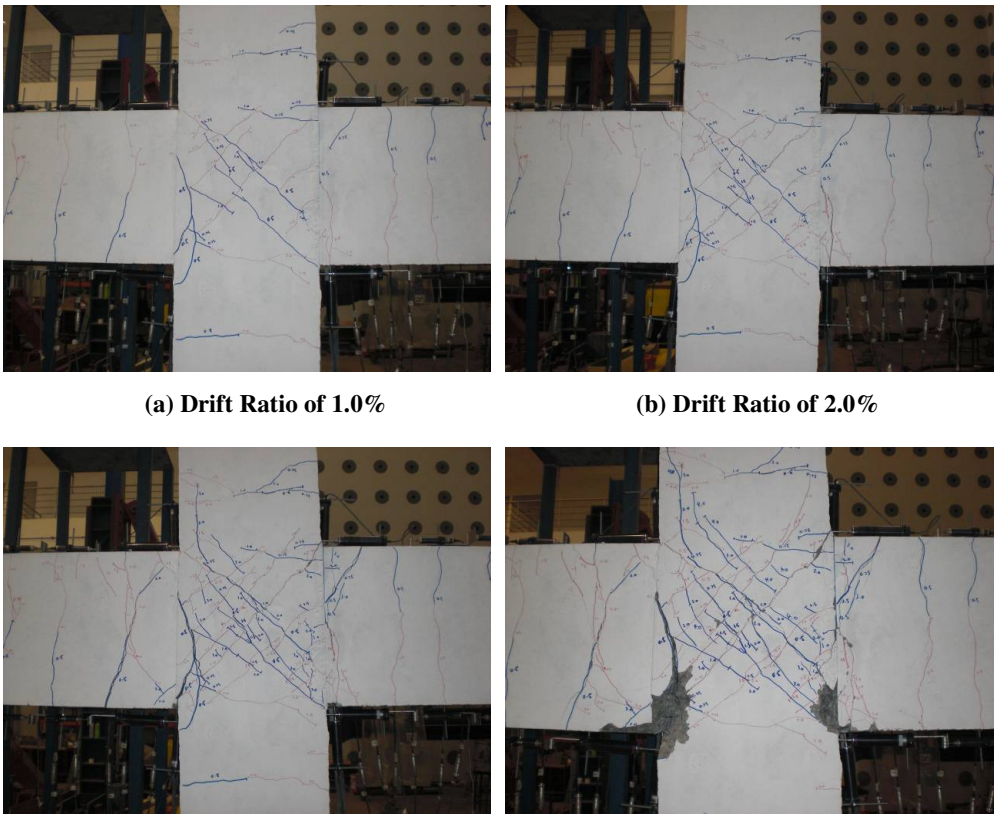

(a) Drift Ratio of 1.0% **(b) Drift Ratio of 2.0%**

(c) Drift Ratio of 3.0% **(d) Drift Ratio of 4.0%**

Figure 4.26 Progressive Cracking Development of NS2

4.2.1.2 Hysteretic Behaviour

Figure 4.27 explains the measured horizontal storey shear versus horizontal

displacement hysteresis loops of NS2 with the theoretical ideal storey horizontal load strength P_i and the theoretical stiffness K included for comparison. The stiffness and strength of NS2 increased as the load was firstly applied till DR 2%. However, pinching was noticed throughout the test after DR 2%. This was due to the rapid opening and closing of the cracks on the beam when the load was applied and then reversed. The maximum load was achieved when DR 3% was attained and yielding of the reinforcement took place. Specimen NS2 showed good characteristics in energy dissipation even though pinching was observed. The maximum horizontal storey shear was maintained when test was stopped at DR 4% as seen in Figure 4.27.

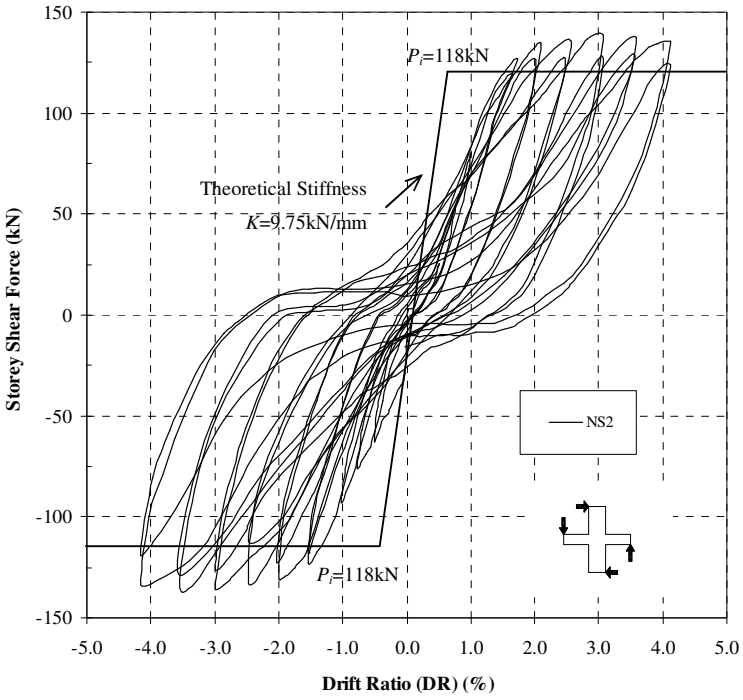

Figure 4.27 Storey Shear Force versus Horizontal Displacement for NS2

4.2.1.3 Decomposition of Horizontal Displacement

The components of the horizontal displacement measured for NS2 at the peak of the loading cycles DR 1%, DR 2%, DR 3% and DR 4% are explained in Figure 4.28.

On the other hand, Figure 4.29 depicts the contributions of each components of the horizontal displacement measured which gave the breakdown of the contribution from each component. Similar to NS1, the major source of the storey drift was the beam displacement, where the maximum contributions of beam flexure and beam fixed-end rotation were 35% and 22%, respectively. The contribution to the total drift of column flexure and column fixed-end rotation was similar in the range of 13% to 17% respectively. The contribution of the displacement due to joint shear distortion remained below 10% despite the observation of concrete spalling near the joint core when test was completed at DR 4%. Generally the contribution of each component did not change significantly during the testing except the contribution of uncounted component such as rigid body movement which reduced at the end of test.

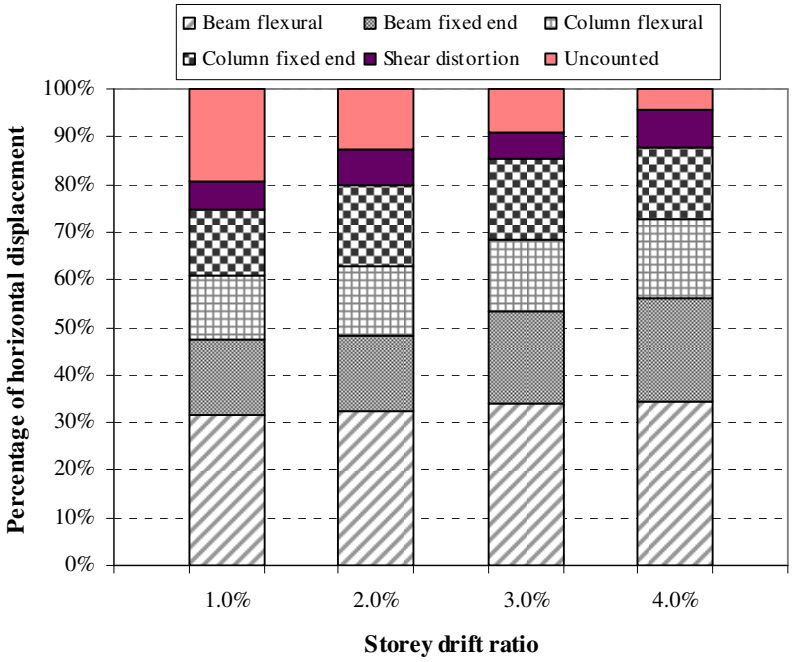

Figure 4.28 Decomposition of Horizontal Components of NS2

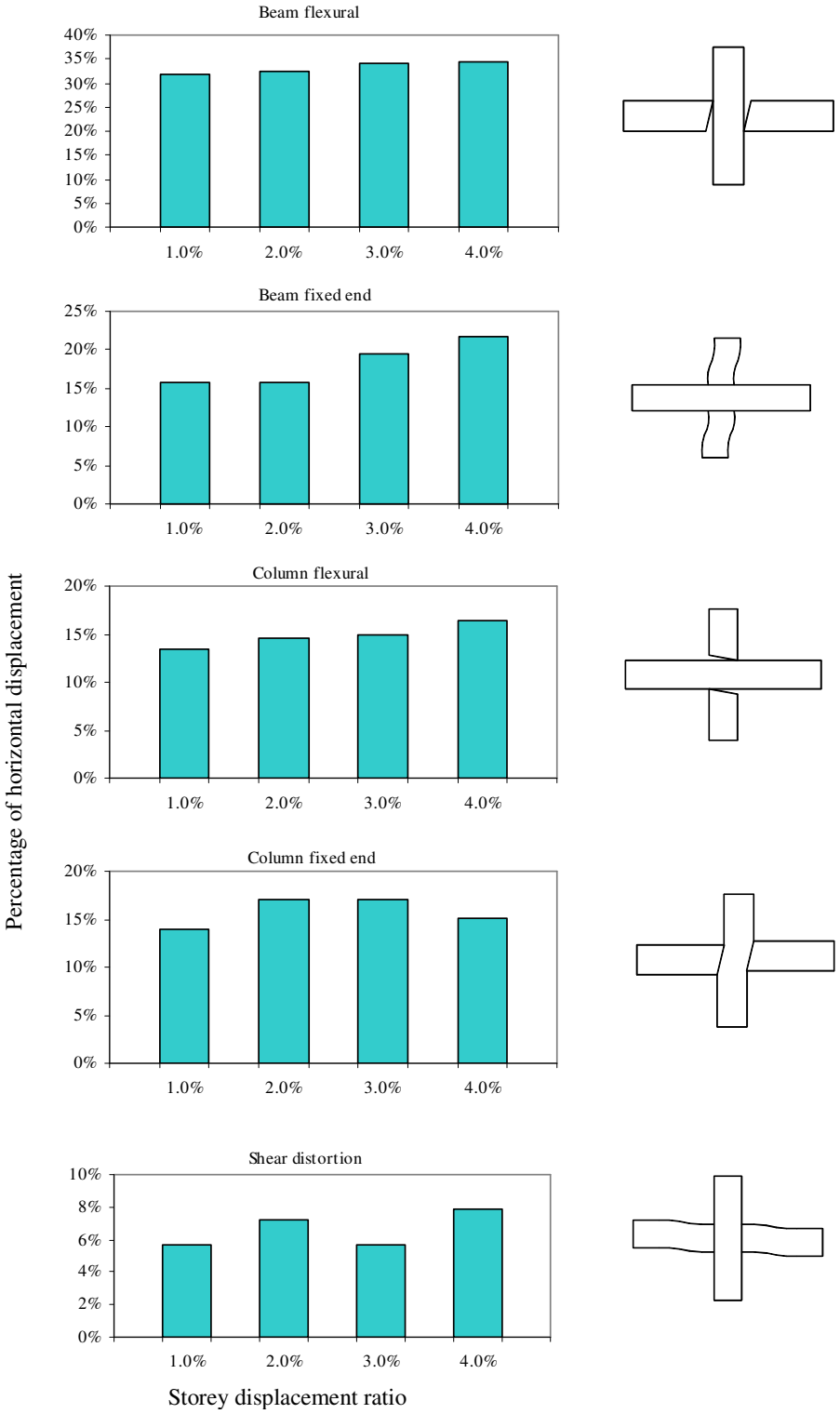

Figure 4.29 Contributions of Horizontal Components of NS2

4.2.1.4 Beam Behaviour

The evaluation of strains in beam reinforcement and beam curvatures are discussed in the following sections based on strain and curvature profiles at DR 1% push/push cycles and DR 3% push/pull cycles:

Beam Reinforcement Strains

Figure 4.30 explains the strain profiles of the top and bottom beam reinforcement of NS2 where beam bars indicated sign of yielding near to column face during DR 1%. Both top and bottom beam bars yieleded at DR 3% and yield penatration was observed where the strain gauges installed within joint core area showed high strain values which was closed to the yield limit. However, the bond of beam reinforcement at joint core was strong enough to transfer the tensile stress at one side to compressive stress at another side. This explained the use of larger bar in both top and bottom reinforcement can give good bond in joint core with certain extent of yield penetration.

Beam curvature

Figure 4.31 depicts the beam curvature distributions estimated from the transducer readings. During DR 1%, no sign of yielding was shown as the theoretical yield curvature was not exceeded. At DR 3%, the measured yield curvature at column face exceeded theoretical yield curvature which confirmed the occurance of yielding at the beam reinforcement. For the loading at the reverse cycles similar situation was observed.

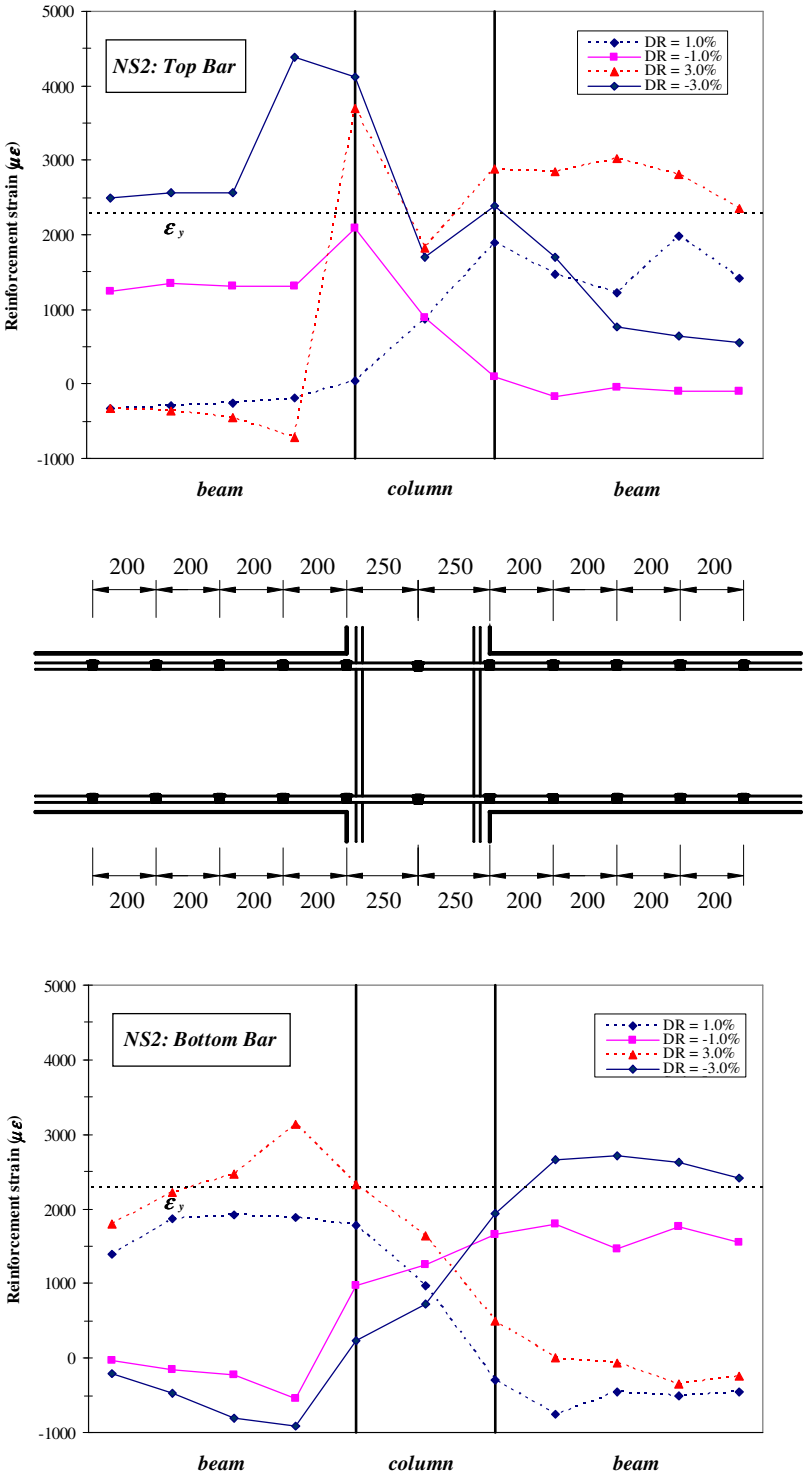

Figure 4.30 Strain Profiles of Beam Bars of NS2

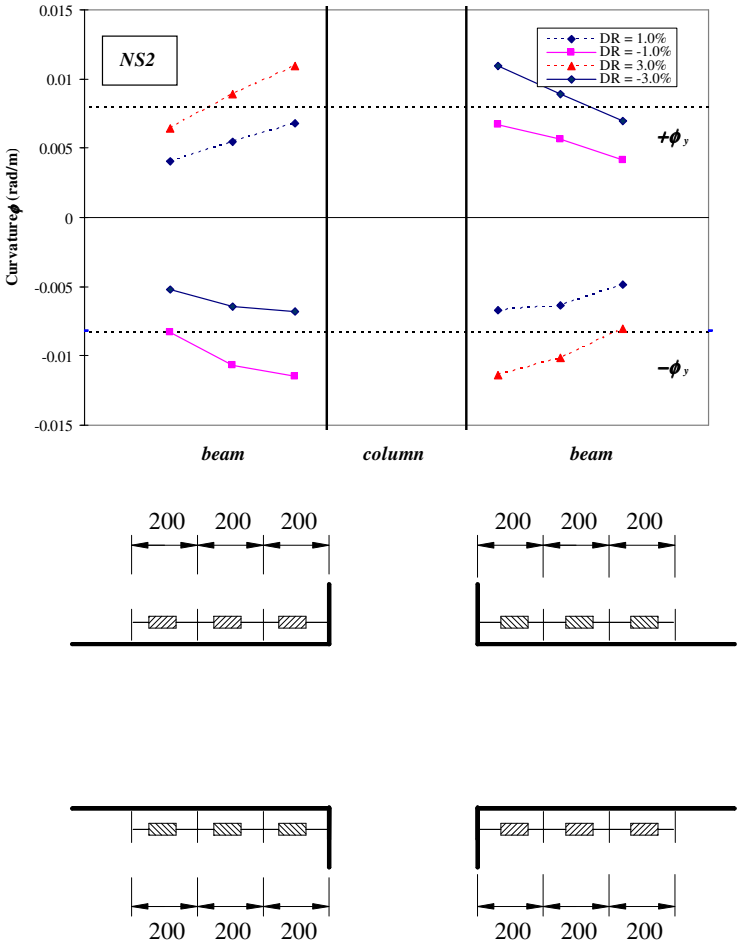

Figure 4.31 Curvature Distribution of Beam of NS2

4.2.1.5 Column Behaviour

The evaluation of strains in column side reinforcement, column middle reinforcement and column curvatures are discussed in the following sections based on strain and curvature profiles at DR 1% push/push cycles and DR 3% push/pull cycles:

Column Reinforcement Strain

Figure 4.32 shows the strains of side bar and central bar of column. Generally the strains did not reach the yield strain throughout the test. The central column bars experienced lower stress compared to the side column bars in general. The column met the characteristic of "strong-column-weak-beam" to give ductile behaviour in reversed cyclic loading.

Column curvature distributions

The column curvature distributions as per instrumented in the test is explained in Figure 4.33. The curvatures measured at the upper column were slightly larger than those at the lower column. Although the curvatures increased gradually, no evident rapid increase was observed. This shows the behavior of the column was still in its elastic range.

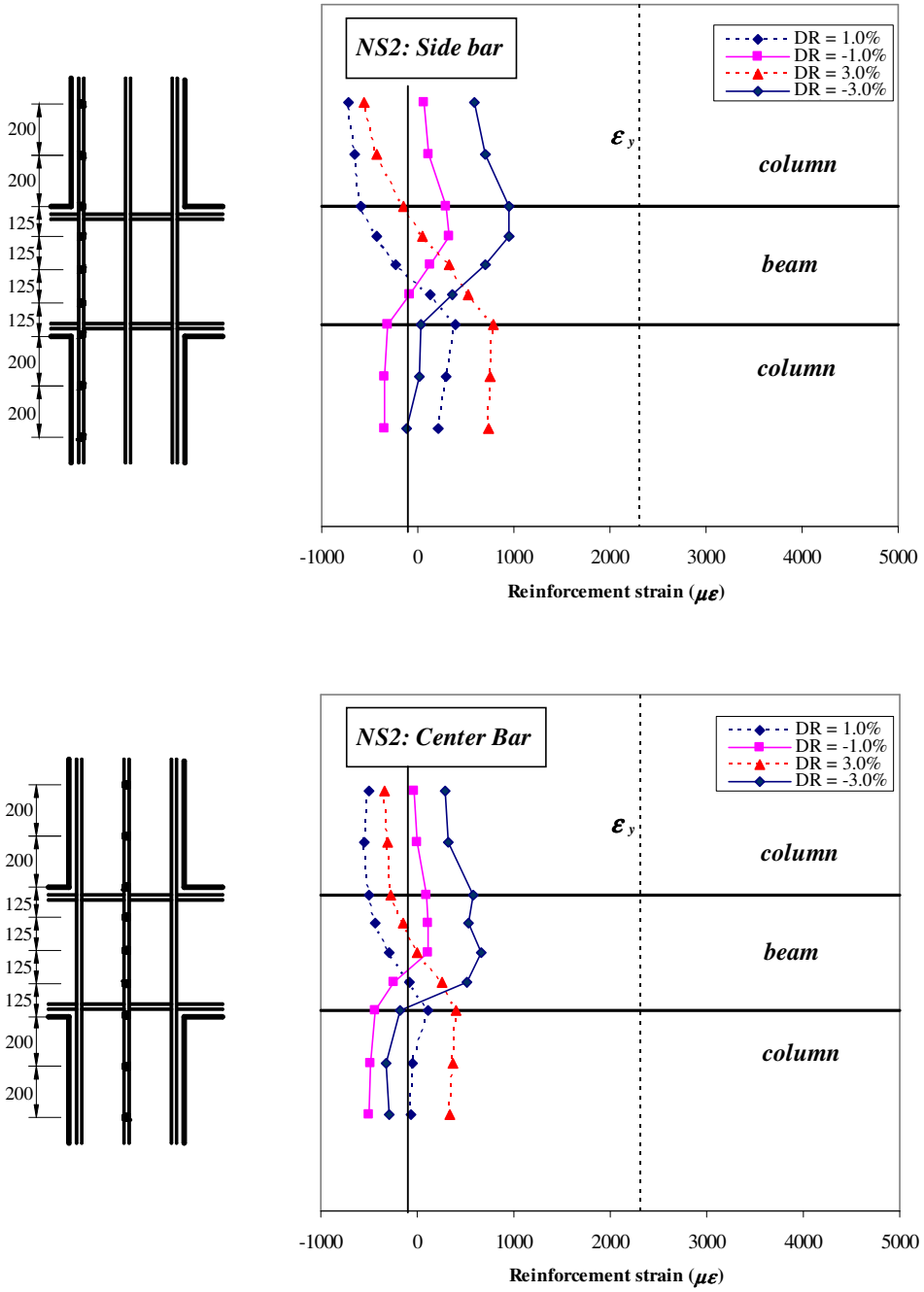

Figure 4.32 Strain Profiles of Column Bars of NS2

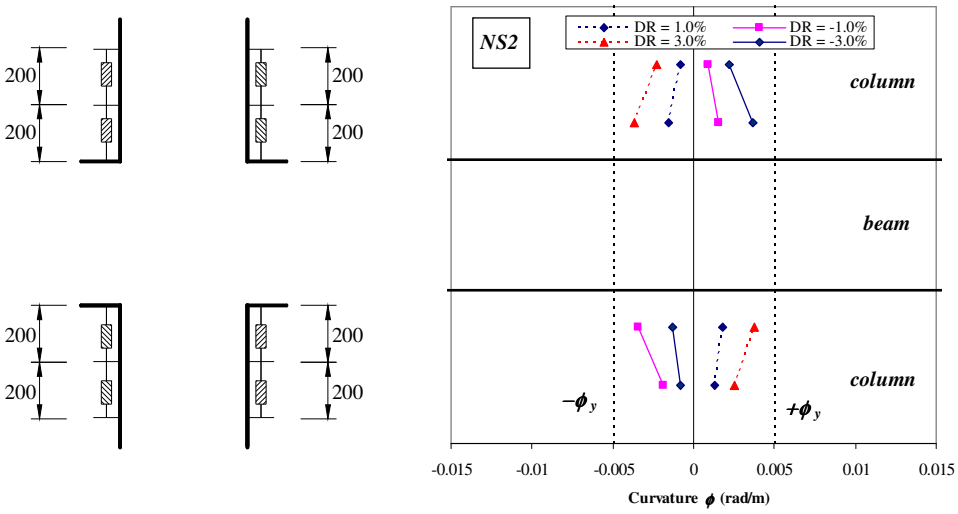

Figure 4.33 Curvature Distribution of Column of NS2

4.2.1.6 Joint Behaviour

The joint behaviour on bond stress of beam reinforcement and column reinforcement, joint shear distortion and joint shear expansion are discussed sections below:

General Behaviour

Diagonal tension cracks were initiated in DR 1% (refer Figure 4.26a) and more cracks appeared on joint core in the subsequent loading cycles. The joint diagonal tension cracks opened wide (see Figure 4.26b) and during DR 3%, the maximum nominal horizontal shear stress in the joint core of 4.72MPa or 0.077 $f_c^{'}$ was observed. At the end of test, strength and stiffness degradation due to joint diagonal tension cracking was noticed.

Bond Stresses of Beam and Column Reinforcement Bars in Joint Core

The average bond stresses was measured along the longitudinal beam and column bars in the joint. The stresses were calculated using the wire strain gauge readings, by assuming the stress was uniformly distributed over the gauge length and were

plotted in Figure 4.34 and Figure 4.35. For top beam bars, the maximum bond stress was found to be 4.81 MPa (=0.079 $f_c^{'}$) while the maximum bond stress observed along bottom beam bars was 5.07 MPa (=0.083 $f_c^{'}$). Bond deterioration was obvious in bottom beam bars where bond stresses decreased rapidly in the end of test. On the other hand, the column reinforcement remained elastic in the end of the test with maximum bond stress of 3.87 MPa (=0.063 $f_c^{'}$) on side bar and maximum bond stress of 4.10 MPa (=0.067 $f_c^{'}$) on centre bar, respectively.

Joint Shear Distortion and Joint Shear Expension

The measured joint shear distortion and expansion are shown in Figure 4.36. There was a small joint shear distortion and expansion in the loading to DR 1% while diagonal tension cracks were observed in the joint core, the joint shear distortion and expansion increased rapidly in the loading to DR 2%. In the subsequent loadings the joint distortion and expansion continued to increase with the maximum joint distortion was 0.25% and the maximum joint expansion was 1.89 mm, respectively.

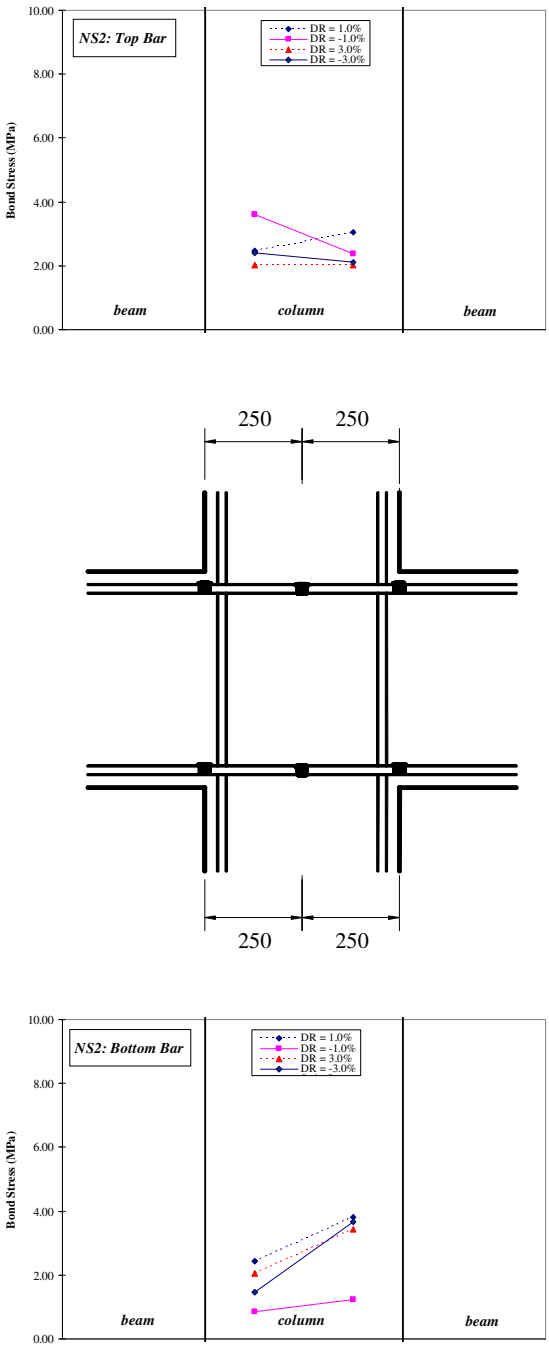

Figure 4.34 Bond Stress of Beam Bar of NS2

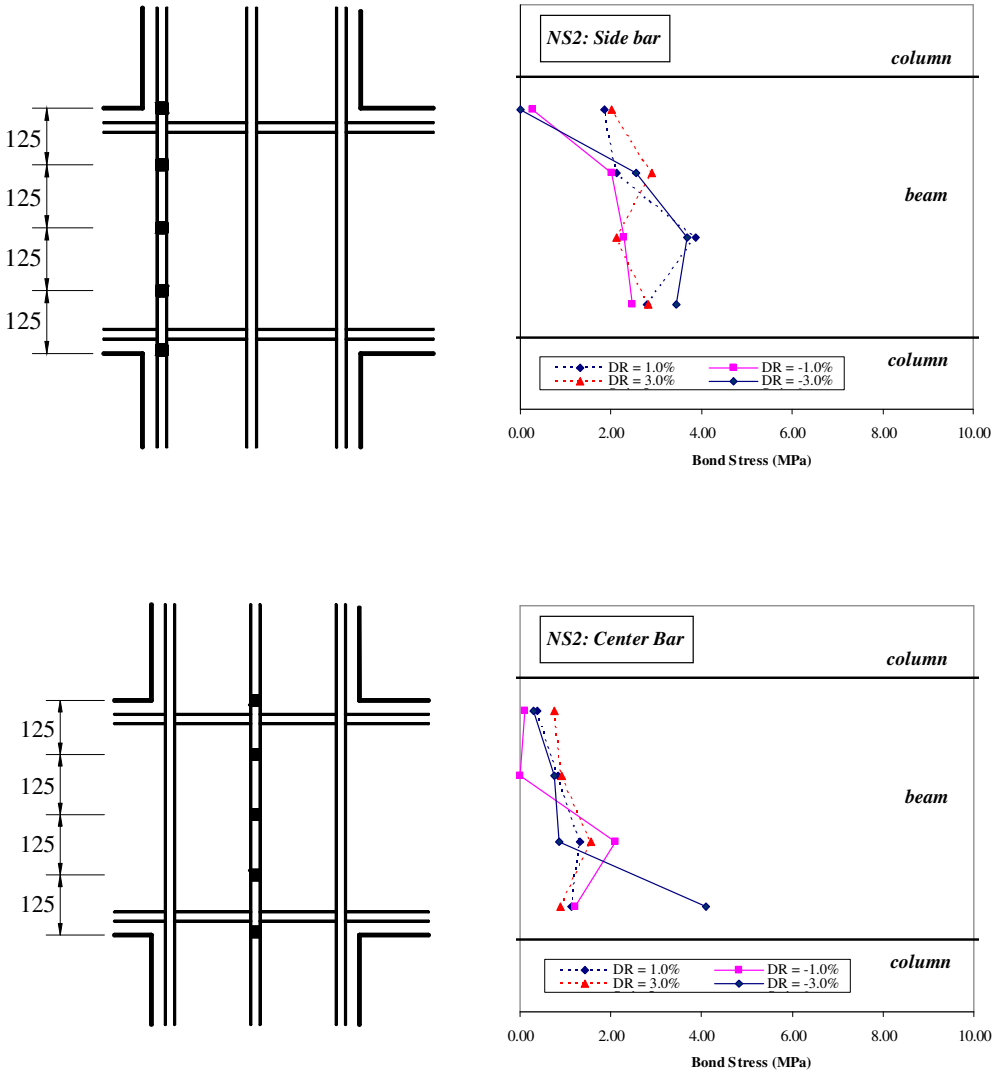

Figure 4.35 Bond Stress of Column Bar of NS2

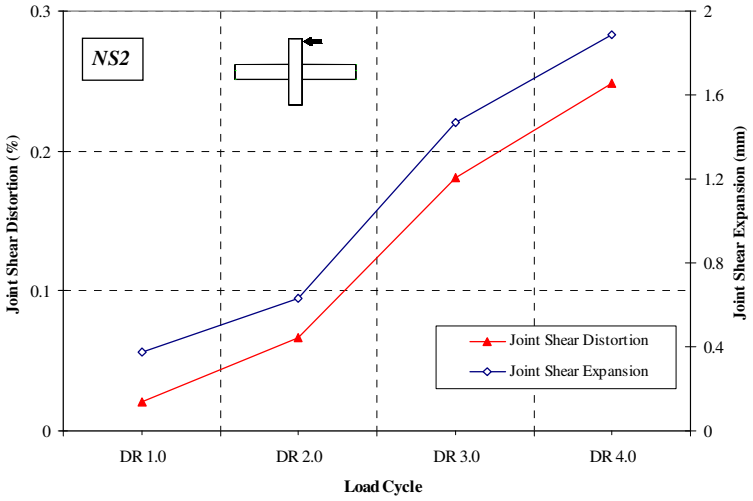

Figure 4.36 Joint Shear Distortion and Expansion of Specimen NS2

4.2.2 Specimen AS2

No crack was found on the column and joint core of AS2 due to the beneficial confinement effect of column axial compressive load. The column remained elastic throughout the test and cracks were mainly found on beams only. Spalling of concrete was noticed at the beam bottom suffix adjacent to column face. Good energy dissipation capacity was observed and AS2 generally behaved in a ductile manner.

4.2.2.1 General Observation

The column and joint core of AS2 stayed elastic throughout the test as explained in the final crack pattern in Figure 4.37. The cracks were mainly formed on beams which explained the energy dissipation contribution were mainly from beams. Due to the unequal beam bar area, concrete of beam bottom face was spalled. The slip of bottom bars was larger than the top bar where the bond condition of beam top was better than beam bottom. The concrete at bottom face was subjected to a large compression force than the concrete at top at the opposite corner when the flexural cracks at beam bottom were fully closed. Hence, spalling due to crushing was

noticed at the beam bottom of AS2. Bottom reinforcement and top reinforcement yielded at the end of test and while column reinforcement remained in elastic range.

Figure 4.37 Final Crack Pattern of AS2

Figure 4.38 elaborates the crack development of AS2 at the peak of storey drift ratio of 1.0% (DR 1%), 2.0% (DR 2%), 3.0% (DR 3%) and 4.0% (DR 4%). During DR 1%, initiation of flexural cracks caused by sagging and hogging moment was noticed on beams as shown in Figure 4.38 but no crack was observed at joint core area at this stage. In the subsequent loading stage of DR 2% and DR 3%, more flexural cracks were observed on beams and some cracks joined each other to form longer flexural cracks. Spalling of concrete took place at beam ends near to column face during DR 3%. At DR 4%, serious spalling of concrete was observed at the bottom surfaces of beam ends due to bond deterioration of beam reinforcement. The column and joint core of AS2 stayed elastic throughout the test and no crack was found in the end of test.

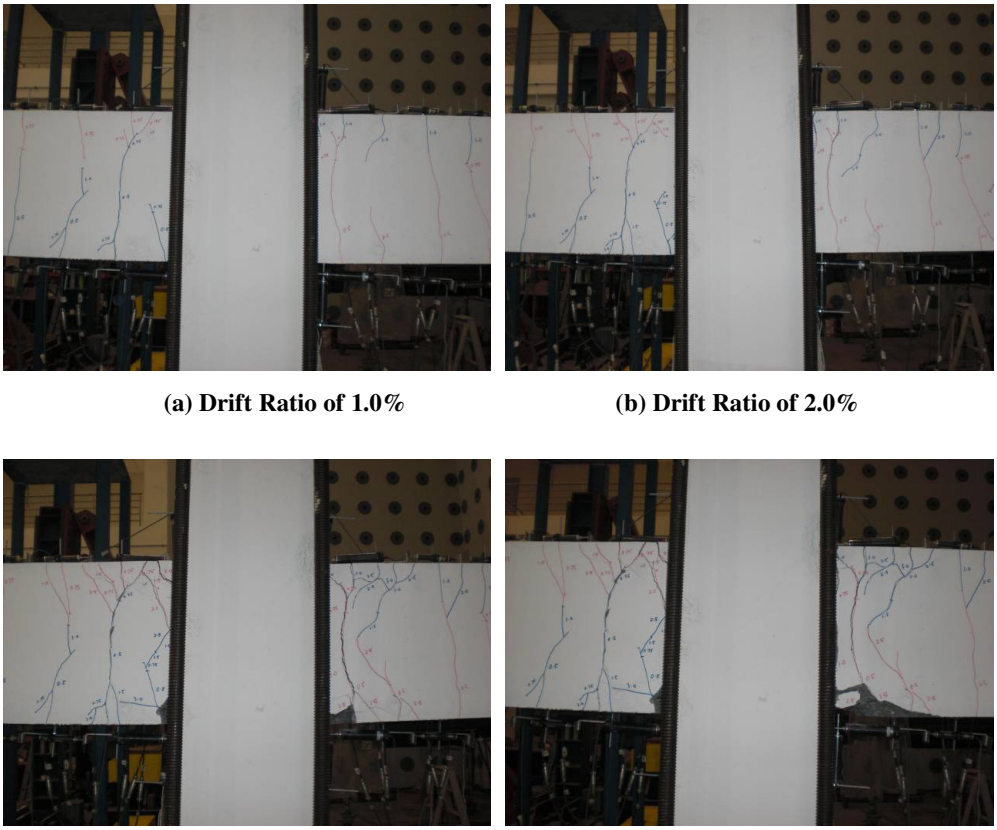

(a) Drift Ratio of 1.0% **(b) Drift Ratio of 2.0%**

(c) Drift Ratio of 3.0% **(d) Drift Ratio of 4.0%**

Figure 4.38 Progressive Cracking Development of AS2

4.2.2.2 Hysteretic Behaviour

The hysteretic behaviour of AS2 is explained in Figure 4.39 with the measured horizontal storey shear versus horizontal displacement hysteresis loops. The theoretical ideal storey horizontal load strength P_i as well as the theoretical stiffness K is included for comparison. AS2 exhibited high initial stiffness when the load was firstly applied till DR 1%. The maximum storey shear force was achieved at DR 2% and the deterioration in storey shear force happened after DR 3%. The shear strength in the end of test was around 70% of the maximum shear force at DR 2%. The energy dissipation capacity of AS2 was satisfactory with large area confined in the hysteresis loops. However, serious pinching was observed in the hysteresis loops when the test was stopped at DR 4% which indicated bond failure happened in beam reinforcement.

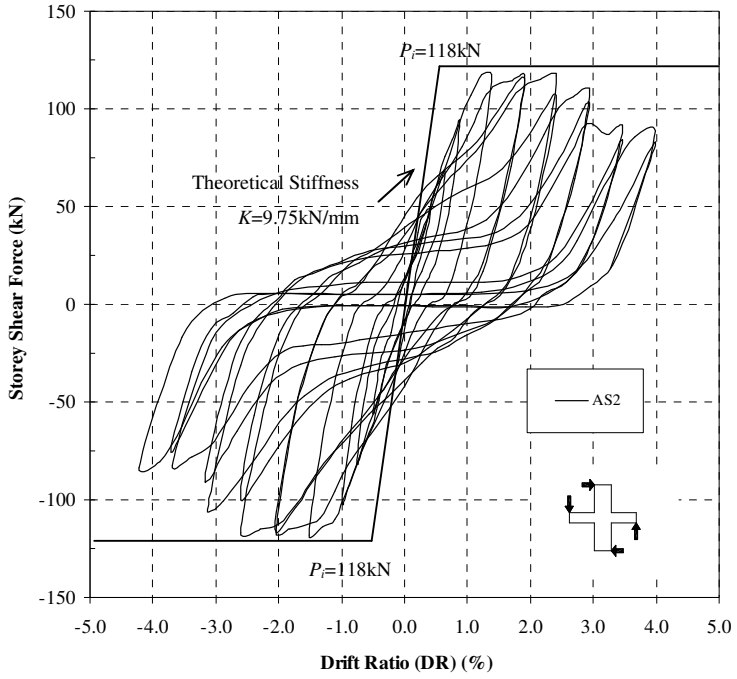

Figure 4.39 Storey Shear Force versus Horizontal Displacement for AS2

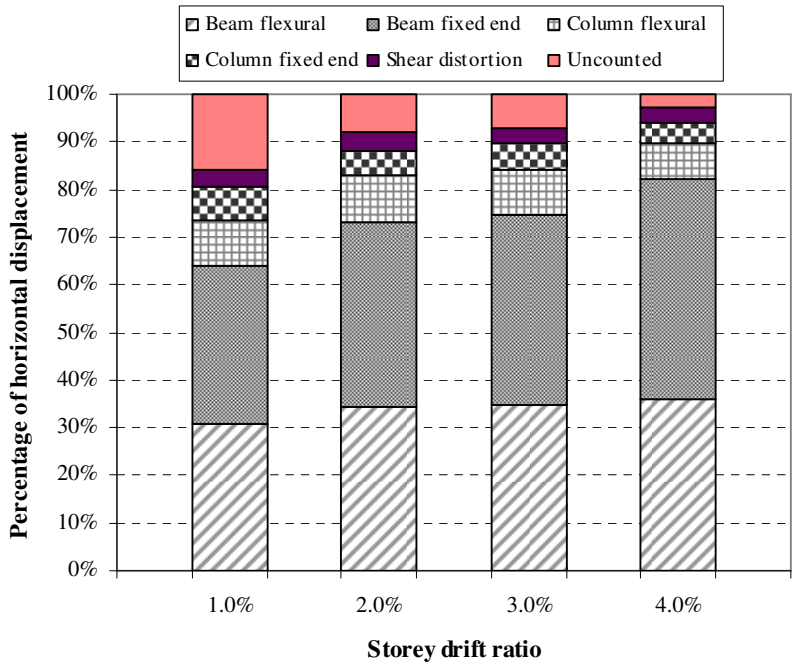

Figure 4.40 Decomposition of Horizontal Components of AS2

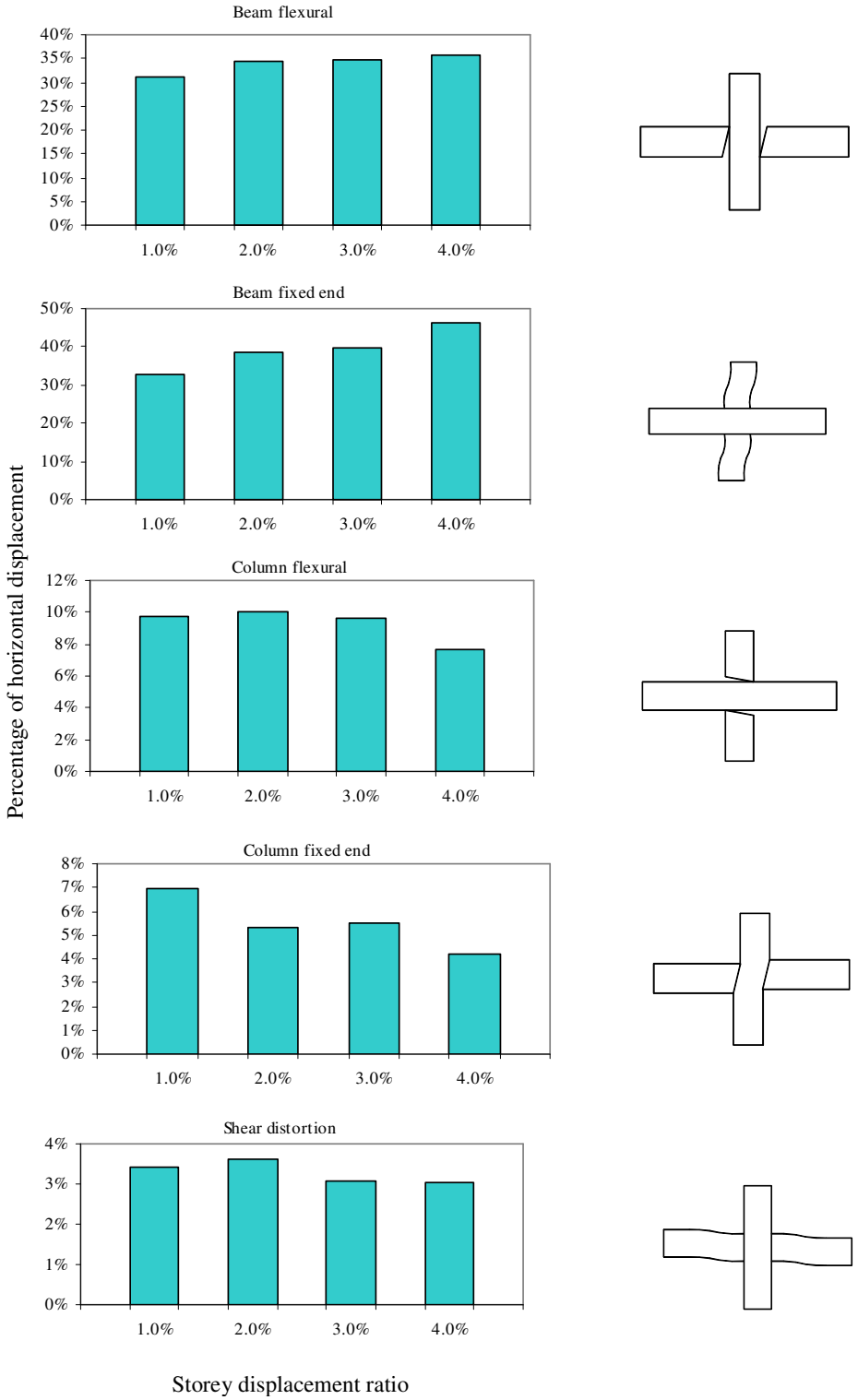

Figure 4.41 Contributions of Horizontal Components of AS2

4.2.2.3 Decomposition of Horizontal Displacement

Figure 4.40 shows the components of horizontal displacement measured for AS2 at the DR 1%, DR 2%, DR 3% and DR 4%. The contribution of uncounted component such as rigid body movement was significant in the early stage of test but greatly reduced in the end of test. As explained in Figure 4.41, the beam components have been the major contribution to the horizontal displacement measured for AS2**.** The contributions of beam flexure and beam fixed-end rotation were ranging from 31% to 36% and 33% to 46% respectively. The contributions of column flexure and column fixed-end rotation to the total drift were relatively small during the testing where the maximum contributions were 10% and 7%, respectively. As the joint core remained intact throughout the test, the contribution of joint shear distortion to horizontal displacement was the smallest at 3% only.

4.2.2.4 Beam Behaviour

The following sections discuss the evaluation of strains in beam reinforcement and beam curvatures:

Beam Reinforcement Strains

As explained in Figure 4.42, top beam reinforcement and bottom reinforcement of specimen AS2 has high strain in strain gauge readings in the initial loading stage of DR 1% near to the column face. The strain gauges at tension face almost reaching its yield strain while the strain of gauges at compression face was still relatively low. When DR 3% was attained, the strain measured along the tension face surpassed the yield strain. Strain gauges installed at the middle of the joint core showed low strain reading which explained the presence of good bond in joint core with the bar size used in both top and bottom reinforcement due to the confinement from applied column axial compressive load.

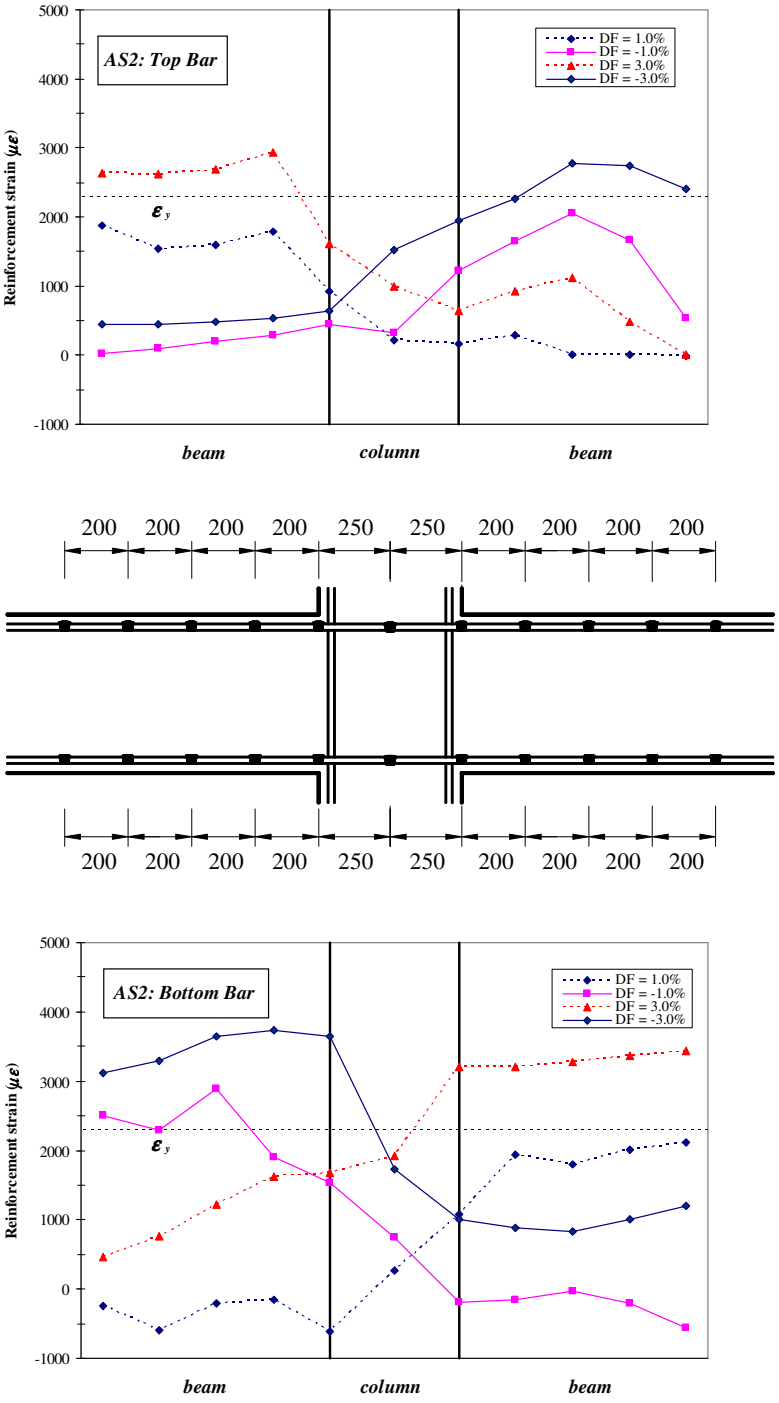

Figure 4.42 Strain Profiles of Beam Bars of AS2

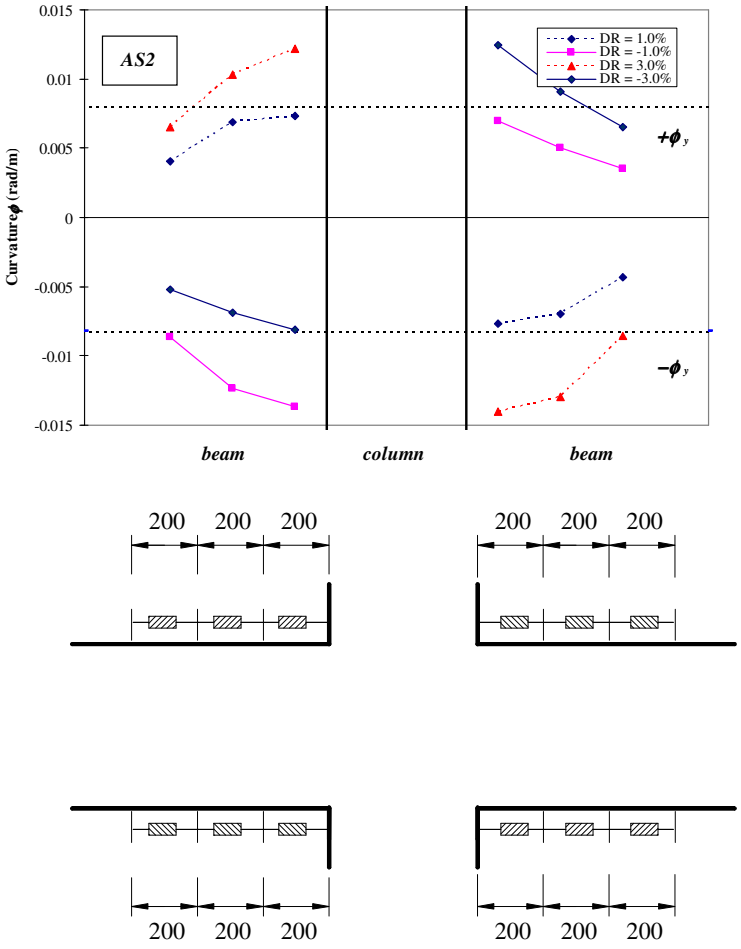

Figure 4.43 Curvature Distribution of Beam of AS2

Beam curvature

Figure 4.43 shows the beam curvature distributions estimated from the transducer readings. In the early loading stage of DR 1%, the beam curvature measured near the column face almost reached the theoretical yield curvature and in the subsequent loading cycles the curvature of the first two segments measured had surpassed its yield curvature limit. A similar situation was also observed in the negative loading cycles as the plastic hinges formed in the beam end near to column face.

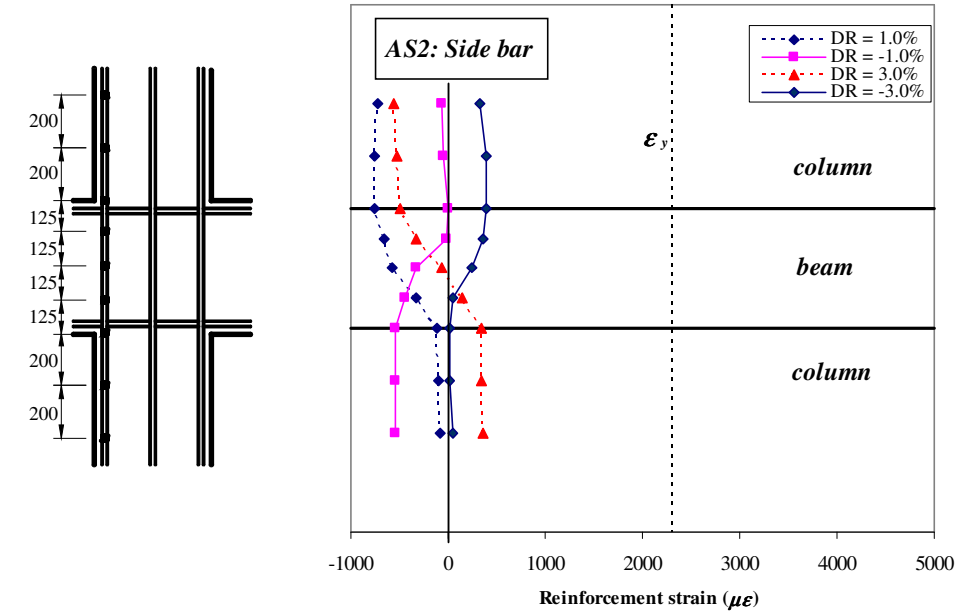

.

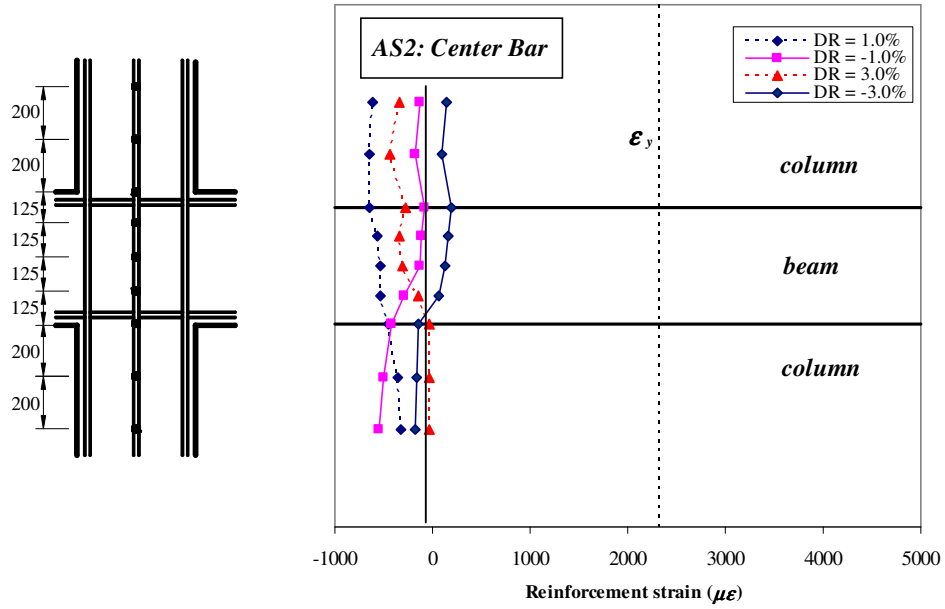

Figure 4.44 Strain Profiles of Column Bars of AS2

4.2.2.5 Column Behaviour

The evaluation of strains in column side reinforcement, column middle reinforcement and column curvatures are discussed in the following sections:

Column Reinforcement Strain

As shown in Figure 4.44, the column basically remained elastic throughout the test due to the confinement from column axial compressive load where the strains of column bar did not reach the yield strain. This is partially due to the confinement from the applied axial compressive load.

Column curvature distributions

Figure 4.45 shows the column curvature distributions where the respective curvatures increased gradually but no rapid increase was observed and the column was still in its elastic range.

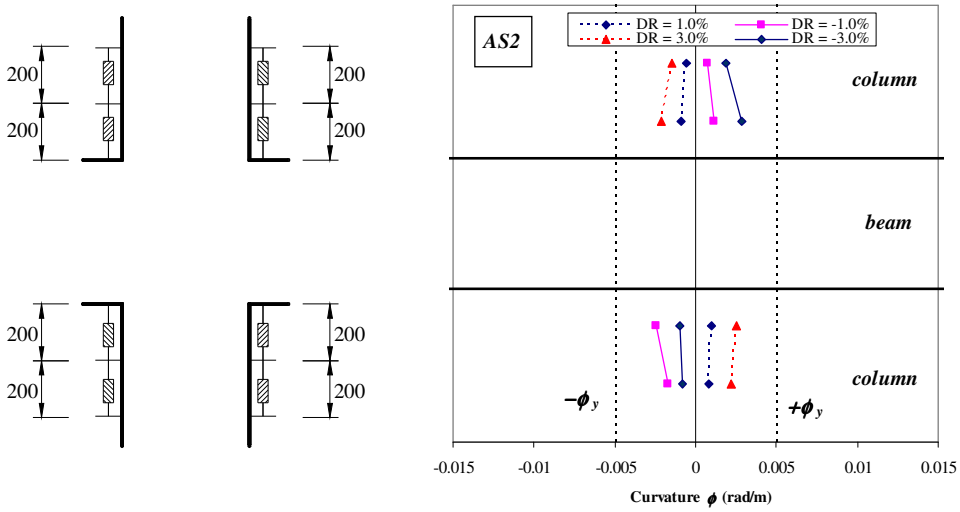

Figure 4.45 Curvature Distribution of Column of AS2

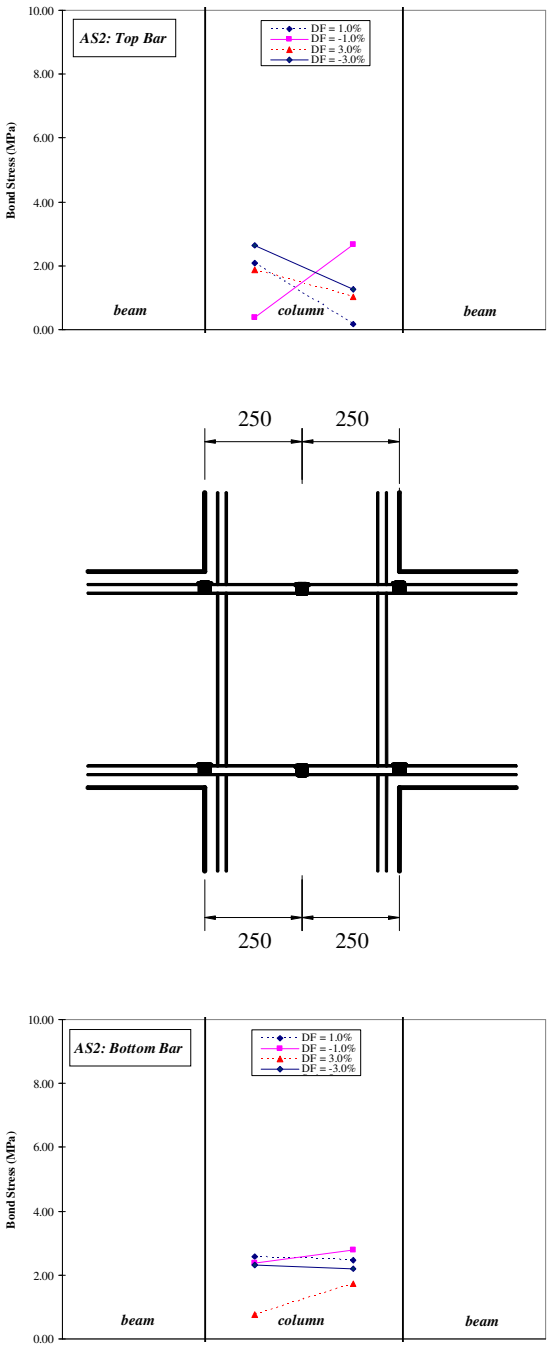

Figure 4.46 Bond Stress of Beam Bar of AS2

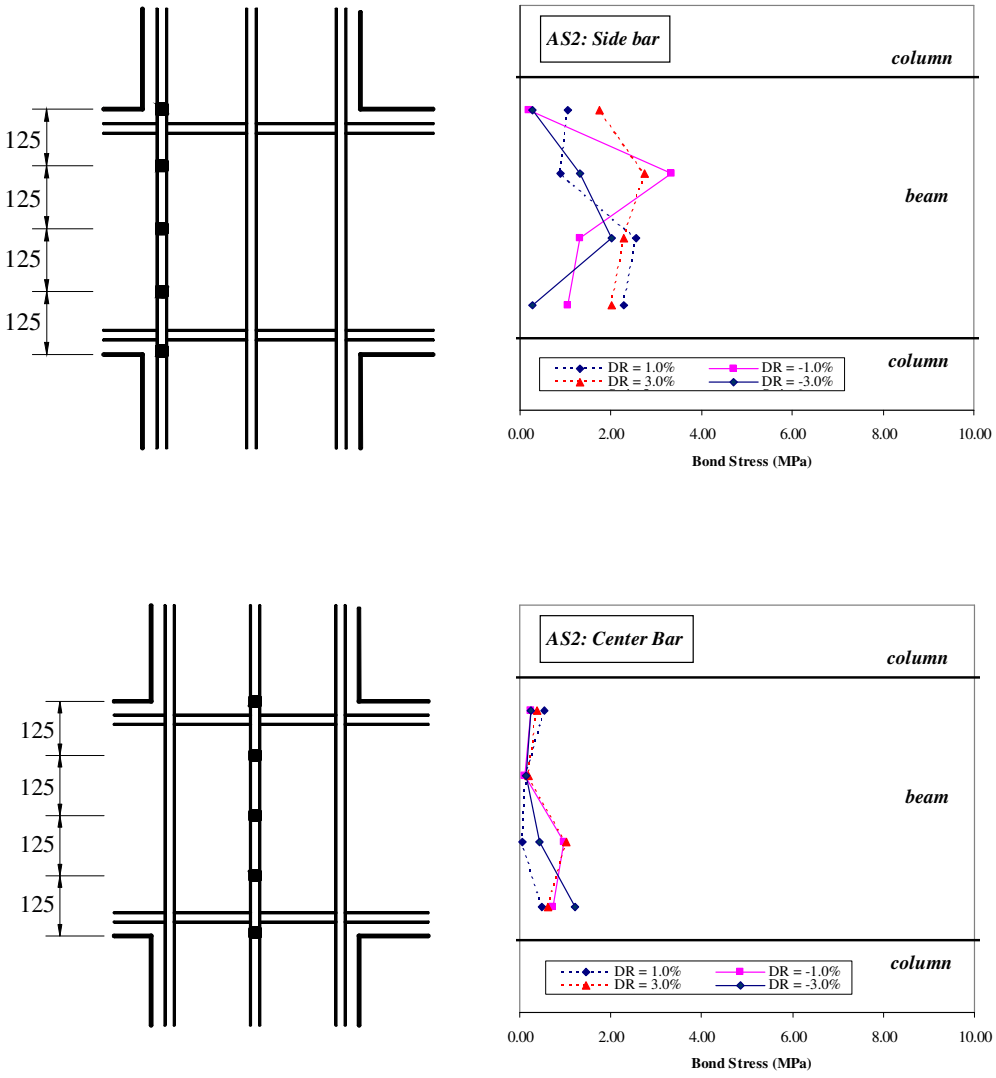

Figure 4.47 Bond Stress of Column Bar of AS2

4.2.2.6 Joint Behaviour

The joint behaviour discussion shall cover bond stress of beam and column reinforcement, joint shear distortion and joint shear expansion:

General Behaviour

Due to the confinement effect from from the applied column axial compressive loading, no crack was found on the joint core of AS2 throughout the test (see Figure

4.38a to Figure 4.38d). The maximum nominal horizontal shear stress was 4.59MPa or 0.075 $f_c^{'}$ was observed which met the requirement in NZS 3101.

Bond Stresses of Beam and Column Reinforcement Bars in Joint Core

The average bond stresses for beam bars and column bars are shown in Figure 4.46 and Figure 4.47 respectively. The maximum bond stress obtained along top beam bars was 2.68 MPa (=0.044 $f_c^{'}$) while the maximum bond stress observed along bottom beam bars was 2.78 MPa (=0.046 $f_c^{'}$). Some bond deterioration was noticed in bottom beam bars where bond stresses decreased in the end of test. On the other hand, the maximum bond stress of 3.34 MPa (=0.055 $f_c^{'}$) and 1.22 MPa (=0.020 $f_c^{'}$) was oberved on column side bar and columncentre bar, respectively. The column reinforcement remained elastic in the end of the test.

Joint Shear Distortion and Joint Shear Expension

The joint shear distortion and expansion was initiated in the loading stage of DR 1% as explained in Figure 4.48. Both the joint shear distortion and expansion increased rapidly in the loading from DR 2% to DR 3%. In the final loading stage of DR 4%, the maximum joint distortion was 0.12% and the maximum joint expansion 1.41 mm, respectively.

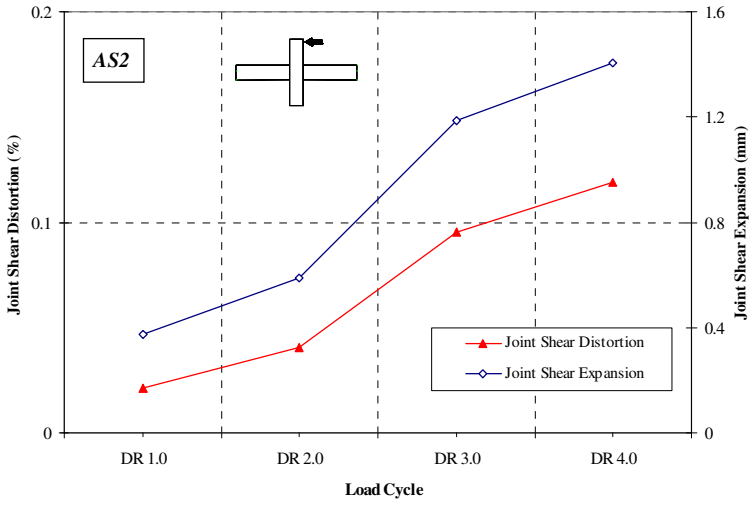

Figure 4.48 Joint Shear Distortion and Expansion of Specimen AS2

4.3 Test Result of Group Three (NS3 and AS3)

Group Three consists of specimens NS3 and AS3 with which was made of larger beam bars and larger column bars as explained in Chapter 3. Similarly, NS3 was tested without column axial compressive loading while AS3 was tested with column axial compressive loading of $0.3f_c'A_c$. The typical features of these specimens are summarised as follows:

- beam reinforcement size of was 33% larger than specimens NS1 (16mm for NS3 and 12mm for NS1)
- equal beam bottom reinforcement and top reinforcement area
- actual maximum beam-bar-to-column-depth = 1/28.13
- actual column-bar-to-beam-depth = 1/15.63
- calculated maximum beam-bar-to-column-depth based on Eq. 7-13 in NZS 3101 :

  NS3= 1/24.74 AS3= 1/24.74
- calculated maximum column-bar-to-beam-depth based on clause 7.5.3.4 in NZS 3101:

  NS3= 1/16.33 AS3= 1/16.33
- NS3 and AS3 only met the requirement of maximum beam-bar-to-column-depth and did not meet the requirement of maximum column-bar-to-beam-depth set in NZS 3101
- Joint core reinforcement detailing complied with the requirement in clause 7.5.3.4 in NZS 3101 (maximum bar spacing = 70mm, allowable bar spacing = 100mm)

The following sections report the test result of these two specimens.

4.3.1 Specimen NS3

Even though NS3 was made of larger bar compared to NS1, it showed satisfactory ductile behaviour throughout the test. The energy dissipation of NS3 was good with high ultimate load attained. The reinforcement of beam was yielded in the end of test. Due to the use of larger beam diameter, splitting bond failure was found and the beam overall height near to column face was found to be slightly expended.

4.3.1.1 General Observation

Figure 4.49 shows the final crack pattern of Specimen NS3 which was made of larger bar with equal top and bottom beam reinforcement area. The energy dissipation capacity was good and consistent throughout the test. Although NS3 did not meet the column bar bond development requirement in NZS3101, no failure was found at column while the major cracks observed were flexural cracks on the beams top and beam bottom. As depicted in Figure 4.49, cracks at joint core spanned across diagonal corners of the joint panel and the formation of concrete compressive strut was noticed. Both the beam top and bottom reinforcement yielded at the end of test and while the column reinforcement remained in elastic range.

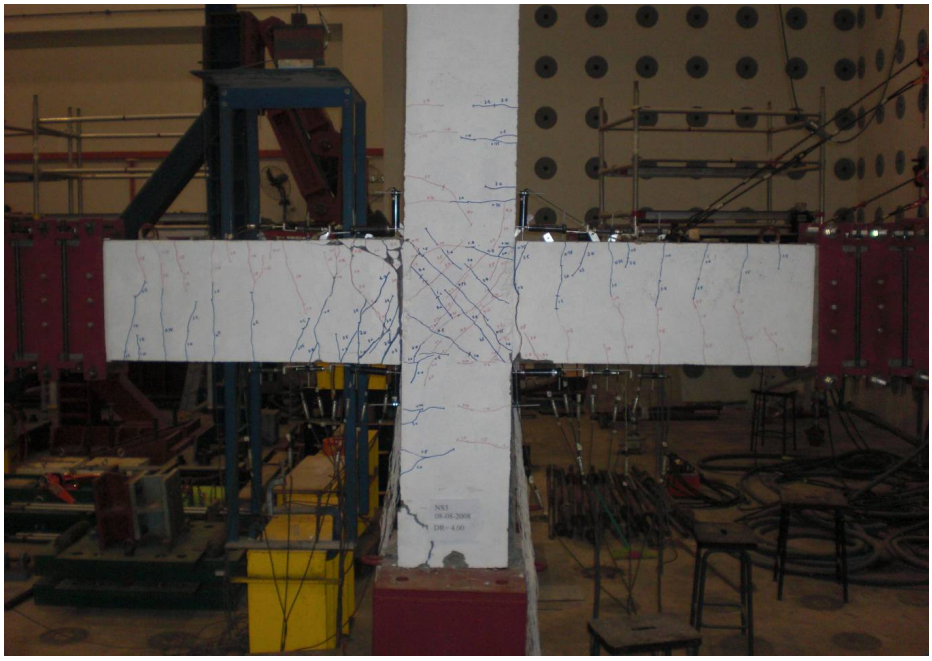

Figure 4.49 Final Crack Pattern of NS3

The crack development of NS3 is at the peak of storey displacement ratio of 1.0% (DR 1%), 2.0% (DR 2%), 3.0% (DR 3%) and 4.0% (DR 4%) are explained Figure 4.50. When DR 1% was attained, the flexural cracks caused by sagging and hogging moment were first observed on top and bottom surface of beams. Besides that, few diagonal cracks were noticed at joint core area which formed the concrete compression strut of the joint core in the later stage. More flexural cracks were

observed at beam while the formation of compressive strut at joint core was significant with more diagonal shear cracks formed and intersected when DR 2% was reached. No new crack was observed when loading stage DR 3% was surpassed. At the final loading stage DR 4%, spalling of concrete was observed at beam end due to excessive buckling of beam reinforcement which caused the distortion of beam depth.

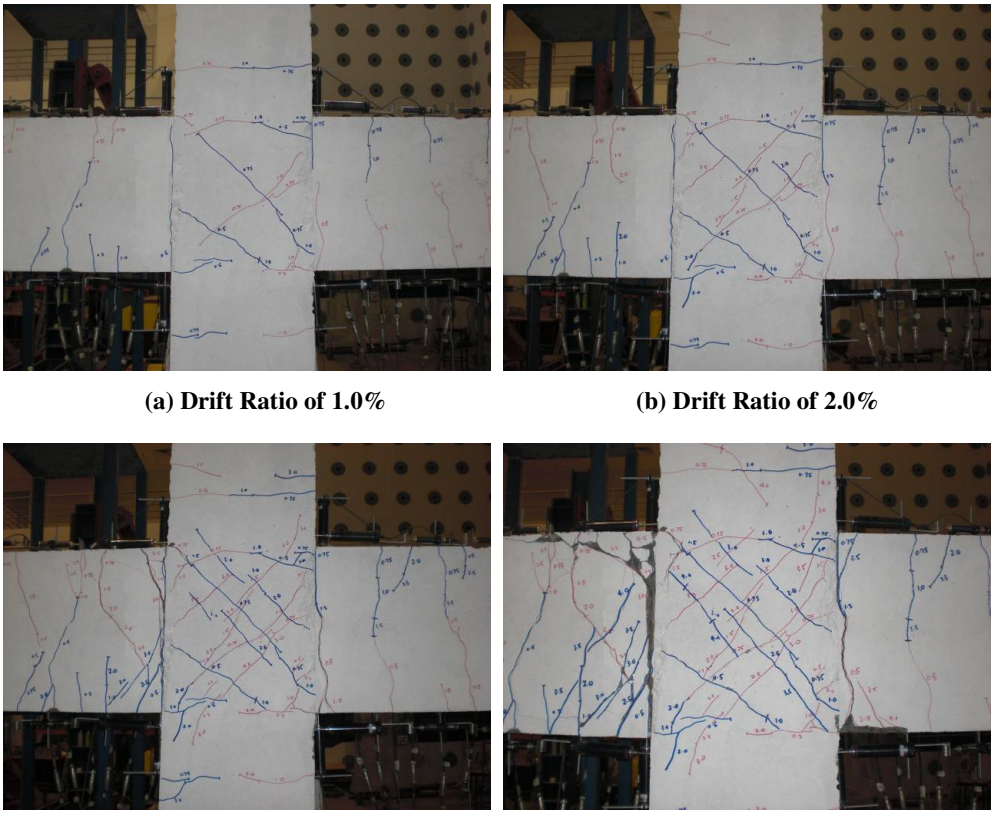

(a) Drift Ratio of 1.0% **(b) Drift Ratio of 2.0%**

(c) Drift Ratio of 3.0% **(d) Drift Ratio of 4.0%**

Figure 4.50 Progressive Cracking Development of NS3

4.3.1.2 Hysteretic Behaviour

Figure 4.51 shows the measured horizontal storey shear versus horizontal displacement hysteresis loops of NS3. For comparison, the theoretical ideal storey horizontal load strength P_i and the theoretical stiffness K are also shown in Figure 4.51. The stiffness and strength developed steadily when the load was applied from beginning until DR 4%. Although NS3 was made of larger beam bar reinforcement, bond failure did not happen in the end of the test. This is explained in the hysteresis loops as pinching was not observed even though cracks were mainly formed in the beams. The maximum horizontal storey shear was achieved at DR 2% and the strength of specimen was maintained at the maximum when the test was halt. With the good energy dissipation in NS3, the use of larger beam bar in high strength concrete beam-column joint is possible.

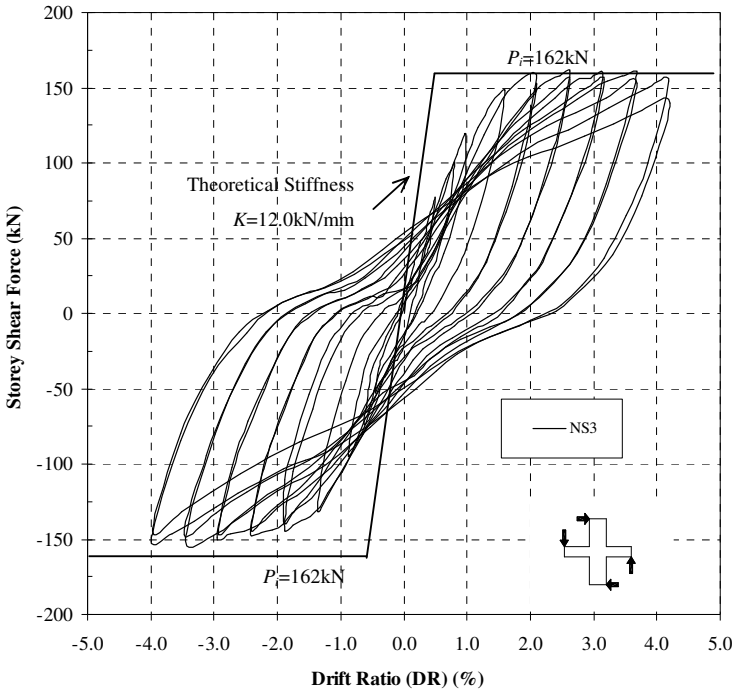

Figure 4.51 Storey Shear Force versus Horizontal Displacement for NS3

4.3.1.3 Decomposition of Horizontal Displacement

Figure 4.52 and Figure 4.53 explain the contribution of each component of the horizontal displacement measured for NS3 at the peak of DR 1%, DR 2%, DR 3% and DR 4%. From the test results, it is noticed that the beam displacement has been the main control in the storey drift. The contributions of beam flexure and beam fixed-end rotation ranged from 33% to 38% and 18% to 22%, respectively. On the other hand, the column has less influence on the story drift where the maximum contributions of column flexure and fixed-end rotation were 14% and 16% respectively. The contribution of the displacement due to joint shear distortion remained constant in the test while the contribution of uncounted component such was significantly reduced in the end of test.

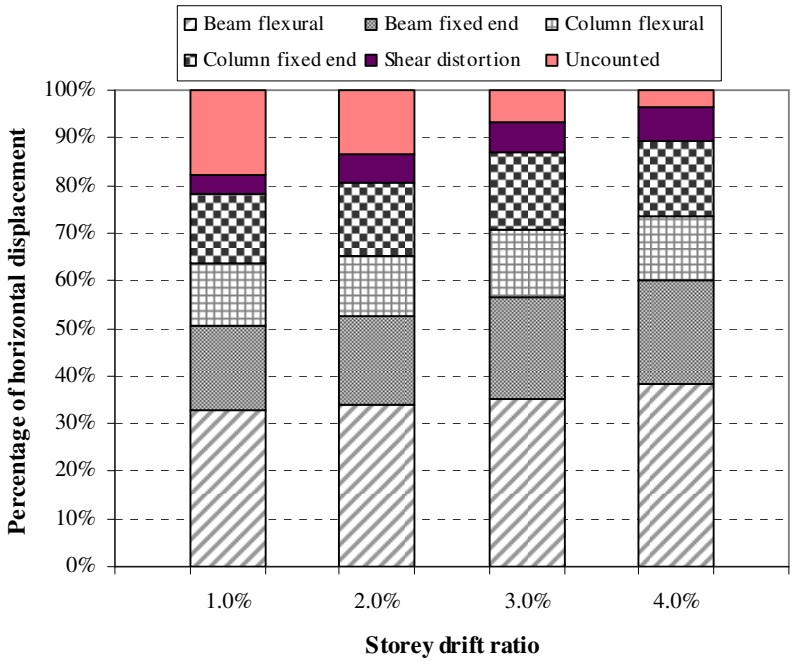

Figure 4.52 Decomposition of Horizontal Components of NS3

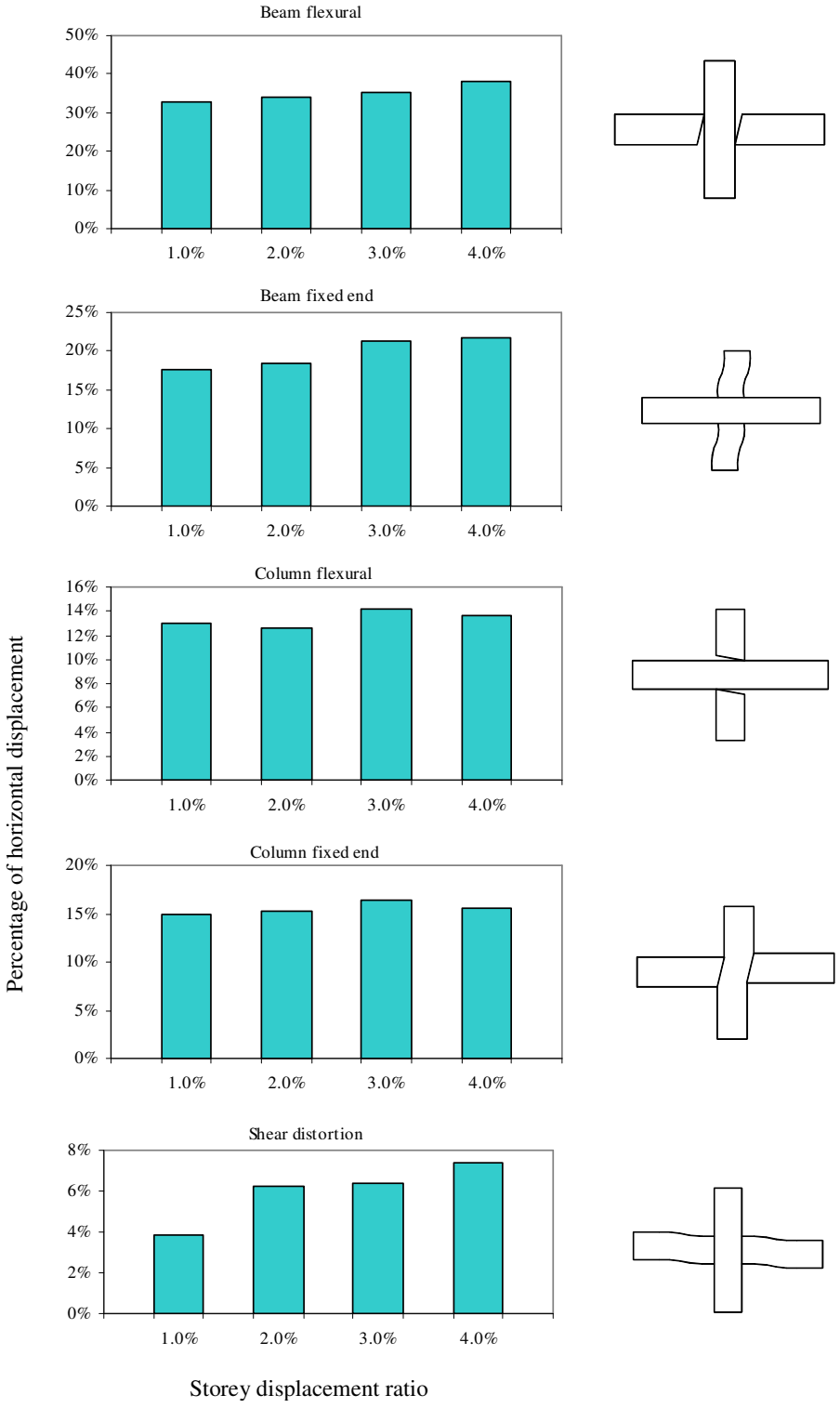

Figure 4.53 Contributions of Horizontal Components of NS3

4.3.1.4 Beam Behaviour

The following section demostrates the evaluation of strains in beam reinforcement and beam curvatures:

Beam Reinforcement Strains

Figure 4.54 depicts the strain profiles of the top and bottom beam reinforcement of NS3. Yielding of top beam reinforcement and bottom reinforcement near the column face was noticed at DR 3%. The strain measured along the joint core was well below its yield strain which confirmed the presence of good bond in joint core even though large bar size was used in both top and bottom reinforcement.

Beam curvature

The beam curvature distributions estimated from the transducer readings is explained in Figure 4.55. The beam curvature was below its theoretical yield curvatures at DR 1%. With the development of plastic hinge at beam near to column face, the measured beam curvature was above its theoretical yield curvatures at DR 3%.

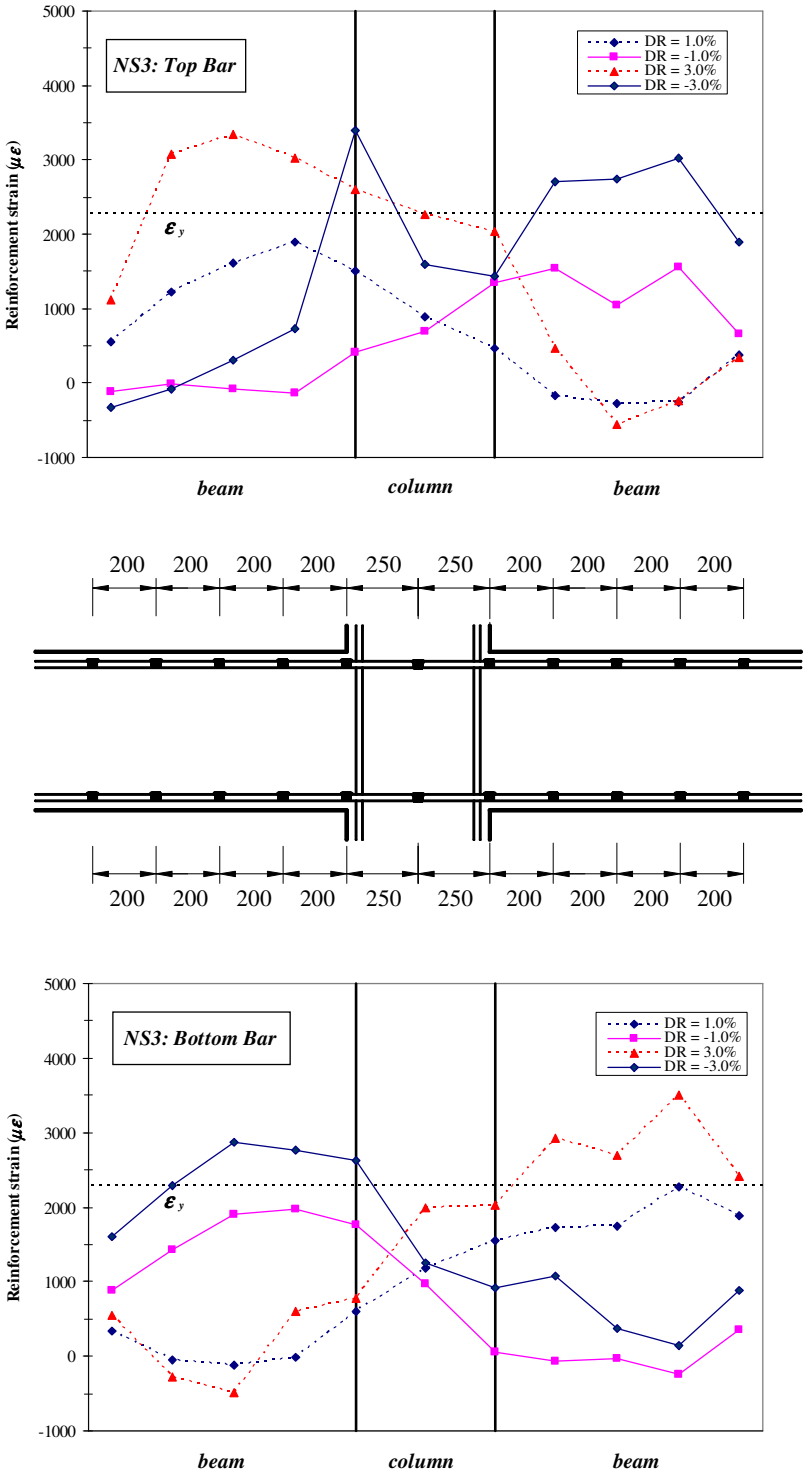

Figure 4.54 Strain Profiles of Beam Bars of NS3

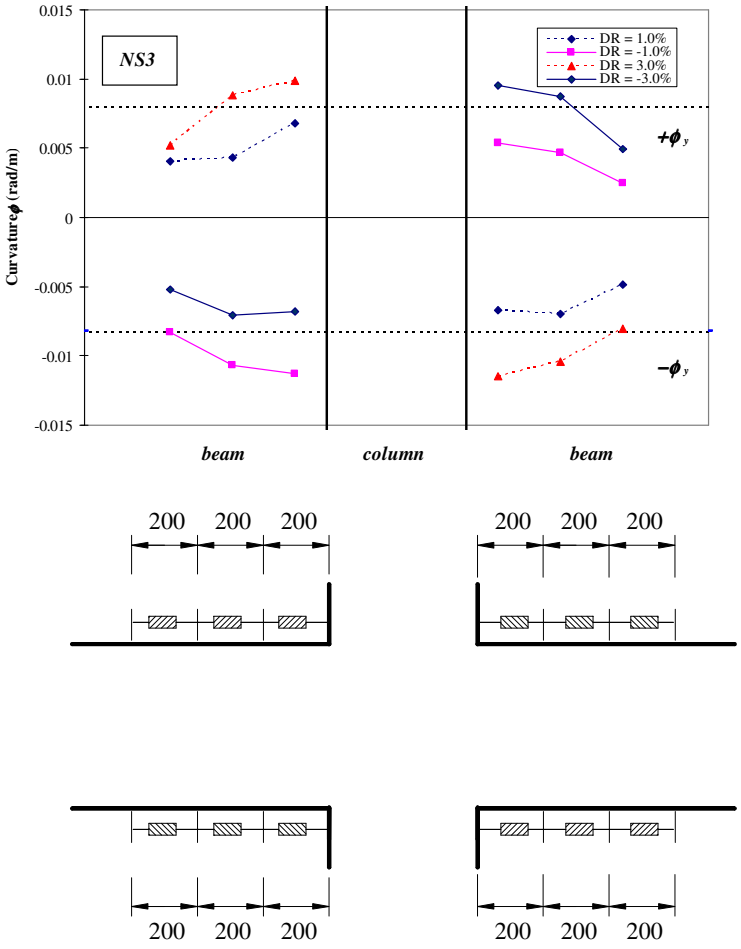

Figure 4.55 Curvature Distribution of Beam of NS3

4.3.1.5 Column Behaviour

The strains in column side reinforcement, column middle reinforcement and column curvatures are addressed as below:

Column Reinforcement Strain

As explained in Figure 4.56, the gauged column reinforcement shows no sign of yielding where the measured strains are well below its yielding strain limit. The strains increase gradually as horizontal force was applied but the gauged reinforcement was elastic when the test reached the maximum.

Column curvature distributions

Figure 4.57 shows the column curvature distributions based on the measured readings by LVDT installed along the column. The curvatures measured at the upper column were slightly larger than those at the lower column but none of the measurement exceeded the theoritical yield curvature limit. The measured curvatures have confirmed the behaviour of the column was still in its elastic range.

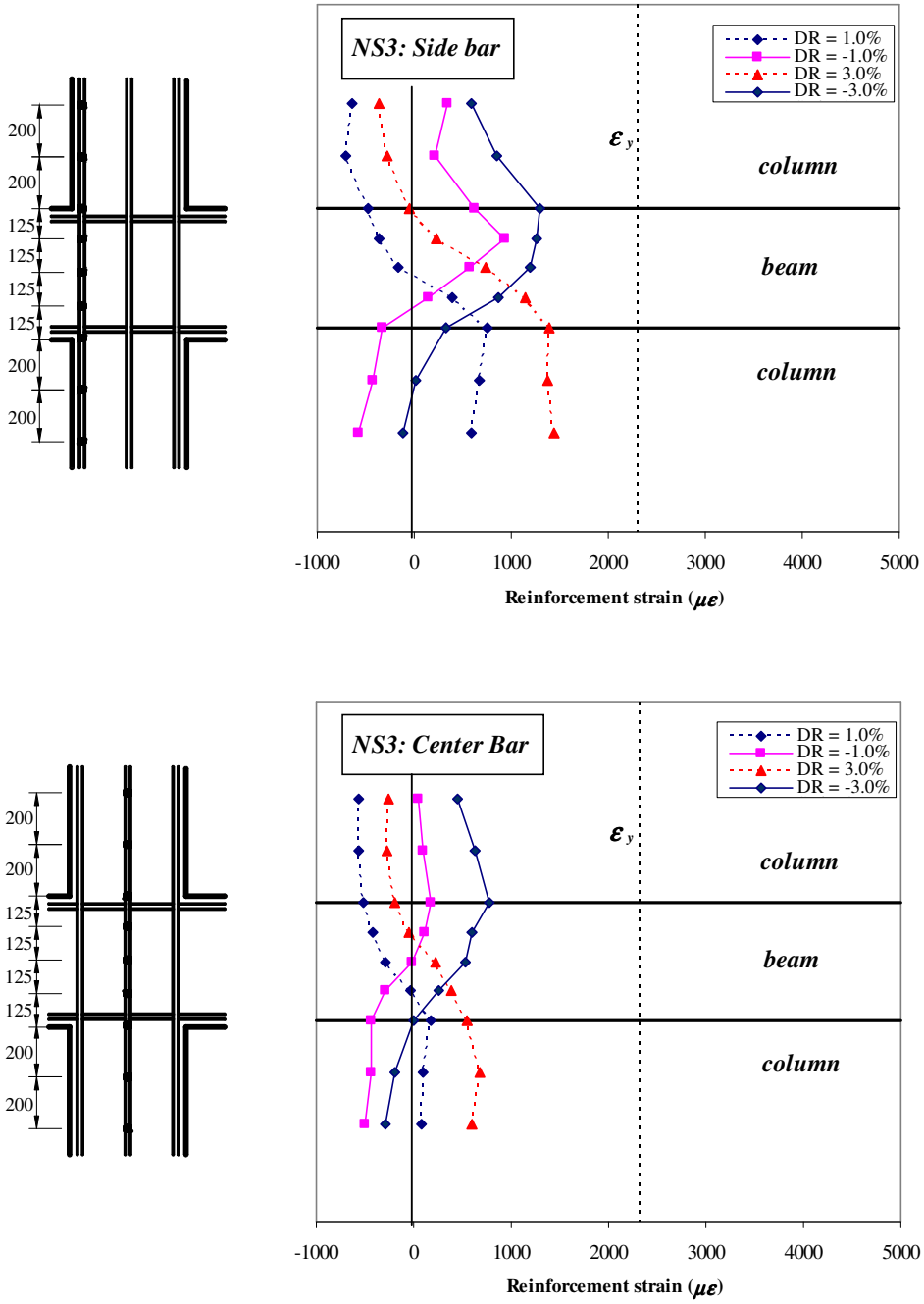

Figure 4.56 Strain Profiles of Column Bars of NS3

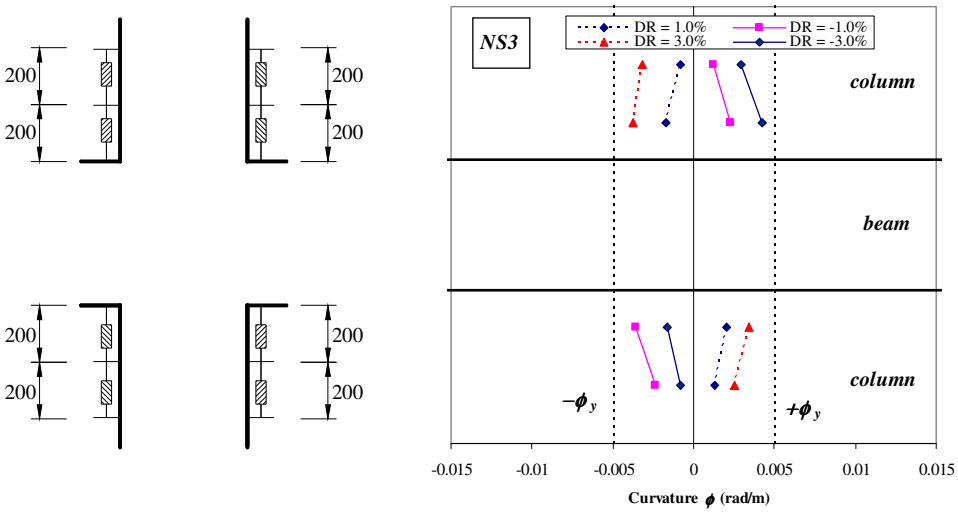

Figure 4.57 Curvature Distribution of Column of NS3

4.3.1.6 Joint Behaviour

The discussion on joint behaviour in the following sections cover the evaluation of bond stress of beam reinforcement and column reinforcement, joint shear distortion and joint shear expansion.

General Behaviour

Initial diagonal tension cracks were observed during DR 1% (see Figure 4.50a). In the subsequent loading cycles, more cracks appeared on joint core and propagated rapidly (see Figure 4.50b to Figure 4.50d). A maximum nominal horizontal shear stress of 6.31MPa or 0.103 $f_c^{'}$ was observed. The strength and stiffness degradation was observed when the test was completed.

Bond Stresses of Beam and Column Reinforcement Bars in Joint Core

The average bond stresses obtained are plotted in Figure 4.58 for beam bars and Figure 4.59 for column bars. The maximum bond stress obtained along top beam bars and bottom beam bars was 3.62 MPa (=0.059 $f_c^{'}$) and 4.99 MPa (=0.082 $f_c^{'}$), respectively. Bond deterioration was obvious in both top and bottom beam bars

where bond stresses decreased rapidly in the end of test. On the other hand, the column reinforcement remained elastic in the end of the test with maximum bond stress of 5.90 MPa (=0.097 $f_c^{'}$) on side bar and maximum bond stress of 1.66 MPa (=0.027 $f_c^{'}$) on centre bar, respectively.

Joint Shear Distortion and Joint Shear Expension

Figure 4.60 depicts the measured joint shear distortion and expansion based on instrumentation in joint core. Generally, the development of joint shear distortion and joint shear expension was rapid in the test from DR 1% to DR 4%. The maximum joint distortion was 0.21% and the maximum joint expansion was 1.64 mm, as measured in Figure 4.60.

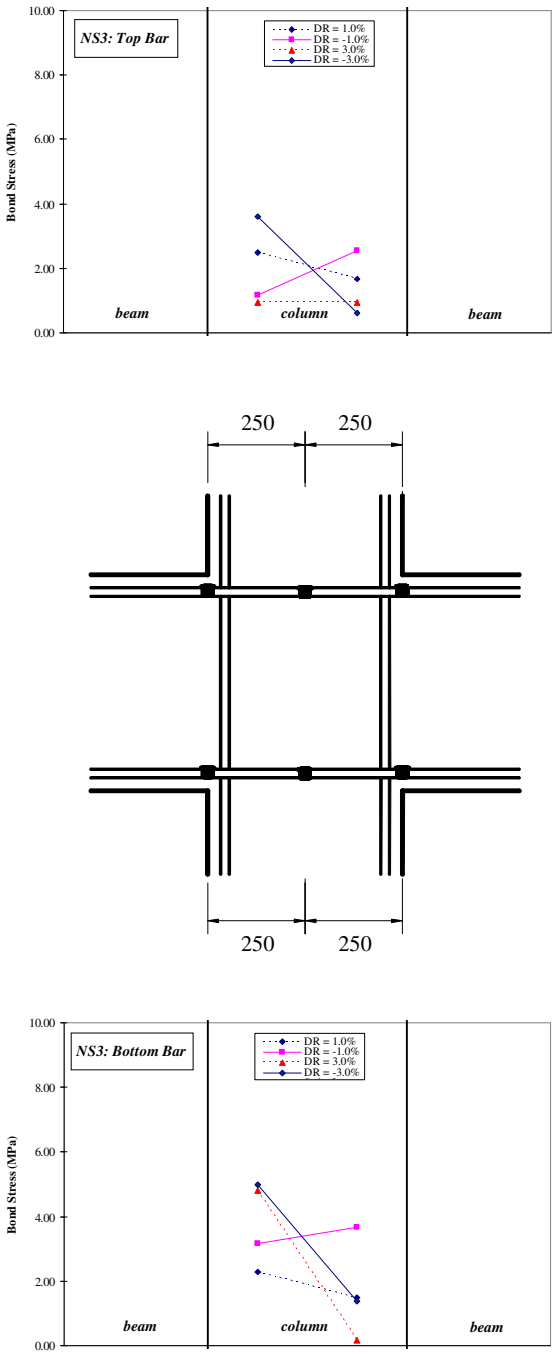

Figure 4.58 Bond Stress of Beam Bar of NS3

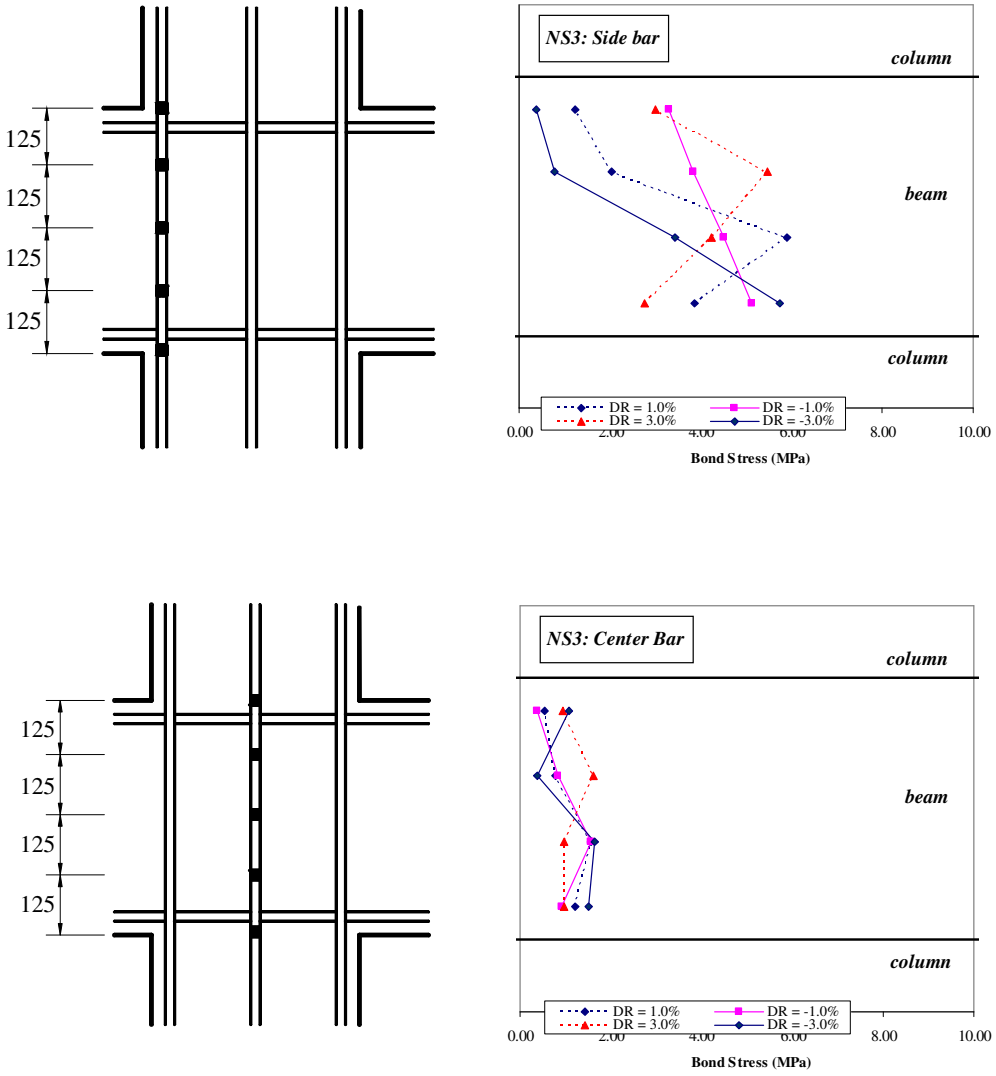

Figure 4.59 Bond Stress of Column Bar of NS3

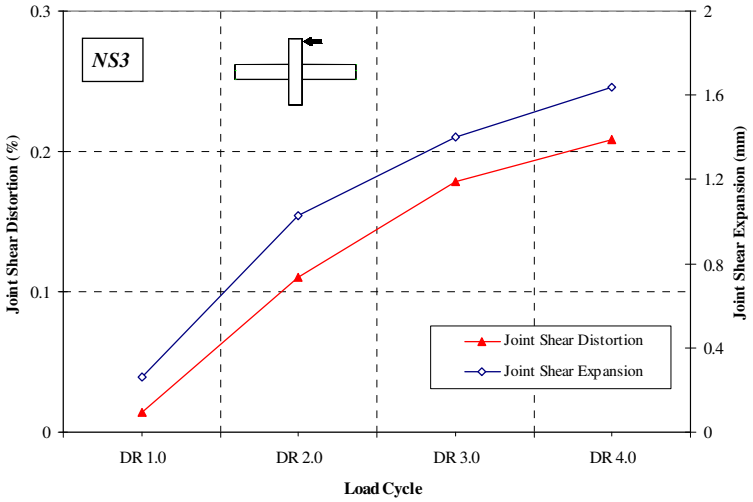

Figure 4.60 Joint Shear Distortion and Expansion of Specimen NS3

4.3.2 Specimen AS3

The energy dissipation of AS3 was good and exhibited ductile behaviour throughout the test. With the beneficial confinement effect of column axial compressive load, the column of AS3 remained elastic throughout the test with no crack was found on the column. Cracks were mainly found on beams and some cracks occurred on joint core panel. Similar to NS3, splitting bond failure was found with the beam near to column slightly expended.

4.3.2.1 General Observation

The final crack pattern of AS3 is shown in Figure 4.61. The major cracks formation was concentrated at the beam and joint core. No crack was detected on the column and its column remained elastic throughout the test due to the confinement by applied column axial loading. Noteworthy that the diagonal cracks formed on joint core panel was relatively steeper than its AS3 tested without column axial compressive load. AS3 exhibited good energy dissipation capacity in general and the major energy dissipation was contributed by beams with the excessive cracks developed at beams. The cracks were mainly formed on beams which explained the energy dissipation contribution were mainly from beams. Both beam top

reinforcement and beam bottom reinforcement were found to yield in the end of test which the column remained elastic in the end of test.

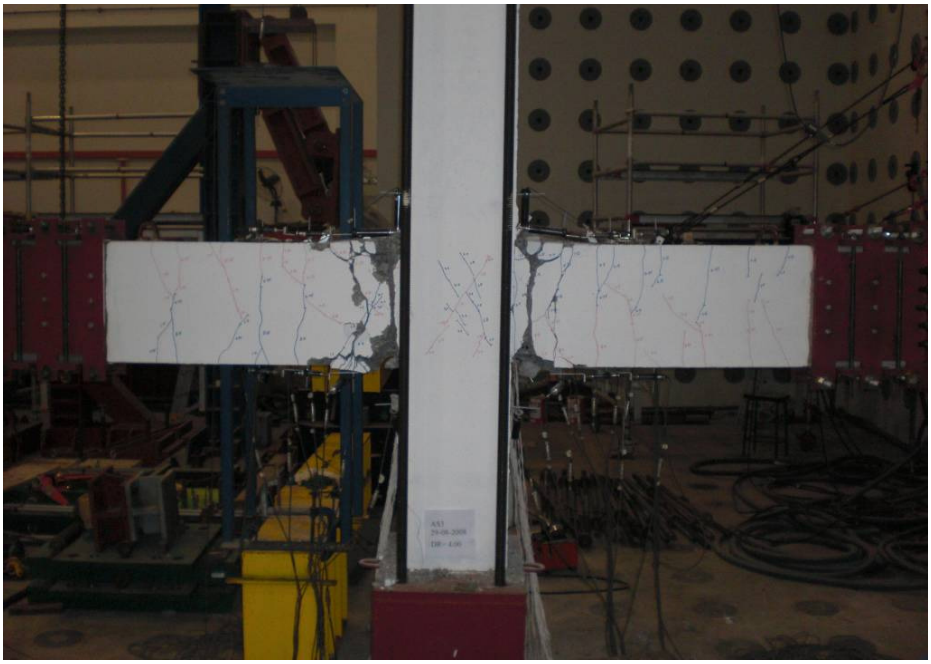

Figure 4.61 Final Crack Pattern of AS3

The crack development of AS3 at the peak of storey drift ratio of 1.0% (DR 1%), 2.0% (DR 2%), 3.0% (DR 3%) and 4.0% (DR 4%) is depicted in Figure 4.62. The flexural cracks on beam was noticed when DR 1% was reached, as shown in Figure 4.62. Few diagonal cracks were formed at joint core area at this stage but with a relatively steeper angle as compared to NS3. The formation of compressive strut at joint core was significant during the subsequent loading stage of DR 2% and DR 3%. More flexural cracks were observed on beams until after DR 3% was reached. At DR 4%, spalling started to take place at beam ends near to column. The spalling was getting more serious in the end of test which was caused by the bond deterioration of beam reinforcement.

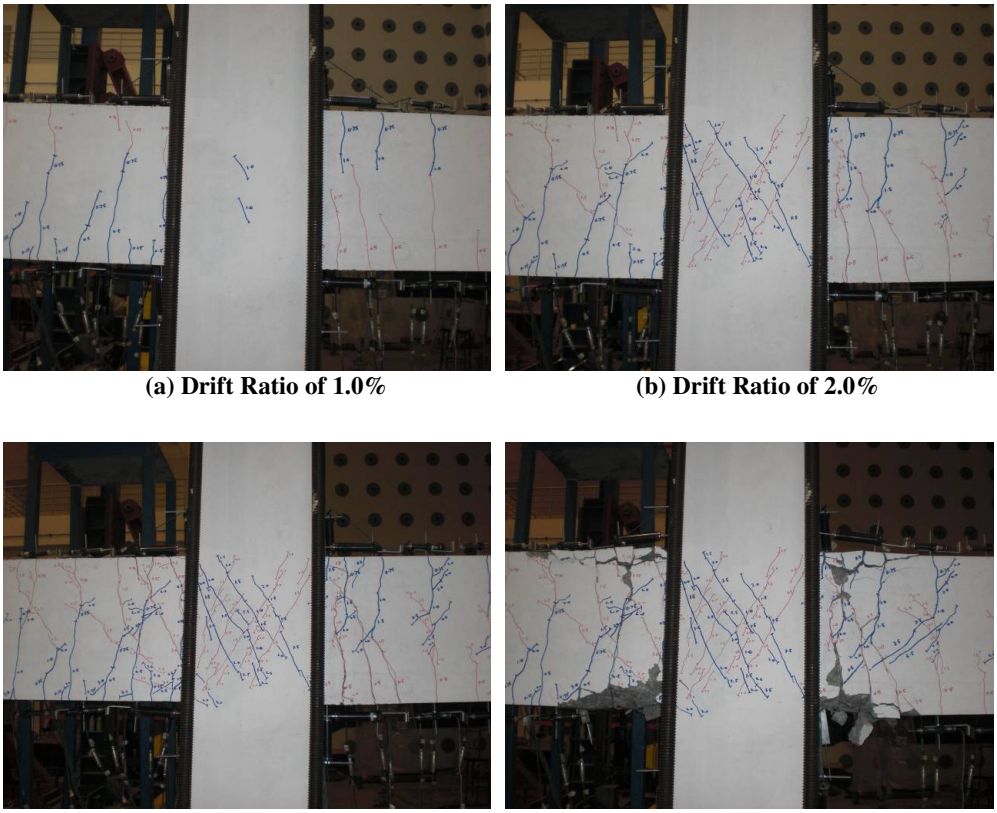

(a) Drift Ratio of 1.0% **(b) Drift Ratio of 2.0%**

(c) Drift Ratio of 3.0% **(d) Drift Ratio of 4.0%**

Figure 4.62 Progressive Cracking Development of AS3

4.3.2.2 Hysteretic Behaviour

Figure 4.63 shows the hysteresis loop which elaborates the hysteretic behaviour of AS3. With the large and stable enclosed areas of the loops, Specimen AS3 exhibited satisfactory energy dissipation capacity. Similar to AS1, no pinching was found in the loops throughout the test which explains no bond slip failure was observed in AS3. The maximum load was reached at DR 2% where yielding of the reinforcement started. Its maximum storey shear force begun to drop after DR 3% and a drop of 25% of strength as compared to its maximum was noticed when the test was ended at DR 4%. The hysteretic behaviour of AS3 indicated the possible of use of larger beam reinforcement in beam of high strength concrete beam-column joint.

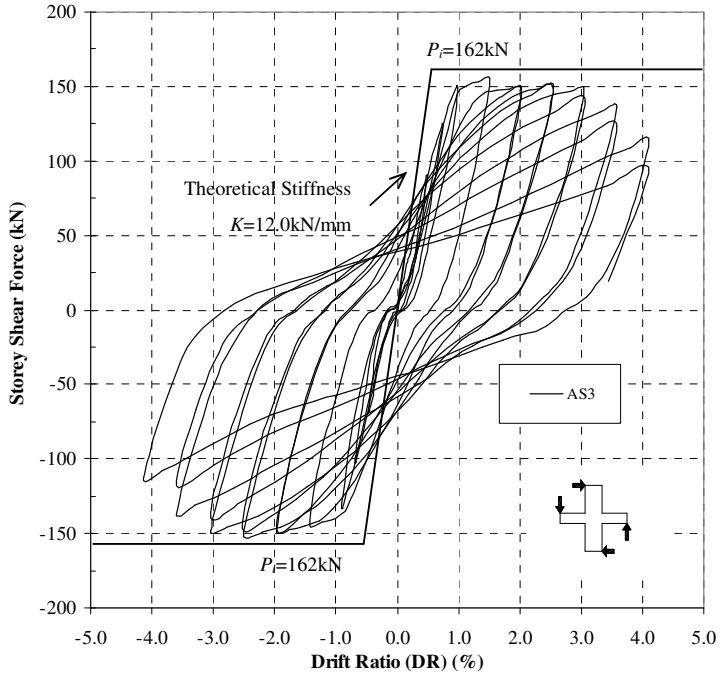

Figure 4.63 Storey Shear Force versus Horizontal Displacement for AS3

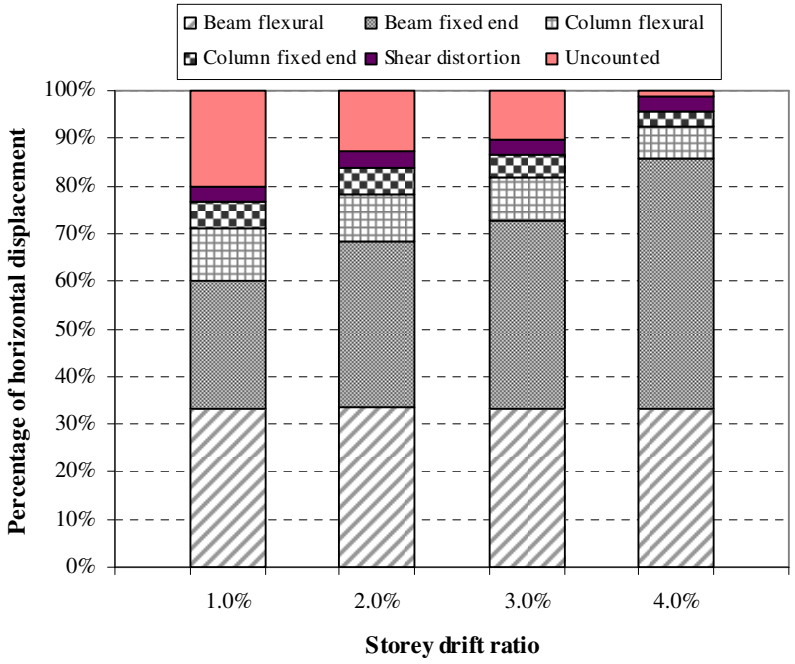

Figure 4.64 Decomposition of Horizontal Components of AS3

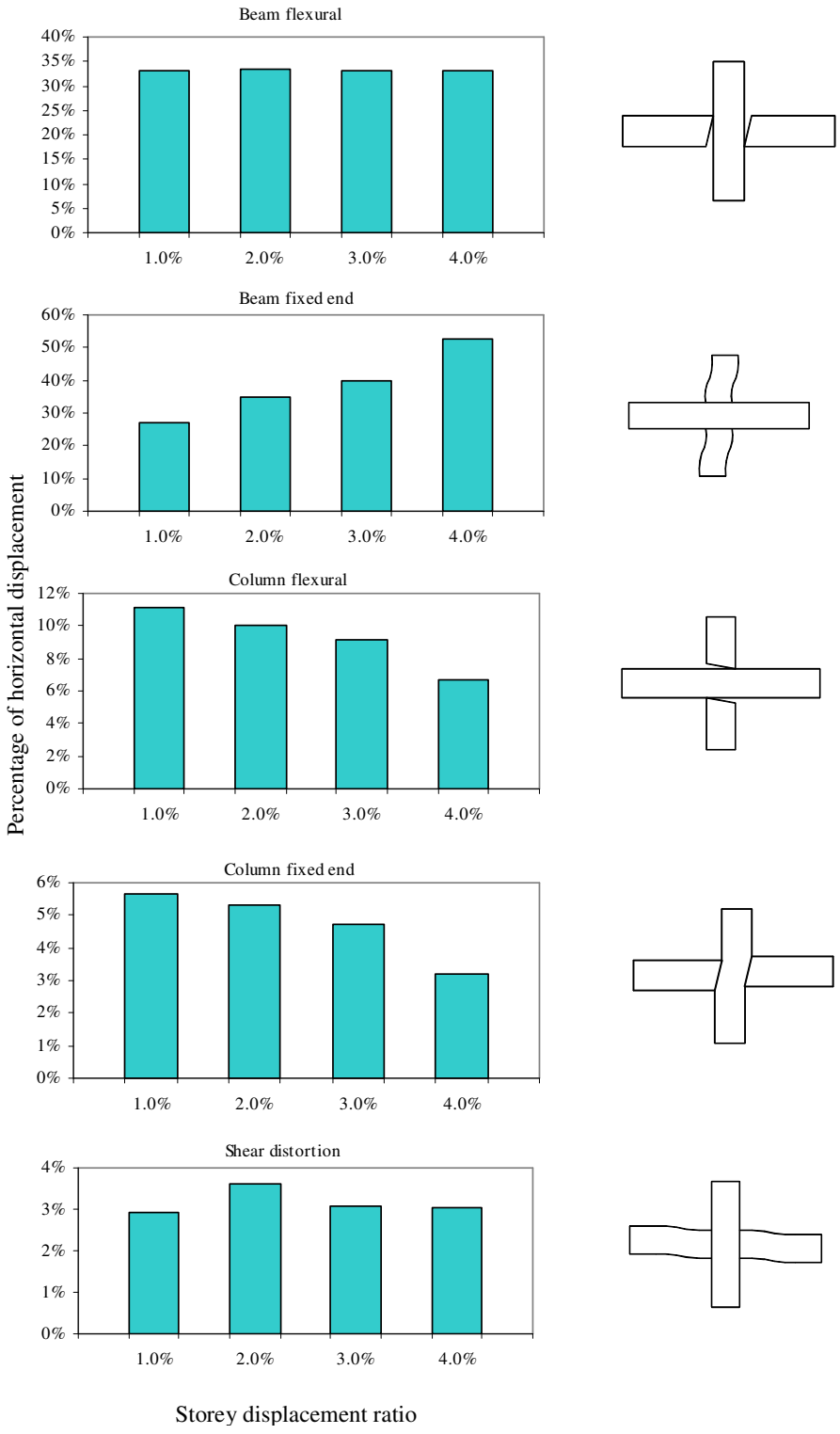

Figure 4.65 Contributions of Horizontal Components of AS3

4.3.2.3 Decomposition of Horizontal Displacement

Figure 4.64 shows the components of horizontal displacement measured for AS3 at the peak of DR 1%, DR 2%, DR 3% & DR 4% while Figure 4.65 explains the contributions of each components of the horizontal displacement measured for AS3**.** The main source of storey drift was beam flexure and fixed-end rotation with maximum contributions of 33% and 53% respectively. The column flexure and column fixed-end rotation has less influence on the horizontal displacement. Similarly, the rigid joint core has little contribution to horizontal displacement in the form of joint shear distortion. The contribution of uncounted component such as rigid body movement was significant in the early stage of test and eventually reduced in the end of test.

4.3.2.4 Beam Behaviour

The beam behaviour is discussed via the evaluation of strains in beam reinforcement and beam curvatures:

Beam Reinforcement Strains

Figure 4.66 explains the strain profiles of the top and bottom beam reinforcement of AS3. At DR 1% the beam reinforcement was in elastic range where none of the strain gauges exceeded its yield strain limit. Plastic hinge was formed at beam near to column face when DR 3% was attained. The respective strain gauges installed near column face yielded at DR 3% which illustates the formation of plastic hinge. Although larger bar was used in AS3, no bond deterioration within the joint was observed.

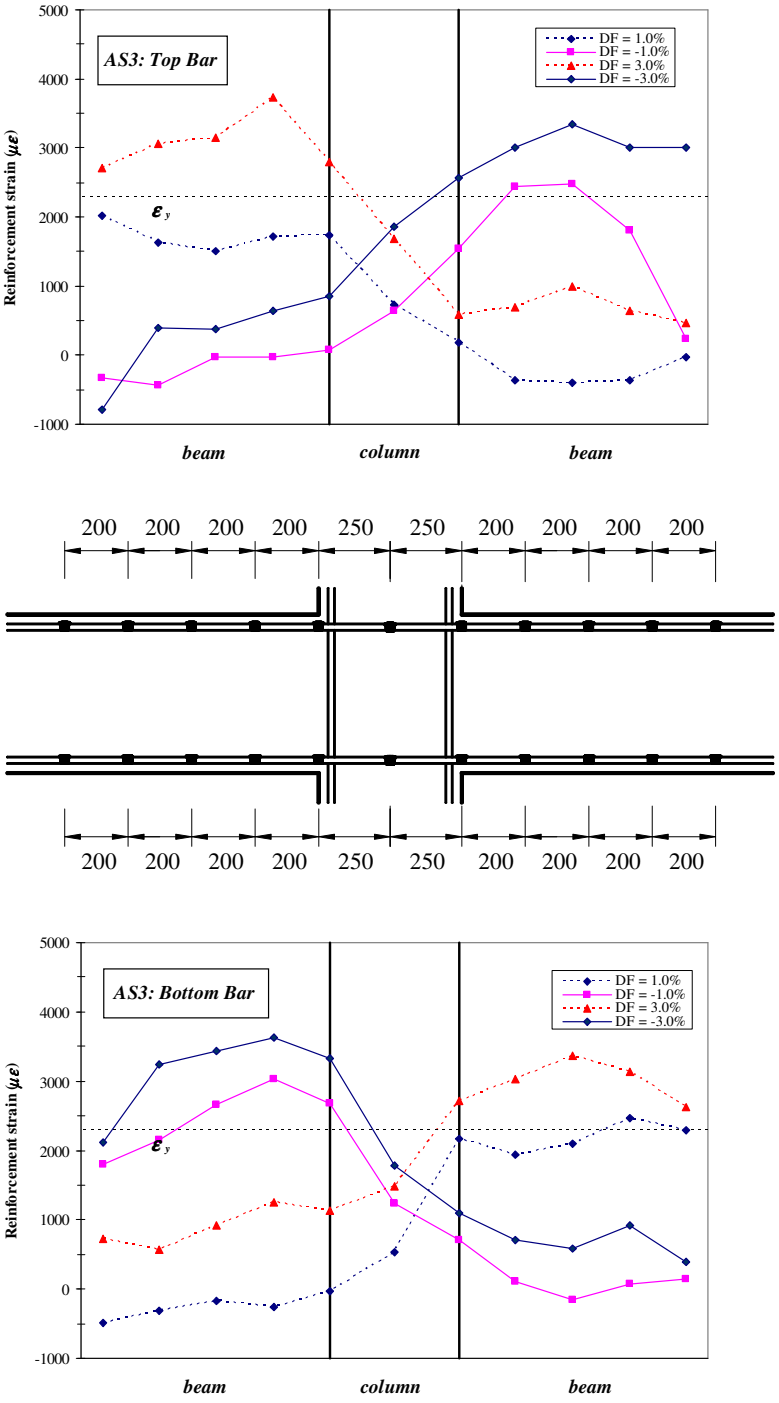

Figure 4.66 Strain Profiles of Beam Bars of AS3

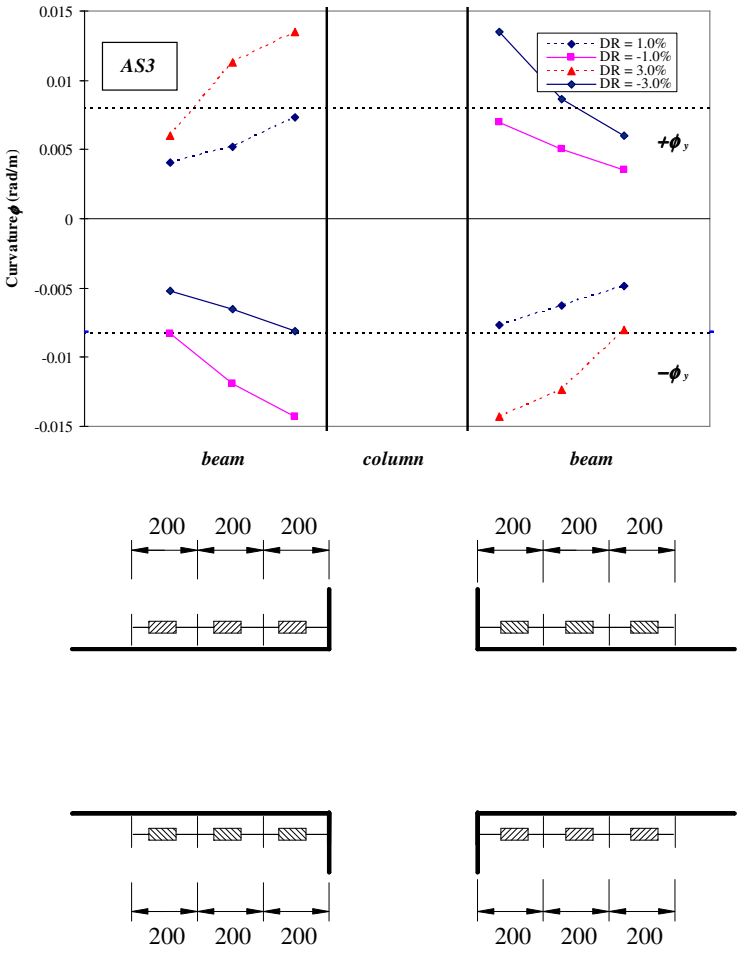

Figure 4.67 Curvature Distribution of Beam of AS3

Beam curvature

Figure 4.67 shows the beam curvature distributions estimated from the transducer readings. The beam curvature measured near the column face almost reached the theoretical yield curvature in the loading stage of DR 1%. Beam curvature increases rapidly after DR 3% and exceeded its theoritical yield curvature. This was mainly due to the plastic hinges forming in the beam end and spalling begun to take place after DR 3%.

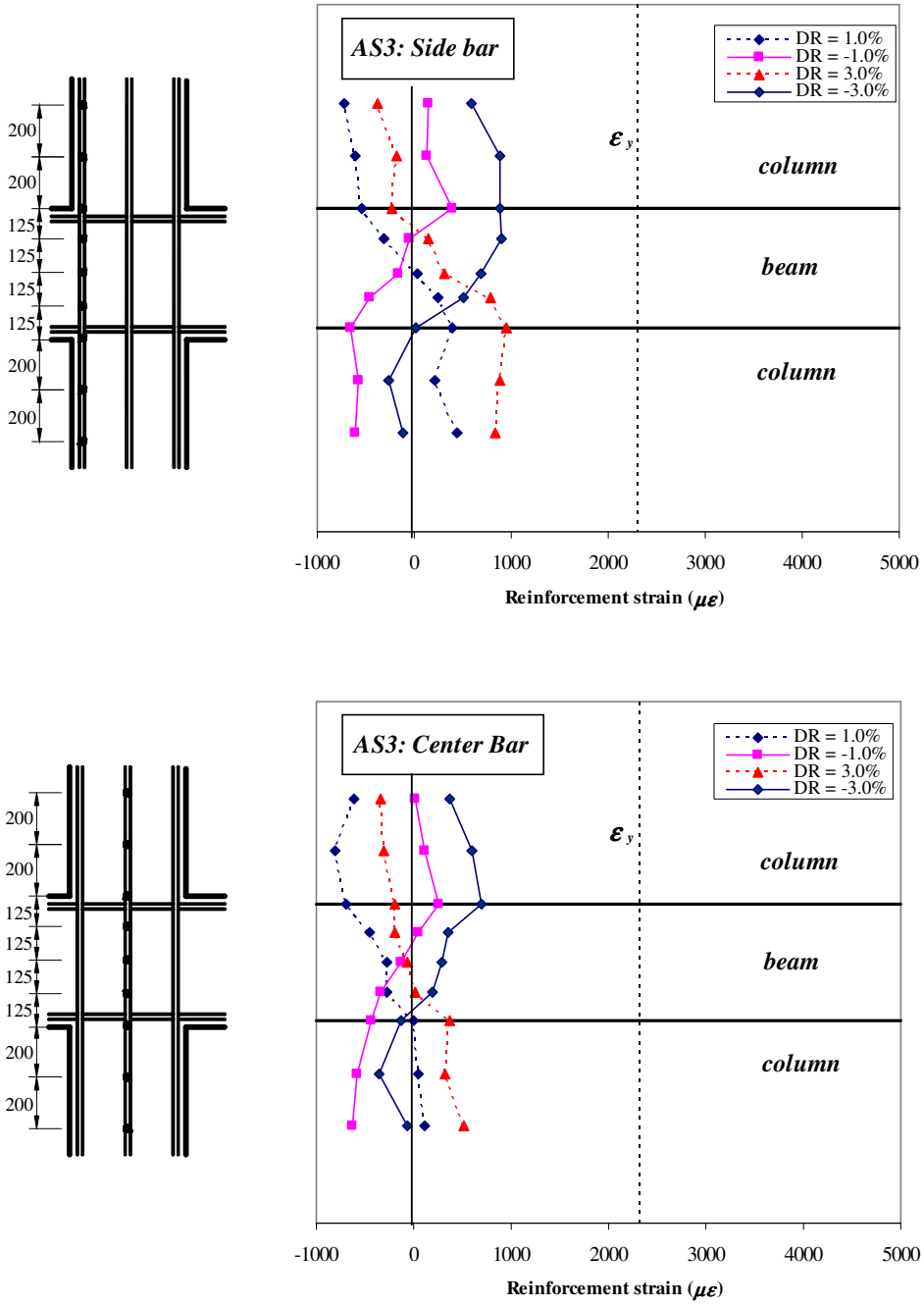

Figure 4.68 Strain Profiles of Column Bars of AS3

4.3.2.5 Column Behaviour

The column behaviour is evaluated based on the measured strains in column side reinforcement and column middle reinforcement. The column curvature was obtained from the measured displacement transducers along the column.

Column Reinforcement Strain

The strains of side bar and central bar of column are explained in Figure 4.68. Due to the confinement from column axial compressive load, the column remained elastic throughout the test; although the strains of column bar increase gradually they did not reach the yield strain.

Column curvature distributions

Figure 4.69 shows the column curvature distributions as per instrumented in the test. The curvatures measured at the upper column were similar to those at the lower column. As the column was still in its elastic range, the respective curvatures increased gradually but no rapid increase was observed.

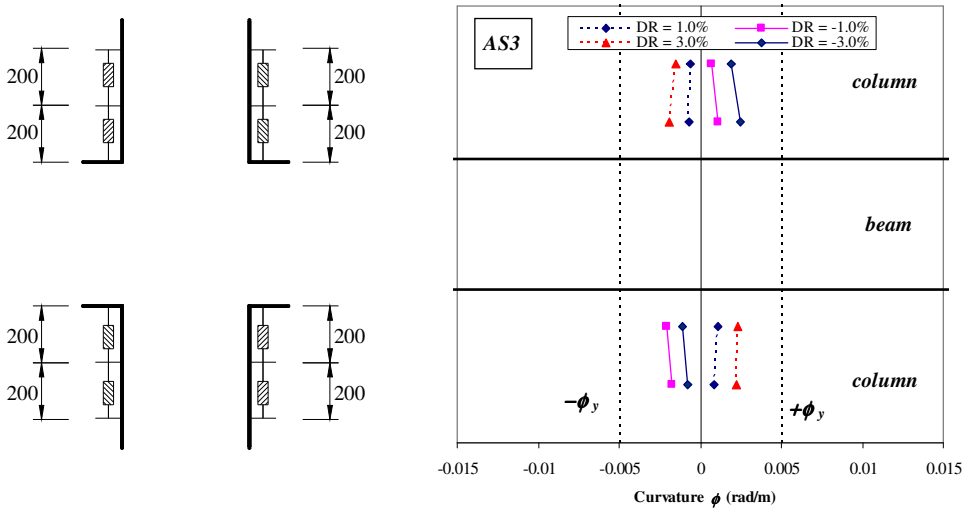

Figure 4.69 Curvature Distribution of Column of AS3

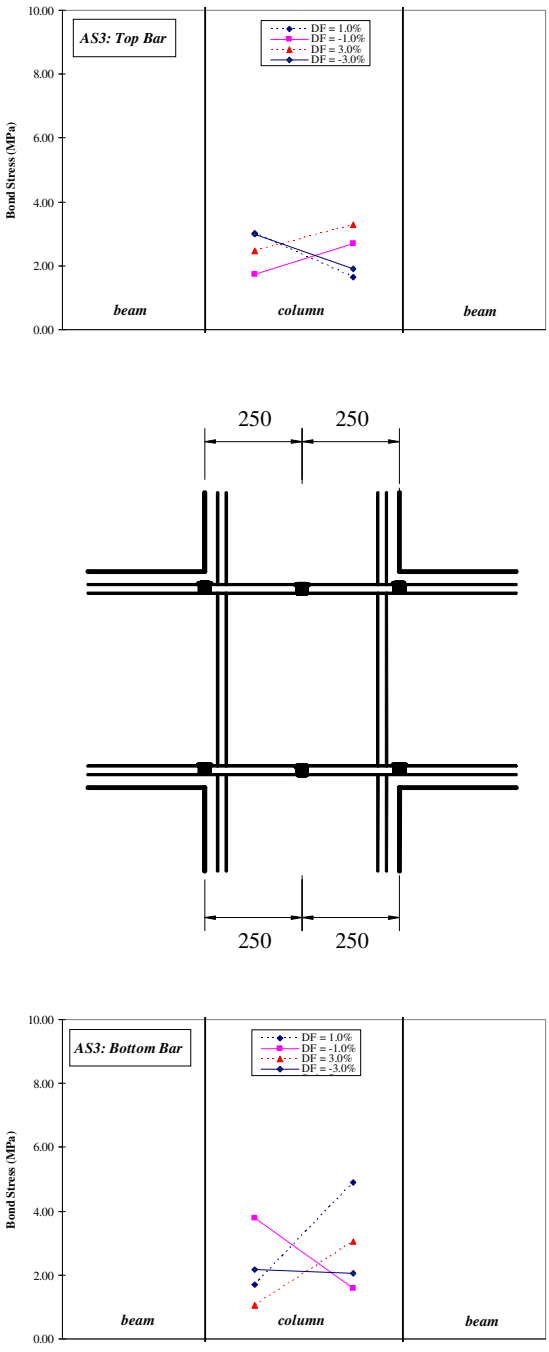

Figure 4.70 Bond Stress of Beam Bar of AS3

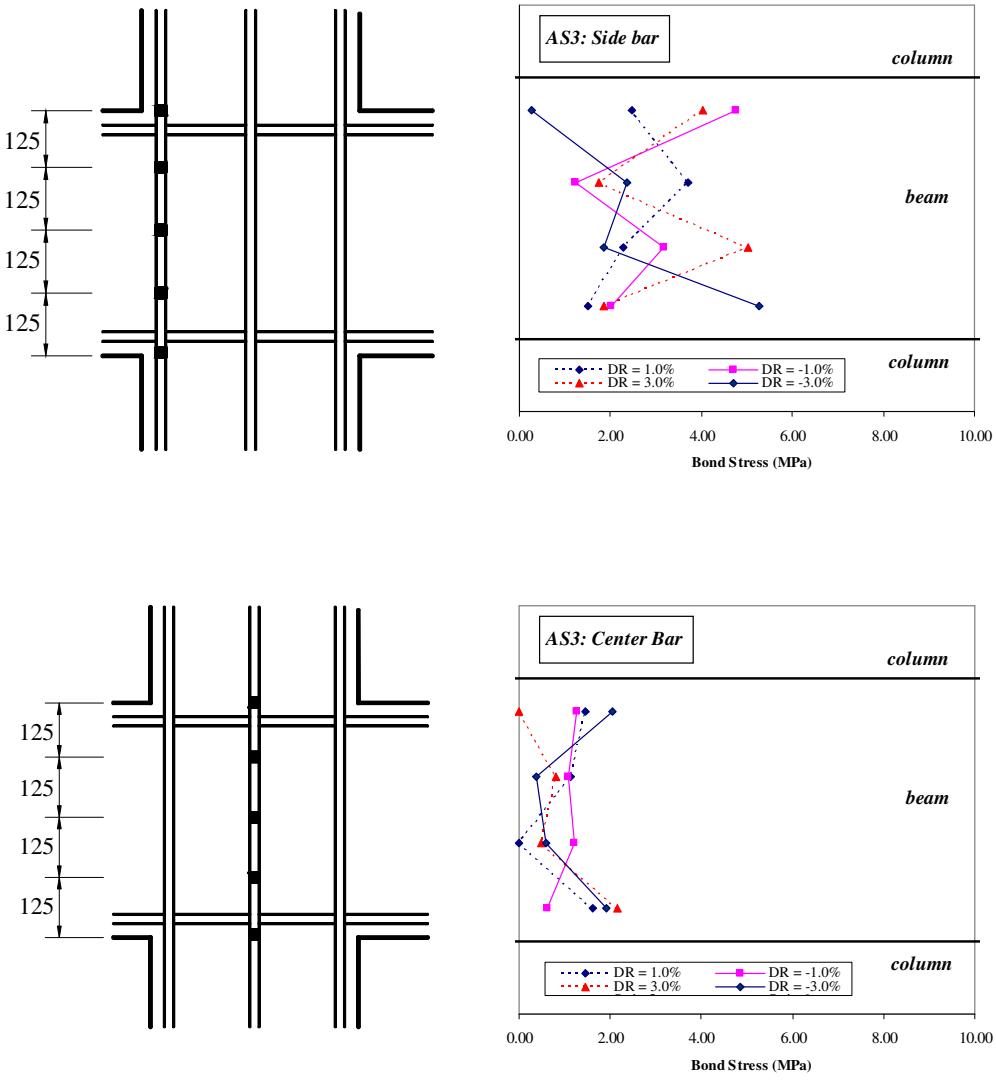

Figure 4.71 Bond Stress of Column Bar of AS3

4.3.2.6 Joint Behaviour

The bond stress of beam reinforcement and column reinforcement, joint shear distortion and joint shear expansion are discussed in the following sections:

General Behaviour

For AS3, the maximum nominal horizontal shear stress in the joint core was 6.27 MPa or 0.103 $f_c^{'}$ which met the requirement in NZS 3101. As shown in Figure 4.62a to Figure 4.62d, the initial diagonal tension cracks formed in the DR 1%. In

the subsequent loading cycles, more cracks appeared on joint and the joint diagonal tension cracks propagated and opened wider till DR 3% was reached. Crack development at joint core stabilised after then and no new crack was observed.

Bond Stresses of Beam and Column Reinforcement Bars in Joint Core

Figure 4.70 and Figure 4.71 show the average bond stresses obtained from beam bars for column bars. The maximum bond stress obtained along top beam bars was 3.28 MPa (=0.054 $f_c^{'}$) while the maximum bond stress observed along bottom beam bars was 3.78 MPa (=0.062 $f_c^{'}$). Bond deterioration was noticed in both top and bottom beam bars where bond stresses decreased rapidly in the end of test. On the other hand, the column reinforcement remained elastic in the end of the test with maximum bond stress of 5.28 MPa (=0.087 $f_c^{'}$) on side bar and maximum bond stress of 2.15 MPa (=0.035 $f_c^{'}$) on centre bar, respectively.

Joint Shear Distortion and Joint Shear Expension

Figure 4.72 explains the measured joint shear distortion and expansion of AS3. The joint shear distortion and expansion of AS3 is generally small due to the beneficial confinement effects from column axial compressive load. In the final loading to DR 4%, the maximum joint distortion is 0.14% and the maximum joint expansion is 1.58 mm.

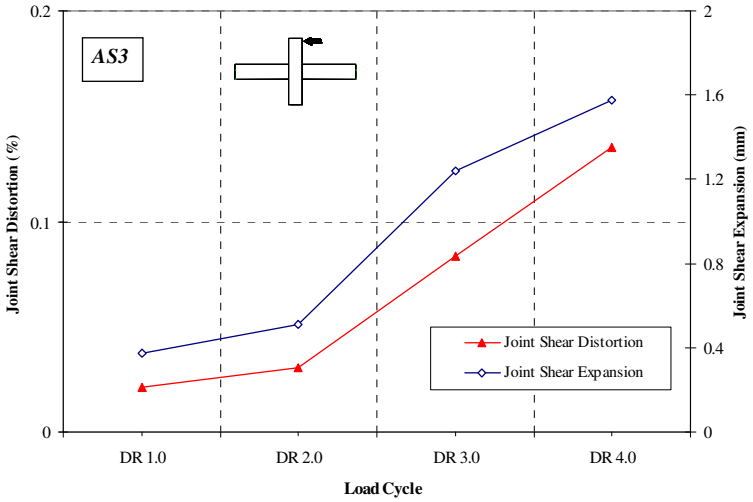

Figure 4.72 Joint Shear Distortion and Expansion of Specimen AS3

4.4 Test Result of Group 4 (NS4 and AS4)

The last group consists of specimens NS4 and AS4 with which was made of the largest beam bars as explained in Chapter 3. As for the test method, NS4 was tested without column axial compressive loading while AS4 was tested with column axial compressive loading of $0.3f_c'A_c$. The typical features of these specimens are summarised as follows:

- beam reinforcement size was the largest among all specimens (20mm for NS4, 16mm for NS2 & NS3 and 12mm for NS1)
- ratio of beam bottom reinforcement to beam top reinforcement area= 0.64
- actual maximum beam-bar-to-column-depth = 1/22.50
- actual column-bar-to-beam-depth = 1/15.63
- calculated maximum beam-bar-to-column-depth based on Eq. 7-13 in NZS 3101 :

  NS4= 1/25.02 AS4= 1/24.74
- calculated maximum column-bar-to-beam-depth based on clause 7.5.3.4 in NZS 3101:

  NS4= 1/16.52 AS4= 1/16.33
- NS4 and AS4 did not meet the requirement of maximum beam-bar-to-column-depth but met the requirement of maximum column-bar-to-beam-depth set in NZS 3101
- Joint core reinforcement detailing complied with the requirement in clause 7.5.3.4 in NZS 3101 (maximum bar spacing = 85mm, allowable bar spacing = 100mm)

The test results of NS4 and AS4 are explained in following sections.

4.4.1 Specimen NS4

Specimen NS4 has the largest beam reinforcement which did not meet the bond development limit in NZS 3101. However, NS4 showed a stable energy dissipation capacity with cracks developed all over the specimens and behaved in a ductile manner. Cracks were mainly concentrated at the joint panel with fewer cracks on

beam and column. The energy dissipation was consistent but the ultimate load was the lowest among the samples.

4.4.1.1 General Observation

Specimen NS4 was made of larger beam bars which did not meet the beam bar bond development limits in NZS3101. Due to this, the top beam reinforcement of NS4 exhibited some slippage and spalling of concrete was observed at the beam near to column face as shown in the final crack pattern of NS4 in **Figure 4.73**. However, NS4 still showed satisfactory energy dissipation capacity and failed in a ductile manner in the end of test. Cracks were mainly found at joint core with spalling observed at both the top and bottom corners of the joint panel. As shown in Figure 4.73, limited crack was formed at the column and flexural cracks were observed on the beams top and beam bottom.

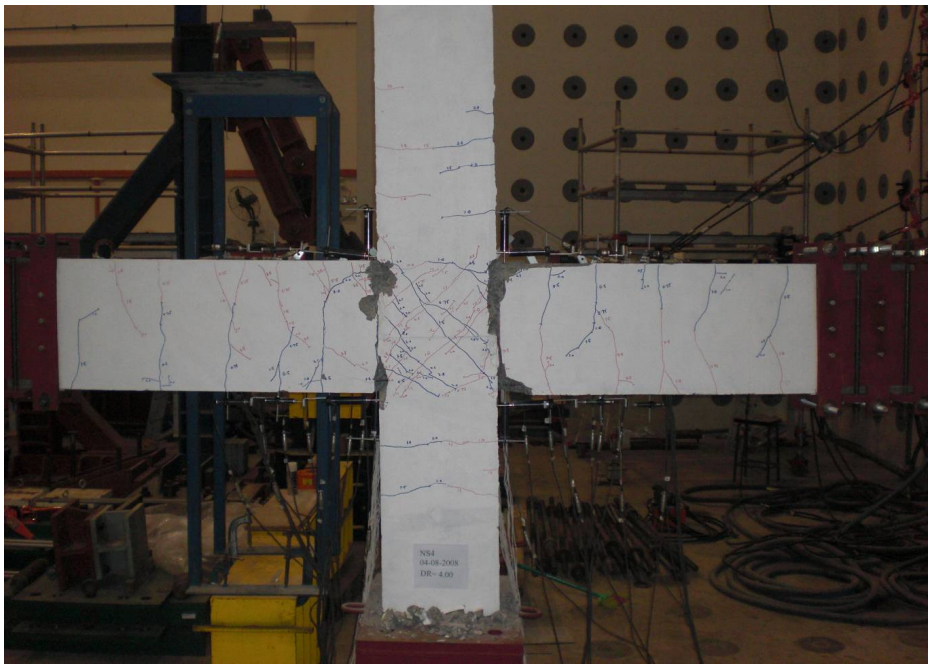

Figure 4.73 Final Crack Pattern of NS4

As illustrated in Figure 4.74, a series of photographs taken at the peak of storey drift ratio of 1.0% (DR 1%), 2.0% (DR 2%), 3.0% (DR 3%) and 4.0% (DR 4%) to explain the crack development of NS4. At loading of DR 1%, diagonal cracks at

the joint core area and column were noticed. Besides that, flexural cracks were also observed at beam bottom when loading at DR 1% was attained as shown in Figure 4.74. The flexural cracks at beams were found to propagate and the cracks at joint core progress rapidly during loading stage of DR 2% and DR 3%. Meanwhile, little new crack was found at column and new cracks were mainly formed at joint core region. Spalling was observed at joint core area as shown in Figure 4.74, due to the excessive fixed-end deflection of beam caused by lower bottom reinforcement that compressed against joint core that eventually crush the joint core to spall at the final loading stage of DR 4%.

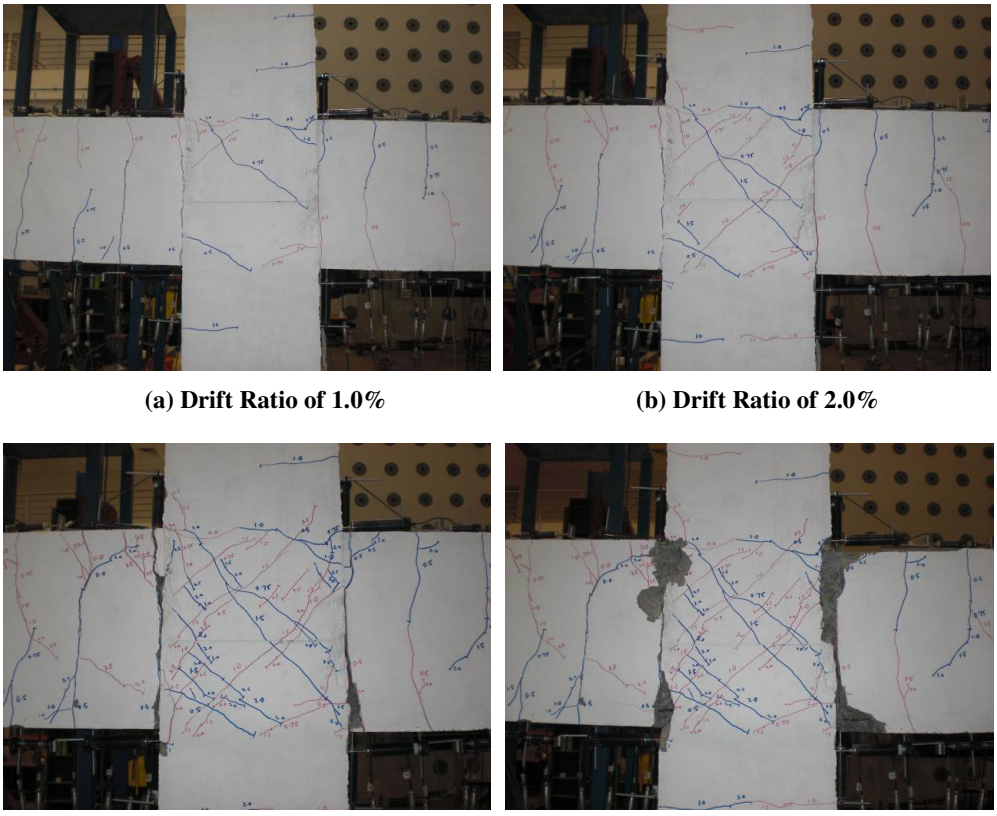

(a) Drift Ratio of 1.0% **(b) Drift Ratio of 2.0%**

(c) Drift Ratio of 3.0% **(d) Drift Ratio of 4.0%**

Figure 4.74 Progressive Cracking Development of NS4

4.4.1.2 Hysteretic Behaviour

Due to the use of larger bar size in beam reinforcement, Specimen NS4 has a higher tendency to have bond failure at the beam. However, the hysteresis loops shown in Figure 4.75 indicates satisfactory energy dissipation behaviour with no serious pinching found. This phenomenon explained bond slip failure in the beam reinforcement in joint core did not happen although the bond development limits in NZS 3101 was not met. The maximum load of NS4 was achieved in DR 2% and yielding of the beam reinforcement begun. The maximum horizontal storey shear was maintained until DR 3% and a drop of 15% was observed when test was completed at DR 4%.

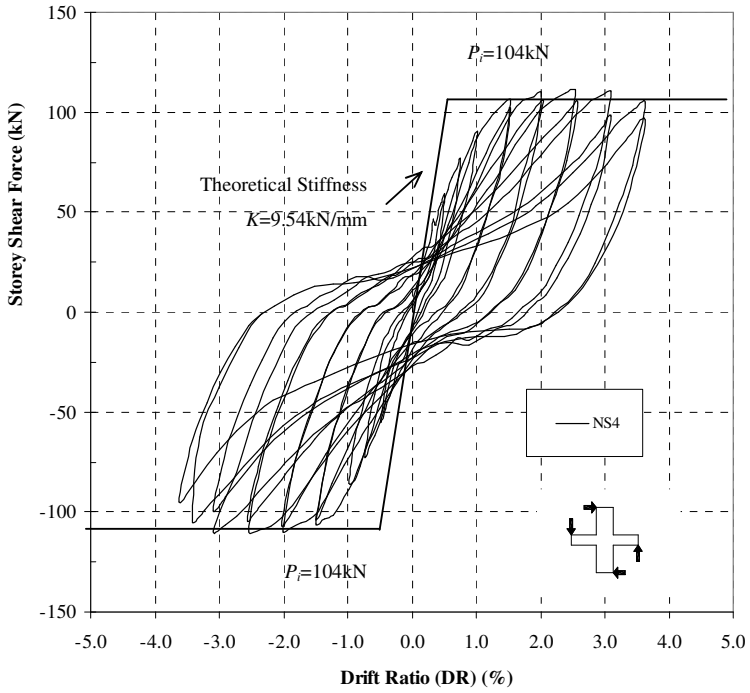

Figure 4.75 Storey Shear Force versus Horizontal Displacement for NS4

4.4.1.3 Decomposition of Horizontal Displacement

As explained in Figure 4.76 and Figure 4.77, the beam displacement has been the dominant component that formed the measured horizontal displacement for NS4. On the other hand, the column displacement has less influence on the total horizontal displacement. The maximum contributions of each component are as follows: beam flexure (34%), beam fixed-end rotation (24%), column flexure (16%) and column fixed-end rotation (16%). Even though larger beam bars passed through the joint core, the contribution of shear distortion was below 10% which explains the rigid joint core of NS4.

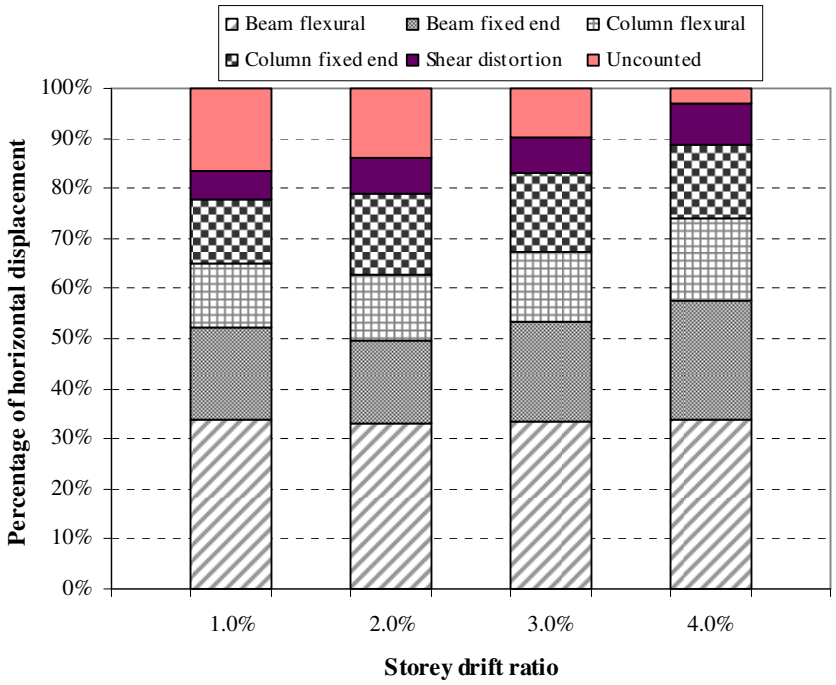

Figure 4.76 Decomposition of Horizontal Components of NS4

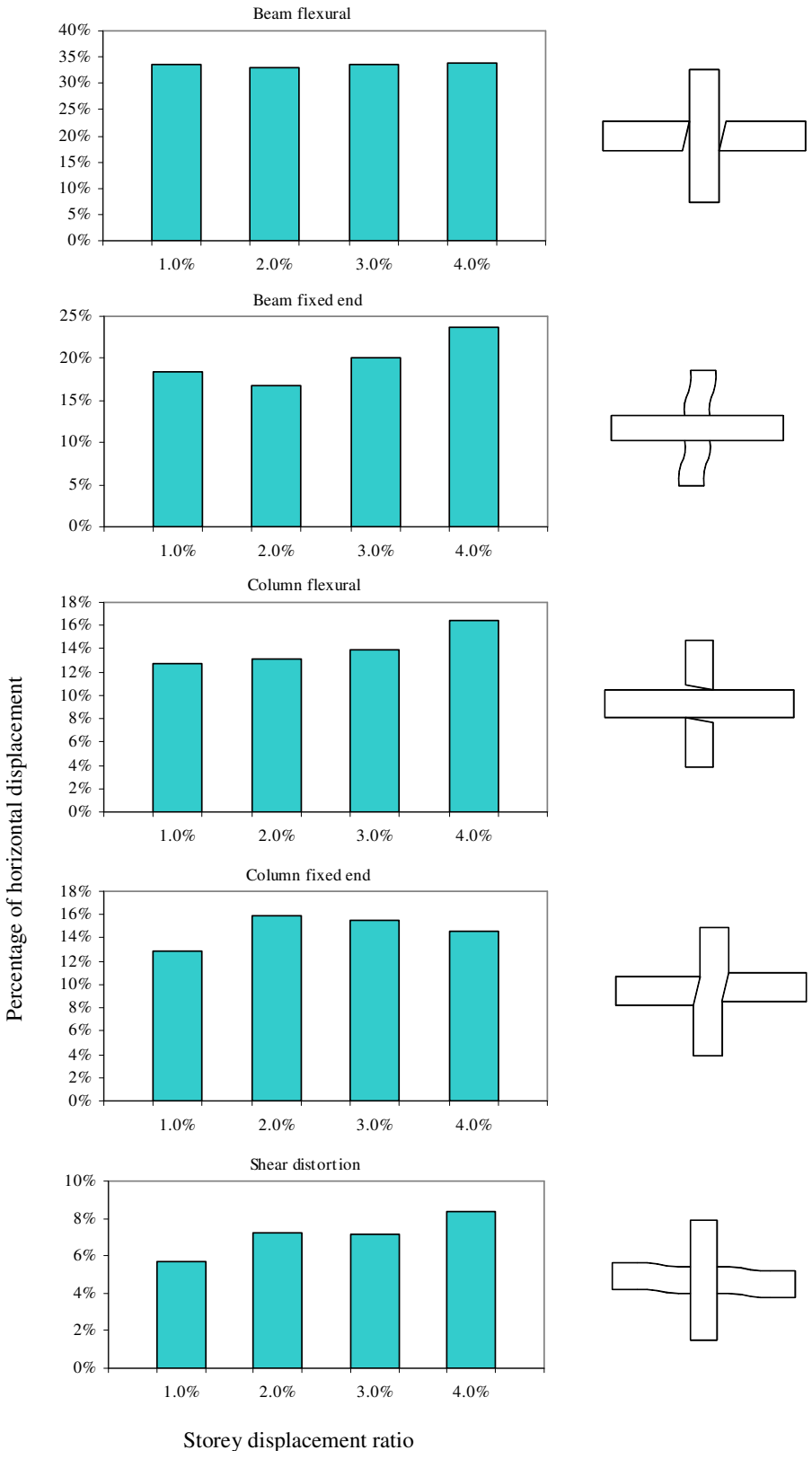

Figure 4.77 Contributions of Horizontal Components of NS4

4.4.1.4 Beam Behaviour

The strain profiles of beam reinforcement and beam curvatures are explained in the following sections:

Beam Reinforcement Strains

As explained in Figure 4.78, top beam reinforcement and bottom reinforcement of specimen NS4 showed a sign of yielding as the strain gauges installed near to column face exceeded the yield strain at DR 1%. When DR 3% was attained, yielding of beam reinforcement was observed in more strain gauges which confirmed the propagation of bar yielding. Yield penetration was noticed where yield strain was penetrated through a certain distance into the joint core. The beam within joint core demotrated good bonding the tensile stress on one face was transferred to compressive stress at another face despite the use of large diameter beam reinforcement.

Beam curvature

The beam curvature distributions estimated from the transducer readings is depicted in Figure 4.79. Due to the formation of plastic hinges in the beam end, the beam curvature measured near the column face exceeded the theoretical yield curvature at DR 1%. Rapid increase of the curvature was observed in the subsequent loading cycles explaining the energy dissipation of beams..

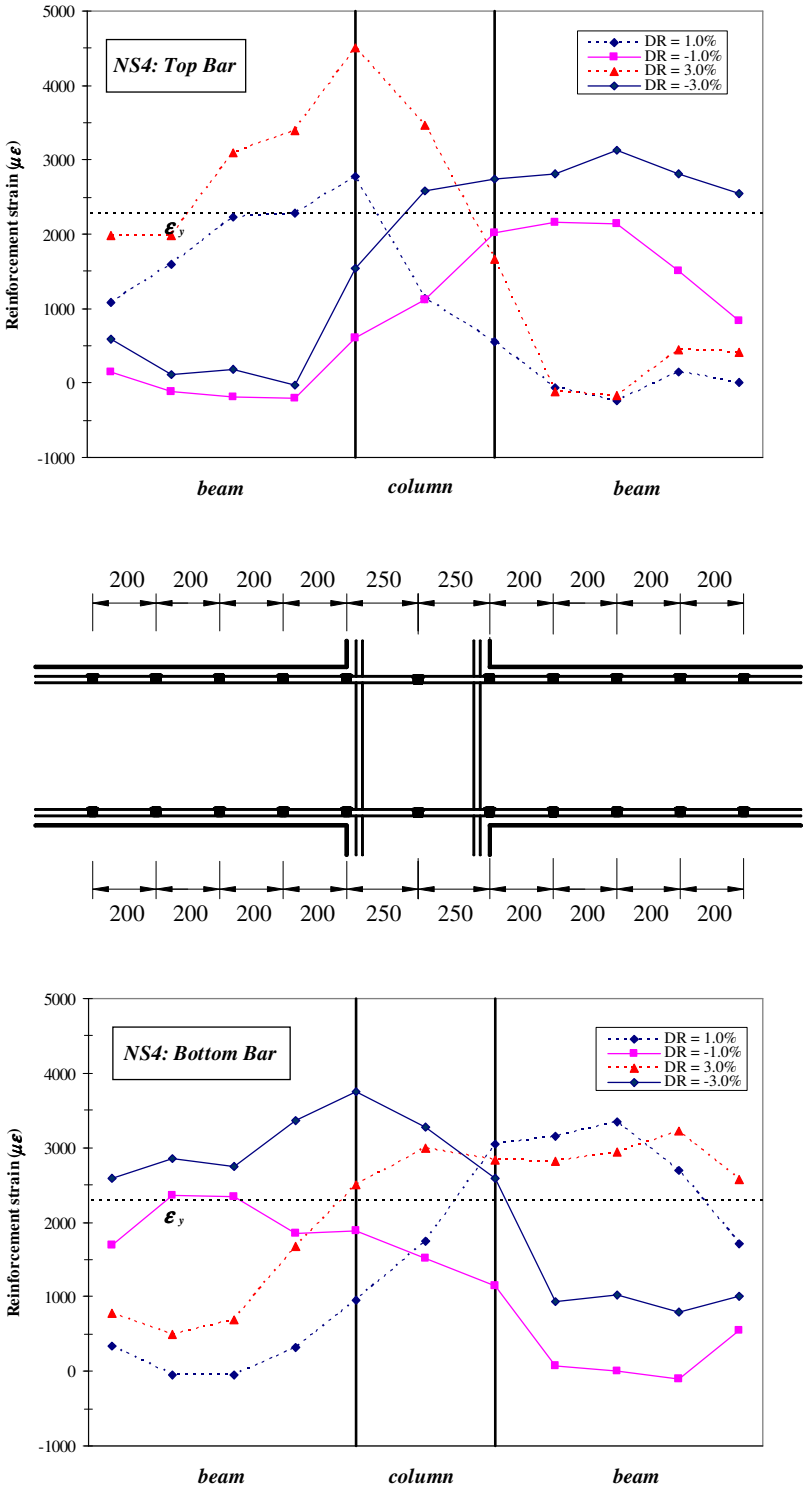

Figure 4.78 Strain Profiles of Beam Bars of NS4

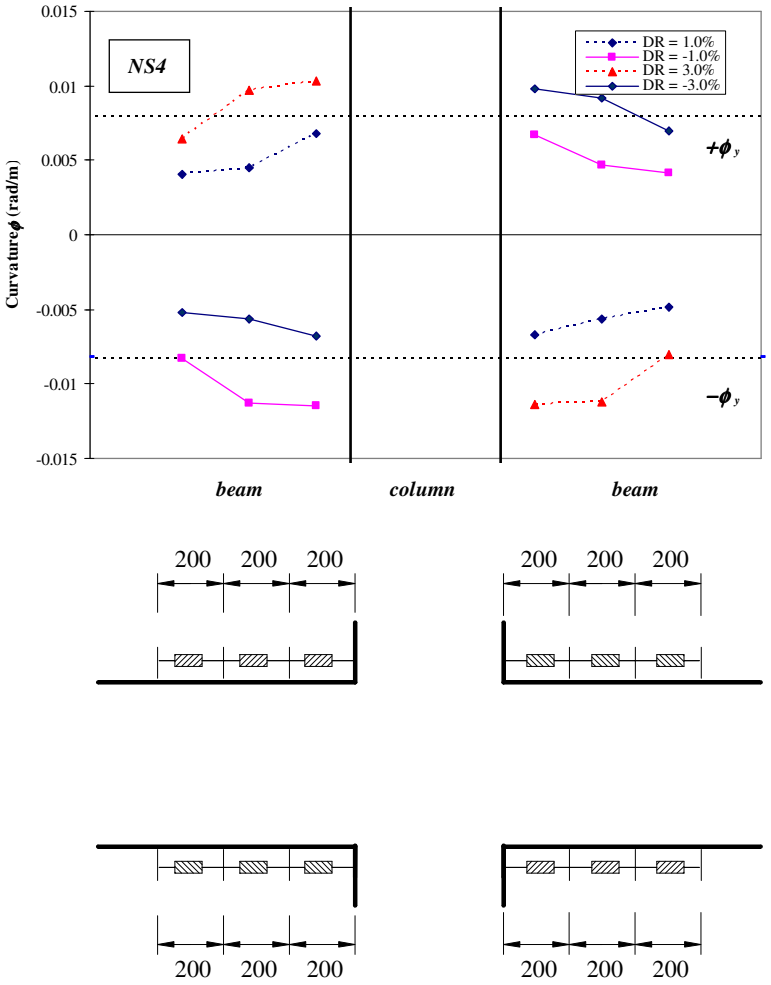

Figure 4.79 Curvature Distribution of Beam of NS4

4.4.1.5 Column Behaviour

The evaluation of strains in column reinforcement and column curvatures are discussed in the following sections:

Column Reinforcement Strain

Generally the strains of column bars did not reach the yield strain as explained in Figure 4.80. The column was strong enough to resist the applied horizontal load in test.

Column curvature distributions

Although the curvatures increased gradually, no evident rapid increase was observed in Figure 4.81. This shows the behavior of the column was still in its elastic range.

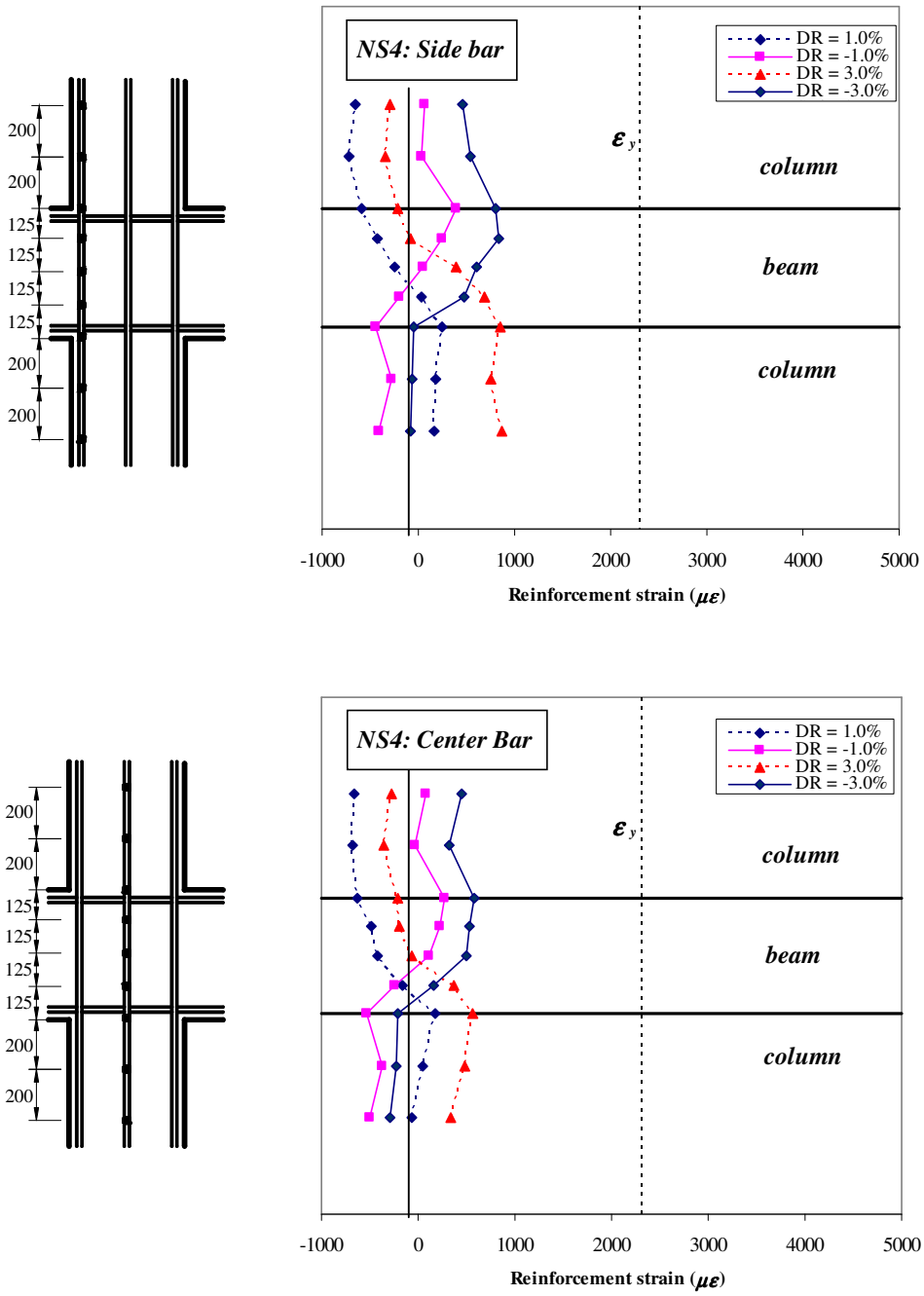

Figure 4.80 Strain Profiles of Column Bars of NS4

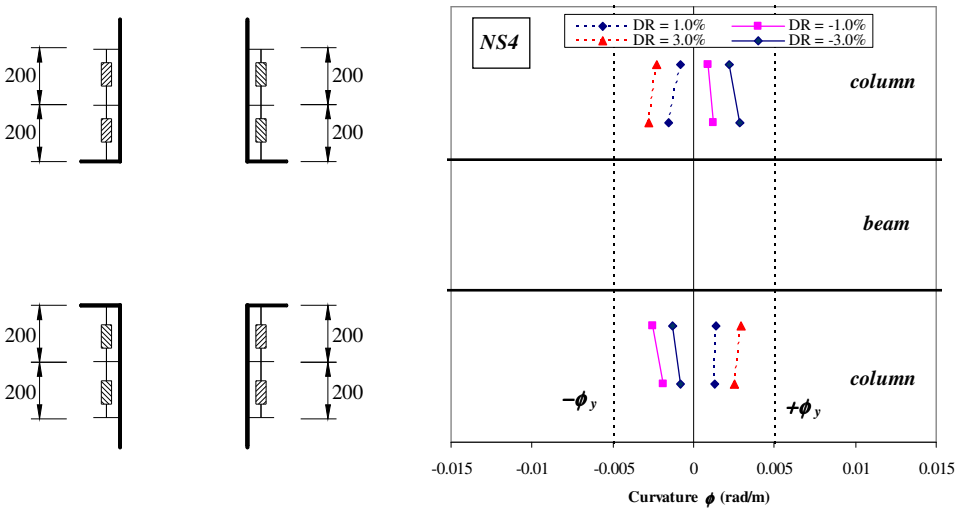

Figure 4.81 Curvature Distribution of Column of NS4

4.4.1.6 Joint Behaviour

The evaluation of joint behaviour on bond stress of beam reinforcement and column reinforcement, joint shear distortion and joint shear expansion are discussed in the following sections:

General Behaviour

The diagonal tension cracks were firstly observed in DR 1% as explained in Figure 4.74a and the cracks were then propagated in the subsequent loading cycles. Figure 4.74d shows the final crack patterns of the joint core where spalling was observed in the conrers of the joint core. The maximum nominal horizontal shear stress in the joint core was 4.00MPa or 0.066 $f_c^{'}$, which met the requirement in NZS 3101.

Bond Stresses of Beam and Column Reinforcement Bars in Joint Core

The average bond stresses measured along the longitudinal beam and column bars in the joint were calculated using the wire strain gauge readings. These calculated bond stresses obtained are plotted in Figure 4.82 for beam bars and Figure 4.83 for column bars.

The maximum bond stress obtained along top beam bars was 6.81 MPa (=0.112 $f_c^{'}$) while the maximum bond stress observed along bottom beam bars was 3.95 MPa (=0.065 $f_c^{'}$). Bond deterioration was obvious in bottom beam bars where bond stresses decreased rapidly in the end of test. As for column, the maximum bond stress of 5.64 MPa (=0.092 $f_c^{'}$) on side bar and maximum bond stress of 2.59 MPa (=0.042 $f_c^{'}$) on centre bar, respectively. It is noteworthy that the column reinforcement remained elastic in the end of the test.

Joint Shear Distortion and Joint Shear Expension

Figure 4.84 explains the measured joint shear distortion and expansion with the procedures for estimating the joint shear distortion and expansion explained in Chapter 3. Joint shear distortion and expension was initially observed in DR 1% and progressed rapidly throughout the test. The maximum joint distortion and expension was 0.24% and 1.81 mm, repsectively.

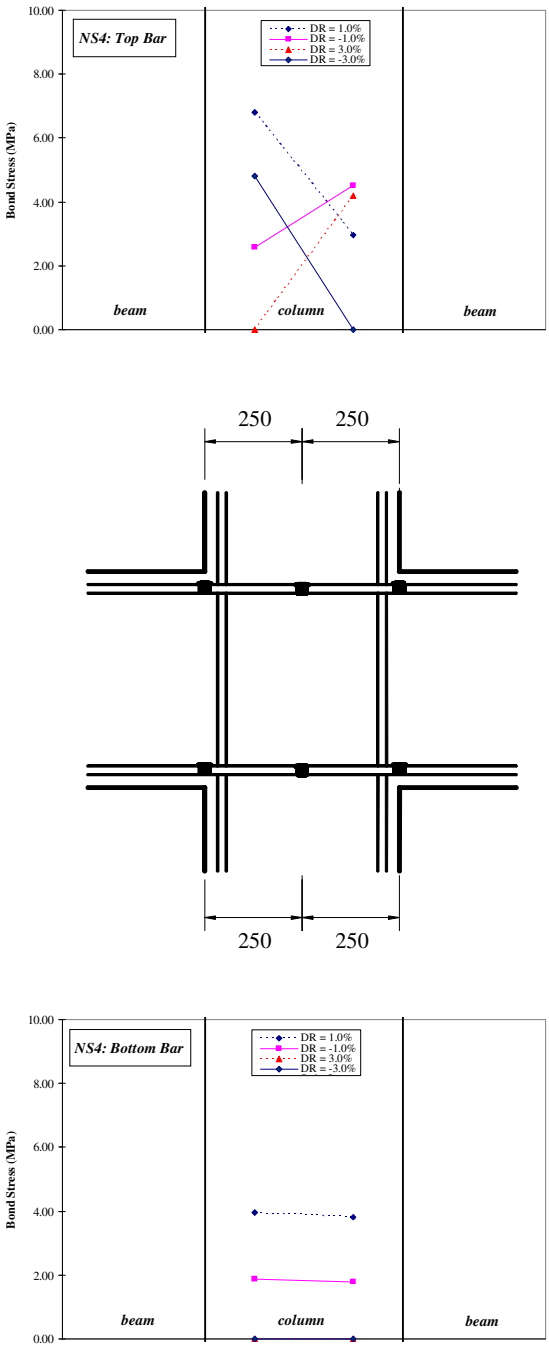

Figure 4.82 Bond Stress of Beam Bar of NS4

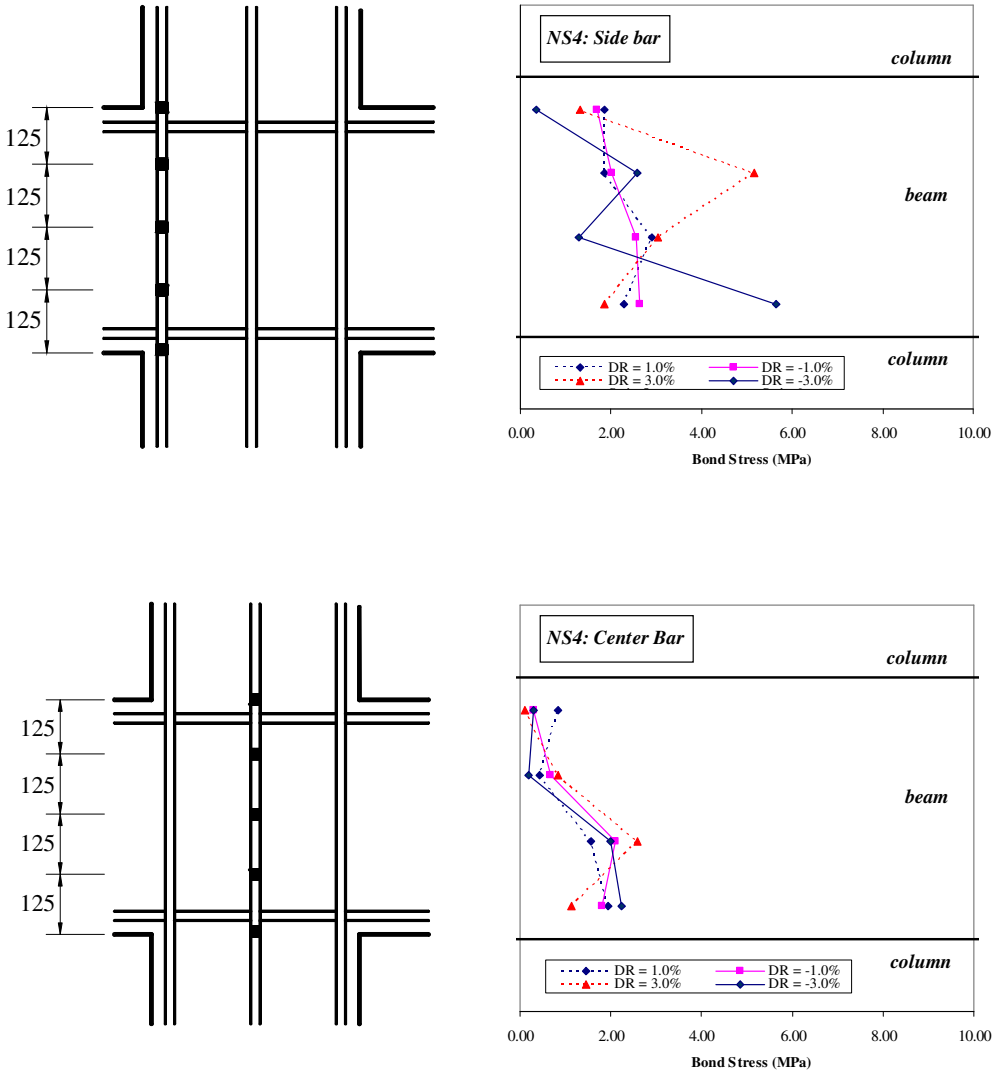

Figure 4.83 Bond Stress of Column Bar of NS4

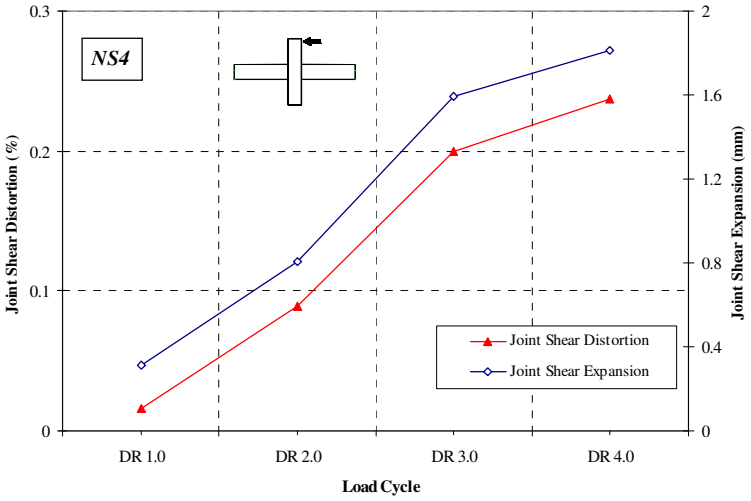

Figure 4.84 Joint Shear Distortion and Expansion of Specimen NS4

4.4.2 Specimen AS4

With the to the beneficial confinement effect of column axial compressive load, no crack was found on the column and joint core of AS4. Cracks were mainly found on beams only while the column remained elastic throughout the test. Even though AS4 was made of large beam bars, its energy dissipation capacity was satisfactory with failure in a ductile manner.

4.4.2.1 General Observation

As seen in the final crack pattern in Figure 4.85, cracks were mainly formed on beams which explained the major contribution of beams in energy dissipation when AS4 were subjected to reverse cyclic loading. The column and joint core of AS4 remained elastic throughout the test as a result of confinement effect from the applied column axial compressive load. Spalling due to crushing of concrete was noticed at the beam bottom of AS4. Bottom reinforcement and top reinforcement yielded at the end of test and while column reinforcement remained in elastic range. The specimen showed serious strength degradation in the final load cycle, which was caused by deterioration of bond in beam bars.

Figure 4.85 Final Crack Pattern of AS4

The crack development of AS4 at the peak of storey drift ratio of 1.0% (DR 1%), 2.0% (DR 2%), 3.0% (DR 3%) and 4.0% (DR 4%) is depicted in Figure 4.86. During DR 1%, limited flexural cracks caused by sagging and hogging moment was noticed on beams but no crack was found on column and joint core area at this stage. More flexural cracks were formed on beams in loading stage of DR 2%. In the subsequent loading stage DR 3%, spalling of concrete was found at beam ends near to column face. At final loading stage DR 4%, serious spalling of concrete was observed at the bottom surfaces of beam ends due to bond deterioration of beam reinforcement. The column and joint core of AS4 was intact throughout the test and no crack was found in the end of test as explained in Figure 4.86.

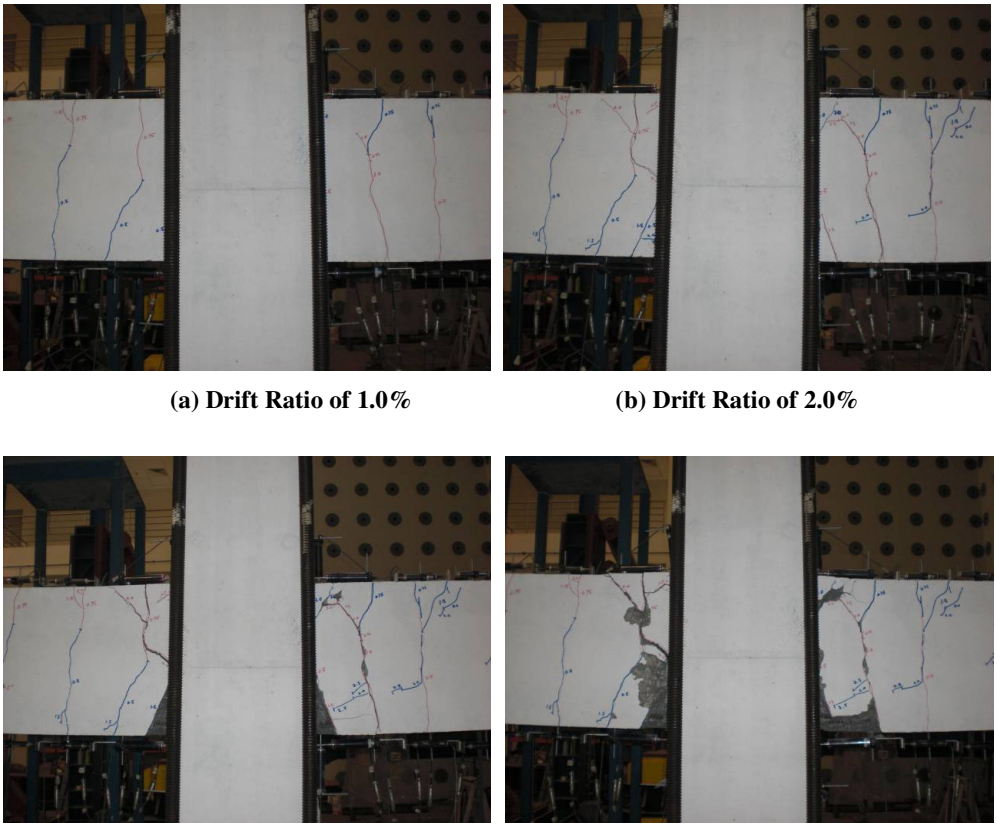

(a) Drift Ratio of 1.0% **(b) Drift Ratio of 2.0%**

(c) Drift Ratio of 3.0% **(d) Drift Ratio of 4.0%**

Figure 4.86 Progressive Cracking Development of AS4

4.4.2.2 Hysteretic Behaviour

The hysteresis loops in Figure 4.87 explains the hysteretic behaviour of AS4. The energy dissipation capacity of AS4 was satisfactory in terms of area confined in the hysteresis loops. High initial stiffness was found in AS4 when the load was firstly applied till DR 1%. The maximum storey shear force was achieved at DR 2% and the deterioration in storey shear force happened after DR 3%. Due to the bond failure of bottom reinforcement, the storey shear force dropped rapidly before DR 4% was attained. The serious pinching found in the hysteresis loops before DR 4% has confirmed the occurance of bond failure in beam reinforcement. The test was halted at DR 4% as storey shear force was merely half of the maximum value achieved at DR 2%.

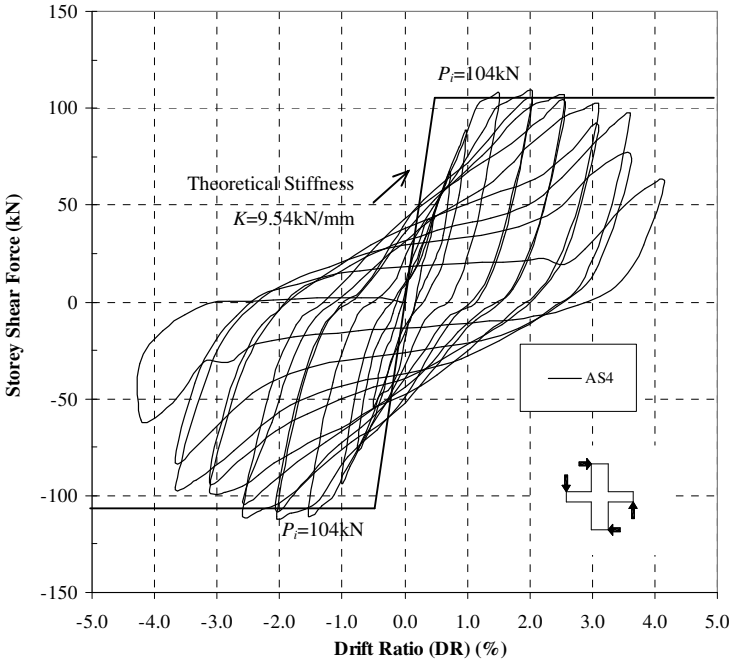

Figure 4.87 Storey Shear Force versus Horizontal Displacement for AS4

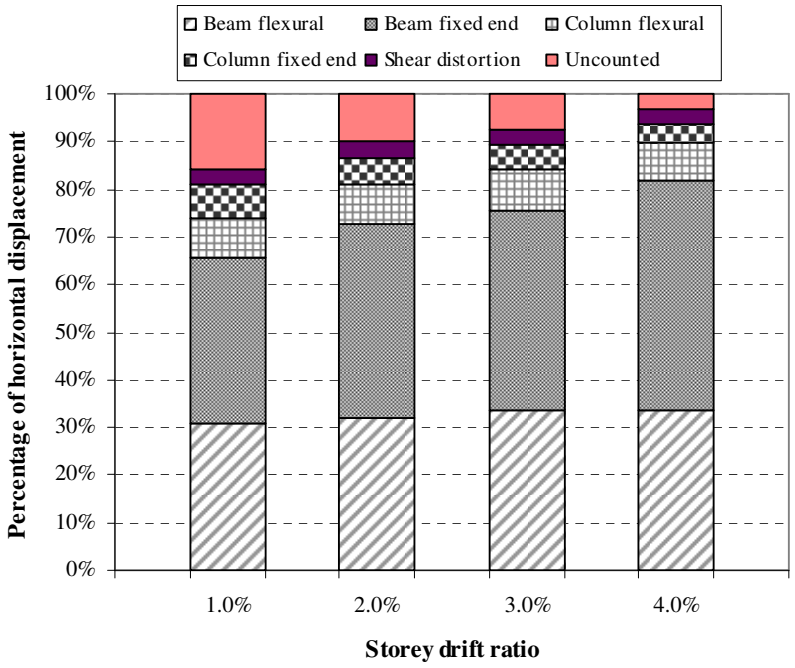

Figure 4.88 Decomposition of Horizontal Components of AS4

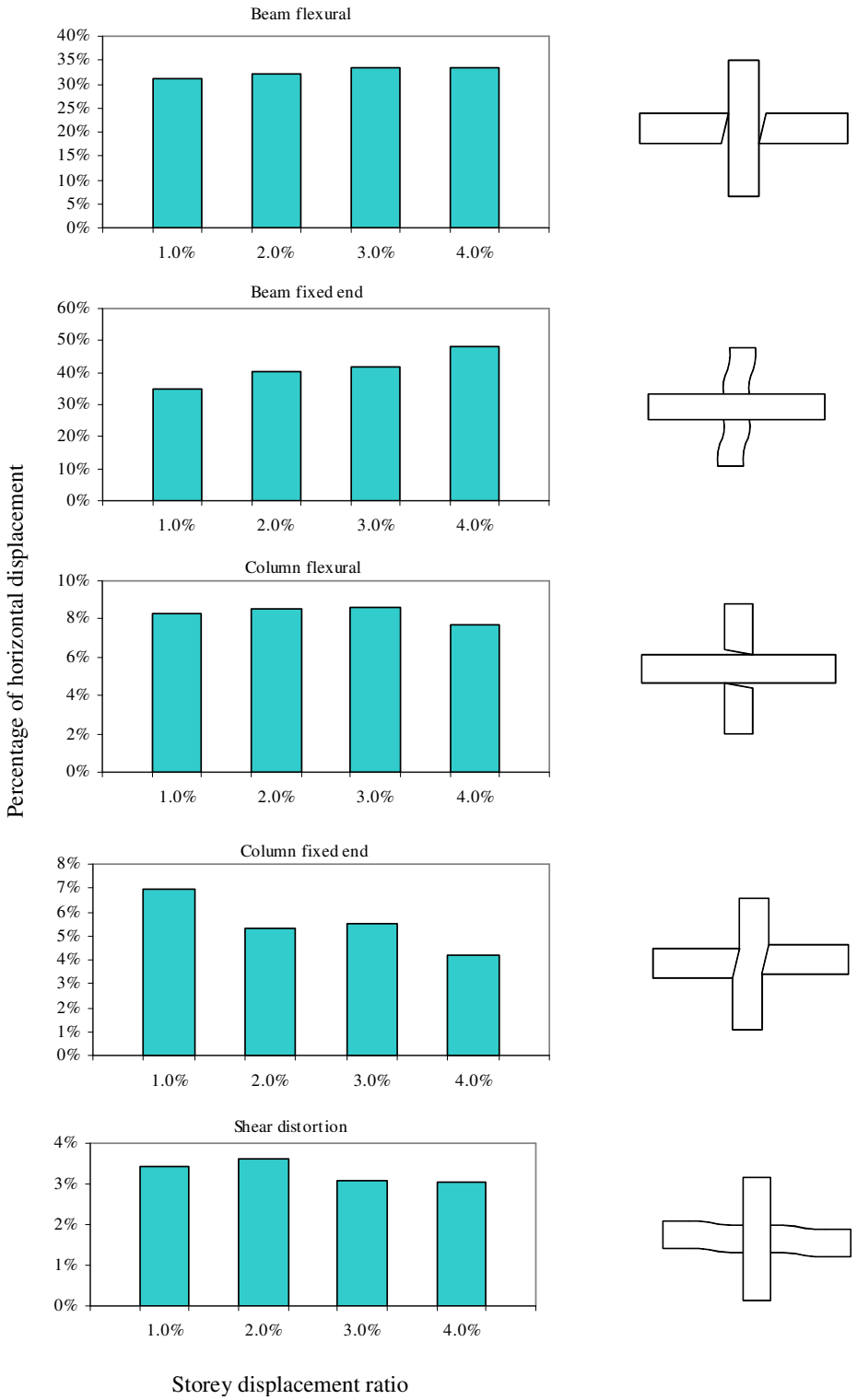

Figure 4.89 Contributions of Horizontal Components of AS4

4.4.2.3 Decomposition of Horizontal Displacement

The breakdown on components of horizontal displacement measured for AS4 at the DR 1%, DR 2%, DR 3% and DR 4% is depicted in Figure 4.88. The contribution of each component is explained in Figure 4.89. The beam components with beam flexure and beam fixed-end rotation have been the major contribution to the horizontal displacement measured for AS4**.** The contributions of beam flexure and beam fixed-end rotation were ranging from 31% to 34% and 35% to 48% respectively. The maximum contributions of column flexure and column fixed-end rotation the contributions were 9% and 7%, respectively. The contribution of joint shear distortion to horizontal displacement was the smallest at 3% as the joint core remained intact throughout the test.

4.4.2.4 Beam Behaviour

The evaluation of strains in beam reinforcement and beam curvatures are discussed in the following sections:

Beam Reinforcement Strains

In the initial loading stage of DR 1%, both top beam reinforcement and bottom reinforcement of specimen AS4 has shown the sign of yielding in its strain gauge readings. As explained in Figure 4.90, strain gauge located near to column face exceeded the yield strain limit. In the later stage, more strain gauge exceeded the strain limit. The larger bar used yielded in the end of test which showed the energy was dissipated through beam yielding and thus a ductile structure was formed.

Beam curvature

The beam curvature measured near the column face almost reached the theoretical yield curvature in the loading stage of DR 1% as explained in Figure 4.91. In the subsequent loading cycles, increase of the curvature was fast and the curvature of the first two segment measured had surpassed its yield curvature at drift ratio of 3.0%.

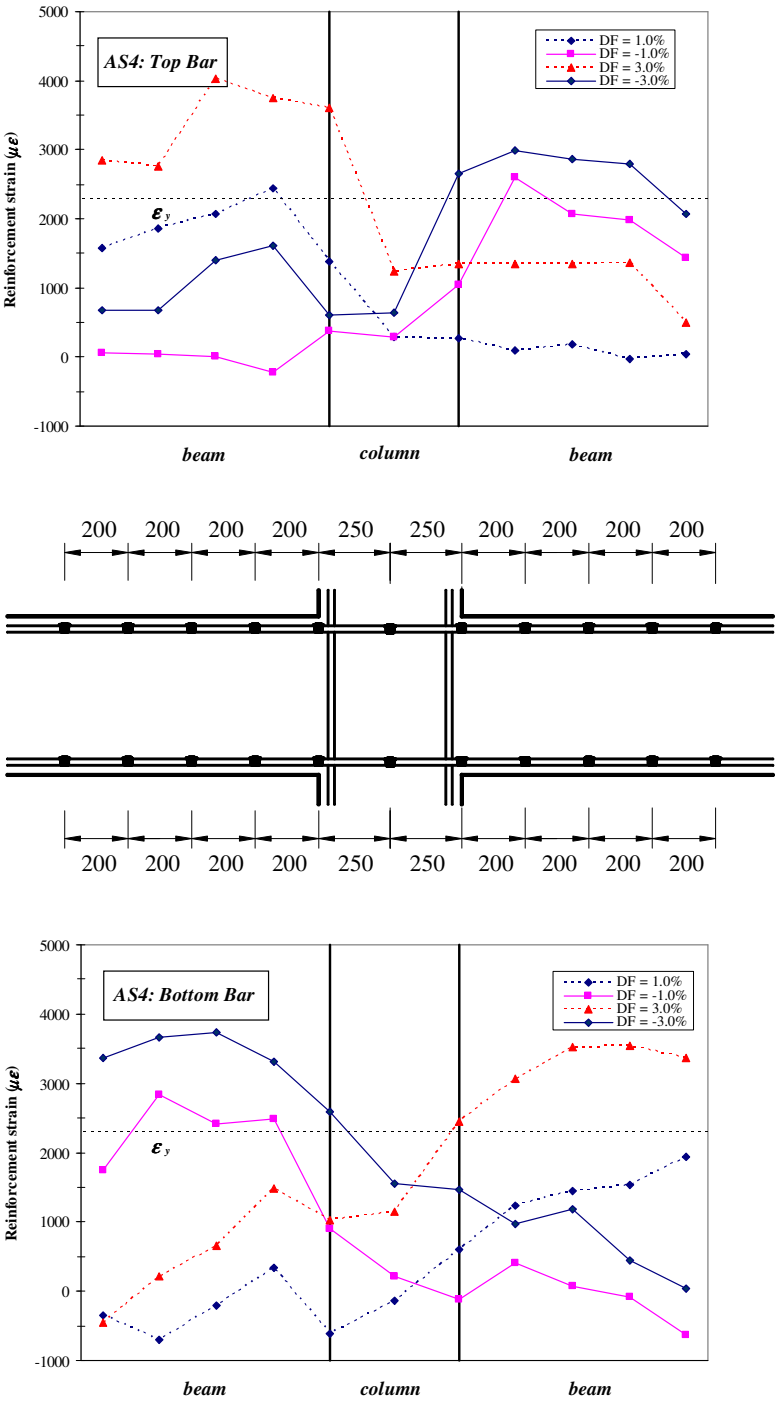

Figure 4.90 Strain Profiles of Beam Bars of AS4

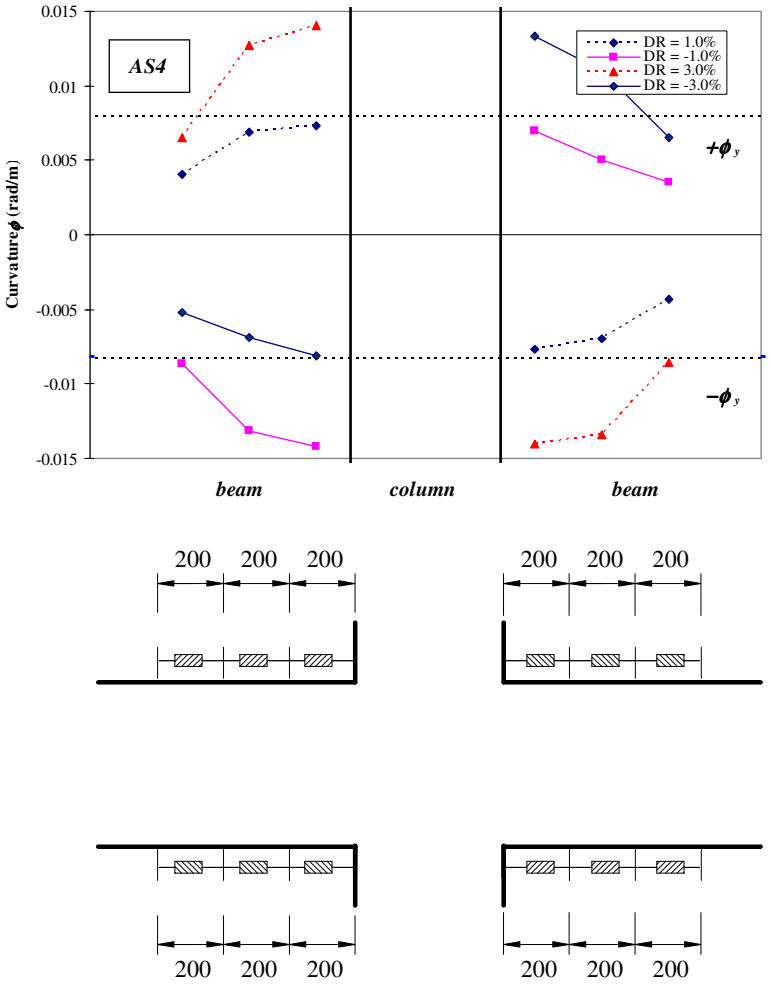

Figure 4.91 Curvature Distribution of Beam of AS4

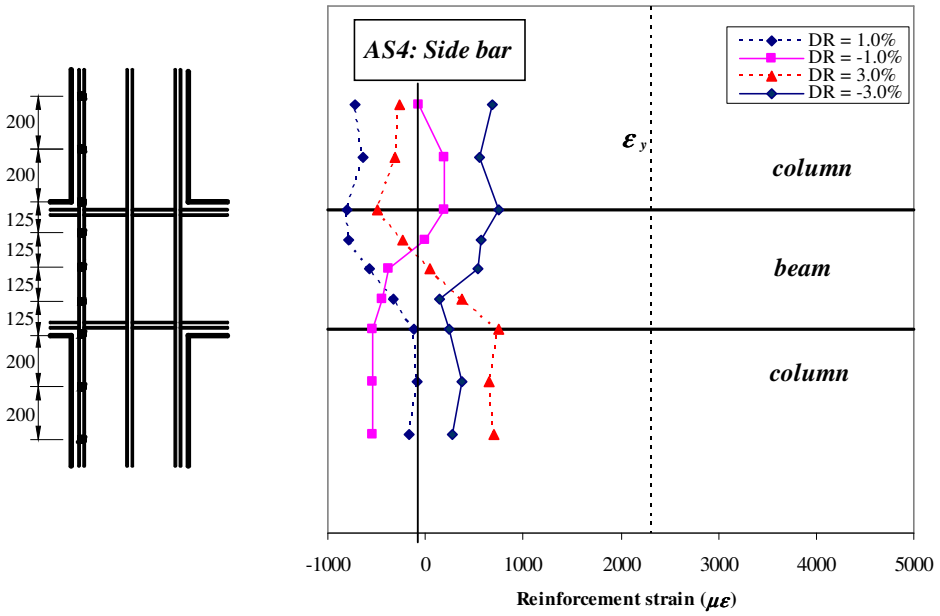

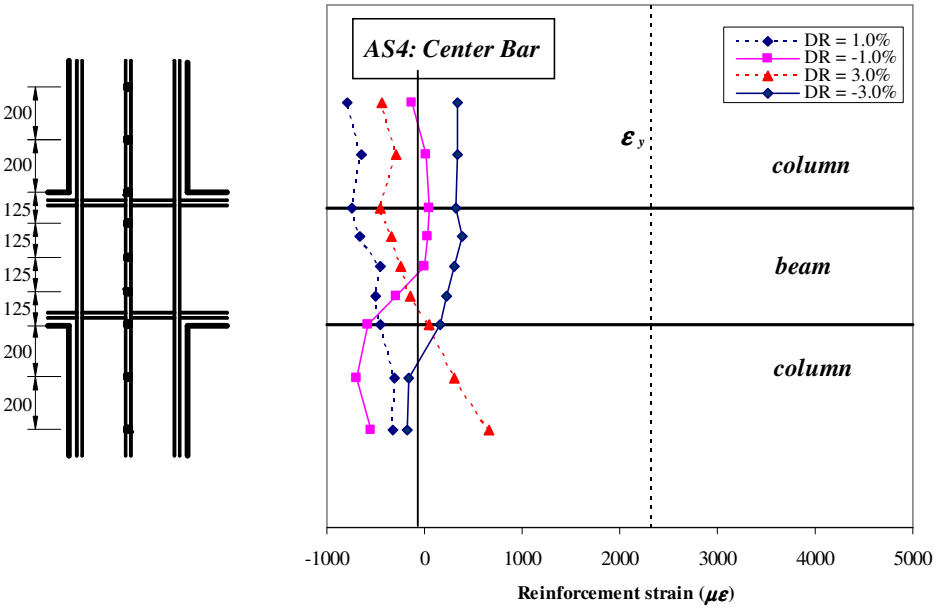

Figure 4.92 Strain Profiles of Column Bars of AS4

4.4.2.5 Column Behaviour

The evaluation of strains in column side reinforcement, column middle reinforcement and column curvatures are discussed in the following sections:

Column Reinforcement Strain

The strains of side bar and central bar of column are explained in Figure 4.92. Due to the confinement from column axial compressive load, the column basically remained elastic throughout the test.

Column curvature distributions

Figure 4.93 shows the column curvature distributions as per instrumented in the test. Since the column was still in its elastic range, the respective curvatures increased gradually but no rapid increase was observed.

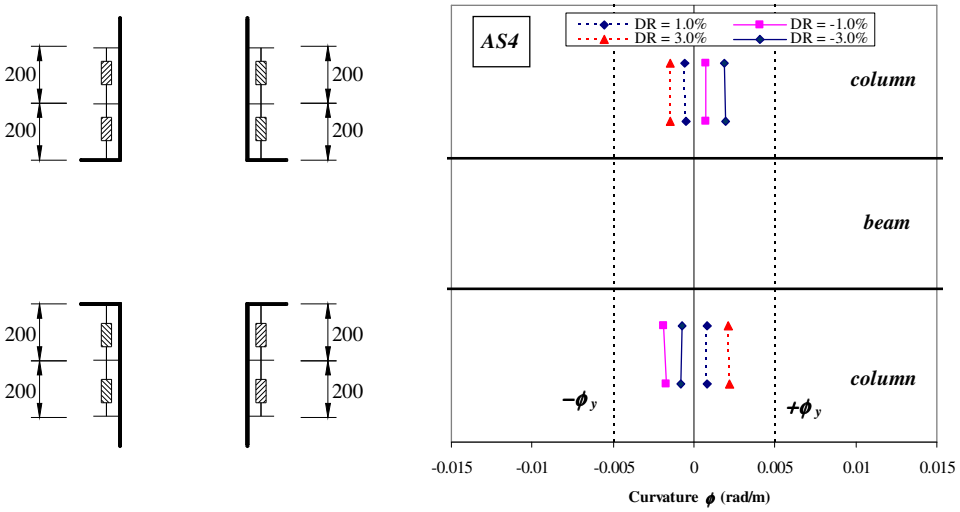

Figure 4.93 Curvature Distribution of Column of AS4

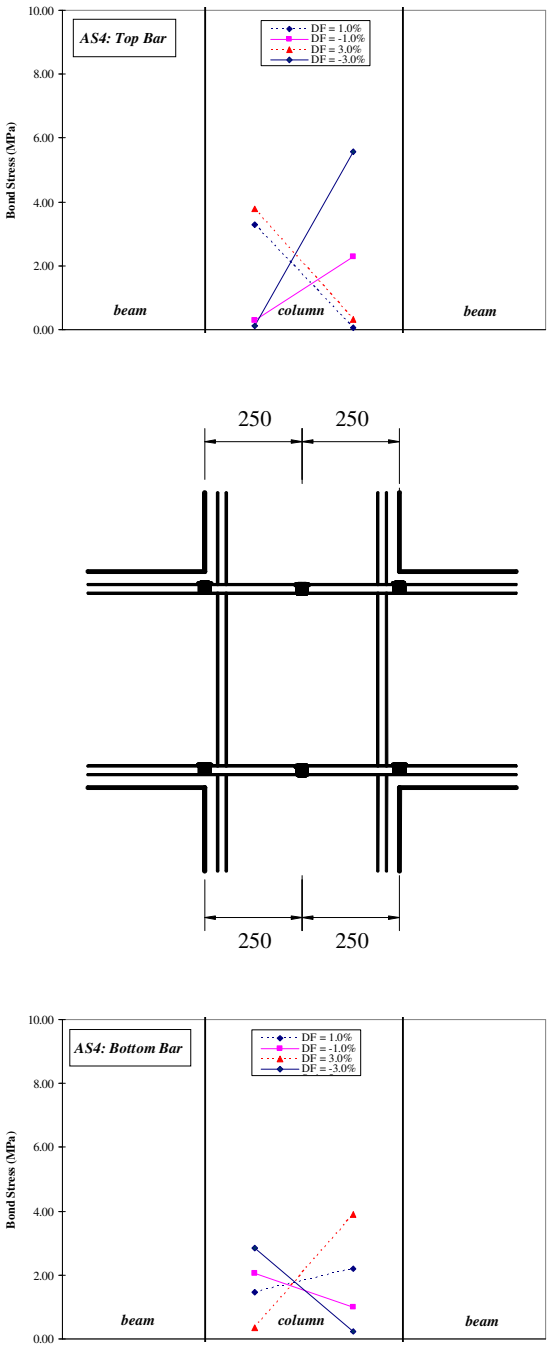

Figure 4.94 Bond Stress of Beam Bar of AS4

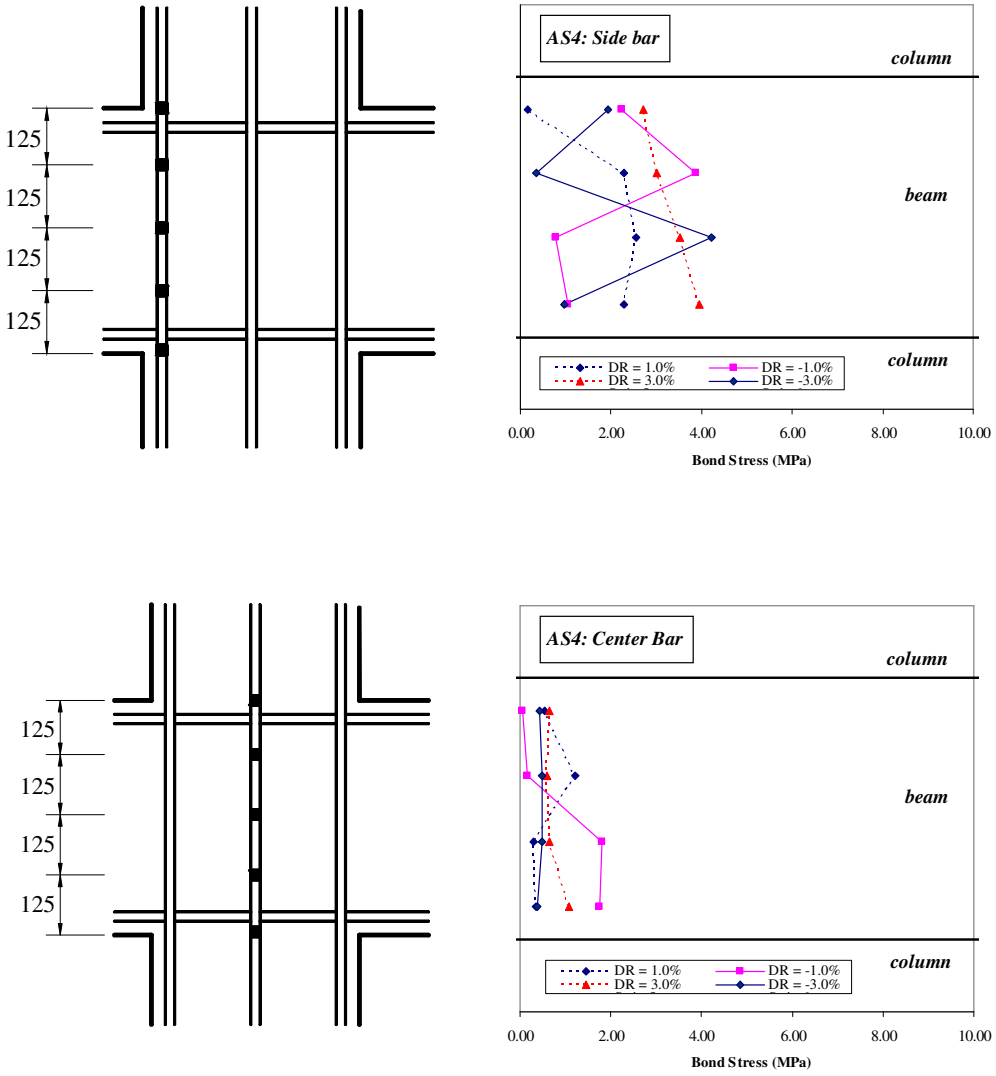

Figure 4.95 Bond Stress of Column Bar of AS4

4.4.2.6 Joint Behaviour

The evaluation on bond stress of beam and and column reinforcement, joint shear distortion and joint shear expansion are discussed in the following sections:

General Behaviour

No crack was found on the joint core of AS2 throughout the test as explained in Figure 4.86a to Figure 4.86d, due to confinement effect from from the applied column axial compressive loading, The maximum nominal horizontal shear stress in

the joint core of 3.96MPa or 0.065 $f_c^{'}$ was observed which met the requirement in NZS 3101.

Bond Stresses of Beam and Column Reinforcement Bars in Joint Core

The average bond stresses for beam bars and column bars were calculated from the wire strain gauge readings. The stresses obtained were plotted in Figure 4.94 and Figure 4.95, respectively. The maximum bond stress obtained along top beam bars was 5.59 MPa (=0.092 $f_c^{'}$) while the maximum bond stress observed along bottom beam bars was 3.90 MPa (=0.064 $f_c^{'}$). Bond deterioration was obvious in bottom beam bars where bond stresses decreased rapidly in the end of test. On the other hand, the column reinforcement remained elastic in the end of the test with maximum bond stress of 4.21 MPa (=0.069 $f_c^{'}$) on side bar and maximum bond stress of 1.81 MPa (=0.030 $f_c^{'}$) on centre bar, respectively.

Joint Shear Distortion and Joint Shear Expension

The measured joint shear distortion and expansion are shown in Figure 4.96. The joint shear distortion and expansion was initiated in the loading to DR 1% while the joint shear distortion and expansion increased rapidly in the loading from DR 2% to DR 4% with the maximum joint distortion and joint expansion was 0.12% and 1.41 mm, respectively.

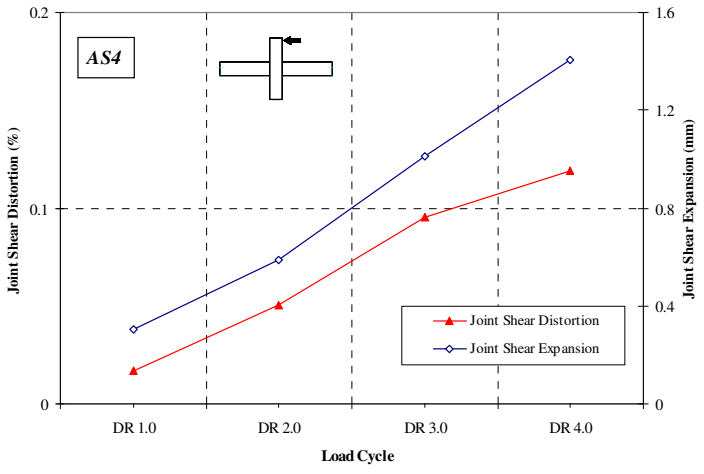

Figure 4.96 Joint Shear Distortion and Expansion of Specimen AS4

4.5 Conclusions

The results of eight HSC beam-column joints were presented. Only Group 1 met the design requirement in NZS 3101 while the remaining 3 groups did not meet either the bond development or detailing in joint core reinforcement. From the test observation, the following points can be concluded:

- Test results revealed that all HSC specimens tested generally show good energy dissipation characteristic. Even though some specimens did not meet the bond development limits in NZS 3101, the specimens did not fail abruptly but still behave ductilely in the end of test. The joint core bond conditions of all specimens were satisfactory where no joint shear failure took place.
- In general, the presence of column axial compressive load in test enhanced the energy dissipation capacity of all specimens with larger confined area within the loops. The presence of column axial compressive load did not change the maximum load of specimens attained.
- The maximum load of specimens tested with column axial compressive load was attained in early loading stage as compared to their counterparts tested without column axial compressive load. This is due to the confinement effects in column that reduced the occurrence of damage in column and joint core hence damage only concentrate at beams.
- Early strength deterioration was observed in test results of specimens tested with the presence of column axial compressive load as the strength of specimens begun to drop when the maximum load was attained.
- The presence of column axial compressive load altered the load path of joint core where the angle of cracks were steeper compared to the test results without column axial compressive load.

The test results showed that the bond development requirement in NZS 3101 can be relaxed since those specimens that did not meet the requirement showed good energy disspipation characterisctics and no serious bond was observed. The following chapters will discuss the possiblity to relax in bond development requirement by parametric studies and finite element modelling.

Chapter 5 Discussion and Analysis of Test Results

This chapter discusses the test results and seismic behaviour of eight high strength concrete beam-column joints. The discussion and analysis cover load-carrying capacity and strength degradation, stiffness degradation, joint shear, member contribution to horizontal displacement and energy dissipation. The development of nonlinear finite element (FE) analysis procedures, especially in nonlinear constitutive laws of materials allows the nonlinear behaviour of reinforced concrete to be reliably simulated. The continual development on computer technology also makes the complicated nonlinear finite element analysis on reinforced concrete structures possible and efficient. It is of great benefit to apply the nonlinear finite element analysis as a parametric study tool. To ascertain the test findings and provide additional information, finite element analyses are carried out on the seismic behaviour of the joints by using finite element program DIANA [D1]. This chapter explains the process which used the advantage of the nonlinear finite element analysis to simulate a laboratory experiment to provide in depth understanding of the structural behaviour of beam-column joints. Moreover, the parameters which have not been considered in the experiment can be applied in the nonlinear finite element simulation.

5.1 Discussion of Experimental Results

The following sections discuss the test results in Chapter 4 and comparisons are made between specimens to understand the influences of parameters such as concrete compressive strength in the structural behaviour of high strength concrete (HSC) beam-column joints. In general, the test data confirmed that joints constructed using high strength concrete can be designed to perform well under severe seismic loading in terms of energy dissipation and failure mode. It would appear that HSC can be used in the structures designed for seismic resistance. For specimens tested with the presence of axial compressive load in columns, the energy dissipation of beam-column joints were found to be improved but the failure

mode remained unchanged. Thus, particular attention should be paid to the problems of degradation in the strength and stiffness due to shear and bond stresses at the joint based on review and discussion, and design recommendations derived for the structural use of HSC.

5.1.1 Load-Carrying Capacity and Energy Dissipation

During a major earthquake, a tremendous amount of energy is released. If the building is designed to withstand the earthquake without collapse, it must be capable of absorbing and dissipating energy. The energy dissipating capability of a structure is very important because it has a strong influence on the response of the structures under dynamic loadings.

The reversed cyclic behaviours of all specimens are shown in Figure 5.1 to Figure 5.2**.** The hysteresis curves of Xin [X1] made of normal strength concrete (NSC) were included in Figure 5.1 (a) to Figure 5.1 (d) for comparison. For each specimen, the energy dissipated in each loading cycle was obtained by calculating the area enclosed by the corresponding load-displacement hysteretic loop. Generally, all specimens showed stable energy dissipation capacity and behaved in a ductile manner. They generally showed satisfactory strength, ductility and energy dissipation characteristics.

In general, the use of high strength concrete (HSC) enhances the strength of beam-column joints with improvement in ultimate load as explained in Figure 5.1a to Figure 5.1d. For specimen NS1, it was observed that the HSC specimen yielded a higher ultimate load in as compared to its NSC counterpart. The enhancement in ultimate load was significant throughout the test with good energy dissipation. On the other hand, for specimens NS2, NS3 and NS4, the enhancement of the ultimate load was less significant compared to NS1. The ultimate loads of these HSC and NSC specimens were load in the test. The stiffness of HSC specimens was generally higher when compared to their respective NSC counterparts. For specimens NS2 and NS4, the pinching of at post-cracked stage was found to be less serious due to the closing of smoother cracks of HSC. Due to the inherent brittle

characteristics of HSC, all HSC specimens showed inferior energy dissipation capacity with a smaller confined area within the curves as compared to its their NSC counterparts.

The test results of NS1 to NS4 and AS1 to AS4 were compared to analyse the effect of the presence of axial loading in test. As explained in Figure 5.2a to Figure 5.2d, the presence of axial load in test enhanced the energy dissipation capacity of all specimens with larger confined area within the loops. The maximum ultimate load was attained in early drift as the confinement effects in column reduced the occurrence of damage in column and joint core hence damage only concentrate at beams. It is noteworthy that the test results with the presence of axial load showed strength deterioration. When the maximum ultimate load was attained, the strength of specimens begun to drop and this is evident in all specimens. This could happen as a result of the damage being concentrated on beam and the deterioration of beams developed too rapidly compared to their counterparts tested without axial load thus leading to strength deterioration upon attaining the maximum ultimate load. It was noticed that specimens tested with axial load have attained the maximum ultimate loads closed to their counterparts tested without axial load, which explained the presence of column axial compressive load has no effect on the maximum ultimate loads. Also, the presence of axial load altered the load path of joint core where the cracks were steeper compared to the test results without axial load. Based on the experimental results, the influence of column axial compressive load is significant in joint shear strength. The axial compressive load of $0.3 f_c' A_g$ was based on the local design code [B5] and the upper threshold of the beneficial effect of axial compressive load has yet to be explored further.

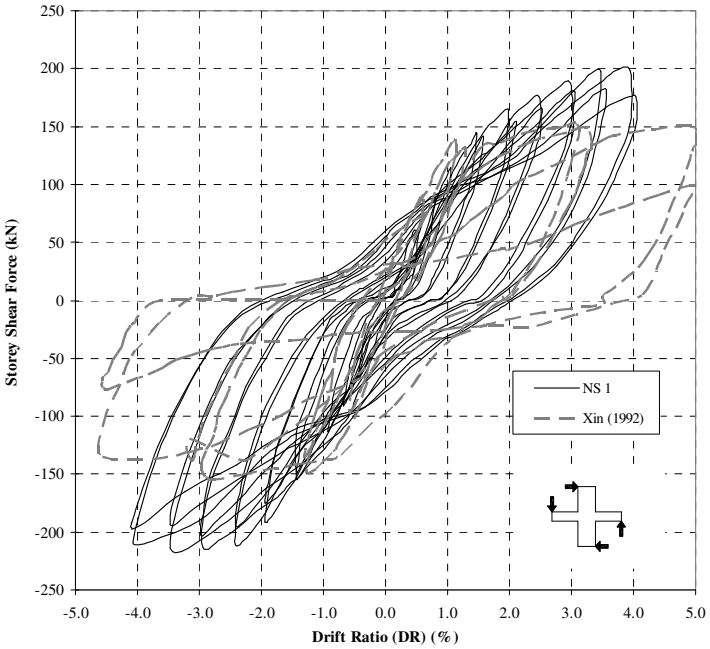
Storey Shear Force (kN)
Drift Ratio (DR) (%)
NS 1
Xin (1992)

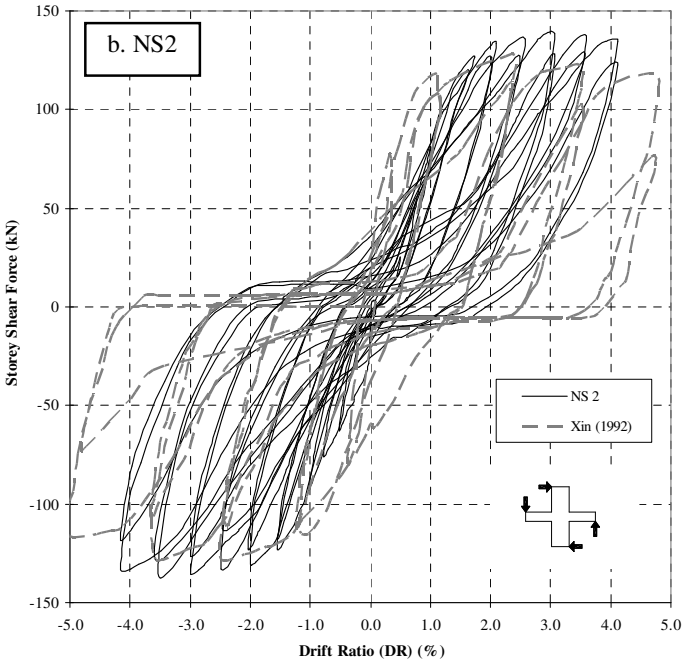
b. NS2
Storey Shear Force (kN)
Drift Ratio (DR) (%)
NS 2
Xin (1992)

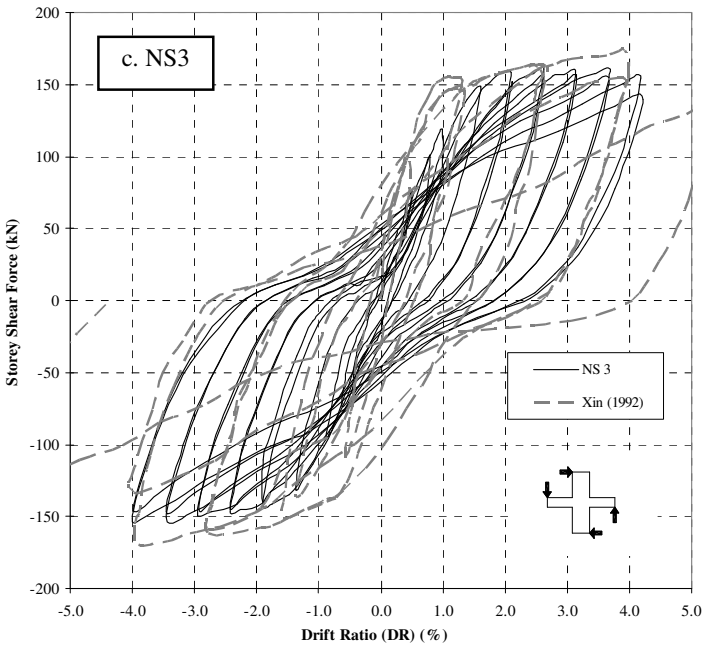

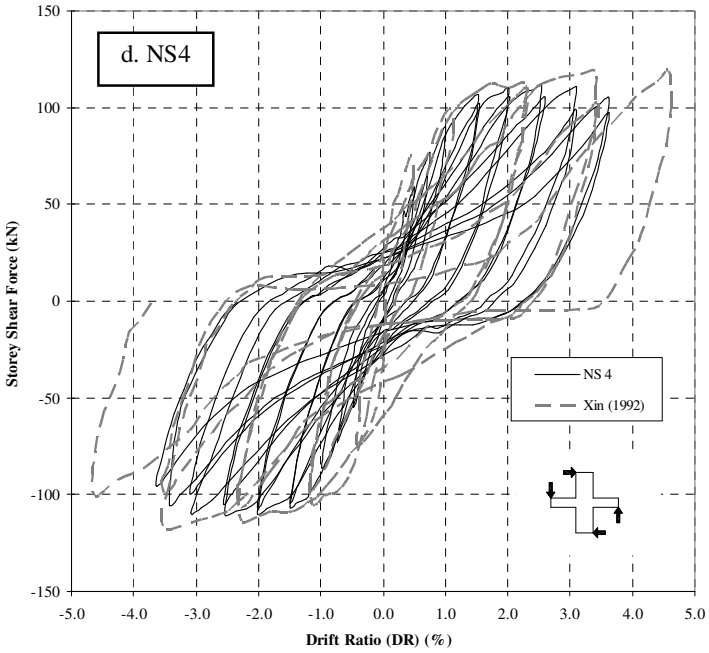

Figure 5.1 Comparison of Hysteresis Loop of NS1 to NS4

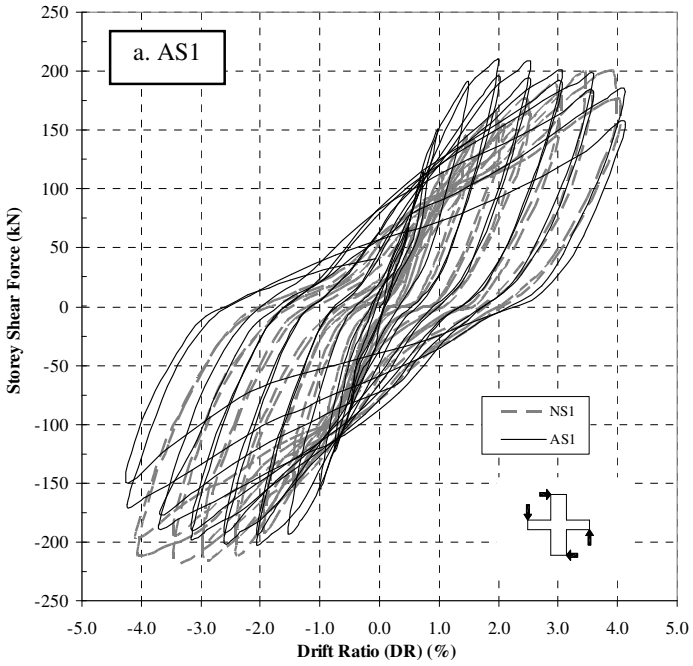
a. AS1
Storey Shear Force (kN)
Drift Ratio (DR) (%)
NS1
AS1
250
200
150
100
50
0
-50
-100
-150
-200
-250
-5.0
-4.0
-3.0
-2.0
-1.0
0.0
1.0
2.0
3.0
4.0
5.0

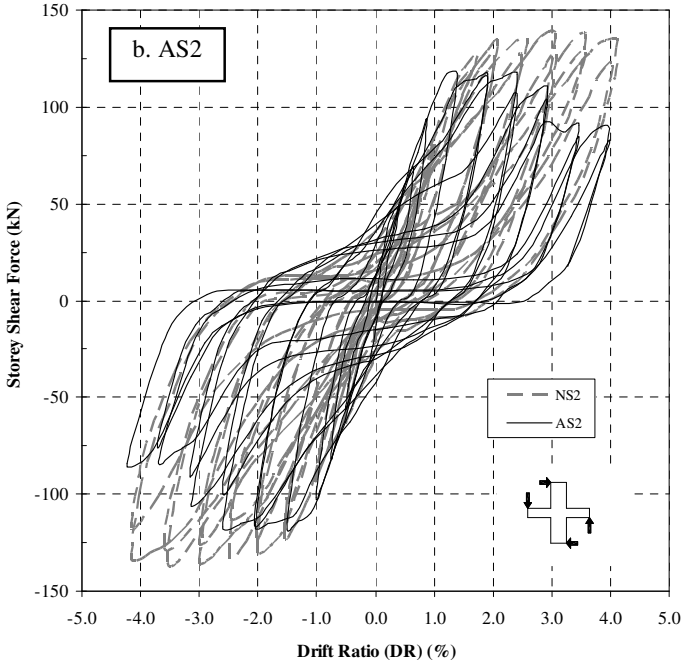
b. AS2
Storey Shear Force (kN)
Drift Ratio (DR) (%)
NS2
AS2
150
100
50
0
-50
-100
-150
-5.0
-4.0
-3.0
-2.0
-1.0
0.0
1.0
2.0
3.0
4.0
5.0

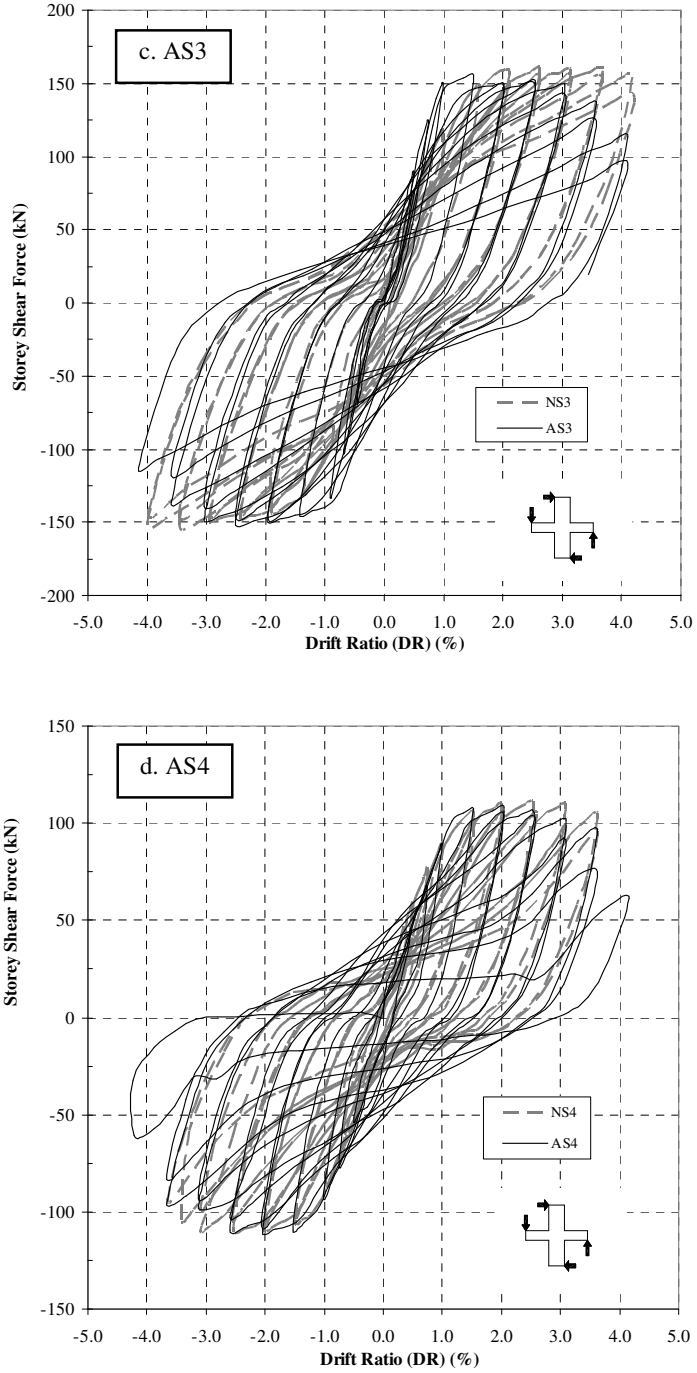

Figure 5.2 Comparison of Hysteresis Loop of AS1 to AS4

5.1.2 Comparison of Stiffness Degradation

The peak-to-peak stiffness versus storey drift ratio (DR) for the specimens at each storey drift level is shown in Figure 5.3a to Figure 5.3d. The comparison was made between specimens tested with and without column axial compressive load. All specimens experienced stiffness degradation with the applied loading and when the deformation level was reached between the storey drift ratios of 1.0% to 1.5%, all specimens had a significant decrease in the global tangent stiffness due to the failure of a critical member. In the final stages, the stiffness continuously decreased to approximately 10% of the predicted elastic stiffness.

There was a large disparity between the drift ratios at which the peak values occurred. Specimens tested with column axial compressive load had accelerated the peak to occur by an average of 25% to 35% and respectively. This observation proved that column compressive axial load could lead to higher stiffness in the early loading stage. Since the column axial load did not really enhance the peak column shear strength, in order to reach the same level of capacity, a smaller deformation is required for a stiffer structural system. With a relatively slower degradation process, the specimens with axial load showed a higher stiffness value by up to 15%. However, the effect of axial load diminished beyond the drift ratio of 2.5% and specimens without axial compressive load had slightly higher stiffness compared to their counterparts till the end of test.

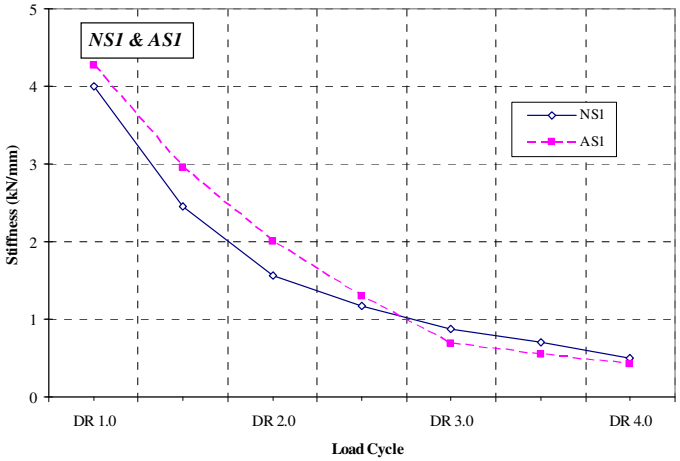

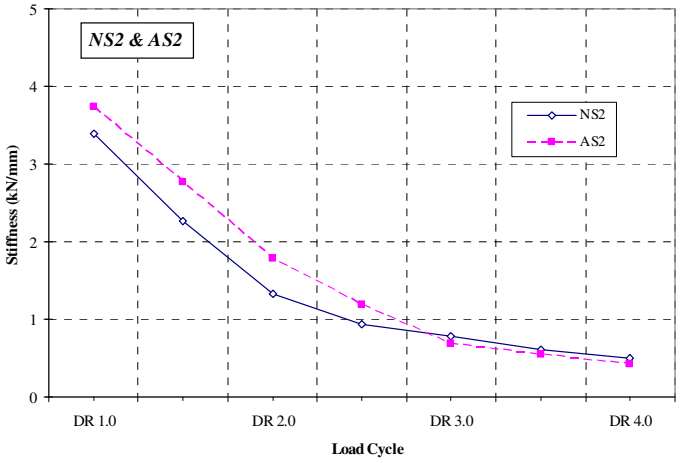

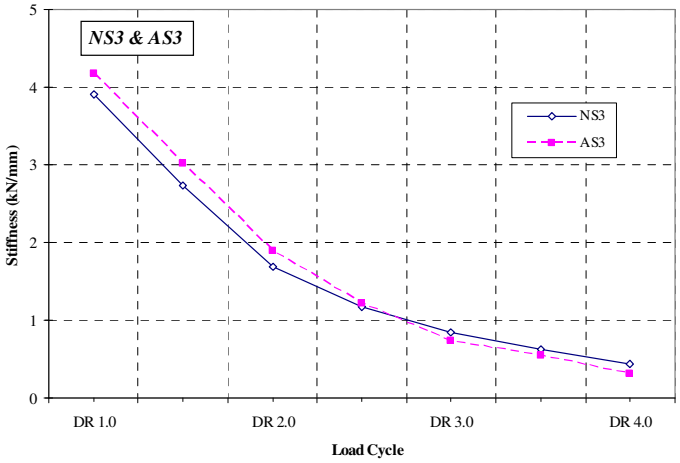

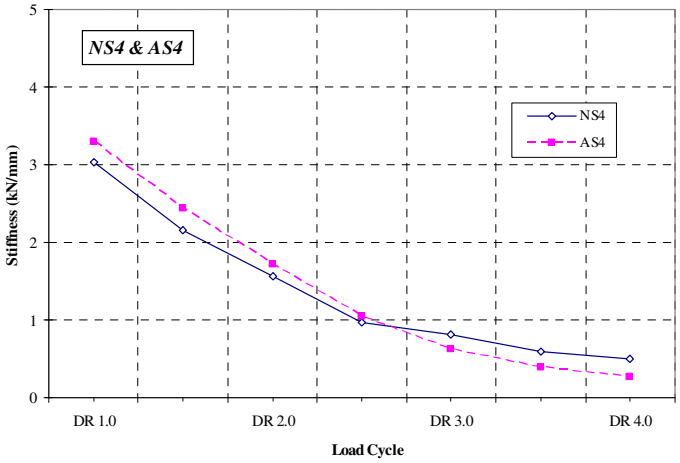

Figure 5.3 Stiffness Degradation of All Specimens

5.1.3 Joint Behaviour

The assessment of the beam-column joint shear strength could be the greatest controversy regarding the structural performance of reinforced concrete frames. Higher shear forces in the joint may lead to deterioration of the joint concrete, as a result of extensive diagonal cracking and or concrete crushing inside of the joint core. In order to prevent the diagonal concrete strut from crushing, the nominal horizontal joint core shear stress in either direction is limited by NZS 3101 [N1] and ACI 318 [A1] to:

$$v_{jh} = \frac{V_{jh}}{b_j h_c} \leq 0.2 f'_c \qquad (5.1)$$

Table 5.1 summarises the joint shear stresses of test results of eight specimens. Comparison was made between NSC specimens of Xin and HSC specimens in Table 5.1a while the effect of column axial compressive load is summarised in Table 5.1b. Apparently, the HSC specimens show a lower joint shear stress demand in term of normalised concrete strength and met the requirement as show in Eq. 5.1. From the test observations, it would appear that all tested specimens did not exhibit serious joint shear failure at the end of the test. The use of HSC improved the joint shear strength of all specimens. For example, no serious joint shear failure occurred in NS1 while its counterpart X1 made of NSC exhibited joint shear failure with spalling of concrete at the joint core due to the opening of diagonal tension cracks, and the crushing of diagonal compression struts was observed [X1].

As shown in Table 5.1b, the presence of column axial compressive load has limited influence on the joint shear stress. For example, the joint shear stress of both specimens NS1 and AS1 were similar. From the test observation, specimens tested with column axial compressive load, no joint shear was observed and for specimen AS2 and AS4, no crack was observed throughout the test due to the beneficial confinement effects of axial compressive load which prevented the opening of diagonal tension cracks as well as the crushing of diagonal compression struts to take place.

Table 5.1 Comparison of Joint Shear Stress of Test Results

a. Comparison on Concrete Grade

Specimen ID	*Joint Shear Stress*	
	(MPa)	*f_c' (MPa)*
X1	*4.87*	*0.157*
NS1	*4.78*	*0.078*
X2	*3.67*	*0.089*
NS2	*3.62*	*0.059*
X3	*4.89*	*0.114*
NS3	*4.97*	*0.081*
X4	*3.04*	*0.065*
NS4	*3.14*	*0.051*

b. Comparison on column axial compressive load

Specimen ID	*Joint Shear Stress*	
	(MPa)	*f_c' (MPa)*
NS1	*4.78*	*0.078*
AS1	*4.65*	*0.076*
NS2	*3.62*	*0.059*
AS2	*3.80*	*0.062*
NS3	*4.97*	*0.081*
AS3	*5.04*	*0.083*
NS4	*3.14*	*0.051*
AS4	*3.14*	*0.052*

It is observed that HSC specimens were much stiffer than NSC specimens. From test observation, the joint core contribution to the overall deformation decreased with the increase in concrete compressive strength. The subsequent deterioration in stiffness occurred mainly due to cracking, spalling and crushing of the concrete. Due to the lack of post-peak ductility of HSC, the cover thickness problem is worth noting again for its importance. If the concrete cover or corner of the column face is crushed, the concrete compression strut mechanism may not be developed effectively. The lost of stiffness consequently results in more pinching of the hysteresis loops.

5.1.4 Member Contribution to Horizontal Displacement

The contributions of different members to specimen deformation give a good understanding of the behaviour of the specimens and help in visualizing the possible failure modes. In general, at a large deformation level, an increase in the participation of the most damaged members was accompanied by a serious loss of strength. For the specimens with a strong column-weak beam system, the beam deformation contributed more to the lateral displacement during the test and the specimens could be considered to have failed due to the beam flexural failure.

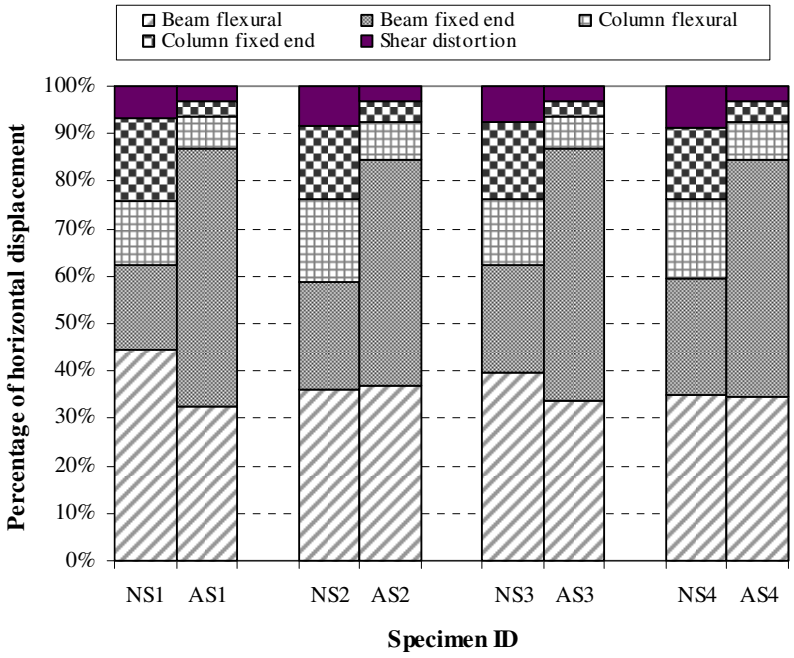

Figure 5.4 Decomposition of Lateral Displacement of All Specimens

The decomposition percentages of the total lateral displacement measured at the top of the column at the end of the test are shown in Figure 5.4. Based on the observation in Figure 5.4, it is evident that lateral displacement contributed by beam flexural and beam fixed end rotation has been dominant in all specimens. The lateral displacement contributed by column flexural and column fixed-end rotation was not significant in all specimens. Similarly, it is noted that the contribution of lateral displacement from shear distortion was not significant in all specimens, the reason being that the joint core region was very strong and rigid. This agreed with the test observation where no joint failure was noticed at the end of test.

As explained in Figure 5.4, the presence of axial compressive load altered the failure mode of specimens AS1 to AS4 as compared to their respective counterparts. Due the beneficial confinement effect from axial compressive load, the columns have been confined with limited flexural rotation thus the lateral displacement contributed by column flexural and column fixed-end rotation was not significant in Specimens AS1 to AS4. On the other hand, the lateral displacement

contribution from beam fixed end were the highest as both the adjoining beams rotated excessively against the confined column which served as rigid ends. This was also confirmed by the observation of spalling of beams adjacent to column at the end of test.

5.1.5 Bond Stress

The average bond stresses measured along the longitudinal beam and column bars in the joint were calculated using the wire strain gauge readings. Due to the complexity of bond stresses within a joint, the strain was assumed to be uniformly distributed over the gauge length of 150 mm to obtain the average bond stress of the measured points. The average bond stresses so obtained are summarized in Table 5.2.

Table 5.2 Summary of Measured Maximum Bond Stress

Specimen Marking	*NS1*	*NS2*	*NS3*	*NS4*	*AS1*	*AS2*	*AS3*	*AS4*
Max Bond Stress (MPa)	*4.54*	*4.81*	*4.85*	*5.23*	*3.81*	*4.05*	*4.12*	*4.83*
Drift ratio (DR)	*4.0%*	*2.0%*	*2.0%*	*1.0%*	*4.0%*	*3.0%*	*3.0%*	*3.0%*

It is obvious that the smaller bar used in NS1 has showed the lowest bond stress. At DR 4%, the highest bond stress of NS1 was 4.54 MPa while for NS2 and NS3 made of a 16mm bar, the maximum bond stress was 4.81MPa and 4.85 MPa at DR 2%. Lastly for NS4 made of larger bar of 20mm, the bond stress of NS4 was 5.23 MPa. However, the bond stress deteriorated after the maximum values at DR 1% was attained. For specimens tested with column axial compressive load, it is evident that the presence of axial compressive load improved the bond condition of specimens. At DR 3%, the bond stress of AS1 was 3.81 MPa while improvement in bond stresses of AS2 and AS3 was observed. The maximum bond stresses for both specimens were found to be 4.05MPa and 4.12 MPa, respectively, reached at DR 3%. Finally for AS4 made of larger bar of 20mm, the bond stress was 4.83 MPa and the bond stress deteriorated after the maximum values at DR 3% was attained.

5.1.6 Concrete Strength Effect

In general, the use of high strength concrete enhances the strength of beam-column joints and load carrying capacity with improvement in stiffness and ultimate load. However, the inherent brittle characteristics of high strength concrete in ductile beam-column joints were also observed. All HSC specimens showed inferior energy dissipation capacity, with a smaller confined area within the curves as compared to the normal strength concrete specimens. The test results revealed that the bond strength of HSC is higher than the corresponding NSC. However, the bond behaviour of HSC is more brittle in comparison with NSC. The use of small reinforcement in NS1 successfully enhanced the performance of HSC beam-column joint with higher ultimate load. As compared to other specimens, the use of larger bar diameter caused a less favourable brittle bond behaviour that has less favourable energy dissipation capacity then the NSC specimens.

It is noteworthy that when HSC is used in beam-column joint, problem such as development of high bond stresses and shear may arise. To overcome this possible problem, the control of column deformation is essential so as to avoid the development of high bond stresses and shear. The bond conditions along the longitudinal reinforcement can be improved if a limit is imposed on the minimum column depth to longitudinal bar diameter ratios. As such, equations for column depth to beam bar diameter could be developed for longitudinal bars passing through joints constructed using HSC in order to incorporate the influence of critical parameters such as column depth, bar diameter, concrete strength in beam-column joint design. In the current practice, the minimum column depth to longitudinal bar diameter ratios limitation set in NZS 3101 [N1]:

$$\frac{d_b}{h_c} \leq 3.3\alpha_f \frac{\sqrt{f_c'}}{\alpha_o f_y} \qquad (5.2)$$

α_f = 0.85 for beam bars in two way frames and
= 1.00 for beam bars in one direction

α_o = 1.25 for plastic hinge in beam developed in column face and

= 1.00 for plastic hinge is relocated and beam section in column face remain elastic range

With the new construction technology that propels the use of HSC, the above equation may be reviewed to ensure the equation is still valid for HSC usage.

5.1.7 Effect of Column Axial Compressive Load

In general, the presence of column axial compressive load in test enhanced the energy dissipation capacity of all specimens with larger confined area within the loops. The maximum ultimate load was attained in early drift as the confinement effects in column reduced the occurrence of damage in column and joint core hence the damage concentrated at beams. It is noteworthy that the strength of specimens with column axial compressive load begun to drop when the maximum ultimate load was attained, and this is evident in all specimens. This could due to the damage was mainly concentrated on beam and the deterioration of beams developed too rapidly compared to their counterparts tested without axial load thus lead to a strength deterioration upon attaining the maximum ultimate load. For comparison, most of the maximum ultimate load of specimens tested with axial load was similar to their counterparts tested without axial load.

On the other hand, the compressive axial load did steepen the diagonal strut by causing a more vertical diagonal cracking in the joint panel. The orientation of the diagonal cracks was primarily determined by the joint panel geometry itself the relative depth of the columns to that of the beams. For instance, in specimen trigonometry gave the orientation of the diagonal line in the joint panel to be 48 degree with respect to the horizontal direction. This complied very well with the observed diagonal cracking orientation. Likewise, in specimen most of the parallel diagonal propagated along a 54 degree orientation. Therefore, it is believed by the author that the ultimate effect of column axial load should be assessed from both aspects together: the beneficial effect from enlarging the diagonal strut and the detrimental effect by imposing more compressive pressure to the concrete strut.

The main parameters that influence the bond performance of the reinforcing bar are confinement, clear distance between the bars and nature of the surface of the bar [P3, P7]. In this test, the confinement of the embedded bar was very essential to improving the bond performance in order to transfer the tensile forces. The relevant confinement was obtained from axial compressive load due to the column and with reinforcement that helps in arresting the splitting cracks. The beneficial confinement effect on specimens made of larger bars was also found to be substantial, as summarized in bond stress of Table 5.2.

Axial compressive loading is a critical parameter in the studies of beam-column joints, but the effect of axial compressive loads on the seismic behavior of beam-column joints is still debated among researchers in this field. Paulay [P7] pointed out that column axial force is beneficial to the joint shear resistance. Because the neutral axis depth in the column increases with axial compression, a larger portion of the bond forces from the beam bars can be assumed to be transferred to the diagonal strut. Thus, the contribution of the concrete to joint shear resistance will increase. This point of view was accepted by NZS 3101 [N1] in which the concrete shear strength is considered to increase alongside the increase in the column axial compressive loading.

Based on the experimental results, the influence of column axial compressive load is significant in joint shear strength. The axial compressive load of $0.3 f_c' A_g$ was based on the local design code [B5] and the upper threshold of the beneficial effect of axial compressive load have yet to be further explored. Recently, a number of researchers [F3, L5] noticed that the effect of axial compressive loads may vary at different axial compressive loading levels or at different joint shear levels. By testing 10 interior beam-column joints, Fu *et al*. [F3] pointed out that if the shear is high, the increase of axial compressive loads is unfavorable, whereas if the shear is small, the increase of axial compressive loading is favorable to the joints.

5.1.8 Effect of Bottom-Reinforcement-to-Top-Reinforcement Ratio, β

From test results of NS1, AS1, NS3 and AS3, no serious pinching was observed in the hysteresis loops of specimens with equal bottom and top reinforcement area ($\beta = 1.0$). On the other hand, pinching was observed in the hysteresis loops of specimens NS2, AS2, NS4 and AS4 with bottom-reinforcement-to-top-reinforcement ratio β of less than unity ($\beta < 1.0$). The pinching of the hysteresis loops was direct related to the lost of bond in the beam reinforcement. Also, spalling of concrete and crushing of corners of joint was observed in specimens NS2, AS2, NS4 and AS4 with β of less than unity. This was due to the difference in bond condition between the bottom and top reinforcement.

For specimens with β of less than unity, larger reinforcement area was used in top bar where the bond condition of top reinforcement was found to be better due to the smaller stress in the top reinforcement in compression than its bottom reinforcement. The slip of bottom reinforcement was larger than that of top reinforcement, the flexural cracks at the bottom of beam at column face was fully closed where the concrete was subjected to a larger compression force than the concrete of the top of the beam on the opposite of the column face. Correspondingly, the force transferred to concrete by the bottom reinforcement was smaller than the top reinforcement in the joint core. Some yield penetration was observed in beam reinforcement of specimens with β of less than unity and it is deduced that yield penetration was the cause of lost of bond strength around beam reinforcement.

By comparing the hysteresis loops of NS2 (β of less than unity, beam bar size 16mm) in Figure 5.1b and NS3 (β of unity, beam bar size 16mm) in Figure 5.1c, the effect of β is evident. The smaller the β, the more significant the pinching of the hysteresis loops. Thus, the value of β affects the shape of the hysteresis loops due to different bond condition of top and bottom beam reinforcement should β is less than unity.

5.2 Finite Element Modelling

A two-dimensional nonlinear finite element analysis on beam-column sub-assemblages using program DIANA is introduced in this chapter to investigate the structural behaviour of the high strength concrete beam-column joints. **DIANA** (**Di**splacement **Ana**lyser) is an extensive multi-purpose finite element software package that is dedicated to a wide range of problems arising in Civil Engineering including structural, geotechnical, tunnelling and earthquake disciplines as well as oil & gas engineering. It is a well proven and tested software package with robust functionality, an extensive material, element and procedure library based on advanced database techniques, linear and non-linear capabilities, full 2D and 3D modelling features and tools for CAD interoperability [D1]. The fundamental concept of DIANA finite element analysis performed is explained in the following sections.

5.2.1 Modelling of Concrete

In DIANA, the constitutive behaviour of quasi-brittle material such as concrete is characterized by tensile cracking and compressive crushing [D1]. Out of all the available cracking models, the Modified Maekawa Concrete Model has been selected as the concrete model throughout the analysis. This model combines a multi-axial damage plasticity model for the compressive regime with a crack model based on total strain for the tensile regime which can simulate the hysteresis in tensile and compressive unloading-reloading loops. The model is defined by engineering parameters such as the tensile and compressive strength and the fracture energy which covers all loading situations. The constitutive model of total strain crack model has been developed along the line with of the Modified Compression Field Theory originally proposed by Vecchio & Collins [D1].

The Modified Maekawa Concrete Model is developed on the "total strain model" in DIANA which describes the stress as a function of the strain. This concept is known as hypo-elasticity when the loading and unloading behaviour is along the same stress-strain path. In the software, the behaviour in loading and unloading is

modelled differently with secant unloading [see Figure 5.5a]. The co-axial stress-strain concept is applied where the stress-strain relationships are evaluated in the principal directions of the strain vector. This approach is also known as the "Rotating Crack Model" which is applied to the constitutive modelling of reinforced concrete and is well suited for reinforced concrete structures. More appealing to the physical nature of cracking is the fixed stress-strain concept in which the stress-strain relationships are evaluated in a fixed coordinate system which is fixed upon cracking. Both approaches are easily described in the same framework where the crack directions are either fixed or continuously rotating with the principal directions of the strain vector [D1].

The basic concept of the total strain crack models is that the stress is evaluated in the directions which are given by the crack directions. The strain vector in the element coordinate system is updated with the strain increment which is transformed to the strain vector in the crack directions with the strain transformation matrix. In a co-axial rotating concept the strain transformation matrix depends on the current strain vector whereas in a fixed concept the strain transformation matrix is fixed upon cracking. The behaviour in compression is evaluated in a rotating coordinate system when the material is not cracked, where in case of a fixed concept the compressive behaviour is evaluated in the fixed coordinate system determined by the crack directions [D1].

In the concrete model, a crack is assumed to be initiated perpendicular to the major principal stress if its value exceeds the concrete tensile strength, independent of the value assumed by the other principal stresses. The orientation of the crack is then stored and the material response perpendicular to the crack is determined by a stress-strain relationship for the cracked material volume. Additional cracks may appear at the same location, but they are assumed to form at an orientation greater than 15 degrees to the existing cracks. If the angle is less than that, the secondary cracks are assumed not to have been generated even when the tensile stress has reached its fracture envelope [D1].

During loading the concrete is subjected to both tensile and compressive stress which can result in cracking and crushing of the material. In a fixed stress-strain concept the shear behaviour is modelled explicitly with a relationship between the shear stress and the shear strain. It is assumed that damage recovery is not possible which implies that the absolute values of the internal damage variables are increasing. The tensile behaviour of reinforced concrete can be modelled using tension softening approach [M1]. For the total strain crack model, softening function based on fracture energy are implemented as shown in softening curve in Figure 5.5b which is related to a crack bandwidth as is usual in smeared crack model. The fracture energy G_F and the tensile strength f_t of the concrete were used to calculate the value of ultimate crack opening w_u [H1]. The fracture energy G_F of the concrete was calculated using a three-point bending test based upon the recommendations of RILEM 50-FMC [H1]. An exponential stress-strain curve was used as shown in Figure 5.5b and the tensile strength of concrete f_t used in the analysis was determined from the compressive strength f_c in accordance to CEB-FIP Model code [M1]:

$$f_t = 0.30\left(f_c\right)^{2/3} \text{ (MPa)} \qquad (5.3)$$

Concrete which is subjected to compressive stresses shows a pressure-dependent behaviour, i.e., the strength and ductility increase with increasing isotropic stress. Due to the lateral confinement, the compressive stress-strain relationship is modified to incorporate the effects of the increased isotropic stress. Furthermore, it is assumed that the compressive behaviour is influenced by lateral cracking. To model the lateral confinement effect, the parameters of the compressive stress-strain function, f_{cf} and ε_p, are determined by a failure function which gives the compressive stress that causes failure as a function of the confining stresses in the lateral directions. The base function in compression, with the parameters f_{cf} and ε_p, is modelled with a number of different predefined curves in which a softening model of concrete after cracking is selected as shown in Figure 5.5c to explain the drop of strength after cracks took place in concrete [D1].

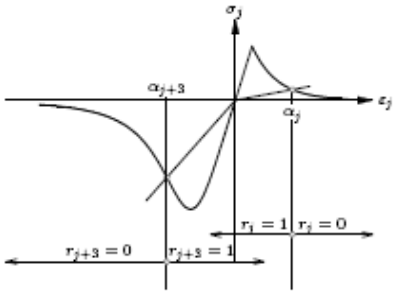

a. Hypo-elasticity of Model

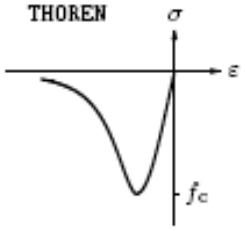

b. Compression Model

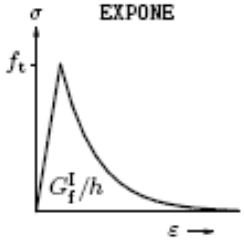

c. Tension model

Figure 5.5 Material Modelling [D1]

In the model the compressive strength f_{cf} is assumed to be under uniaxial stress situations and its essence is calibrated on experimental data. The compressive strength of the model only matches with the maximum compressive stress under uniaxial loading conditions when the specified Young's modulus and Poisson's ratio are close to the values for concrete. As such, the cylinder compression strength test results were used as the concrete compressive strength in the modelling with the assumption of Poisson's ratio of 0.20 in the analysis.

5.2.2 Modelling of Reinforcement

The Von Mises yield criterion with isotropic strain hardening and an associated flow rule were used to describe the constitutive behaviour of the reinforcement. The bars were modelled with the DIANA options of separate truss elements. Figure 5.6 defines the stress-strain relationship for the reinforcing steel, which was modelled with an elasto-plastic curve. During the test, bond deterioration along the beam

longitudinal bars and column main bars, particularly within the joint region, was found and necessary slippage of the steel bars was expected to occur. Bond-slip models with the DIANA options were accounted for the reinforcement and surrounding concrete [D1].

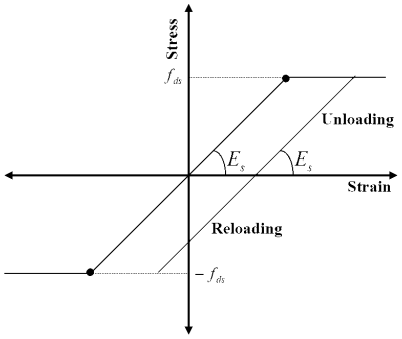

Figure 5.6 Material Modelling of Reinforcement [D1]

5.2.3 Bond Slip Law

The bond law used in the analysis is based on CEB-FIP Model Code-2010 [C2] with the following equations of bond stress:

$$\tau = \tau_{\max}\left(\frac{s}{s_1}\right)^{\alpha} \text{ for } 0 \le s \le s_1 \tag{5.4a}$$

$$\tau = \tau_{\max} \text{ for } s_1 \le s \le s_2 \tag{5.4b}$$

$$\tau = \tau_{\max} - \left(\tau_{\max} - \tau_f\right)\frac{s - s_1}{s_3 - s_2} \text{ for } s_2 \le s \le s_3 \tag{5.4c}$$

$$\tau = \tau_f \text{ for } s_3 \le s \tag{5.4d}$$

The bond law model parameters depend on the properties of the bar surface, and can be referred from the CEB-FIP Model Code [C2].

5.2.4 Mesh Generation

To simulate the structural behaviour of a HSC beam-column joint, the model should firstly be built based on the geometrical properties of the as-built models. Figure 5.7a explains the construction of FE model of NS1 where the geometry definition was performed to outline the overall dimension of the model. Prior to assigning the element to the model, the model was meshed and discritised to an appropriate element size as shown in Figure 5.7b. It is noteworthy that the joint core was meshed to a denser element size to cater for the inherent more complex stress-strain relation of a joint core.

In the FE analysis, the 8-node 2D quadratic solid elements (CQ16M) were used for the concrete modelling, while the embedded reinforcing bars were modelled using truss elements as depicted in Figure 5.7c and Figure 5.7d. The material properties of concrete and steel were then assigned to the respective elements to complete the element modelling process. To simulate the specimen as close as possible, the material test results were utilised as the material properties during the FE modelling.

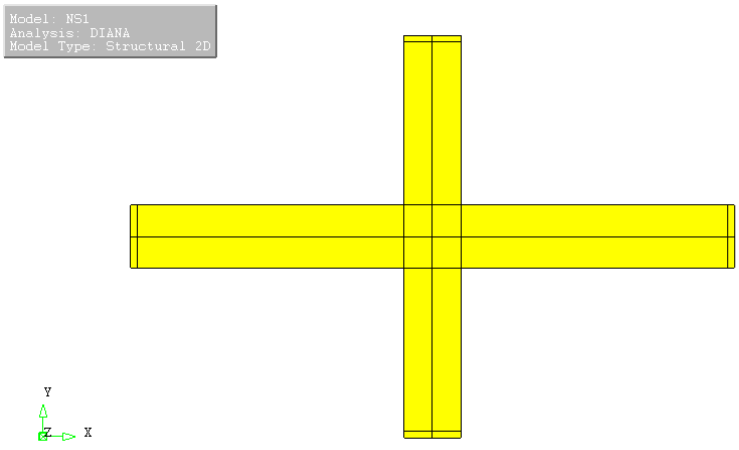

a. Geometry Definition

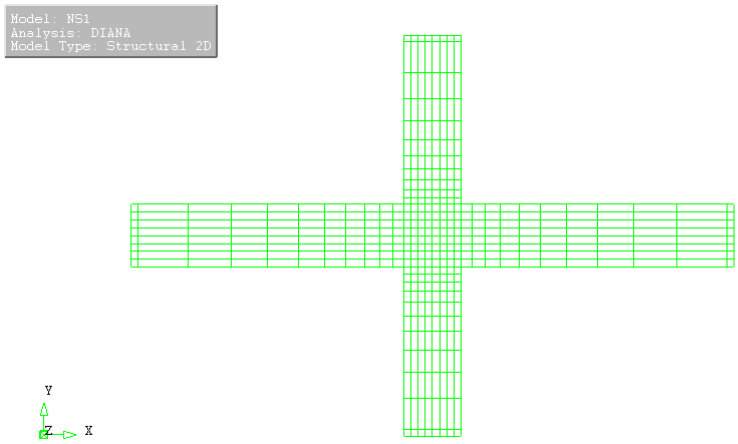

b. Meshing of Model

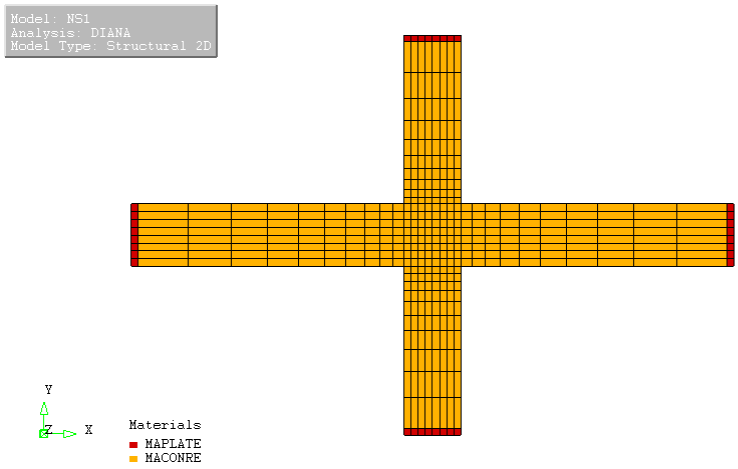

c. Assign of Element on Model

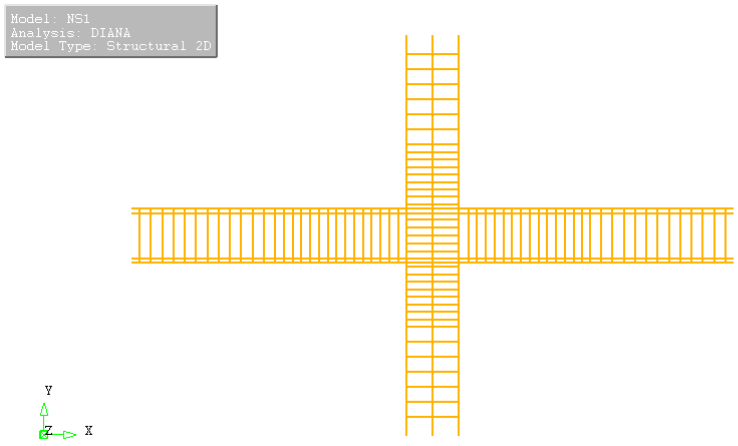

d. Reinforcement Bar Element

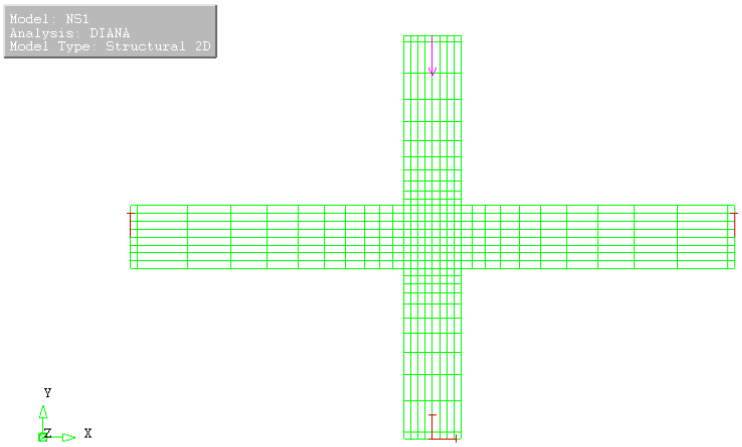

e. Boundary Condition

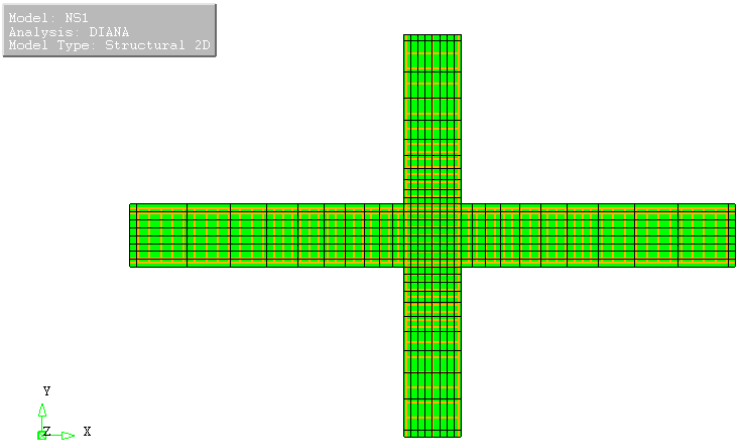

f. Complete Meshing

Figure 5.7 Typical Meshing of Model

5.2.5 Boundary Condition and Loading Condition

Boundary condition is the most important control parameter in FE modelling. As explained in Figure 5.7e, the column was restrained in x and y direction in its base while the beam was restrained in y direction to allow horizontal displacement. Horizontal load was then applied on the top of column to simulate the quasi-static load in the test. No axial compressive load was applied on the column of Specimens NS1 to NS4 while a constant axial compressive load of $0.3f_c^{'}A_g$ was applied on column of Specimens AS1 to AS4 throughout the FE simulation. The

complete model is shown in Figure 5.7f. Upon completion of modelling, the FE analysis can be performed. All the load cycles of the simulation were carried out in the displacement controlled mode as explained in Figure 5.8 which is similar to the loading condition of the test performed.

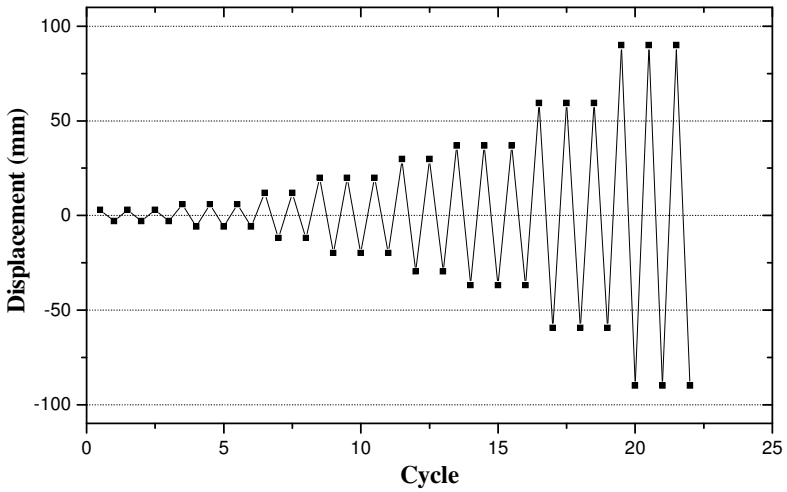

Figure 5.8 Loading Procedures

5.2.6 Material Properties

Table 5.3 summarised the material parameters used in finite element analysis of high strength concrete beam-column joints. Since test results in Chapter 4 were used as benchmarks to the analysis, the material properties based on material test were adopted as to minimise the variation in the FE analysis.

Table 5.3 Material Properties of Finite Element Model

Material Parameters	*Values*
Concrete tension strength, f'_t	*3.12 to 3.34 MPa (based on each specimen)*
Concrete compression strength, f'_c	*60.2 to 61.4 MPa (based on each specimen)*
Concrete elastic modulus, E_c	*20000 MPa*
Concrete poisson ratio υ	*0.16*
Steel tension yield strength, f_y	*473 to 526 MPa (based on each bar size used)*
Steel ultimate strain, ε	*0.16*
Steel elastic modulus, Es	*2.1e+5 MPa*
Fracture energy, G_f	*0.2*

5.3 Finite Element Models Results Verification

Upon the completion of an FE modelling, the FE result needs to be verified against the test results to ascertain its validity. Even though the actual loading conditions in test were simulated in the FE modelling to reflect the actual behaviour of HSC beam-column joint under cyclic loading, the output from FE can be misleading sometimes. The control parameters in shear behaviour, tension behaviour and compression behaviour need to be fine-tuned in the FE simulation process to closely simulate the actual structural behaviour of HSC beam-column joints. The fine-tuning process was performed based on the comparison between the hysteresis loops from FE simulations and test results to study the general trend of the analysis while stress contour and crack profiles were plotted to understand the stress distribution in the end of simulation. Until the confirmation of values in control parameters, the full FE simulations were then carried out on the eight test samples. The following sections discuss the comparison between test observations and FE findings to verify the validity of the FE analysis as well as provide a clearer picture on the structural behaviour of high strength concrete beam-column joints.

5.3.1 Hysteretic Behaviour

Figure 5.9 and Figure 5.10 present the comparison of hysteretic behaviour obtained through the FE numerical predictions and the experimental investigations. There is a good agreement between the analytical and the experimental results where the general trend of the hysteresis loops from FE is similar to the test results. FE models of NS2, NS4, AS2 and AS4 exhibited a significant pinching in the loops which was quite similar to those observed during the experiments. The FE numerical models generally give lower maximum loads compared to the test data which explained the conservatism in the FE simulation.

As explained in Figure 5.9a to Figure 5.9d, the FE simulation successfully estimated the energy dissipation capacity of HSC beam-column joint which is close to the test results. However, conservatism was observed when 3.0% drift was surpassed where FE tended to estimate a lower energy dissipation capacity when

maximum load was attained. Note that the maximum load estimated in FE is about 20% to 25% less than those found in the test investigation for Specimens NS1 to NS4 tested with zero axial compressive loading. On the other hand, the FE estimation underestimated the energy dissipation of HSC beam-column joints with smaller confined area within the curves as explained in Figure 5.10a to Figure 5.10d. The conservatism in structural performance is particularly significant in the later loading stage where the estimated maximum loads from FE simulation are around 20% lower than those of the test results.

5.3.2 Overall Strength and Stress Contours

The stress contours during the peak of 4.0 drift of all models are depicted in Figure 5.11a to Figure 5.11d and Figure 5.12a to Figure 5.12d. In general, the joint core was highly stressed in the end of the simulation. The compression strut was formed at the adjacent corners of the joint core which agreed with the test observations. The softening of the FE models after maximum load had attained was not as significant as the actual test observation but the overall energy dissipation capacity of the models are good enough to closely simulate the behaviour of HSC beam-column joints. Table 5.4 and Figure 5.13 summarise the comparison between both test and FE results where the FE can predict the maximum strength fairly good with mean value of 0.87 and standard deviation of 0.07.

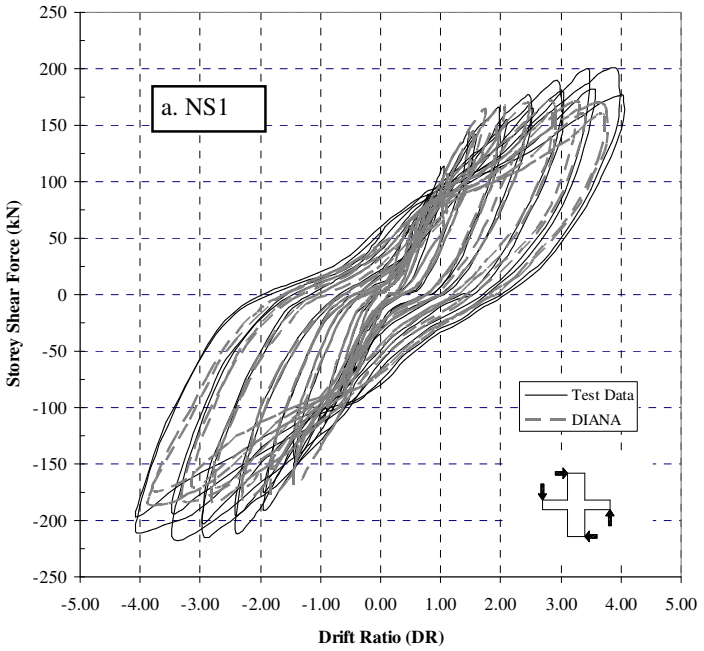
a. NS1
Storey Shear Force (kN)
Drift Ratio (DR)
Test Data
DIANA
250
200
150
100
50
0
-50
-100
-150
-200
-250
-5.00
-4.00
-3.00
-2.00
-1.00
0.00
1.00
2.00
3.00
4.00
5.00

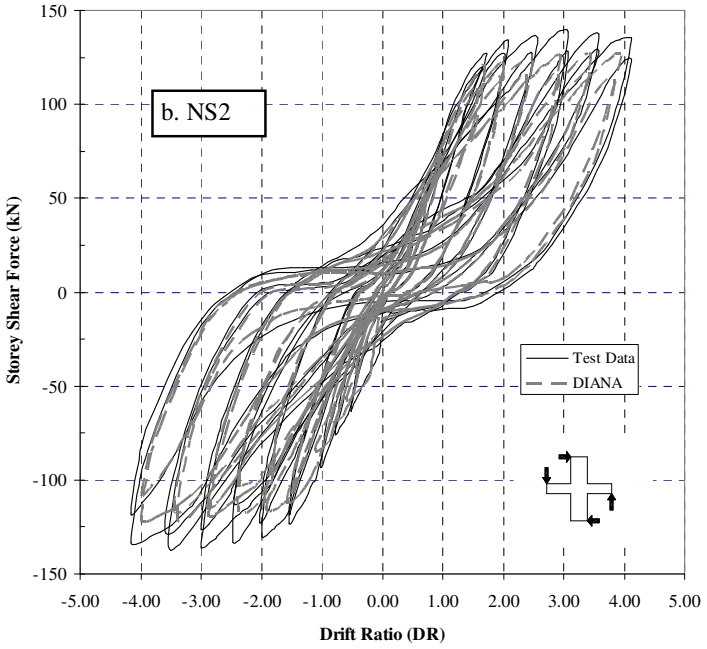
b. NS2
Storey Shear Force (kN)
Drift Ratio (DR)
Test Data
DIANA
150
100
50
0
-50
-100
-150
-5.00
-4.00
-3.00
-2.00
-1.00
0.00
1.00
2.00
3.00
4.00
5.00

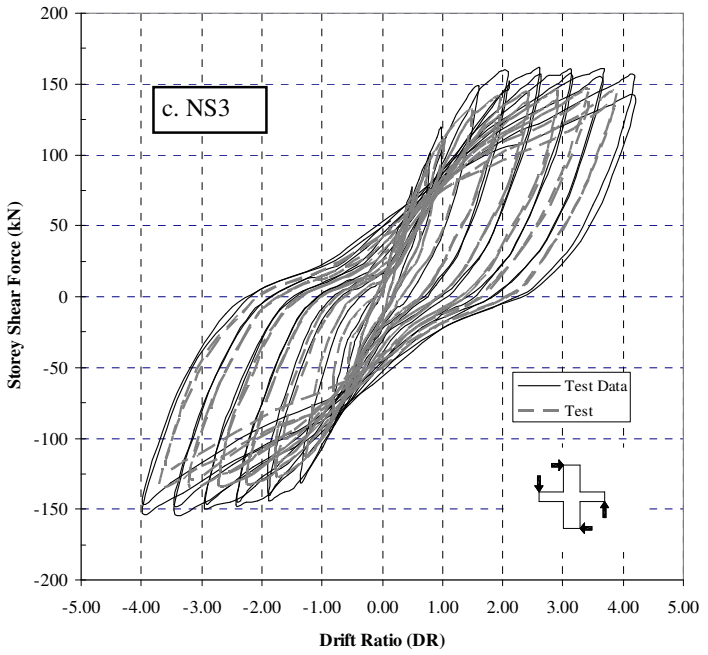

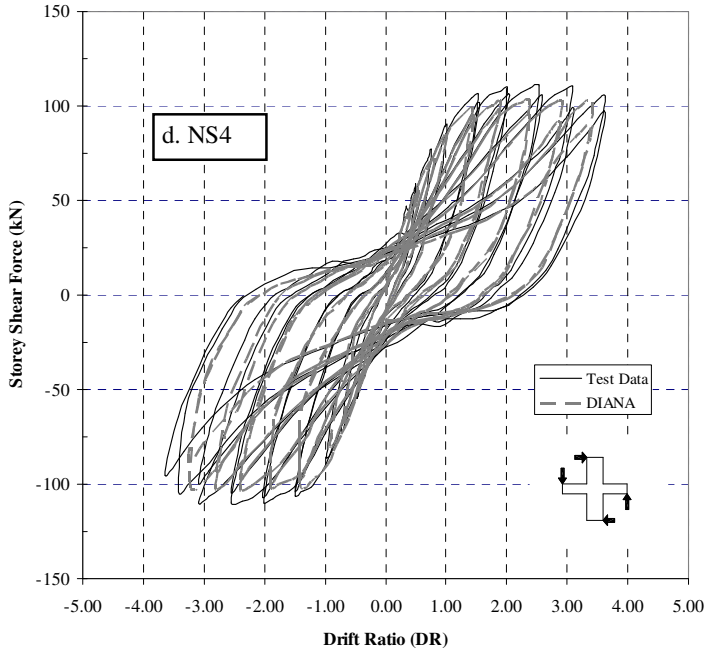

Figure 5.9 Hysteresis Loop of Specimens NS1 to NS4

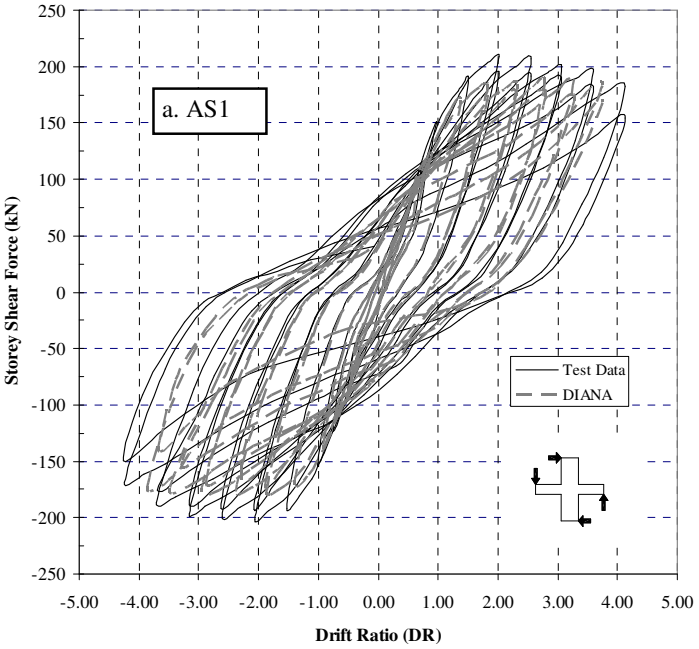
a. AS1
Storey Shear Force (kN)
Drift Ratio (DR)
Test Data
DIANA
250
200
150
100
50
0
-50
-100
-150
-200
-250
-5.00
-4.00
-3.00
-2.00
-1.00
0.00
1.00
2.00
3.00
4.00
5.00

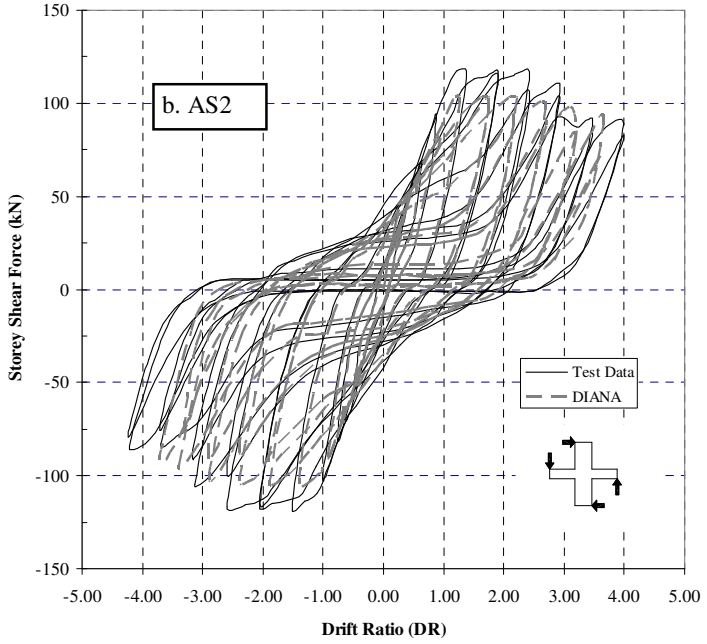
b. AS2
Storey Shear Force (kN)
Drift Ratio (DR)
Test Data
DIANA
150
100
50
0
-50
-100
-150
-5.00
-4.00
-3.00
-2.00
-1.00
0.00
1.00
2.00
3.00
4.00
5.00

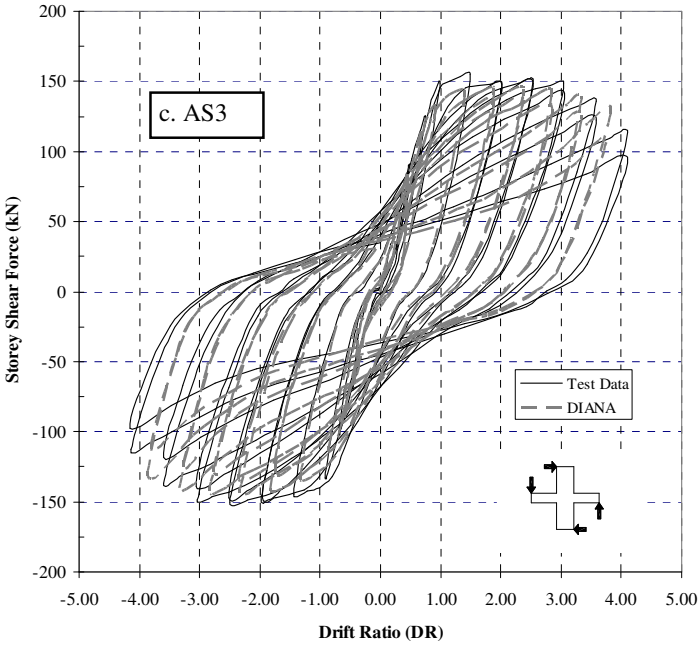

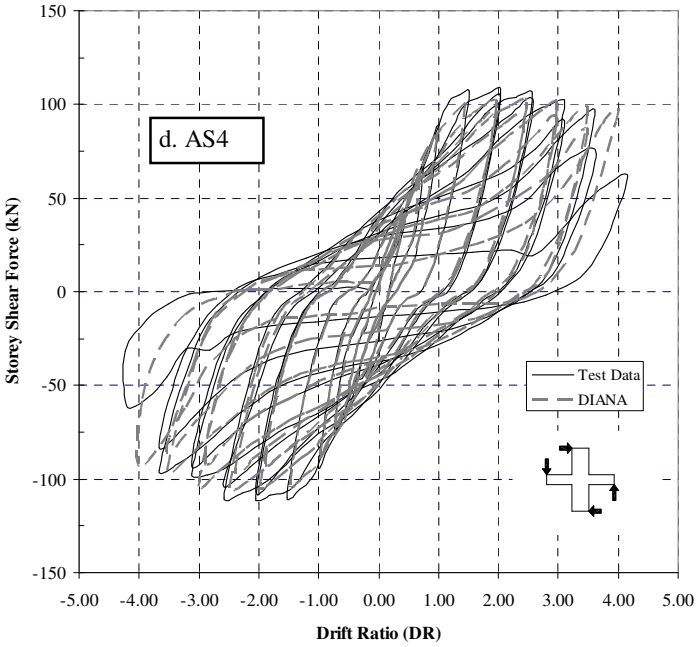

Figure 5.10 Hysteresis Loop of Specimens AS1 to AS4

a. NS1

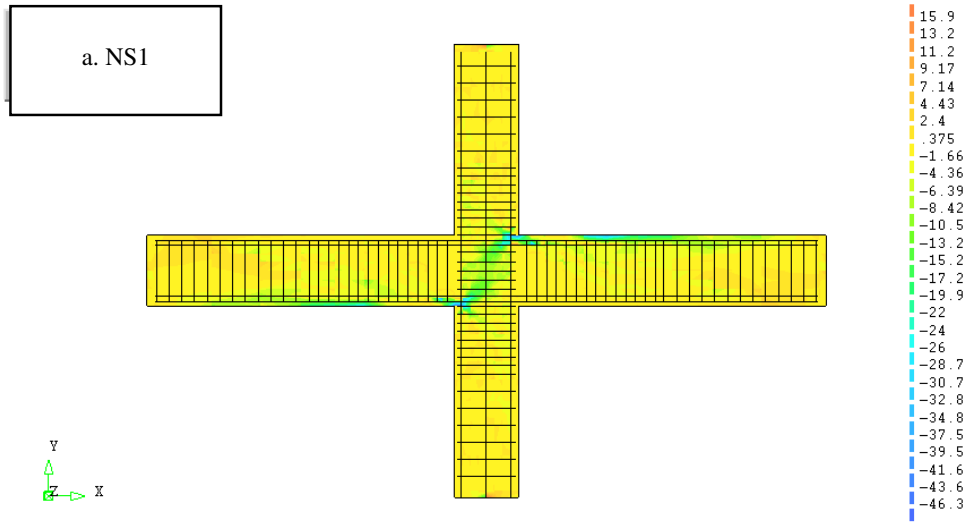
15.9
13.2
11.2
9.17
7.14
4.43
2.4
.375
-1.66
-4.36
-6.39
-8.42
-10.5
-13.2
-15.2
-17.2
-19.9
-22
-24
-26
-28.7
-30.7
-32.8
-34.8
-37.5
-39.5
-41.6
-43.6
-46.3
Y
Z
X

b. NS2

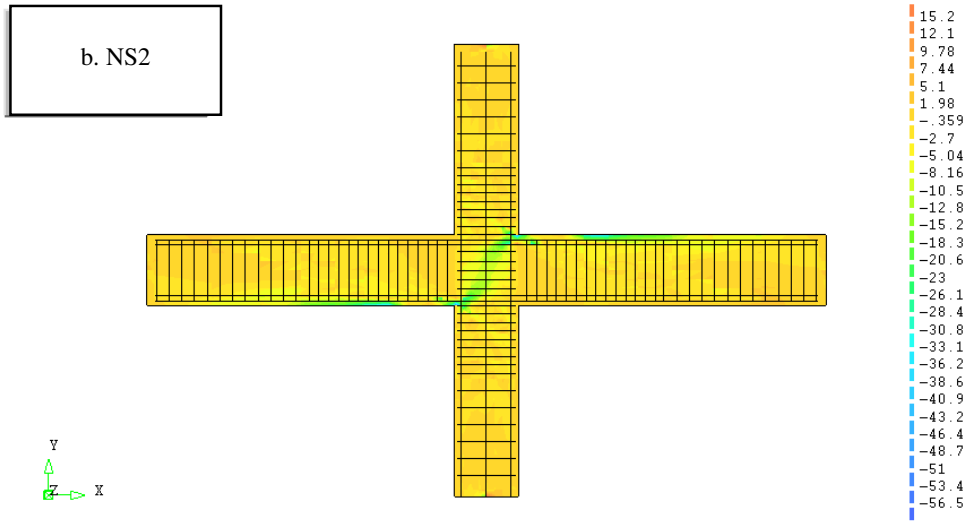
15.2
12.1
9.78
7.44
5.1
1.98
-.359
-2.7
-5.04
-8.16
-10.5
-12.8
-15.2
-18.3
-20.6
-23
-26.1
-28.4
-30.8
-33.1
-36.2
-38.6
-40.9
-43.2
-46.4
-48.7
-51
-53.4
-56.5
Y
Z
X

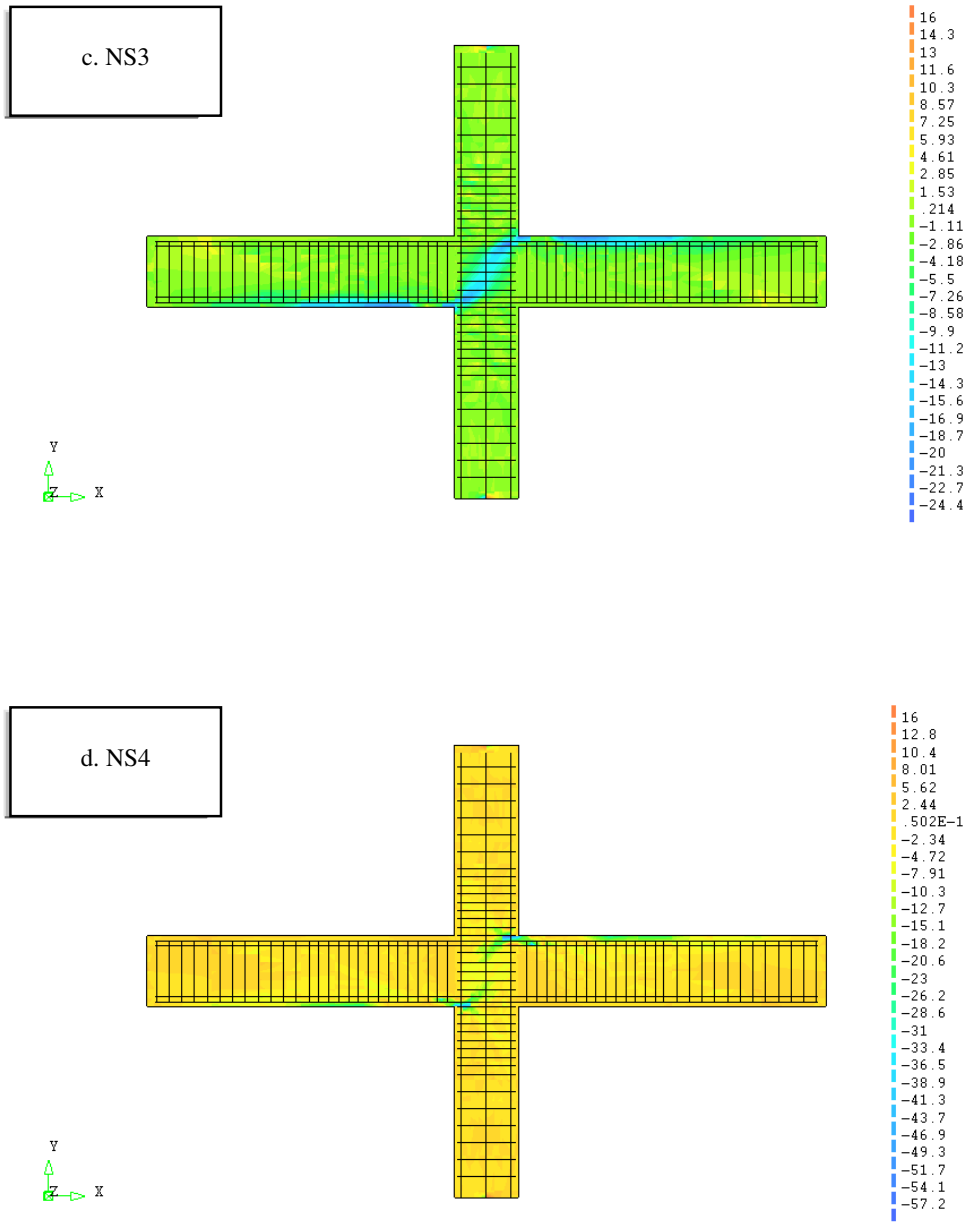

Figure 5.11 Stress Contour of Specimens NS1 to NS4

a. AS1

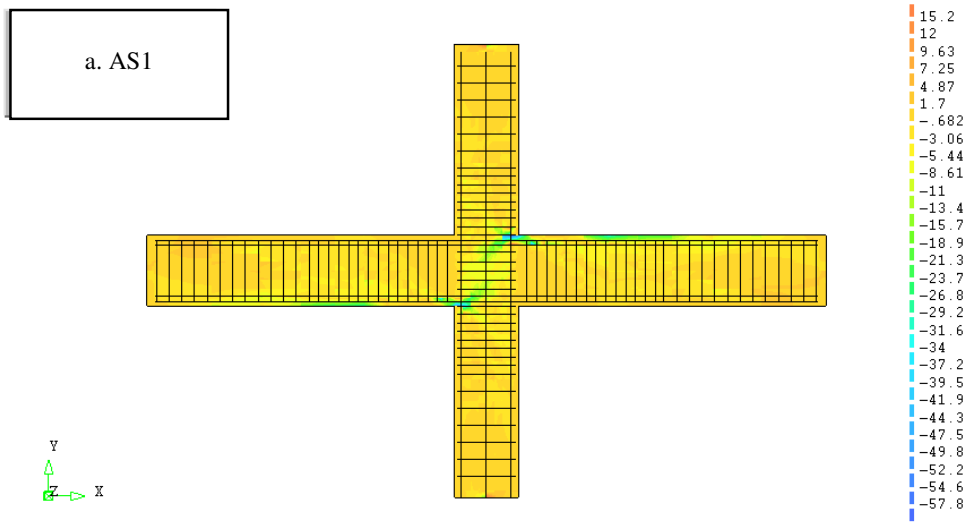
15.2
12
9.63
7.25
4.87
1.7
-.682
-3.06
-5.44
-8.61
-11
-13.4
-15.7
-18.9
-21.3
-23.7
-26.8
-29.2
-31.6
-34
-37.2
-39.5
-41.9
-44.3
-47.5
-49.8
-52.2
-54.6
-57.8
Y
Z
X

b. AS2

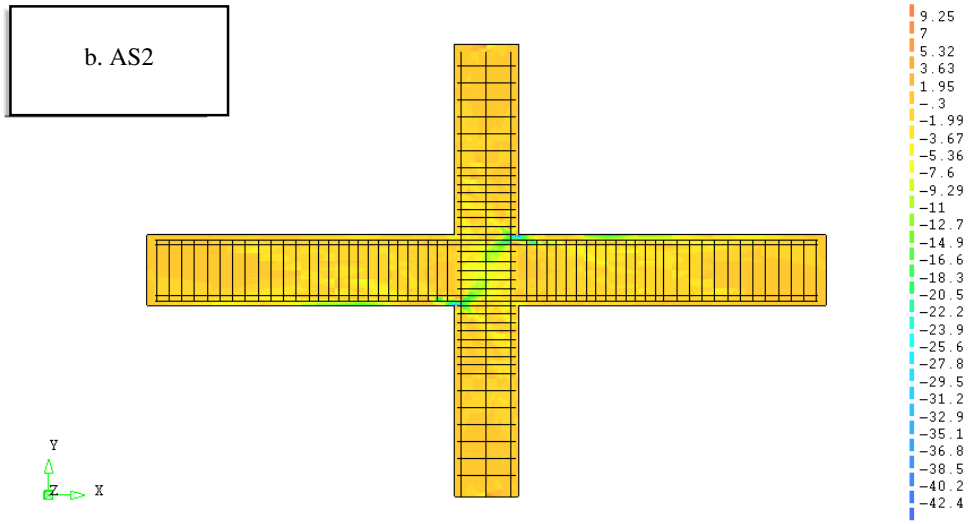
9.25
7
5.32
3.63
1.95
-.3
-1.99
-3.67
-5.36
-7.6
-9.29
-11
-12.7
-14.9
-16.6
-18.3
-20.5
-22.2
-23.9
-25.6
-27.8
-29.5
-31.2
-32.9
-35.1
-36.8
-38.5
-40.2
-42.4
Y
Z
X

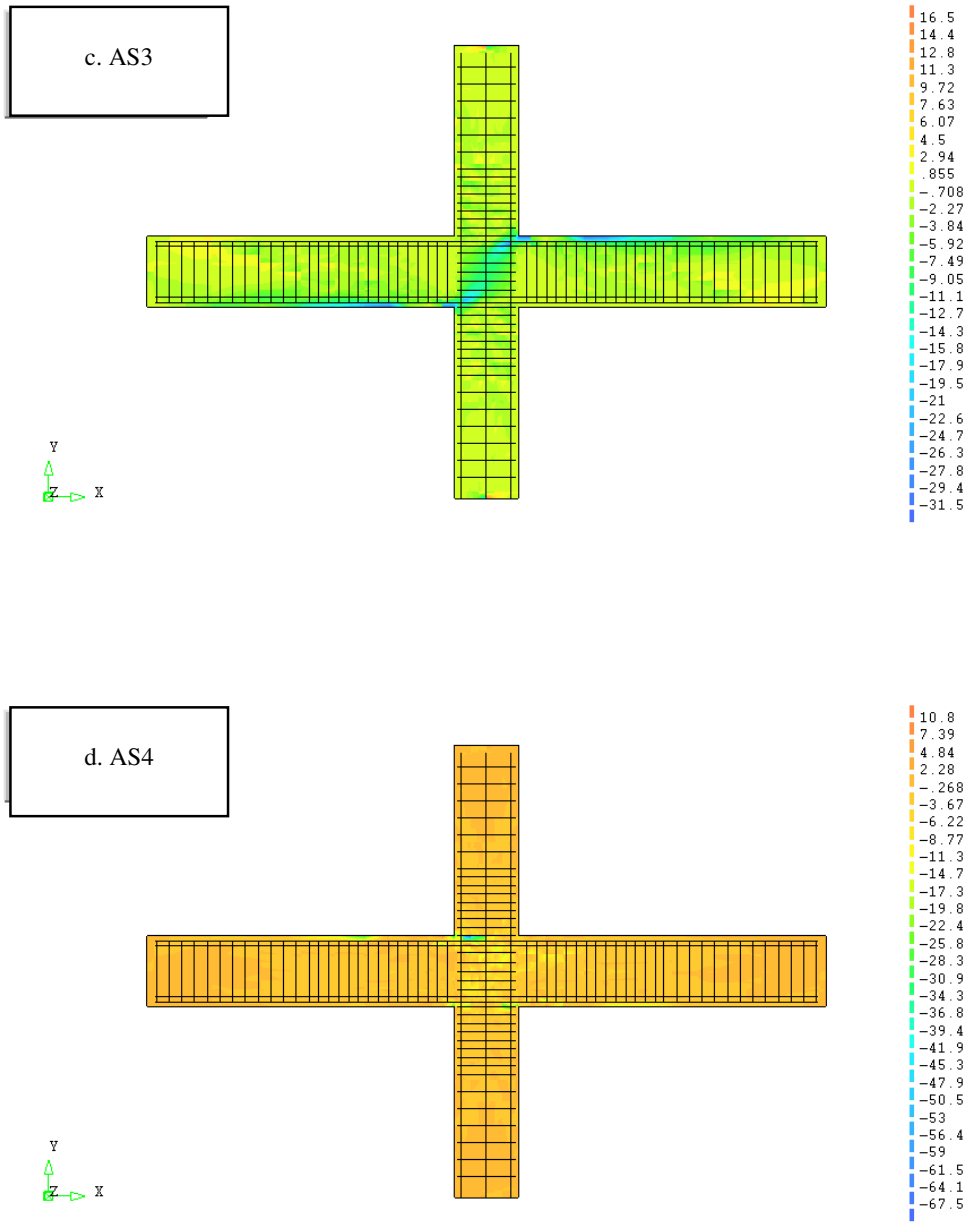

Figure 5.12 Stress Contour of Specimens AS1 to AS4

Table 5.4 Comparison of Test Results and Analysis

Specimen ID	$V_{(test)}$ *(kN)*	$V_{(FE)}$ *(kN)*	$V_{(FE)} / V_{(test)}$
NS1	*220*	*162*	*0.74*
NS2	*140*	*126*	*0.90*
NS3	*165*	*150*	*0.91*
NS4	*110*	*102*	*0.93*
AS1	*220*	*180*	*0.82*
AS2	*120*	*102*	*0.85*
AS3	*155*	*140*	*0.90*
AS4	*110*	*101*	*0.92*
		Mean	*0.87*
		Standard Deviation	*0.07*

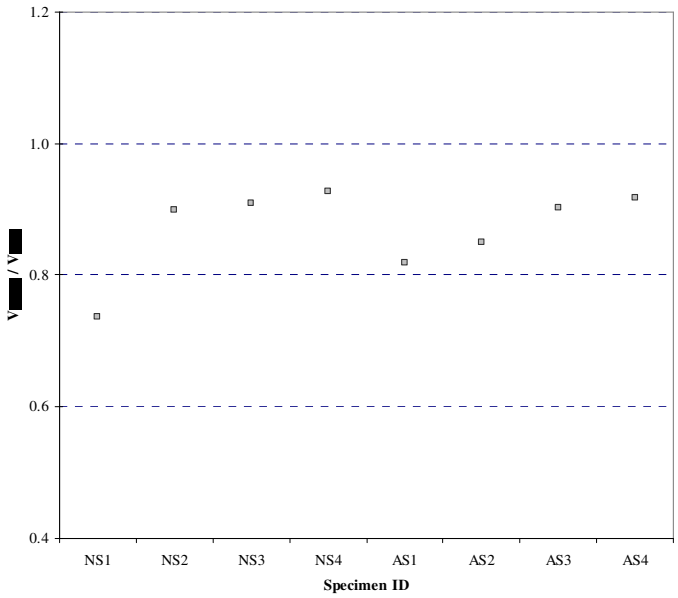

Figure 5.13 Ratio of Shear Strength Predictions to Test Results

5.3.3 Cracking Patterns

Figure 5.14 to Figure 5.17 depict the cracking patterns observed during the test, obtained through a finite element approach. The crack patterns from FE analysis were not physical cracks but they only indicated the concrete cracks limits of the particular FE elements were exceeded. As such the crack patterns from FE analysis only explained the region of cracks to take place should not be simplified as the predicition of physical cracks. In the analysis, diagonal tension cracks started to occur as early as the models were loaded to a drift ratio of 0.5% and subsequently the extensive diagonal cracking was found concentrated within the joint core. Similar to the test observation, the crack patterns from FE analysis explained the present of column axial compressive load prevented the crack to take place in columns while limited or no crack was found in joint core of AS2 and AS4.

5.3.4 Strains in Beam and Column Longitudinal Bars

The strains of reinforcement bar elements were extracted to explain the general behaviour of finite element models as compared to test data obtained. The compared results presented here only consist of the strain profiles of the beam top bars and column side bars when the models were loaded in a single loading direction. Figure 5.18 to Figure 5.19 show the comparison of strain profiles of the beam longitudinal bars and the trend of finite element analysis was close to the test observation where bar near to beam-column interface yielded in the end of test and the strain of reinforcement within the joint core was below the yield limits. The strain magnitude of the analytical and experimental models was in good agreement, where the strain magnitude of the analytical models was more conservative than that obtained through experiments. Figure 5.20 to Figure 5.21 explain the comparison of strain profiles of column longitudinal bars. In general, the strain distribution as well as strain magnitude of the analytical and experiential models was basically in good agreement. The reinforcement of columns remained in elastic range throughout the test which explained the characteristics of the combination of "strong-column-weak beam".

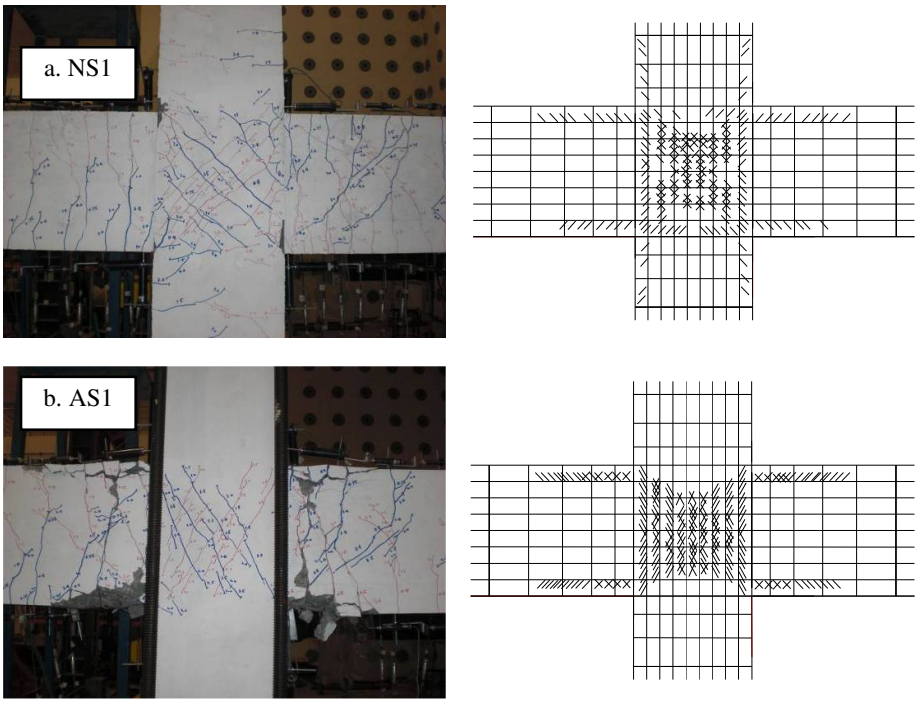

Figure 5.14 Comparison of Crack Profiles of NS1 and AS1

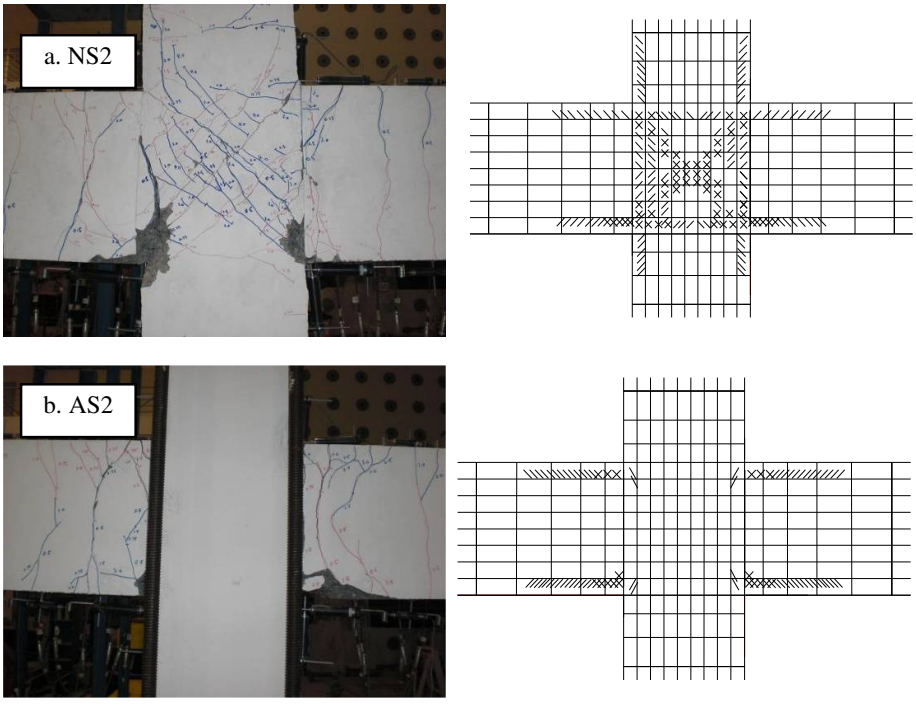

Figure 5.15 Comparison of Crack Profiles of NS2 and AS2

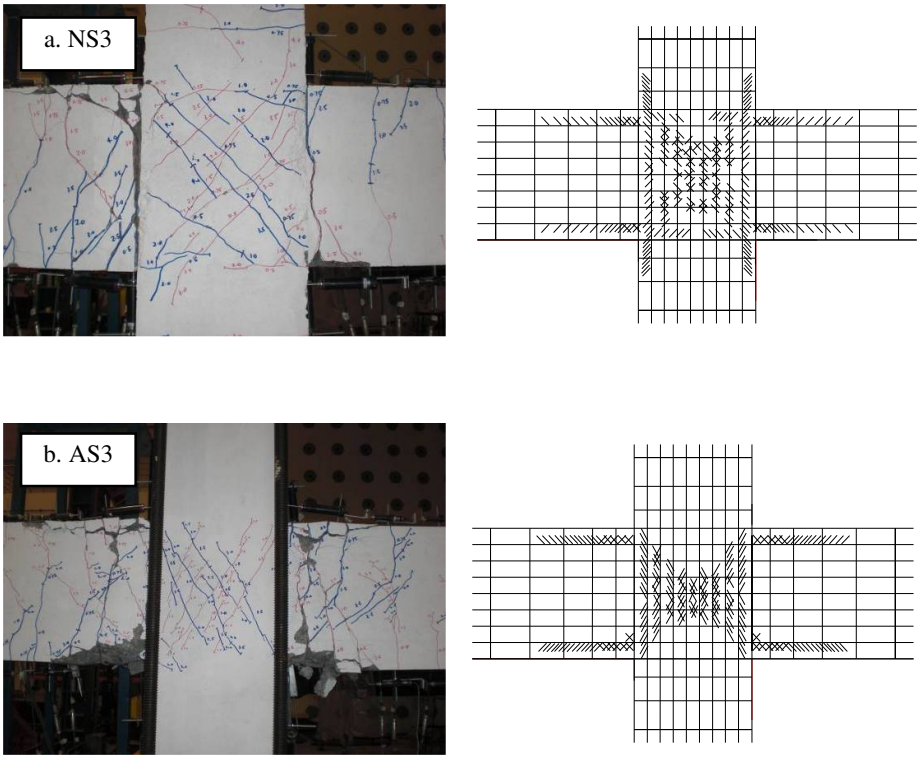

Figure 5.16 Comparison of Crack Profiles of NS3 and AS3

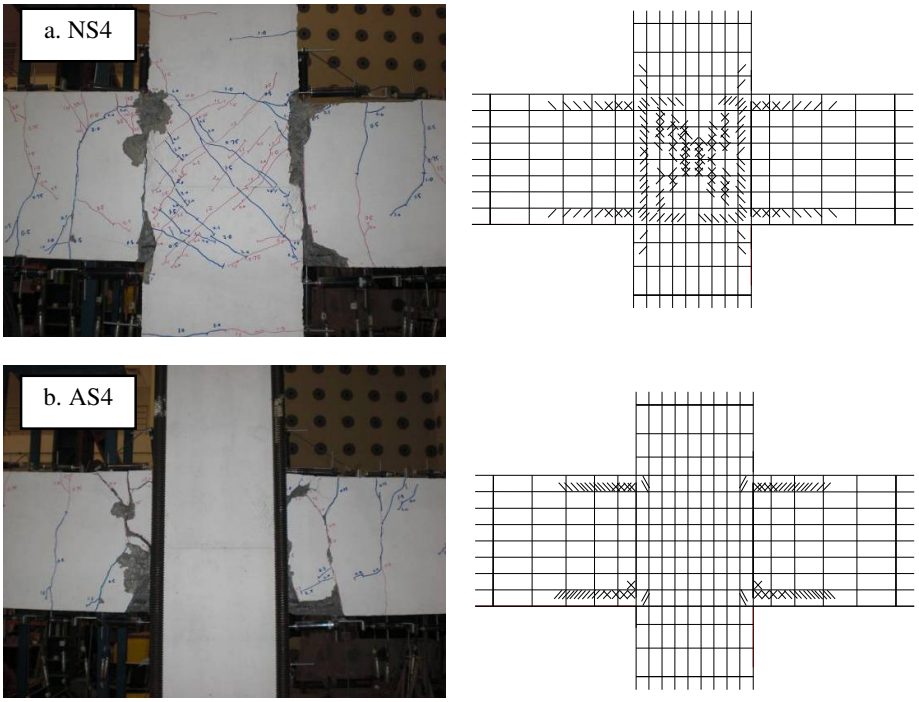

Figure 5.17 Comparison of Crack Profiles of NS4 and AS4

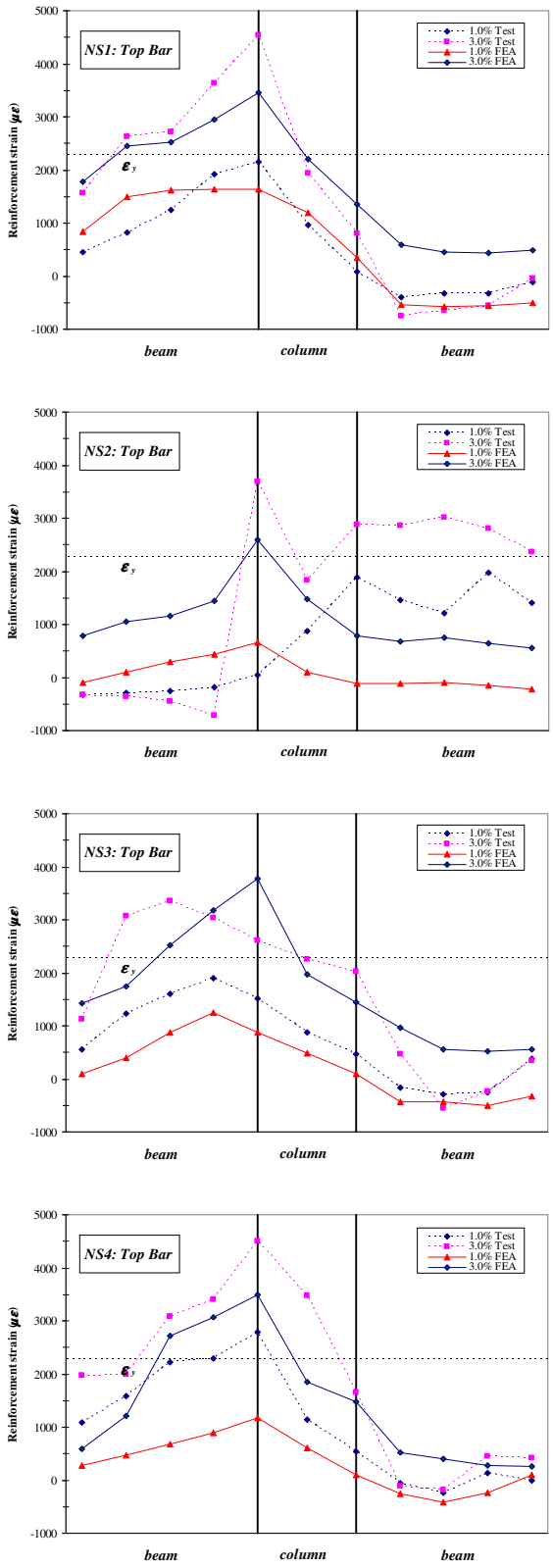

Figure 5.18 Comparison of Beam Strain Profiles of NS1 to NS4

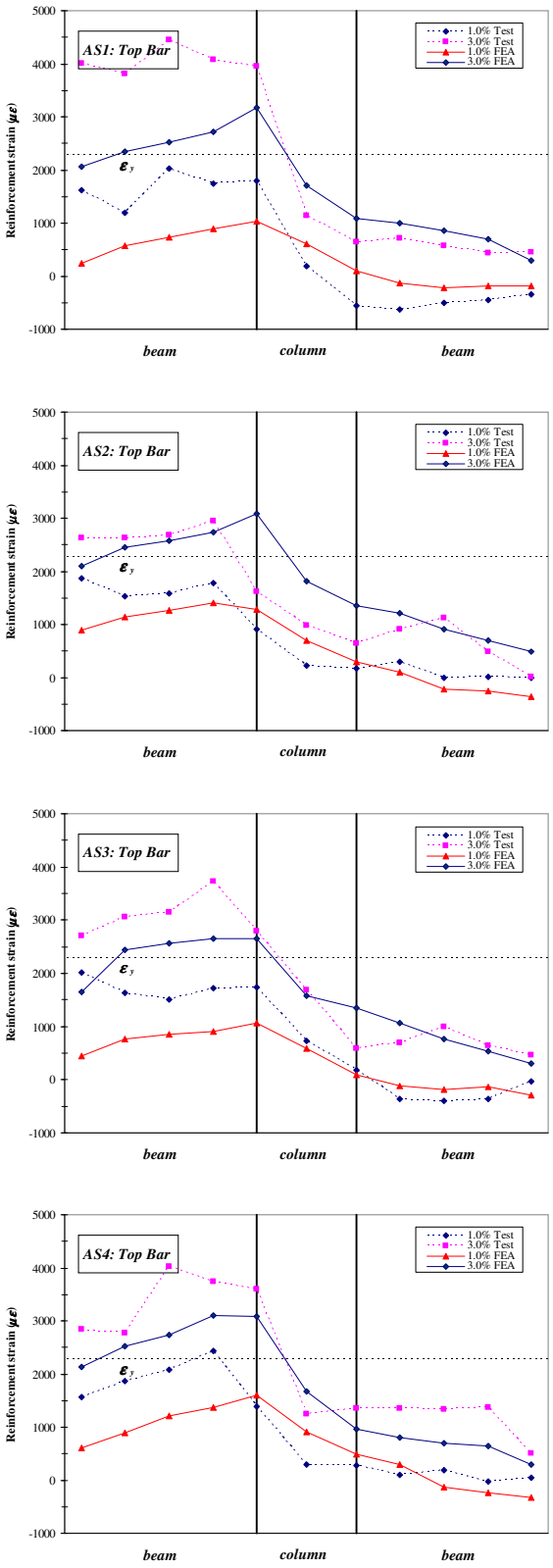

Figure 5.19 Comparison of Beam Strain Profiles of AS1 to AS4

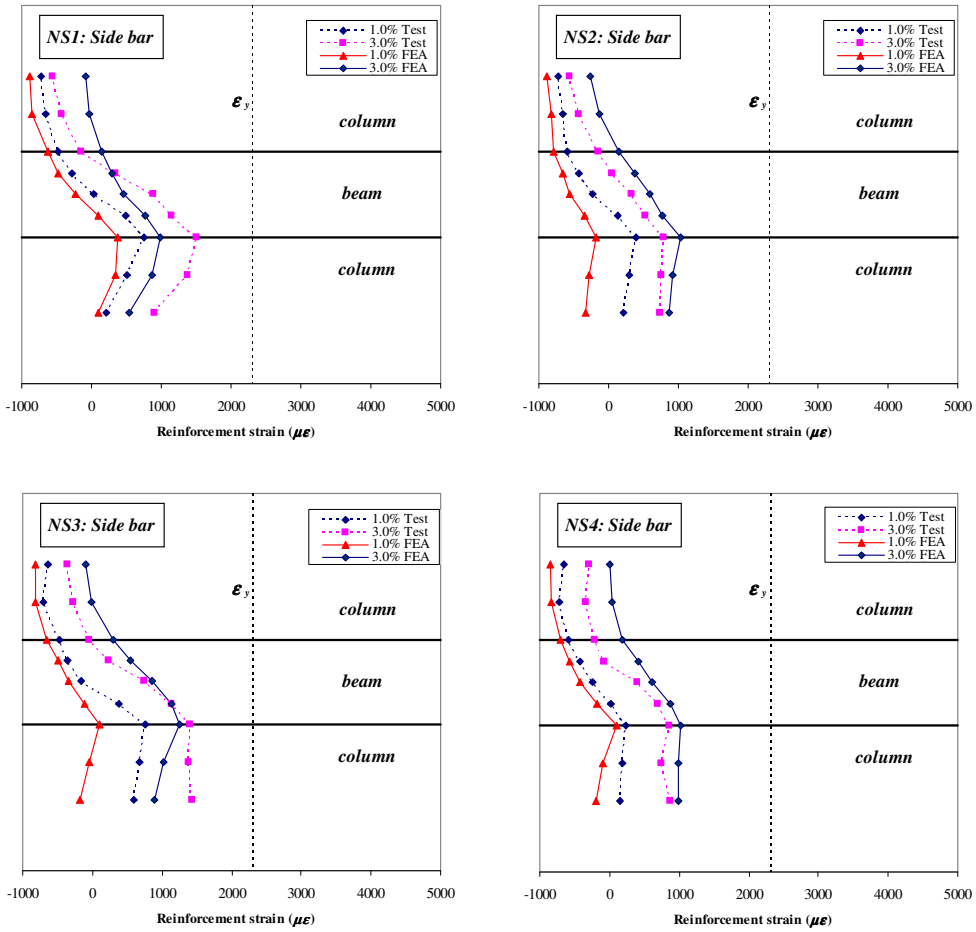

Figure 5.20 Comparison of Column Strain Profiles of AS1 to AS4

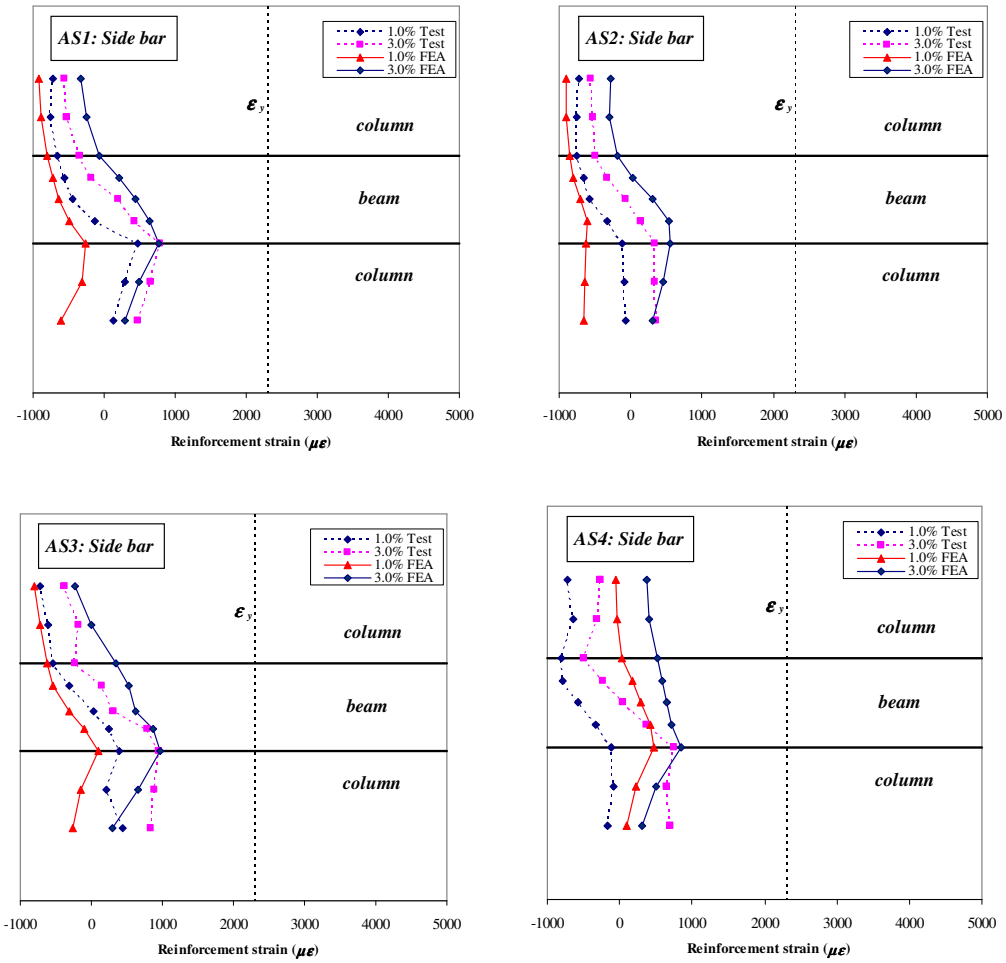

Figure 5.21 Comparison of Column Strain Profiles of AS1 to AS4

5.3.5 Joint Shear Stres

Table 5.5 tabulates the comparison of calculated joint shear stress through experimental and analytical approaches. The following expression was used to determine joint shear force,

$$V_t = A_s f_s + A'_s f'_s - V_{col} \quad (5.5)$$

where, V_t = the total joint shear force,

A_s and A'_s = the area of the tension and compression bars in the beam,

f_s and f'_s = the stress in the tension and compression bars in the beam

V_{col} = the column shear force.

As explained in Table 5.5, it is clear that, finite element models showed higher joint shear stress demands than those observed in the experiment due to the lower column shear force from the analysis. The higher joint shear force in finite element analysis may result in a more conservative design with the required larger joint reinforcement area for the joint core. The normalised joint shear stresses explain that the joint shear strength met the requirement in NZS 3110.

Table 5.5 Comparison of Joint Shear Stress of Test Results and Analysis

Specimen ID	*Joint Shear Stress (Test)*		*Joint Shear Stress (FE Analysis)*	
	(MPa)	f_c' *(MPa)*	*(MPa)*	f_c' *(MPa)*
NS1	*4.78*	$0.078 < 0.2 f_c'$	*4.35*	$0.071 < 0.2 f_c'$
NS2	*3.62*	$0.059 < 0.2 f_c'$	*3.52*	$0.058 < 0.2 f_c'$
NS3	*4.97*	$0.081 < 0.2 f_c'$	*4.85*	$0.080 < 0.2 f_c'$
NS4	*3.14*	$0.051 < 0.2 f_c'$	*3.08*	$0.050 < 0.2 f_c'$
AS1	*4.65*	$0.076 < 0.2 f_c'$	*4.35*	$0.071 < 0.2 f_c'$
AS2	*3.80*	$0.062 < 0.2 f_c'$	*3.67*	$0.060 < 0.2 f_c'$
AS3	*5.04*	$0.083 < 0.2 f_c'$	*4.93*	$0.081 < 0.2 f_c'$
AS4	*3.14*	$0.052 < 0.2 f_c'$	*3.08*	$0.050 < 0.2 f_c'$

5.4 Summary of Test Results Analysis

In this chapter, the seismic performance of the high strength concrete beam-column joints was evaluated through experimental and analytical approaches. Based on these studies, some conclusions can be summarized as follows:

- High strength concrete (HSC) and the presence of column axial compressive load in test improved the bond condition of specimens.
- The use of HSC enhances the strength of beam-column joints with improvement in ultimate load. The stiffness of HSC specimens was generally higher when compared to their respective NSC counterparts.
- Due to the inherent brittle characteristics of HSC, all HSC specimens showed inferior energy dissipation capacity with a smaller confined area within the curves as compared to its their NSC counterparts.
- The use of HSC improved the joint shear strength of all specimens. For example, no serious joint shear failure occurred in NS1 while its counterpart X1 made of NSC exhibited joint shear failure with spalling of concrete at the joint core due to the opening of diagonal tension cracks, and the crushing of diagonal compression struts was observed.
- The presence of column axial compressive load in test enhanced the energy dissipation capacity of all specimens with larger confined area within the loops but the failure mode remained unchanged. The maximum ultimate load was attained in early drift as the confinement effects in column reduced the occurrence of damage in column and joint core hence damage only concentrate at beams.
- The presence of column axial compressive load in test helped to prevent joint shear failure as observed in test. No joint shear failure was observed in specimens tested with column axial compressive load.
- Strength deterioration was observed in test results of specimens tested with the presence of column axial compressive load where the strength of specimens begun to drop when the maximum ultimate load was attained.

- The test results proved that column compressive axial load could lead to higher stiffness in the early loading stage. However, the effect of axial load diminished beyond the drift ratio of 2.5% and specimens without axial compressive load had slight higher stiffness compared to their counterparts till the end of test.
- Particular attention should be paid to the problems of degradation in the strength and stiffness due to shear and bond stresses at the joint based on review and discussion, and design recommendations derived for the structural use of HSC.
- It is evident that lateral displacement contributed by beam flexural and beam fixed end rotation has been dominant in all specimens. The lateral displacement contributed by column flexural, column fixed-end rotation and shear distortion was not significant in all specimens. The joint core regions of all specimens were very strong and rigid where no joint failure was noticed at the end of test.
- The value of bottom-reinforcement-to-top-reinforcement ratio β affects the shape of the hysteresis loops due to different bond condition of top and bottom beam reinforcement should β is less than unity
- The verification of FE numerical results against the experimental results of all eight specimens showed good agreement in their respective general trends in the hysteresis loops. It is clear that these models are acceptable, despite some minor variations, and therefore, they can be utilized to predict the joint behaviour by varying critical parameters.

The test results reviewed in this chapter confirmed that joints constructed using HSC can be designed to perform well under seismic loading in terms of energy dissipation and failure mode. It would appear that HSC can be used in the structures designed for seismic resistance.

Chapter 6 Parametric Investigations on High Strength Concrete Beam-Column Joints

The research findings in Chapters 4 and 5 have confirmed that the use of high strength concrete (HSC) could lead to some relaxation of the bond requirements in beam-column joints in design. This relaxation should be possible because the bond strength increases with the increase in concrete compressive strength even though not in a linear manner. On the other hand, the shear design equations in NZS 3101 have been developed based on test data in the last century and mostly on normal strength concrete (NSC). With the gaining popularity of HSC in modern building construction technology, it is timely to review the design equation to suit the usage of HSC. Thus, parametric studies by using the test data from experiment and nonlinear finite element analysis to develop the relationship between various variables and joint shear resistance under lateral loads are performed in this chapter. Also, the existing shear design equation in New Zealand Standard (NZS 3101) [N1] is reviewed and improvement is proposed so that it is applicable to both NSC and HSC. The research described in this chapter helps to improve the understanding of the influences of variables on the behaviour of both normal strength concrete (NSC) and high strength concrete (HSC) beam-column.

6.1 Findings on Concrete Beam-Column Joints

Due to the various interactions between shear, bond, compression and also the inherent complexity in the material properties, the structural behaviour of beam-column joint is not well understood. However, the induced maximum shear stress within a joint is always the key parameters in assessing the performance of a beam-column joint. As such, to provide detailed description of the shear strength and behaviour of high strength concrete beam-column joints, an extensive parametric study on the variables that affect the behaviour of beam-column joints is deemed crucial. As explained in literature review in Chapter 2, most researchers have been using experimental observations as a basis to postulate conceptual models while

most of these experimental tests were done on isolated beam-column joints where boundary conditions were highly simplified. These results could have been influenced by the various design concepts as design standards differ worldwide. Therefore, the variables for the parametric study must be chosen according to design procedures and the uncertainties of being adopted by current code provisions.

Failure mechanism control has been the goal in the design of a reinforced concrete structure and the values and influences of various parameters must be well understood. However, the variable influences are normally implicitly reflected in the design code equations. For examples, the maximum nominal joint shear stress is normally limited in relation to the concrete compressive strength such as the ACI-ASCE 352 [A2] recommendation, in which the joint shear stresses are limited by a square root of the concrete compressive strength multiplied by a factor. On the other hand, design codes NZS 3101 [C1] and AIJ [A5] are described in terms of the concrete compressive strength multiplying a different factor according to the joint type.

By considering possible problems in the high-strength concrete beam-column joints especially on the change of bond condition, the current design code and the respective control limits might not be directly applicable on these kinds of beam-column joints. To understand the possible problem in NSC and HSC beam-column joints, parametric study on the variables that affect the behaviour of beam-column joints is carried out and as explained in the following sections.

6.2 Assembly of Database for Parametric Studies

The aim of this parametric study is to study the various influential parameters which have been investigated through years by various researchers. These parameters are: concrete compressive strength, bond index, column axial load, joint hoop reinforcement ratio and beam reinforcement ratio. To correlate the influences of various factors in the structural behaviour of beam-column joints, parametric analysis of the experimental data or from numerical analysis of the joint shear mechanism can be an alternative way to serve the purpose. For instance, Bakir [B1] and Vollum [V2] proposed shear design equations for interior and exterior joints derived from regression analysis of the experimental data or from numerical analysis of the joint shear mechanism. Pantazopoulou's and Bonacci's [P2] equations provide general maximum limits for the joint shear stresses regardless of the joint types and developed with an idealized joint shear mechanism. As such the use of test data as well as finite element analysis findings formed the basis of the parametric study and the following section will explain the details of parametric studies with the findings from the parametric studies.

6.2.1 Experimental Results of Conventional Beam-Column Joints

A total of eighty three (83) interior beam-column joints were summarised to study the influences of parameters such as concrete compressive strength, bond index, column axial load, joint hoop reinforcement ratio and beam reinforcement ratio on structural behaviour of beam-column joints. These specimens were made of concrete grade 15MPa to 63MPa and the ratio of column axial load to column cross-sectional area ranges from -1.1MPa to 18MPa were considered in this study. The specimens also covered a wide range of joint shear reinforcement ratio, beam flexural reinforcement ratio and column to beam width ratio. All selected specimens failed mostly on pure shear mechanism of the joint or beam flexural associated with significant deterioration inside the joint panel to ensure the joint closely attained its maximum shear strength. Table 6.1 tabulates the design parameters of these specimens with the maximum joint shear force.

Table 6.1 Parameters of Database

Reference	Specimen	$f_{c'}$ (MPa)	Yield Strength (MPa)			Reinforcement Ratio			Axial Load N $(f_c'A_g)$
			Beam	Column	Joint	ρ_b	ρ_c	ρ_j	
Leong	NS1	60.1	510	512	354	0.0146	0.0140	0.0052	0.00
	NS2	61.2	508	512	354	0.0107	0.0092	0.0071	0.00
	NS3	60.5	508	512	354	0.0142	0.0160	0.0052	0.00
	NS4	60.3	513	512	354	0.0092	0.0129	0.0042	0.00
	AS1	61.4	510	512	354	0.0146	0.0140	0.0052	0.30
	AS2	60.8	508	512	354	0.0107	0.0092	0.0071	0.30
	AS3	60.5	508	512	354	0.0142	0.0160	0.0052	0.30
	AS4	61.7	513	512	354	0.0092	0.0129	0.0042	0.30
Xin [X1]	X1	28.2	453	447	348	0.0146	0.0140	0.0052	0.00
	X2	30.3	445	447	348	0.0107	0.0092	0.0071	0.00
	X3	32.0	445	447	348	0.0142	0.0160	0.0052	0.00
	X4	36.9	492	447	348	0.0092	0.0129	0.0042	0.00
	X5	60.7	492	447	327	0.0168	0.0160	0.0113	0.00
	X6	59.3	461	447	327	0.0165	0.0160	0.0113	0.00
Fenwick & Irvine [F2]	Unit 1	42.9	280	280	275	0.0349	0.0372	0.007	0.00
	Unit 3	39.3	318	318	275	0.0251	0.0134	0.0158	0.00
Briss [B3]	B1	27.9	288	427	346	0.0252	0.0194	0.0111	0.05
	B2	31.5	288	427	398	0.0252	0.0194	0.0111	0.44
Otani, *et-al* [O1]	J1	25.6	374	374	367	0.0282	0.0157	0.0106	0.08
	J2	24	374	374	367	0.0282	0.0157	0.0106	0.08
	J3	24	374	374	367	0.0282	0.0157	0.0106	0.08
	J4	25.7	374	374	367	0.0282	0.0157	0.0106	0.23
	J5	28.7	374	374	367	0.0282	0.0157	0.0	0.07
Durani & Wight [D2]	X1	34.3	276	413	351	0.0487	0.0351	0.0117	0.05
	X2	33.6	276	413	351	0.0487	0.0351	0.0117	0.06
Meinheit & Jirsa [M4]	I	26.2	434	455	407	0.0351	0.0168	0.0192	0.40
	II	41.8	434	448	407	0.0351	0.0144	0.0279	0.25
	III	26.6	434	400	407	0.0351	0.0271	0.0310	0.39
	IV	35.8	434	441	407	0.0241	0.0456	0.0179	0.30
	V	35.8	434	448	407	0.0351	0.0244	0.0279	0.04
	VI	36.5	434	448	407	0.0351	0.0244	0.0279	0.49
	VII	37.2	434	441	407	0.0241	0.0456	0.0179	0.47
	VIII	33.1	434	448	407	0.0351	0.0244	0.0279	0.32

	IX	31.0	434	448	407	0.0351	0.0244	0.0279	0.35
	X	29.6	434	448	407	0.0351	0.0244	0.0279	0.36
	XI	25.5	434	441	407	0.0241	0.0456	0.0179	0.42
	XII	35.1	434	448	407	0.0351	0.0244	0.0279	0.30
	XIII	41.3	434	448	407	0.0351	0.0244	0.0279	0.25
	XIV	33.1	434	441	407	0.0241	0.0456	0.0179	0.32
Bessho [Z1]	J1	31.6	379	379	317	0.0449	0.0221	0.0127	0.08
	J2	31.6	379	379	317	0.0449	0.0221	0.0127	0.08
	J3	33.4	379	379	317	0.0449	0.0184	0.0127	0.08
Ishibashi [I1]	D19-S1	44.2	524	524	524	0.0325	0.0245	0.0123	0.00
	D19-S2	43	524	524	524	0.0186	0.0245	0.0123	0.00
	D19-S3	47.5	508	524	508	0.0330	0.0245	0.0123	0.00
	D19-S4	47.5	508	524	508	0.0220	0.0245	0.0123	0.00
	D19-S5	47.5	506	524	506	0.0280	0.0245	0.0123	0.00
Ohwada [Z1]	JO1	20	434	434	455	0.0452	0.0391	0.0149	0.00
	JO2	20	434	434	455	0.0452	0.0391	0.0149	0.00
	JE1	20	434	434	455	0.0452	0.0391	0.0149	0.00
	JE2	20	434	434	455	0.0452	0.0391	0.0149	0.00
	JI1	20	434	434	455	0.0452	0.0391	0.0149	0.00
	JI2	20	434	434	455	0.0452	0.0391	0.0149	0.00
Attaalla [A6]	SOC1	30.4	422	419	551	0.0183	0.0251	0.0	-0.01
	SOC2	41.1	422	419	551	0.0183	0.0251	0.0	-0.03
	SOC3	47.1	431	427	551	0.0183	0.0251	0.0	0.05
	SHC1	56.5	431	427	551	0.0183	0.0251	0.0	0.04
	SHC2	59.5	431	427	551	0.0183	0.0251	0.0	0.04
Leon [L1]	BCJ2	30.5	413	413	438	0.0123	0.0245	0.0098	0.00
	BCJ3	27.6	413	413	438	0.0123	0.0196	0.0079	0.00
	BCJ4	27.6	413	413	438	0.0123	0.0131	0.0065	0.00
Ishibashi [I1]	D51-1	24.3	395	395	395	0.0203	0.0186	0.0	0.24
	D51-2	25.9	395	395	395	0.0303	0.0186	0.0	0.23
	D51-3	30.7	402	402	402	0.0203	0.0186	0.0	0.19
	D51-4	31.4	402	402	402	0.0203	0.0186	0.009	0.19
	D41-1	40.7	377	377	377	0.0129	0.0180	0.0	0.14
	D41-2	40.7	377	377	377	0.0129	0.0180	0.0	0.00
	D29-SLS	18.7	382	382	382	0.0158	0.0912	0.0304	0.00
	D29-LSL	20.9	382	382	382	0.0158	0.0912	0.0304	0.00
	D29-KSK	19.2	382	382	382	0.0158	0.0912	0.0304	0.00

	D29-SSS	18.5	382	382	382	0.0158	0.0912	0.0304	0.00
	D29-LLL	19.4	382	382	382	0.0195	0.0912	0.0304	0.00
	D29-LSS	18.7	382	382	382	0.0158	0.0912	0.0304	0.00
	D29-PJN	24.7	382	382	382	0.0292	0.0211	0.0528	0.17
	D29-BJN	23.1	382	382	382	0.0292	0.0211	0.0528	0.18
	D29-PJO	24.7	382	382	382	0.0292	0.0211	0.0528	0.00
	D29-BJO	23.1	382	382	382	0.0292	0.0211	0.0528	0.00
	D29-20N	28	395	395	395	0.0197	0.0211	0.0528	0.00
	D29-30N	31.4	395	395	395	0.0296	0.0211	0.0528	0.00
	D29-30S	34	395	395	395	0.0296	0.0211	0.0528	0.00
	D29-30W	34.5	395	395	395	0.0296	0.0211	0.0528	0.00
	D22-SJP	23.2	377	377	377	0.0117	0.0122	0.0304	0.13
	D22-SJB	24	377	377	377	0.0117	0.0122	0.0304	0.12

6.2.2 Finite Element Modelling

The preceding review of experimental data shows conclusively that the number of parameters affecting the behaviour of beam-column joints might exceed the breadth of the available database. To compensate the possible limitations of the experimental studies, analytical modelling is used to supplement the parametric study where a series of finite element analysis is adopted in this study. The models were built and analysed using finite element analysis program DIANA [D1] and the following sections explain the details of modelling.

6.2.2.1 Analytical Models and Material Properties

The finite element models studied in this section were two-dimensional idealization of beam-column connections with geometries similar to that of beam-column assemblies tested in experiments in Chapter 3. The prototype of conventional beam-column joint's models was derived from the Specimen NS1. The section of columns and beams were 300 mm × 450 mm and 250 mm x 500 mm respectively. The details of reinforcement can be is the same as shown in Figure 3.1 to Figure 3.4 of Chapter 3. The material properties of the models are summarised in Table 6.2 while Table 6.3 summarises the variables in the finite element models

Table 6.2 Summary of Material Properties of Analytical Studies

Properties	***Input Value (MPa)***
Es	*210000*
f_c'	*varies from 30 to 70*
f_t	*varies from 5.5 to 8.4*
f_y *(for beam)*	*510*
f_y *(for column)*	*512*
f_y *(for joint)*	*354*

Table 6.3 Summary of Parameters Investigated in Analytical Studies

Concrete Grade (f_c')	*30*	*40*	*50*	*60*	*70*
Axial Compressive Load ($A_g f_c$')	*0.0*	*0.1*	*0.2*	*0.3*	*0.4*
Ratio of beam bottom bar area to top bar area (A_s/A_s')	*0.5:1*		*0.75: 1*		*1:1*

6.2.2.2 Parameters Investigated for Finite Element Model

In the study with finite element, the concerns regarding the influence of parameters on the behaviour of beam-column connections focus on the effect of concrete compressive strength, column axial compressive loads and beam longitudinal reinforcing ratios. Table 6.3 summarises the parameters investigated in the analytical studies where the variation in each combination formed total of seventy five (75) data for analytical studies. These data were assembled to complement the test data from literatures according to the findings or limitations below:

a. Concrete Compressive Strength

As explained in Table 6.1, the concrete compressive strength in literature database varies from 18.7 to 60.2 MPa. The database for parametric studies generally covered normal strength concrete (NSC) to high strength concrete (HSC) beam-column joints. In the FE analysis studies, the concrete grades of beam-column joint

models ranging from 30 MPa to 70 MPa, in order to have better understand in the structural behaviour of both NSC and HSC beam-column joints due to the difference in the inherent characteristic of both NSC and HSC.

b. Column Axial Compressive Load

In the database of previous tests shown in Table 6.1, it is clear that the column axial compressive load was applied and was kept constantly in certain test while axial compressive load was absent in certain tests due to test setup limitation. In the current study using finite element method, the column axial loads were applied with a magnitude ranging from 0.0 to $0.4A_g f'_c$ where the column axial load is expressed as a percentage of the product of the column gross area and concrete compressive strength.

c. Beam Longitudinal Reinforcing Ratio

In the experimental database, the beam longitudinal reinforcing ratio ρ_b ranged from 1.17% to 4.87%. The longitudinal reinforcing ratio ρ_b alone is not sufficient to analyse the structural behaviour of beam-column joints without comparing to the ratio of beam bottom bar area to top bar area A_s/A_s'. Thus, in the analytical study, three A_s/A_s' ratio are considered in the current study, which are 0.50:1, 0.75:1 and 1:1 resulting in the total beam reinforcing ratios being 0.95%, 1.21% and 1.46%, respectively.

6.2.2.3 Analytical Model Verification

The boundary condition and loading arrangement of models were explained Section 5.2.5 and all models were loaded based on the test loading sequence as explained in Section 3.3. The outputs from finite element analysis were then plotted as shear strength envelopes to study the general trend to ascertain the validity of each modelling. Figure 6.1 to Figure 6.3 explain the general trend of each parameters based on the shear strength envelopes of several parameters combinations.

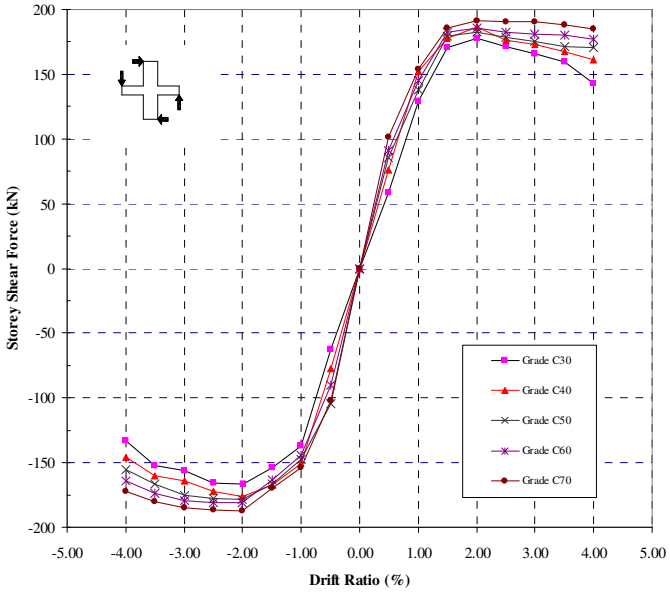

Figure 6.1 Shear Strength Envelopes for Various Concrete Compressive Strength (with A_s'/A_s 1:1, Axial Compressive Load $0.3A_g f'_c$)

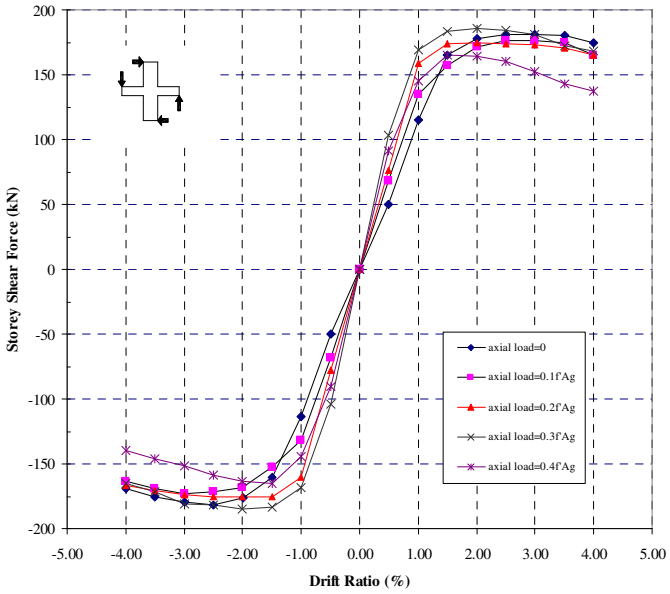

Figure 6.2 Shear Strength Envelopes for Various Axial Compressive Load (with f_c' 60MPa, A_s'/A_s 1:1)

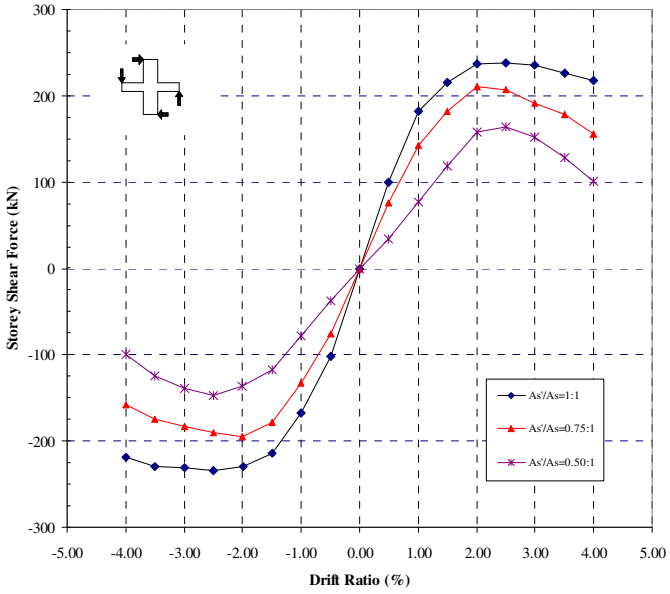

Figure 6.3 Shear Strength Envelopes for Various Beam Bottom Bar to Top Bar Ratio (with f_c' 60MPa, Axial Compressive Load $0.3A_g f'_c$)

Shear strength envelopes for models with A_s'/A_s 1:1 and axial compressive load $0.3A_g f'_c$ is plotted in Figure 6.1 to study the influence of concrete compressive strength. As shown in Figure 6.1, the maximum storey shear of model increased by around 12%, as the concrete compressive strength increased from 30MPa to 70MPa respectively. The general trend of the hysteresis loops was similar in regardless of the change of concrete grade. The maximum load at each drift ratio increased as the concrete grade is increased. The observation in FE analysis agreed well in the test results where the strength of beam-column joint was greatly improved when concrete grade was changed from 30MPa to 60MPa.

Figure 6.2 shows the shear strength envelopes for models with A_s'/A_s 1:1 and concrete grade f_c' 60MPa to verify the influence of column axial compressive load. In the FE analysis, column axial compressive load varied from zero to $0.4\, f_c' A_g$ were applied to the FE models. As observed by Figure 6.2, the storey shears of model increased by around 10%, as the axial load was changed from zero to $0.3\, f_c' A_g$ respectively. However, any increase in the axial load beyond $0.3\, f_c' A_g$ did not enhance the storey shears. The application of axial compressive loads above

0.3 $f_c^{'}A_g$, led a slight reduction in storey shears and a degradation of stiffness. The improvement in joint shear strength was observed in the test data of comparison of NS1 and AS1 when the axial load level was increased from zero to 0.3 $f_c^{'}A_g$.

Lastly, the shear strength envelopes for models with axial compressive load $0.3A_gf'_c$ and concrete grade f_c' 60MPa is shown in Figure 6.3 to verify the influence of the ratio of total area of bottom beam bars to top beam bars β. In the study, the ratio of total area of bottom beam bars to top beam bars β varies from 0.5 to 1.0. From Figure 6.3, stiffness degradation is observed in the respective shear strength envelopes as the ratio gets smaller. From test observation, for units with unsymmetrical beam bars, the bond condition was better in the top bar than the bottom bar in the joint core due to smaller stress in the top beam bar in compression than bottom bar. The significant pinching of the hysteresis lops resulted in a reduction in the dissipated energy after the bottom beam bars lost bond strength. The storey displacement increased suddenly without any change in resistance until the crack in the beam at the column face was completely closed at the bottom. In summary, the value of β has influence on the shape of the hysteresis loops as well as to certain extent of storey shear force.

The FE models were verified with findings from test observation and the results from FE modelling is reliable as explained in Figure 6.1 to Figure 6.3. As such, the maximum loads of each model were then recorded to calculate the maximum joint shear stress for analytical studies in the following sections to supplement the test data from literature.

6.3 Discussion of Database Results

Total of eighty three (83) interior beam-column joints from test data were summarised in Table 6.1 to study the influences of parameters such as concrete compressive strength, bond index, column axial load, joint hoop reinforcement ratio and beam reinforcement ratio on structural behaviour of beam-column joints. Besides that, the maximum joint shear stress of seventy five (75) finite element models explained in Section 6.2.2 were verified and to study the influence of column axial load on structural behaviour of beam-column joints

Except the study on the effect of concrete compressive strength f_c' in Section 6.2.2, a dimensionless factor - maximum joint shear stress factor k has been used in the parametric studies in Sections 6.3.2 to 6.3.6. The factor k is defined as the maximum joint shear stress v_{jh} over the square root of concrete compressive strength f_c'.

6.3.1 Effect of Concrete Compressive Strength

The joint shear failure of beam-column joints is due to the weakened concrete compressive strength after extensive diagonal tension cracking in the joint panel [P4]. The cracks propagated into the concrete block due to the change in the compression flexural reinforcement from compressive stress to tensile stress when bond deterioration within the joint panel took place. For the panel truss mechanism, it relies very much on a good bond condition along the main reinforcement passing through the joint. The high concrete compressive strength f_c' is one of the primary factors to achieve the favourable bond condition [P4]. As such, the concrete compressive strength f_c' is the most essential factor to influence the joint shear behaviour. However, in contrast the concrete compressive strength has been used as the only gauging factor to limit the joint shear input in many design codes [A1, N1].

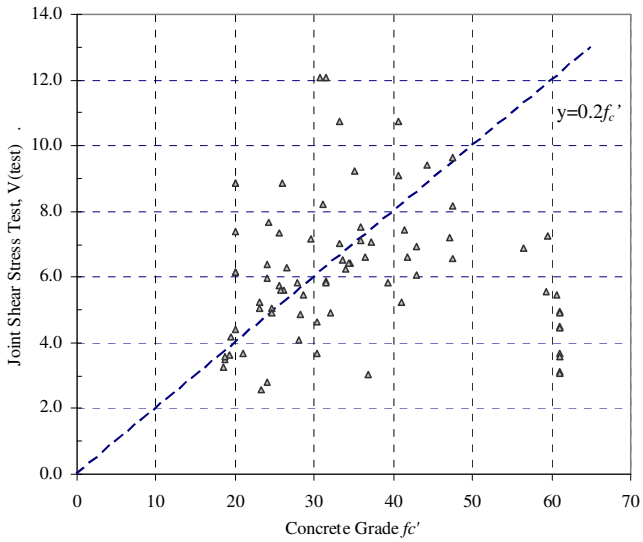

Figure 6.4 Joint Shear Strength versus Concrete Compressive Strength Relation via Experimental Approach

The effect of concrete strength on joint shear stress in this parametric study is presented in Figure 6.4. The concrete compressive strength ranged from 18MPa to 62MPa. Although New Zealand Code NZS 3101 heavily relies on the panel truss mechanism and almost ignores the contribution from the main strut, it still sets the joint shear stress limit to be 0.2 f_c' [N1]. Thus, the limiting values of joint shear stress in NZS3101 has been included in the graph to understand the relation between the concrete compressive strength, joint shear stress as well as the limiting threshold value set in design code.

From Figure 6.4, the general relation between concrete compressive strength and the joint shear stress is not clear. For example, concrete of higher strength of above 60MPa, the joint shear stress is far lower than the limits set in NZS 3101. This explains that the higher concrete compressive strength has a positive influence on the joint shear strength. However, for concrete of lower strength for example 30MPa, the joint shear stress obtained was scattered and no direct conclusion can be drawn. The other factors such as joint shear reinforcement have significant influence on the joint shear strength and further analysis is needed to understand the joint shear strength better.

Noteworthy that the joint shear limits in NZS 3101 could be conservative for high strength concrete and the influence of other control parameters may need to be considered when setting the limit joint shear strength. To incorporate the effect of concrete grade in the remaining control parameters, a dimensionless factor - maximum joint shear stress factor *k*, which is defined as the maximum joint shear stress divided by the square root of concrete compressive strength, $\sqrt{f_c'}$ is used in the analysis of the following sections.

6.3.2 Effect of Column Axial Load

The column axial load is believed to be beneficial to the joint shear resistance because it either confines the joint core, or equilibrates part of the diagonal concrete compression strut that formed inside the joint because of joint shear actions. The neutral axis depth in the column at the column-joint interface would increase with the presence compressive load on the column, as stated by Paulay *et al* [P5]. Due to the increase in the steepness of the diagonal shear cracking in the joint panel, the diagonal strut compression mechanism in the joint would be enhanced as well. Also, the presence of column compressive load helped to prevent the diagonal concrete cracking where the beam reinforcement anchorage condition can be improved. For design practice, the contribution of the main strut mechanism is not taken into consideration in the NZS 3101, unless the column axial compressive load is greater than to $0.1A_g f_c'$. On the other hand, when axial compressive load is taking into consideration, the joint transverse reinforcement can be reduced recommended in Sections 11.4.4.1 and 11.4.5.1 in NZS 3101 [N1].

To study the effect of column axial load to the magnitude of the joint shear resistance, the experimental joint shear stresses factor *k* versus column axial loads is plotted in Figure 6.5. As shown in Figure 6.5, the experimental data are considerably scattered. It is noticed that there is no direct relation between the applied column axial load and the joint shear stresses. The influence of axial compressive loading on joint shear strength is not clear, for instance a larger magnitude of joint shear stresses can be obtained even though no column axial

compressive load is applied. The relation between the axial compressive loading and joint shear strength from test data became more complicated with the variations in the geometrical dimension of specimens as well as the differences in the reinforcement details.

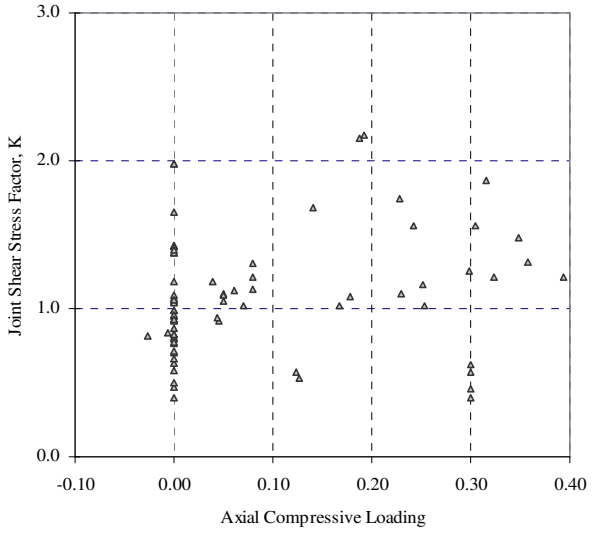

Figure 6.5 Joint Shear Stress Factor *k* versus Column Axial Compressive Loading Relation via Experimental Approach

To simplify the analysis of influence of column axial compressive loading, it would be ideal to fix the dimension of specimens and allow the minimum variables in the study. From the parametric studies using experimental data, a firm relationship between the applied column axial loads and nominal joint shear stresses was not directly comparable with the differences in geometry and reinforcing details. To complement the missing relation due to variation in many control parameters, a series of "ideal" beam-column joints with same dimension were introduced as explained in Section 6.2.2. Through finite element analysis, finite element models with different applied column axial compressive loads while the other variables are fixed were studied. The nominal joint shear stresses from analysis versus applied column axial compressive loads are plotted in Figure 6.6. Based on results shown in Figure 6.6, for specimens with equal beam top and bottom reinforcement, the maximum nominal joint shear stresses of these analytical models ranged from $0.7\sqrt{f_c'}$ to $1.22\sqrt{f_c'}$ when zero column axial loads were applied. When the

magnitude of the column axial load increased to maximum 0.4Ag fc', the maximum nominal joint shear stresses was improved with values ranged from $0.79\sqrt{f_c'}$ to $1.24\sqrt{f_c'}$, respectively.

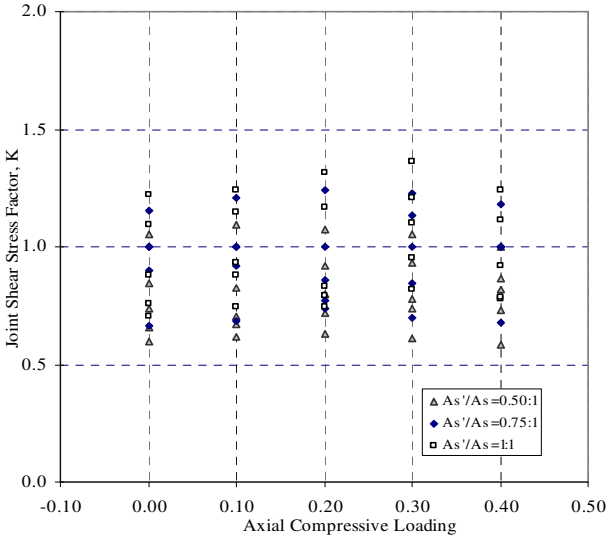

Figure 6.6 Joint Shear Stress Factor *k* versus Column Axial Compressive Loading Relation via Analytical Approach

For comparison of influence of column axial compressive loadings, NSC specimens of 30MPa and HSC specimens of 70MPa were selected and presented in Figure 6.7a and b. Based on results shown in Figure 6.7a, the joint shear demand of the NSC analytical model with A_s'/A_s ratio of 1:1 increased with the applied column axial loads until $0.3A_gf_c'$; whereas the other two models reached their maximum joint shear stresses at the column axial load of $0.2A_gf_c'$, which the joint shear demands of these two models decreased gradually. On the other hand, the joint shear demand of the HSC analytical model with A_s'/A_s ratio of 1:1 peaked at $0.3A_gf_c'$ while the other two models reached their maximum joint shear stresses at the column axial load of $0.2A_gf_c'$. The threshold value of beneficial column axial compressive load was found ranged between $0.2A_gf_c'$ and $0.3A_gf_c'$ and the influence of difference in beam top reinforcement area and beam bottom reinforcement area might override the influence of column axial compressive load.

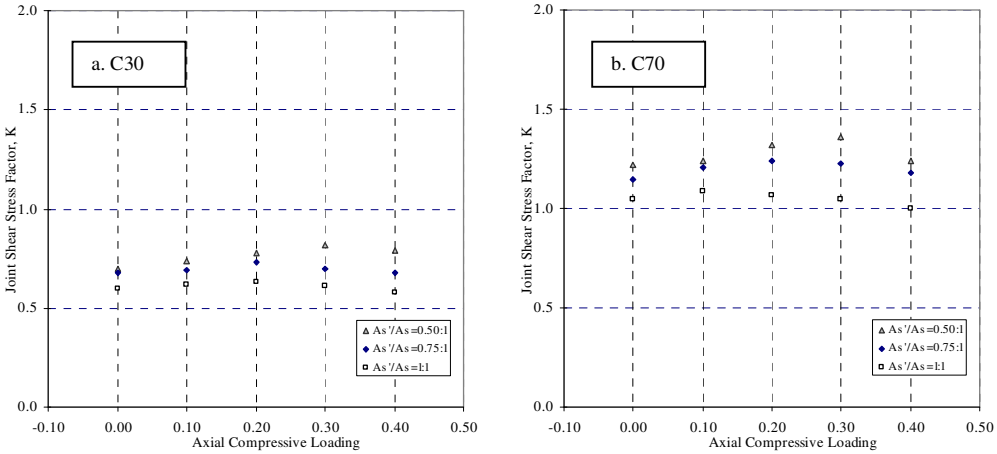

Figure 6.7 Joint Shear Stress Factor *k* for Concrete C30 and C70

The influence of column axial compressive on joint cores could be more significant in joint deformability rather than joint shear strength which involves the story drift levels at the maximum column shears and the contribution of the joint shear deformation to the total story drift, as explained by some researchers [Y1]. Based on the test results in Chapter 4, all specimens with compressive axial load effect had their peak shear strengths occur much earlier by up to about 30% in terms of story drift compared to their counterparts. A stiffer joint were obtained in specimens with compressive axial load effect compared to their counterparts where contribution of the joint shear deformation to the total story drift was less significant. Even though the significant influence of column axial compressive on joint cores in joint deformability is observed in Chapter 4, the influence of column axial compressive on joint cores in joint deformability could not be fully verified due to the scarcity of available experimental data on joint deformation in this study.

6.3.3 Effect of Beam Reinforcing Ratio and Reinforcing Details

The participation of longitudinal reinforcement in joint shear resisting system could be important as the portion of bars that passing through the joint core helped to clamp the opening of diagonal cracks to certain extent which function as joint hoops. In NZS 3101, the design of joint reinforcement is directly related to the area of beam reinforcement passing through the joint as explained in Section 11.4.4

[N1]. Based on experimental findings, Wong [W2] concluded that the amount of joint core hoops necessary would be significantly less than for conventional beam design when vertically distributed reinforcement was used in beams. On the other hand, the joint shear stresses was found to increase with the increasing of total beam longitudinal reinforcement ratios as concluded in parametric study by Tan [T1] in terms of nominal joint shear stresses versus total beam longitudinal reinforcement ratio. Thus, the function of longitudinal reinforcement in joint shear resisting is critical in certain extent.

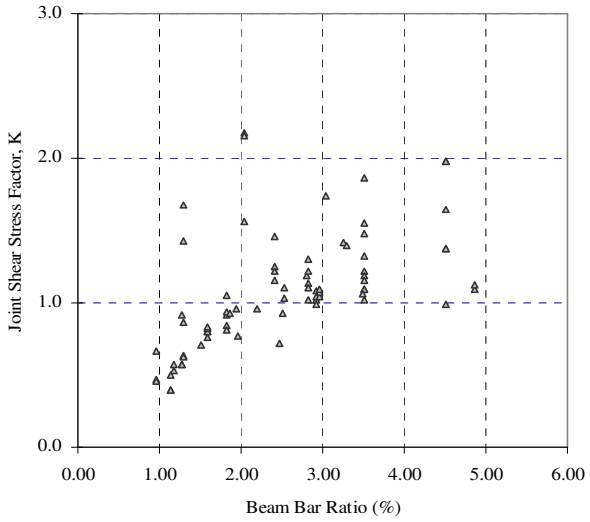

Figure 6.8 Joint Shear Stress Factor *k* versus Beam Bar Ratio Relation via Experimental Approach

Figure 6.8 shows the influence of beam reinforcing details on the joint shear stresses. A general trend was observed where the increase in total beam longitudinal reinforcing ratios can cause the rise in joint shear stresses. However, the joint shear stresses was capped at 4.5% bar ratio and begun to decrease. As such, an upper bound limit for maximum bar ratio is needed to ensure the satisfactory joint shear behaviour. An excessive longitudinal reinforcement in the framing members especially in the beams should be avoided as much as possible since excessive longitudinal reinforcement in the beams could be detrimental especially for lightly reinforced joints. A higher shear stress could be induced in the joint panel when heavy reinforcement passing through the joint panel. With the presence of excessive beam reinforcement, the increase in the flexural capacities of the beams could be

more than the increase in the joint capacity and this could cause the joint to be relatively weaker than the framing members. Therefore the failure mechanism of the sub-assemblage might be changed to joint shear instead of beam hinging.

In design practice, it is rare to have equal top and bottom reinforcement in a beam, especially for lightly reinforced joints where the area of the top reinforcement is normally twice as large as that of the bottom since the framing members are catered for resisting gravity load only [B5]. The ratio of beam top reinforcement to beam bottom reinforcement can be critical in joint shear resistance due to the force equilibrium in a joint core. In NZS 3101, the ratio of beam top reinforcement to beam bottom reinforcement is taken into consideration in control of diameter of longitudinal beam bars passing through the joint core. As explained in Section 7.5.2.5 of NZS 3101, allowable bar size passing through the joint core is reduced when ratio of beam top reinforcement to beam bottom reinforcement (or vice-visas) is less than unity [N1]. This is to ensure better bond condition when an uneven bar area of top and bottom reinforcement is used.

6.3.4 Effect of Joint Core Reinforcement

The role of the transverse hoops in the joint is to provide shear resistance and to promote good confinement to the joint volume. Joint shear reinforcement design has been an important chapter in major design codes to ensure the frames not fail at joint shear should an earthquake happened. From a parametric study, Yin [Y1] summarised that the interactions within the beam-column joint are rather complex, and it is not sufficient to just rely on the transverse reinforcement to provide the required joint shear capacity. Quite a number of test specimens in the literature were failed by joint shear even though the beam column joint was strictly following the code requirement to have the failure mode as beam hinging.

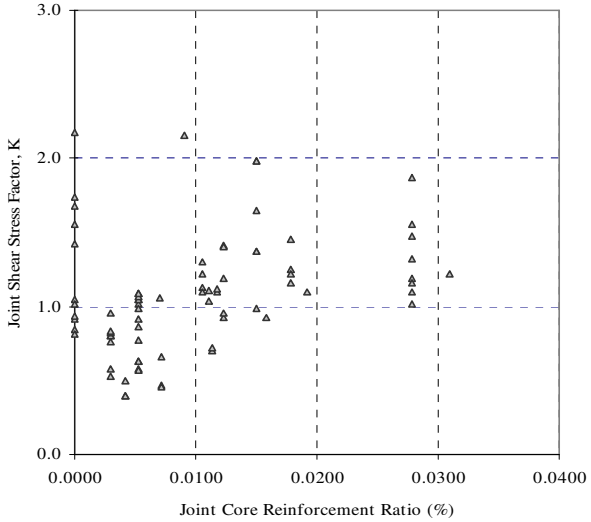

Figure 6.9 Joint Shear Stress Factor *k* versus Joint Core Reinforcement Ratio Relation via Experimental Approach

The effect of joint hoop and joint confinement on maximum joint shear strength is graphically presented in Figure 6.9. The joint hoop reinforcement ratio in this case is defined as the total cross sectional area of the hoops in the loading direction over the total area obtained from the product of column width and beam depth. The general assumption in a ductile frames design is the formation of plastic hinges at beams and the columns remain elastic. To avoid the failure of joints, joint hoops are provided to provide shear resistance and provide confinement to the joint volume. There is a vast variation in design requirement in modem seismic design codes such as ACI 318-08, NZS 3101-2006 and AIJ-1994, which give different minimum joint hoop requirement and design equations. The NZS 3101-2006 has the most stringent requirements on joint shear reinforcement as because the force transfer from members to the joint panel only rely on the panel truss mechanism. It is noteworthy that the joint shear strength is not as sensitive as beam shear strength to shear reinforcement as stated in the design standard ACI 318-08. If the design of the beam column joint is strictly following the code requirement, the preferred failure mechanism i.e. beam hinging should always be expected.

As shown in Figure 6.9, the relation between joint hoop reinforcement ratio and joint shear stress is not clear. The shear stress demand for lightly reinforced beam

column joint with no joint core reinforcement can be as high as those with high joint core reinforcement. The parametric studies shows the possibility of overestimation in the contribution of joint hoops, even though it is generally accepted that joint core reinforcement serves to provide shear resistance and provide confinement to the joint volume. From the test of lightly reinforced beam-column joints that failed in beam hinging, Hakuto *et al.* [H2] pointed the importance of good bond condition for the main rebars passing through the joint panel, as compared to the provision of joint. Hakutu *et al.* [H2] concluded that no joint core hoops were required for shear reinforcement if the column was large enough. A large column depth can lead to better anchorage condition and the horizontal nominal shear stress in the joint core could be reduced to a smaller magnitude. Meanwhile, Yin [Y1] reported that the ductile joints apparently reached higher joint shear stress level than the lightly reinforced joints from a parametric study and suggested to investigate the effect of joint hoops with respect to the joint shear deformation, instead of joint shear capacity.

6.3.5 Effect of Bond Condition

Based on the reseach by Kitamaya *et al.* [K1], the relation between the severities of bond stress relative to the bond strength is termed as Bond Index (BI) where the average bond stress μ_b is divided by bond strength which is assumed to be the square root of the concrete strength $\sqrt{f_c'}$:

$$\text{BI} = \frac{\mu_b}{\sqrt{f_c'}} \qquad (6.1)$$

Besides serving as indicator bond condition, bond index can be a tool to evaluate the joint failure mechanism. In a parametric study, Yin [Y1] recommended the following upper boundary of the bond index based on the failure modes of the collected literature data: 1.0 for lightly reinforced joints, 1.5 for ductile joints and BI is greater than 2.0 for joint shear failure.

Figure 6.10 shows the relation of Bond Index and joint shear stress. Since no joint shear failure was observed in the failure mode of the data, the BI of test data shall be in the range of BI <2.0. However, as explained in Figure 6.10, the BI of test data mostly concentrated around 1.0 and some scattered around 3.0. Thus, the use of BI as indicator could be risky without studying the influence of other control parameters for example beam bar ratio.

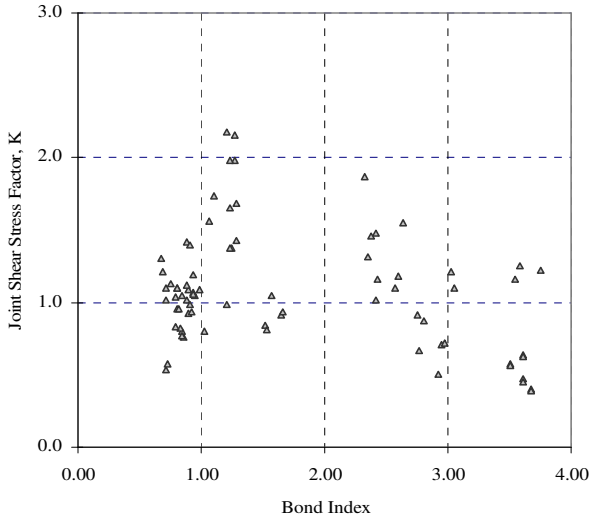

Figure 6.10 Joint Shear Stress Factor *k* versus Bond Index via Experimental Approach

The bond index was initially defined based on a single reinforcing bar passing through the joint [K1]. When multiple rebars with different size and property exist in a beam section along the beam-joint interface, the BI is referring to the rebar that has the largest bond index value. However, the flexural capacity of beams and columns is correspondingly increased when the amount of longitudinal reinforcement is increased. This could cause the joint panel be the weakest part within a beam-column joint sub-assemblage. As such, if there is a large amount of reinforcing bars passing through the joint, joint shear failure is not always prohibited although its BI is low. For a safer design, the application of BI in a design for the development length of reinforcement in joint core should be companied by the checking of longitudinal reinforcement ratio. The structures itself should comply with the detailing requirement in the design code so that the development length of reinforcement in joint core is safe to be used.

6.3.6 Effect of Transverse Beams

In real buildings, the transverse beams as well as slabs are structural elements that have direct interaction with the beam-column joints which may influence the structural behaviour of a joint. Due to the complexity in specimen preparation and test setup, the study of beam-column joint behaviour is always simplified as two dimensional (2D) frame or cruciforms. However, the influence of transverse beams and slabs on a beam-column joint in terms of confinement is important to study.

The seismic codes generally acknowledge the beneficial effects of transfer beams in joint shear strength. The NZS 3101 recommends the area of transverse joint reinforcement be halved for joints connecting beams at all four column faces [N1]. Also, the ACI 318-08 code accepts the beneficial effect of transverse beams where the total horizontal reinforcement within the joint can be reduced by 50% when beams are framing into all four sides of the joint [A1]. On the other hand, the model of AIJ-1994 highlights that the allowable nominal shear strength of the joint may be enhanced up to 1.3 times if beams frame into all four faces of the joint [A5].

Even though the design codes recommend the reduction of joint hoops area with the presence of transverse beam, some research on beam-column joint with transverse beams explained otherwise. Cheung *et al* [C3] carried out a series of full scale beam-column-slab tests and concluded that there was no evidence during the test to indicate that the presence of floor slabs or beams in two directions provided significant confinement to the joint cores during bidirectional seismic loading.

On the other hand, Tan [T1] analysed a series of analytical models with different transverse beam configurations with the main variable being the dimension of the transverse beam. The study concluded that a well-reinforced transverse beam with a large cross section may contribute to the superior behaviour of the beam longitudinal bars outside the column. This can be achieved by increasing the reinforcing ratio of the transverse beam or the dimension of the transverse beam, which leads to an increase in the torsion strength and stiffness of the transverse beam. However, the significant role of a transverse beam can only be expected

before it reaches the cracking torsional strength.

6.3.7 Summary of Parametric Studies

From the parametric studies, the following findings were summarised:

- In general the following parameters have significant effects on the joint shear capacity: concrete compressive strength, bond index, joint hoop reinforcement and beam reinforcement ratio. The column axial load on the other hand has more influence on the deformational behaviour of an interior beam-column joint than on the strength capacity.
- The influence of concrete strength on joint shear strength is not in a direct manner due to the additional influences of other parameters such as joint hoop reinforcement area. As such, the joint shear strength is normalised to the concrete strength to study the influences of other control parameter.
- Column axial load in general has no direct effect on the maximum joint shear strength, but it does affect the joint shear deformation and it may lead to different deterioration behaviour after the peak column shear strength is reached depending on the availability of joint hoops.
- Longitudinal reinforcement passing through the joint panel helps to resist the joint shear. However, excessive longitudinal reinforcement in the beams and columns could be detrimental especially for lightly reinforced joints, as they might change the failure mechanism of a joint from beam hinging to joint shear.
- Even though it is generally accepted that joint core reinforcement serves to provide shear resistance and provide confinement to the joint volume, the parametric studies shows the possibility of overestimation in the contribution of joint hoops. The shear stress demand for lightly reinforced beam column joint with no joint core reinforcement can be as high as those with high joint core reinforcement.
- Bond Index (BI) can be a good indication to estimate the bond condition of a joint. It is recommended that the application of BI in a design for the

development length of reinforcement in joint core should be companied by the checking of longitudinal reinforcement ratio.

The transverse beams and slabs are structural elements that have direct interaction with the beam-column joints which may provide significant confinement to the joint cores during bidirectional seismic loading. The major design codes such as NZS 3010 and ACI 318 allow the reduction of joint hoops area with the presence of transverse beam.

6.4 Joint Shear Design of New Zealand Standard NZS 3101

The findings from parametric studies in Section 6.3 revealed that concrete compressive strength, bond index, joint hoop reinforcement and beam reinforcement ratio has significant influence on the joint shear capacity while the column axial load is more influential on the deformational behaviour of an interior beam-column joint. To have a ductile structure, the design equations must have incorporated various aspects that have been addressed in Section 6.3. In the following sections, the joint shear design of New Zealand Standard NZS 3101 is reviewed and improvement is proposed to produce a more thorough design code.

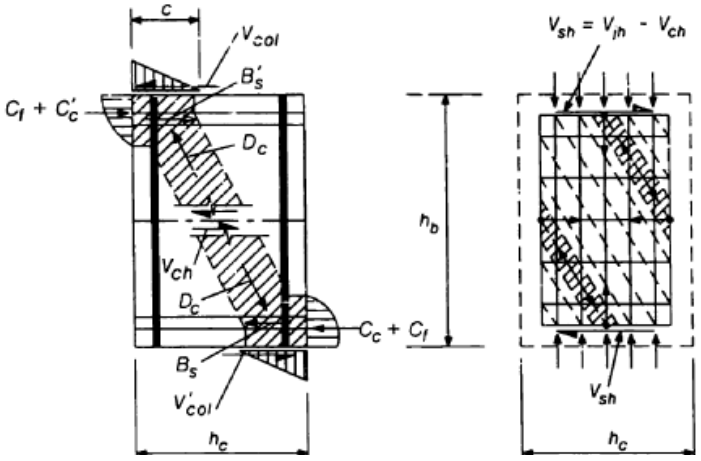

(a) Diagonal compression strut **b) Truss mechanism**

Figure 6.11 Shear Resisting Mechanisms in Beam-Column Joints [P3]

The shear provision in the NZS 3101 has been developed based on strut-and-tie models for joint behaviour and experimental test that have been conducted in New Zealand since the 1970s. [P3, P4] The NZS 3101 model postulates that an adequately detailed joint should be able to mobilize two self-equilibrating mechanisms of shear transfer namely diagonal compression strut V_c and truss mechanism V_s as shown in Figure 6.11 [P3].

The diagonal compression strut V_c is initiated at the initial stage of response before the beam yielding starts to penetrate from the adjacent beam-column interface into the joint. After several significant cycles of loading, the yield penetration of beam bar and bond deterioration is taking place with the formation of full-depth cracks. The normal stresses acting on the concrete compression zones of the framing members will eventually be eliminated. Then, both the horizontal members shear and vertical members shear forces will have to be transferred through bond effects. As the yield penetration destroyed the bond, it is noticed that the stress transfer moves towards the central region of the joint which causes significant stress distribution within the joint. At this point, the concrete strut mechanism is assumed to be no longer activated. A self equilibrium truss mechanism, formed by both horizontal and vertical shear reinforcement and column longitudinal reinforcement starts to carry the distributed forces. The concrete core supplies the necessary compression field which is balanced by the tension forces in the reinforcement. To sustain such mechanism, a large amount of horizontal and possible vertical joint reinforcement is required [P3].

In the design code, the truss mechanism is assumed to take a large portion of joint shear when full depth flexural cracks occurred in the beams at column face upon the formation of plastic hinge at beam adjacent to column faces as well as the diminish of concrete compression capacity. The contribution of main strut mechanism is neglected except the presence of column axial compressive load greater than $0.1f_c'A_g$ [N1]. This conservatism which ignores the contribution of main strut mechanism with insignificant axial load causes the diagonal compression strut V_c is generally taken as zero in design and the truss mechanism V_s on the other hand

undertakes all the forces. The horizontal shear reinforcement is considered to take all the probable horizontal forces. Similarly, the vertical reinforcement inclusive of intermediate column reinforcement placed in the plane of bending between corner bars is assumed to take all the vertical forces. The NZS 3101 also requires provision of horizontal transverse confined reinforcement to prevent possible concrete dilation. The amount of confinement reinforcement can be halved if a joint is framed at all four faces. The axial compressive load is assumed to contribute to the compression strut by increasing the steepness towards the vertical plane which in turn enhances the joint shear strength especially when the axial compressive load is insignificant. The beneficial effect of axial compressive load is reflected in the design equation of horizontal and vertical shear reinforcement in the next section.

6.4.1 Structural Behaviour of Beam-Column Joints

The beam-column joint has been a critical region in reinforced concrete frames designed for inelastic response to severe seismic attack. As a consequence of seismic moments in columns of opposite signs immediately above and below the joint (and similar for beam moment reversal across the joint), the joint region is subjected to shear forces of vertical and horizontal with magnitude of many times higher than the adjacent beams and columns. Shear failure could take place if no design consideration was taken place. The reversal in moment across the joint also means that the beam reinforcement is required to be in compression on one side of the joint and at tensile yield on the other side of the joint. Bond failure could also happen as high bond stresses required to sustain the force gradient across the joint and corresponding degradation of moment capacity accompanied by excessive drift.

Reinforced concrete frames can achieve ductile behaviour provided that brittle failure of structural elements and instability can be prevented in severe earthquakes. The design and detailing of beam-column joints is important in achieving satisfactory performance of RC frames. The design should be able to prevent brittle shear failure of the joint and maintain integrity of the joint to develop the ultimate strength of the connecting beams and columns. Besides that, the design should also

reduce joint stiffness degradation by minimizing cracking of the concrete at joint core by preventing the loss of bond between the concrete and longitudinal beam and column reinforcement.

The ductility and associated energy dissipating capacity of a reinforced concrete frame is anticipated to originate primarily from chosen and appropriately detailed plastic hinges in beams or columns [P3]. Due to the control of shear and bond mechanism, the joint should never be regarded as being suitable to be the major source of energy dissipation if any of the both exhibited poor hysteretic properties. Hence the response of the joint should be restricted essentially to the elastic domain. To better understand the structural behaviour of a beam-column joint, a typical interior beam-column joint subjected to lateral force on the column is illustrated in Figure 6.12 to explain the joint shear force in an internal beam-column joint.

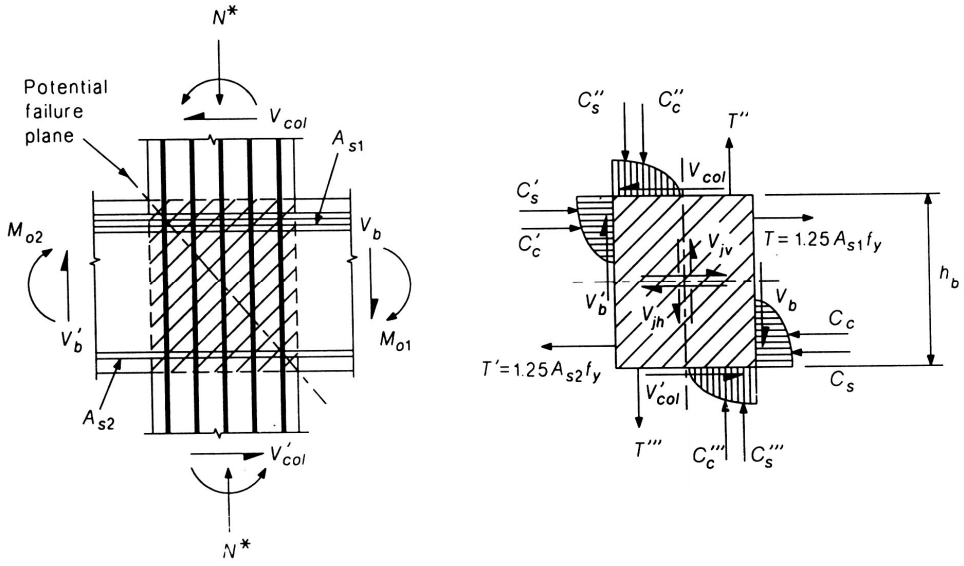

(a) External Action **b) Internal Action**

Figure 6.12 External and Internal Actions of Interior Beam-Column Joints [P3]

By taking column shear force V_{col} acts on the top column of an interior joint and plastic hinges formed in the beams at the column faces, the tension force of the bottom longitudinal beam bar was taken as T with overstrength factor of α on the

yield strength of bar f_y. On the opposite face, the steel and concrete were in compression (C_c', C_s') and to evaluate the force V_{jh} within the joint, the following equilibrium is obtained:

$$V_{jh} = T + C_c' + C_s' - V_{col} \quad (6.2a)$$

On the other hand, to maintain force equilibrium, the top longitudinal beam bar has the following equilibrium:

$$V_{jh} = T' + C_c + C_s - V_{col} \quad (6.2b)$$

Since the approximation of $T' = Cc' + Cs'$ can be made, the joint shear force is simplified to:

$$V_{jh} = T + T' - V_{col} \quad (6.3a)$$

The above relation can be simplified by taking α as 1.25, the area of top reinforcement as A_{s1} and bottom reinforcement as A_{s2}:

$$V_{jh} = 1.25 f_y (A_{s1} + A_{s2}) - V_{col} \quad (6.3b)$$

The nominal horizontal shear stress v_{jh} in the joint is estimated to be:

$$v_{jh} = \frac{V_{jh}}{b_j h_c} < 0.2 f_c' \text{MPa} \quad (6.4)$$

As explained in Figure 6.11, the two shear resisting mechanisms in joints namely, diagonal compression strut V_c and truss mechanism V_s are strongly influenced by the distribution of bond forces along the longitudinal bars anchored within the joints core. Although the bond forces require a major part of the joint shear force to be transferred by the truss mechanism, some deterioration of bond and a consequent reduction in the ability of beam bars to resist compression forces resulted in an increase in the shear resistance of the diagonal compression strut mechanism. Hence the joint shear reinforcement is deduced in NZS 3101: 2006 based on the aforesaid findings and the shear reinforcement is estimated as below:

$$A_{jh} = \frac{V_{sh}}{f_{yh}} = \frac{(V_{jh} - V_{ch})}{f_{yh}} \quad (6.5a)$$

$$A_{jv} = \frac{V_{sv}}{f_{yv}} = \frac{(V_{jv} - V_{cv})}{f_{yv}} \qquad (6.5b)$$

The design equation for horizontal shear reinforcement of an interior beam-column joint is:

$$A_{jv} = \frac{6v_{jh}}{f_c'} \alpha_i \frac{f_y}{f_{yh}} A_s^* > \frac{0.4v_{jh}}{f_c'} \qquad (6.6)$$

where: $0.85 < \frac{6v_{jh}}{f_c'} < 1.2$

$$\alpha_i = 1.4 - 1.6\frac{C_j N^*}{f_c' A_g} \qquad (6.7)$$

A_s^* = greater of area of top or bottom reinforcement passing though the joint

N^* = axial compressive load acting on the column

C_j = taken as 1.0 for on way frame

The spacing of shear reinforcement shall be the lesser of 200mm or 10 times the diameter of smallest longitudinal column bar. Noteworthy that f_c' only appears in the limiting value of v_{jh} and A_{jh}, and ductile frames which are capped at 70 MPa.

6.4.2 Bond Deterioration Control Review

The structural behaviour of an internal beam-column joint as well as the detailing of beam-column joints was explained in Section 6.4.1. Besides providing sufficient joint core reinforcement to create truss mechanism to resist the diagonal crack opening, the bond condition of reinforcement bars passing through the joint core is crucial. To control the bond deterioration within the joint core upon the formation of plastic hinges form in the beams at the column faces, NZS 3101 [N1] specifies the longitudinal bar diameter d_b passing through a column depth h_c should satisfy the limit below:

$$\frac{d_b}{h_c} \le 3.3\alpha_f \frac{\sqrt{f_c'}}{\alpha_o f_y} \qquad (6.8)$$

α_f = 0.85 for beam bars in two way frames and
= 1.00 for beam bars in one direction

α_o = 1.25 for plastic hinge in beam developed in column face and
= 1.00 for plastic hinge is relocated and beam section in column face remain elastic range

Eq. 6.8 set the basis in bond deterioration control for beam-column joints as the beam bar size has the direct relation with bond strength of a joint core with respect to the column depth as well as the material properties of concrete and steel. The research findings in experimental data and FE parametric studies proposed some relaxation of the bond requirements in beam-column joints in Eq. 6.8 with the use of HSC. The relaxation in aforesaid equation should be possible because the bond strength increases with the increase in concrete compressive strength as explained in the test results of HSC specimen NS3 as compared to its NSC counterpart X3.

Based on test observations and FE analysis findings, the bond deterioration control limits in Eq. 6.8 can be refined by considering the followings facts:

- The influence of concrete grade on the ultimate load of beam-column joints tended to be less significant as the concrete strength is above 70MPa
- The beneficial effects of axial compressive load was less significant when the axial compressive load more than $0.3A_gf_c'$ and the ultimate load of the beam-column joints did not enhance when axial compressive load was increased above $0.3A_gf_c'$

As such, improvement on the bond deterioration control for an internal beam-column joint is proposed.

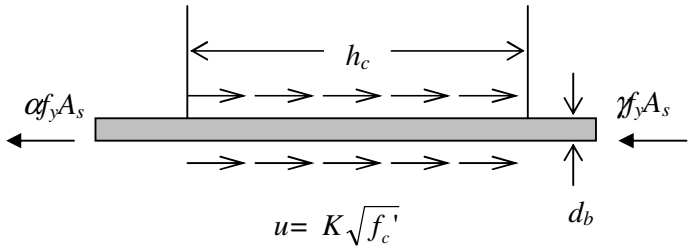

Figure 6.13 Illustration of Bond in Reinforcement Bar in a Joint

Figure 6.13 illustrates the bond within a beam-column joint by considering a longitudinal beam bar with diameter d_b passing through a column of depth h_c. The bar is assumed to reach its yielding strength with overstrength of αf_y at one column face and has compressive force of γf_y at the opposite column face with $\gamma \leq 1$.

The average ultimate bonding stress u is assumed to be $K\sqrt{f_c'}$ and for equilibrium,

$$\frac{\pi}{4} d_b{}^2 \left(\alpha f_y + \gamma f_y\right) = \pi d_b h_c K \sqrt{f_c'}$$

$$\therefore \frac{d_b}{h_c} = \frac{4K\sqrt{f_c'}}{(\alpha f_y + \gamma f_y)} \qquad (6.9)$$

The basic value of K is denoted as K_o and it is estimated by equating Eq. 6.8 to Eq. 6.9 and assumed that $\alpha_f = 1.00$ and $\alpha_o = 1.25$:

$$\frac{4}{(\alpha+\gamma)} \frac{K_o\sqrt{f_c'}}{f_y} = 3.3\alpha_f \frac{\sqrt{f_c'}}{\alpha_o f_y}$$

$$\frac{4}{(\alpha+\gamma)} \frac{K_o\sqrt{f_c'}}{f_y} = 2.64 \frac{\sqrt{f_c'}}{f_y}$$

$$K_o = 0.66(\alpha+\gamma) \qquad (6.10)$$

The factor K_o in Eq. 6.10 is a function of bar stress condition upon the formation of plastic hinge. Besides the factors addressed in Eq. 6.8, the NZS 3101 incorporates two more factors namely, α_t, and α_p in the design. The factor α_t considers the bond condition of a joint due to the casting process. Inferior bond condition always occurred in top reinforcement due to sedimentation during casting of concrete. On the other hand, α_p is another factor that considers the effect of axial compressive loading on the bond condition of a joint as the presence of axial compressive load generally improve the bond condition of beam reinforcement. The limiting values of α_t, and α_p in NZS 3101 are summarised as below:

α_t =0.85 for top beam with more than 30mm of fresh concrete is cast below the bar

=1.00 for other case

$$\alpha_p = \frac{N^*}{2f'_c A_g} + 0.95 \text{ with limitation of } 1.0 \leq \alpha_p \leq 1.25.$$

As such, K in Eq. 6.9 is expressed as below after incorporating the above factors:

$$K = \alpha_t \alpha_p K_o \tag{6.11}$$

By summarizing the aforesaid factor in Eq. 6.11 into Eq. 6.9:

$$\frac{d_b}{h_c} = \frac{4}{(\alpha + \gamma)} \frac{K\sqrt{f_c'}}{f_y}$$

$$\frac{d_b}{h_c} = \frac{4}{(\alpha + \gamma)} \frac{K_o \alpha_t \alpha_p \sqrt{f_c'}}{f_y}$$

$$\frac{d_b}{h_c} = K_m \left(\frac{\alpha_t \alpha_p}{\alpha_m} \right) \frac{\sqrt{f_c'}}{\alpha f_y} \tag{6.12}$$

where $K_m = 4K_o$ and $\alpha_m = \left(1 + \frac{\gamma}{\alpha}\right)$

The factor α_m in Eq. 6.12 is a function of the overstrength factor α of bar at tension face and γ at the compression face which have to be considered based on the design concept and test data. As suggested in the NZS 3101, the overstrength factor α can be assumed as 1.25. Alternatively, the value of α can be determined based on tensile test of reinforcement bars used. From test results and literatures, the overstrength factor α of bars were generally ranging from 1.20 to 1.40.

Figure 6.14 shows a beam section near to column face where the top reinforcement is subjected to compression force C_{s1} and tension force T_1 on bottom reinforcement where $C_{s1} = \gamma f_y A_s$ and $T_1 = \alpha f_y A_s'$

Since: $C_{s1} \leq T_1$

$$\gamma f_y A_s \leq \alpha f_y A_s'$$

$$\gamma \leq \alpha \frac{A_s'}{A_s}$$

$$\gamma \leq \alpha\beta \tag{6.13}$$

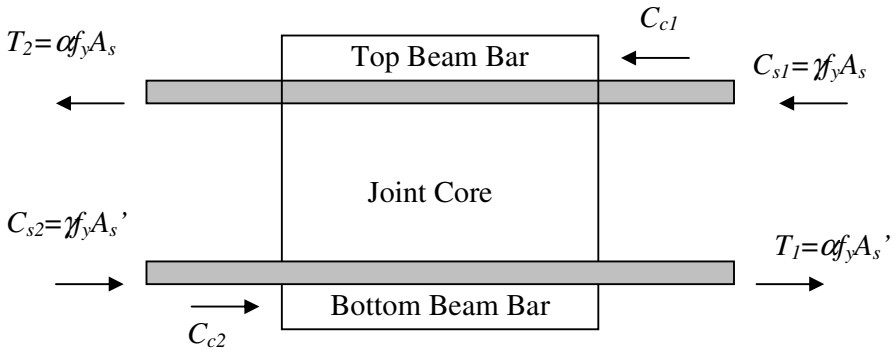

Figure 6.14 Bond Development in a Joint

From the test observation, the γ of top beam reinforcement was unlikely to exceed 0.60 and thus γ shall be the lesser of 0.60 or Eq. 6.13. On the other hand, for equilibrium the bottom reinforcement generally could be subjected to higher stress in compression when β is less than unity. Hence when β is 0.5 which is the minimum value based on the limit of reinforcement ratio in NZS 3101, the γ of bottom bar can set as unity. When β is unity, the γ can be reduced to 0.60 which is same as the threshold of top reinforcement and for β in between unity and 0.5, the γ can be estimated in inverse proportion to β as below:

$$\gamma = 1.00 \qquad \text{for } \beta = 0.50$$

$$\gamma = 0.6+0.8(1-\beta) \qquad \text{for } 0.50 < \beta \leq 1.00 \qquad (6.14)$$

To better understand the relation between α, β and γ, the factor α_m is derived based on the limits of γ explained in Eq 6.13 and Eq 6.14 for α ranging from 1.20 to 1.40. The value of α_m is then plotted against β to study the trend in the relationship.

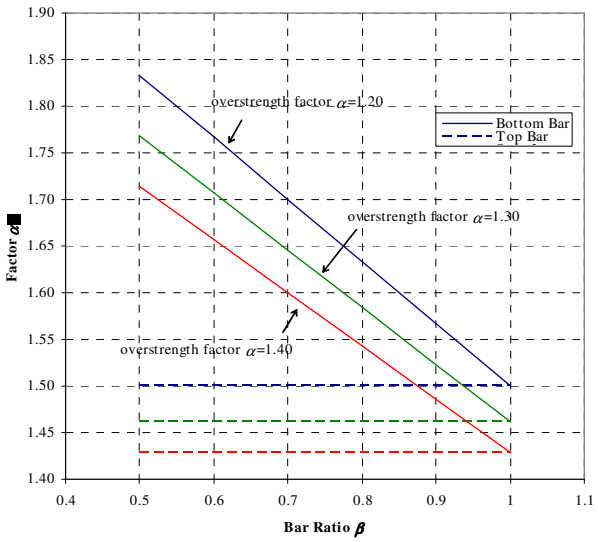

Figure 6.15 Relation between Parameters α, β and α_m

Figure 6.15 shows the factor α_m of the top and bottom reinforcement for α ranging from 1.20 to 1.40 with β ranging from 0.50 to 1.00. For all cases of equal top and bottom reinforcement area (β =1.0), both top and bottom reinforcement have the same α_m. As β is less than 1.0, the values of α_m for top and bottom reinforcement are no longer the same. The α_m of bottom reinforcement is increased as the β is less than 1.0, which required the bar diameter be reduced as explained in Eq. 6.12. On the other hand, the α_m of top reinforcement is consistent even though the β is less than unity as γ was capped at 0.60 as explained in Eq. 6.14. This scenario in Figure 6.15 explains that the top reinforcement is always subjected to more serious bond deterioration and the bar size shall be kept small regardless of the change in ratio of top to bottom reinforcement. The bond condition of bottom reinforcement is less critical compared to its counterpart and thus, the bar size used can be relaxed in the case of smaller ratio of β.

As explained in Figure 6.15, the general trend of α_m for top and bottom reinforcement with α of 1.20 to 1.40 is the same. Hence, to facilitate the design process, to estimate K_o, the overstrength factor α of bar is assumed to be 1.30 and γ

at the compression bar is taken to be 0.60. Hence, by substituting α and γ into Eq. 6.11, the basic value K_o is 1.254 and K_m = 5.016 thus Eq. 6.12 is updated to:

$$\frac{d_b}{h_c} = 5.016\left(\frac{\alpha_t \alpha_p}{\alpha_m}\right)\frac{\sqrt{f_c'}}{\alpha f_y} \qquad (6.15)$$

NZS 3101 has set the maximum value of f_c' at 70MPa to develop a ductile structure [N1]. On the other hand, to reflect the limitation of axial compressive load beyond $0.3A_g f_c'$ the limit of α_p is revised. Based on the maximum limiting value of α_p of 1.25, the equivalent axial compressive load N^* should be $0.6A_g f_c'$. However, from the test observation and FE analysis, any axial compressive load exceeded $0.3A_g f_c'$ has limited influence on the performance of beam-column joint. As such, a capped limit on axial compressive load is proposed to set at $0.3A_g f_c'$ to better reflect the influence of axial compressive load and thus the limit of α_p is changed to $1.0 \leq \alpha_p \leq 1.10$.

To verify the proposed improvement in design equations, Eq. 6.15 was applied to test data of authors and Xin [X1]. The comparison as shown in Table 6.4 explains that by using the proposed design equation, generally the maximum allowable bar size was relaxed to a larger size by considering the beneficial effects from higher concrete grade and presence of axial compressive load which may help to improve the energy dissipation capacity of the beam-column joints. For example, based on the new design limit of the maximum column depth to longitudinal bar diameter ratios, NS1 can be made of bar size of 20mm. On the other hand, for NS2 made of unsymmetrical top bar area and bottom bar area, the maximum size of top and bottom bars shall be 20mm and 16mm respectively, which may give satisfactory joint core bond performance.

Table 6.4 Verification of Proposed Equations

Sample Marking	Bar Location	Bar Size d_b (mm)	Concrete Grade f_c' (MPa)	Steel Grade f_y (MPa)	Axial Load N ($f_c'A_g$)	Bottom bar to top bar ratio β	Calculated d/h	Actual d/h
N1	Top	12	60.1	510	0	1.00	1/22.21	1/37.50
	Bottom	12		510			1/22.21	1/37.50
N2	Top	16	61.2	508	0	0.50	1/21.92	1/28.13
	Bottom	16		508			1/26.54	1/28.13
N3	Top	16	60.5	508	0	1.00	1/22.05	1/28.13
	Bottom	16		508			1/22.05	1/28.13
N4	Top	20	60.3	513	0	0.64	1/22.30	1/22.50
	Bottom	16		508			1/25.43	1/28.13
A1	Top	12	61.4	510	0.3	1.00	1/19.97	1/37.50
	Bottom	12		510			1/19.97	1/37.50
A2	Top	16	60.8	508	0.3	0.50	1/19.99	1/28.13
	Bottom	16		508			1/24.20	1/28.13
A3	Top	16	60.5	508	0.3	1.00	1/20.04	1/28.13
	Bottom	16		508			1/20.04	1/28.13
A4	Top	20	61.7	513	0.3	0.64	1/20.04	1/22.50
	Bottom	16		508			1/22.86	1/28.13
X1	Top	12	30.9	453	0	1.00	1/27.51	1/37.50
	Bottom	12		453			1/27.51	1/37.50
X2	Top	16	40.8	445	0	0.50	1/23.52	1/28.13
	Bottom	16		445			1/28.47	1/28.13
X3	Top	16	42.5	445	0	1.00	1/23.04	1/28.13
	Bottom	16		445			1/23.04	1/28.13
X4	Top	20	47.2	492	0	0.64	1/24.17	1/22.50
	Bottom	16		445			1/25.18	1/28.13
X5	Top	20	60.7	492	0	1.00	1/22.44	1/22.50
	Bottom	20		492			1/22.44	1/22.50
X6	Top	24	59.3	461	0	0.50	1/20.74	1/18.75
	Bottom	20		492			1/26.11	1/22.50

The New Zealand concrete design code NZS 3101: 2006 relaxed the allowable concrete strength from the previous 55MPa to the maximum of 100 MPa, except for the ductile element in seismic design which is capped at maximum of 70 MPa. As explained earlier, the nominal horizontal shear stress v_{jh} in the joint is estimated to be:

$$v_{jh} = \frac{V_{jh}}{b_j h_c} < 0.2 f_c' \text{MPa} \qquad (6.4)$$

The limit of $0.2f_c'$ replaced the limits $1.5\sqrt{f_c'}$ set in NZS 3101: 1982 which reflected the change in the concrete strength limits. The shear provision in the code was developed based on strut-and-tie models for joint behaviour and experimental test that have been conducted in New Zealand since the 1970s which were mainly made of NSC.

To compare the changes made to the limiting values v_{jh}, both the v_{jh} limits were plotted against concrete grade from 20MPa to 90 MPa. The limiting values of both v_{jh} of NSZ is plotted in Figure 6.16a for comparison. The curves in Figure 6.16a shows that the v_{jh} of code version 2006 is conservative for NSC while the v_{jh} of code version 1982 is conservative for HSC above grade C60. The limit v_{jh} of code version 2006 has considered the beneficial of HSC which can yield a better bond strength. However the conservatism of the limit in Eq. 6.4 can lead to over-designed in beam-column joint made of NSC. As such, a limiting value for v_{jh} which take the advantages of both v_{jh} limits shown in Figure 6.16a is preferred in order to cater for the use of both NSC and HSC.

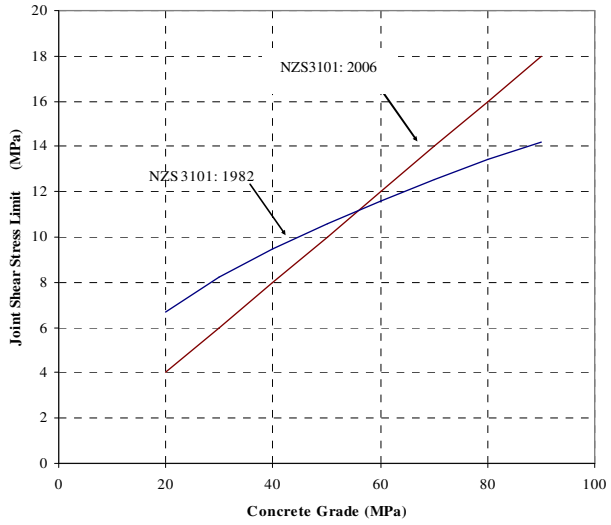

a. Comparison between Limits in NZS (1982) and NZS (2006)

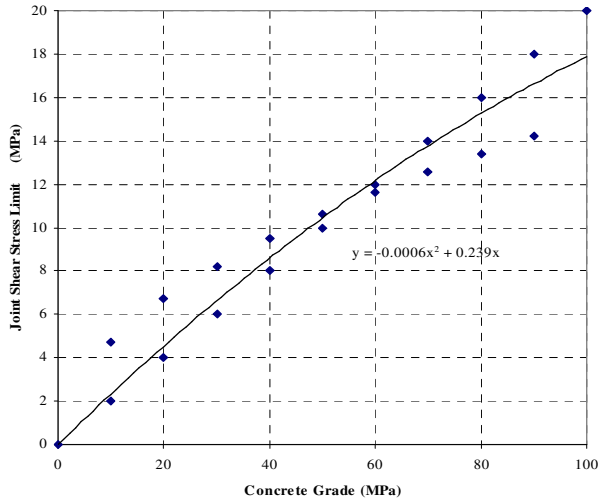

b. Correlation of Limits between NZS (1982) and NZS (2006)

Figure 6.16 Joint Shear Stress Limits in NZS (1982) and NZS (2006)

In Figure 6.16b, all the data points of both v_{jh} limits ranging from 0 to 100MPa were plotted and data regression was performed. From the best fit curve, the joint shear strength limit v_{jh} were found to be:

$$v_{jh} = \frac{V_{jh}}{b_j h_c} < -0.0006 f_c'^2 + 0.239 f_c' \qquad (6.16)$$

which is more suitable to be used in both HSC and NSC beam-column joint.

6.4.3 Parametric Study on Shear Design

To evaluate the shear design equations in NSZ 3101, parametric studies on the interior beam-column joints in summarised in Table 6.1 were performed. The ultimate shear strength these interior beam-column joints were computed using equation in NSZ3101 and normalised with their respective test results as shown in Figure 6.17a. These specimens were made of concrete grade 15MPa to 63MPa and the ratio of column axial load to column cross-sectional area ranges from about -1.1MPa to 18MPa were considered in this study. The specimens also covered a wide range of joint shear reinforcement ratio, beam flexural reinforcement ratio and column to beam width ratio. All selected specimens failed mostly on pure shear mechanism of the joint or beam flexural associated with significant deterioration inside the joint panel to ensure the joint closely attained its maximum shear strength. As explained in Figure 6.17a, the result of linear regression analysis indicates the calculated ultimate shear strength is about 20% more conservative than the actual ultimate shear strength. The conservatism could be partly due to the assumption of overstrength factor α of 1.25 in NZS 3101 instead of the proposed α of 1.30 as demonstated in Section 6.4.2.

To verify this finding, the ultimate shear strength of the 83 specimens was recalculated based on α of 1.30 and normalised with their respective test results as shown in Table 6.5. The proposed joint shear strength limit v_{jh} in Eq. 6.16 was used in the parametric study since it gives good control to joint shear stress limits of both NSC and HSC specimens. As explained in Figure 6.17b, the result of linear regression analysis explains that marginal improvement was found in the calculated ultimate shear strength by revising α from 1.25 to 1.30.

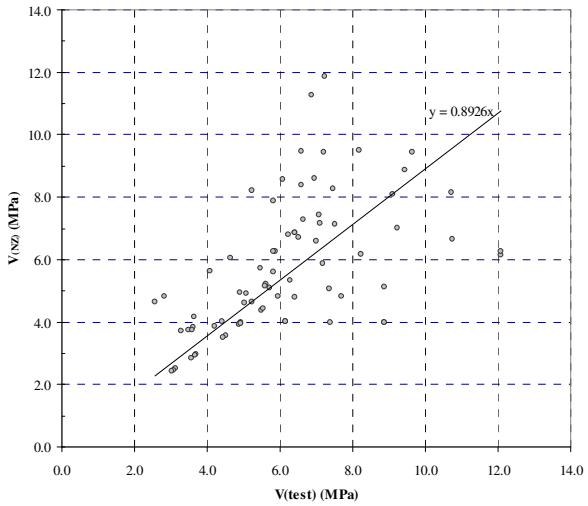

(a) Current NZS

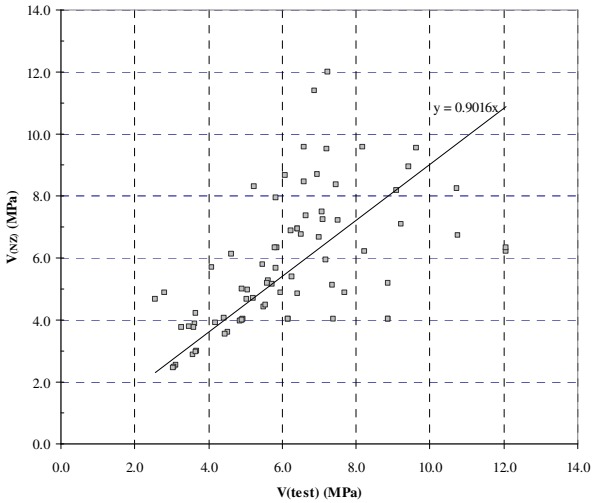

(b) Modified NZS

Figure 6.17 Prediction of Shear Strength versus Experimental Results

Figure 6.18a depicts the ratio between nominal shear stress obtained from modified shear design equation versus the concrete grade of specimens. In general, the equations match reasonably well the test shear strength with better correlation for beam-column joints of 30 to 40MPa. Also, Figure 6.18b explains the ratio between nominal shear stress obtained from modified shear design equation versus applied axial compressive loading of specimens. The equation matches with the test shear

strength of beam-column joints with axial compressive loading of $0.1A_g f_c'$ to $0.3A_g f_c'$.

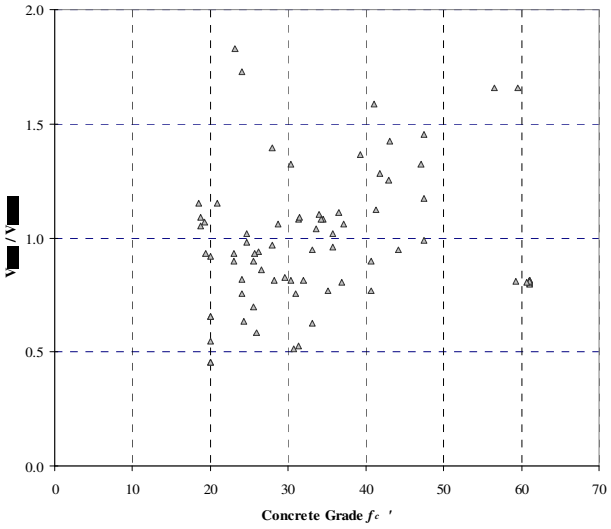

a. Concrete Strength

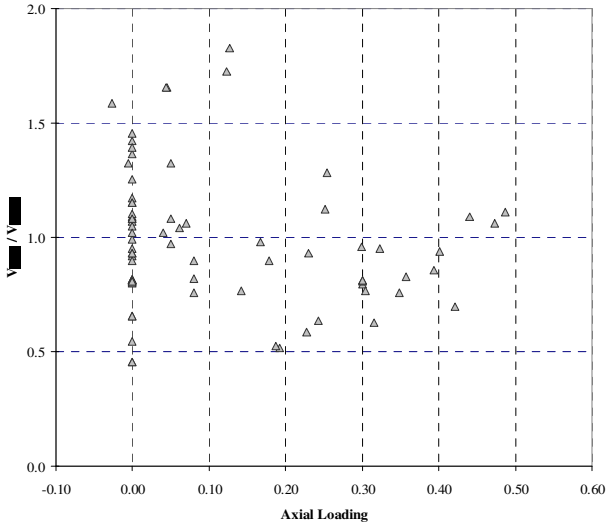

b. Axial Compressive Loading

Figure 6.18 Normalised Shear Strength versus Control Parameters

From the calculated ultimate shear strength of the interior beam-column joints shown in Table 6.5, it is evident that the NZS 3101 gives good correlation with test result in terms of average strength ratio of 0.98, standard deviation of 0.29 and coefficient of variation of 0.30.

Table 6.5 Parametric Studies on Shear Design Equations

Reference	Specimen	$f_{c'}$ *(MPa)*	f_y *(MPa)*	Axial Load N $(f_c'A_g)$	v_{exp} (MPa)	v_{nz} (MPa)	v_{nz} / v_{exp}	v_{jh} (Eq 6.16) (MPa)	limit check
Leong	NS1	60.1	510	0.00	4.51	3.61	0.80	12.35	ok
	NS2	61.2	508	0.00	3.69	3.01	0.81	12.35	ok
	NS3	60.5	508	0.00	4.94	4.02	0.81	12.35	ok
	NS4	60.3	513	0.00	3.12	2.54	0.81	12.35	ok
	AS1	61.4	510	0.30	4.44	3.54	0.80	12.35	ok
	AS2	60.8	508	0.30	3.56	2.88	0.81	12.35	ok
	AS3	60.5	508	0.30	4.90	3.99	0.81	12.35	ok
	AS4	61.7	513	0.30	3.08	2.49	0.81	12.35	ok
Xin [X1]	X1	28.2	453	0.00	4.86	3.96	0.82	6.26	ok
	X2	30.3	445	0.00	3.66	2.98	0.81	6.69	ok
	X3	32.0	445	0.00	4.91	4.00	0.81	7.03	ok
	X4	36.9	492	0.00	3.03	2.45	0.81	8.00	ok
	X5	60.7	492	0.00	5.48	4.41	0.80	12.30	ok
	X6	59.3	461	0.00	5.54	4.48	0.81	12.06	ok
Fenwick & Irvine [F2]	Unit 1	42.9	280	0.00	6.95	8.70	1.25	9.15	ok
	Unit 3	39.3	318	0.00	5.83	7.95	1.36	8.47	ok
Briss [B3]	B1	27.9	288	0.05	5.83	5.65	0.97	6.20	ok
	B2	31.5	288	0.44	5.81	6.34	1.09	6.93	ok
Otani, *et-al* [O1]	J1	25.6	374	0.08	5.73	5.15	0.90	5.73	ok
	J2	24	374	0.08	5.96	4.88	0.82	5.39	ok
	J3	24	374	0.08	6.4	4.85	0.76	5.39	ok
	J4	25.7	374	0.23	5.59	5.19	0.93	5.75	ok
	J5	28.7	374	0.07	5.46	5.79	1.06	6.37	ok
Durani & Wight [D2]	X1	34.3	276	0.05	6.41	6.93	1.08	7.49	ok
	X2	33.6	276	0.06	6.51	6.77	1.04	7.35	ok
Meinheit & Jirsa [M4]	I	26.2	434	0.40	5.62	5.28	0.94	5.85	ok
	II	41.8	434	0.25	6.6	8.47	1.28	8.94	ok

	III	26.6	434	0.39	6.27	5.38	0.86	5.93	ok
	IV	35.8	434	0.30	7.51	7.21	0.96	7.79	ok
	V	35.8	434	0.04	7.1	7.24	1.02	7.79	ok
	VI	36.5	434	0.49	6.63	7.37	1.11	7.92	ok
	VII	37.2	434	0.47	7.07	7.50	1.06	8.06	ok
	VIII	33.1	434	0.32	10.75	6.73	0.63	7.25	ok
	IX	31.0	434	0.35	8.22	6.23	0.76	6.83	ok
	X	29.6	434	0.36	7.18	5.95	0.83	6.55	ok
	XI	25.5	434	0.42	7.36	5.13	0.70	5.70	ok
	XII	35.1	434	0.30	9.22	7.08	0.77	7.65	ok
	XIII	41.3	434	0.25	7.45	8.35	1.12	8.85	ok
	XIV	33.1	434	0.32	7.01	6.66	0.95	7.25	ok
Bessho [Z1]	J1	31.6	379	0.08	9.75	8.95	0.95	9.39	ok
	J2	31.6	379	0.08	9.75	8.66	1.42	9.17	ok
	J3	33.4	379	0.08	10.42	9.54	0.99	10.00	ok
Ishibashi [I1]	D19-S1	44.2	524	0.00	9.43	9.57	1.45	10.00	ok
	D19-S2	43	524	0.00	6.08	9.58	1.17	10.00	ok
	D19-S3	47.5	508	0.00	9.64	4.05	0.92	4.54	ok
	D19-S4	47.5	508	0.00	6.58	4.04	0.66	4.54	ok
	D19-S5	47.5	506	0.00	8.18	4.04	0.66	4.54	ok
Ohwada [Z1]	JO1	20	434	0.00	4.41	4.03	0.55	4.54	ok
	JO2	20	434	0.00	6.16	4.03	0.45	4.54	ok
	JE1	20	434	0.00	6.16	4.03	0.45	4.54	ok
	JE2	20	434	0.00	7.38	6.13	1.32	6.71	ok
	JI1	20	434	0.00	8.87	8.29	1.59	8.81	ok
	JI2	20	434	0.00	8.87	9.53	1.32	9.93	ok
Attaalla [A6]	SOC1	30.4	422	-0.01	4.63	11.40	1.66	11.59	ok
	SOC2	41.1	422	-0.03	5.23	11.99	1.66	12.10	ok
	SOC3	47.1	431	0.05	7.2	4.89	0.64	5.45	ok
	SHC1	56.5	431	0.04	6.88	5.19	0.59	5.79	ok
	SHC2	59.5	431	0.04	7.24	6.22	0.52	6.77	ok
Leon [L1]	BCJ2	30.5	413	0.00	6.89	6.34	0.53	6.91	ok
	BCJ3	27.6	413	0.00	7.62	8.24	0.77	8.73	ok
	BCJ4	27.6	413	0.00	6.68	8.18	0.90	8.73	ok
Ishibashi [I1]	D51-1	24.3	395	0.24	7.68	3.80	1.09	4.26	ok
	D51-2	25.9	395	0.23	8.86	4.20	1.15	4.73	ok
	D51-3	30.7	402	0.19	12.07	3.88	1.07	4.37	ok

	D51-4	31.4	402	0.19	12.07	3.77	1.15	4.22	ok
	D41-1	40.7	377	0.14	10.73	3.90	0.93	4.41	ok
	D41-2	40.7	377	0.00	9.1	3.77	1.05	4.26	ok
	D29-SLS	18.7	382	0.00	3.48	4.97	0.98	5.54	ok
	D29-LSL	20.9	382	0.00	3.65	4.69	0.90	5.20	ok
	D29-KSK	19.2	382	0.00	3.62	5.00	1.02	5.54	ok
	D29-SSS	18.5	382	0.00	3.27	4.67	0.93	5.20	ok
	D29-LLL	19.4	382	0.00	4.2	5.69	1.39	6.22	ok
	D29-LSS	18.7	382	0.00	3.59	6.33	1.08	6.91	ok
	D29-PJN	24.7	382	0.17	5.07	6.87	1.10	7.43	ok
	D29-BJN	23.1	382	0.18	5.22	6.94	1.08	7.53	ok
	D29-PJO	24.7	382	0.00	4.9	4.68	1.83	5.22	ok
	D29-BJO	23.1	382	0.00	5.03	4.87	1.73	5.39	ok
	D29-20N	28	395	0.00	4.08	5.63	1.38	5.60	ok
	D29-30N	31.4	395	0.00	5.86	6.27	1.07	6.28	ok
	D29-30S	34	395	0.00	6.24	6.80	1.09	6.80	ok
	D29-30W	34.5	395	0.00	6.42	6.87	1.07	6.90	ok
	D22-SJP	23.2	377	0.13	2.56	4.63	1.81	4.64	ok
	D22-SJB	24	377	0.12	2.82	4.82	1.71	4.80	ok
						Mean	0.98		
						Standard Deviation	0.29		
						COV	0.30		

6.5 Conclusions

Based on test results, certain level of relaxation of the rigorous bond requirements in beam-column joints is possible as improvement of bond strength was noticed. The congestion of reinforcement in a HSC beam-column joint can be improved when larger bars are allowed to be used. This relaxation should be possible because the bond strength increases with the increase in concrete compressive strength as shown in test results. However the test data was found to be quantitatively insufficient. Therefore, a FE analytical research was supplemented to elucidate the understanding of the high strength concrete joints. The FE models were initially validated with the experimental results, and subsequently applied to study the effect

of varying key parameters influencing the joint performance. Thus, to incorporate the effect of concrete grade, ratio of total area of bottom beam bars top beam bars and axial compressive load in the bond condition of larger bar in HSC beam-column joint, a new design equation was proposed to the current NZS 3101. The design equations were verified by test data and FE results which agreed well the findings. The overstrength factor in NSZ was proposed to change from 1.25 to 1.30 and the limit of joint shear stress was modified based on test findings.

Chapter 7 Summary and Conclusion

Beam-column joints have been identified as one of the most critical parts of frame structures under seismic loading due to the concentration of large shear force and bending moment around joint panel. In this research program, the behaviour of high strength concrete (HSC) interior beam-column joints under reversed cyclic loading was investigated through test programme, finite element analysis and parametric studies. Firstly, the experimental studies of eight high strength concrete interior beam-column joints were conducted under reversed cyclic loadings. Based on test findings, finite element modelling (FEM) using DIANA was performed where the FEM models were verified against test results. The models were fine-tuned based on the general trends of test findings as to give the closest simulations of structural behaviour of high strength concrete beam-column joints. Meanwhile, parametric studies were conducted to identify the influence of variables and to understand the interactions among various parameters. Lastly, based on the findings of these works, design recommendation was proposed. The research program summarised in this thesis is aimed at investigating the performance of normal strength concrete (NSC) and high strength concrete (HSC) beam-column joints subjected to earthquake actions, which are not addressed in Singapore. This chapter summarises the findings of both experimental and parametric studies, and the recommendation for future work is proposed in the end of chapter.

7.1 Experimental Studies on High Strength Concrete Beam-Column Joint

A total of eight (8) high strength concrete (HSC) beam-column joints were built and tested under reversed cyclic loadings to study the structural behaviour of high strength concrete beam-column joints. Based on the NZS 3101: 2006 design limits checking, except for NS1 and AS1, all specimens only partially met the seismic detailing in NZS 3101: 2006. The respective test findings helped to explore the possible room to improve on the design code NZS3101 in order to be applicable to the design of both NSC and HSC.

Two (2) sets of identical HSC beam-column joint specimens were cast where each set of specimens consists of four (4) HSC beam-column joints based on the details of NSC specimens by Xin [X1]. The first set of four (4) HSC specimens were tested with zero column axial compressive loading and another set of four (4) HSC specimens were tested with the presence of column axial compressive loading of $0.3A_cf_c'$.

The structural behaviour of all HSC interior joints were assessed in terms of cracking patterns, column shear strength deterioration, stiffness degradation, energy dissipation, joint shear deformation, bond deterioration and joint shear stress. The test findings were summarised as below:

- Test results revealed that all HSC specimens tested generally show good energy dissipation characteristic. None of the specimens failed abruptly but all specimens behave ductile in the end of test, even though some specimens did not meet the bond development limits in NZS 3101.
- The joint core regions of all specimens were very strong and rigid where no joint failure was noticed at the end of test.
- In general, the presence of column axial compressive load in test enhanced the energy dissipation capacity of all specimens with larger confined area within the loops in the hysteresis graphs.
- The presence of column axial compressive load did not change the maximum load of specimens attained.
- The maximum load of specimens tested with column axial compressive load was attained in early loading stage as compared to their counterparts tested without column axial compressive load. This is due to the confinement effects in column that reduced the occurrence of damage in column and joint core hence damage only mainly found at beams.
- Early strength deterioration was observed in test results of specimens tested with the presence of column axial compressive load as the strength of specimens begun to drop when the maximum load was attained

- The presence of column axial compressive load altered the load path of joint core where the cracks had a steeper inclination angle compared to the test results without column axial compressive load.
- It is evident that lateral displacement contributed by beam flexural and beam fixed end rotation has been dominant in all specimens. The lateral displacement contributed by column flexural, column fixed-end rotation and shear distortion was not significant in all specimens.
- The value of bottom-reinforcement-to-top-reinforcement ratio β affects the shape of the hysteresis loops due to different bond condition of top and bottom beam reinforcement should β is less than unity

The test results showed that the bond development requirement in NZS 3101 can be relaxed since those specimens that did not meet the requirement showed good energy dissipation characteristics and no serious bond was observed.

7.2 Parametric Studies on Influence of Variables

Total of eighty three (83) interior beam-column joints from test data were summarised to study the influences of parameters such as concrete compressive strength, bond index, column axial load, joint hoop reinforcement ratio and beam reinforcement ratio on structural behaviour of beam-column joints. To compensate the possible limitations of the experimental studies, analytical modelling is used to supplement the parametric study where seventy five (75) finite element models were built and analysed. These models were built and analysed using finite element analysis program DIANA [D1]. Prior to performing parametric studies using DIANA, the programme was verified based on test data to ensure the closest simulation on the structural behaviour of HSC beam-column joints.

Based on the findings from parametric studies, some conclusions can be summarized as follows:

- In general the following parameters have significant effects on the joint shear capacity: concrete compressive strength, bond index, joint hoop reinforcement and beam reinforcement ratio. The column axial compressive

load on the other hand has more influence on the deformational behaviour of an interior beam-column joint than on the strength capacity.

- The influence of concrete strength on joint shear strength is not in a direct manner due to the additional influences of other parameters such as joint hoop reinforcement area. As such, the joint shear strength was normalised to the concrete strength to study the influences of other control parameter.
- Column axial compressive load in general have no direct effect on the maximum joint shear strength, but it does affect the joint shear deformation and it may lead to different deterioration behaviour after the peak column shear strength was reached depending on the availability of joint hoops.
- Longitudinal reinforcement passing through the joint panel helps to resist the joint shear. However, excessive longitudinal reinforcement in the beams and columns could be detrimental especially for lightly reinforced joints, as they might change the failure mechanism of a joint from beam hinging to joint shear.
- Even though it is generally accepted that joint core reinforcement serves to provide shear resistance and provide confinement to the joint volume, the parametric studies showed the possibility of overestimation in the contribution of joint hoops. The shear stress demand for lightly reinforced beam column joint with no joint core reinforcement can be as high as those with high joint core reinforcement.
- Bond Index (BI) can be a good indication to estimate the bond condition of a joint. It is recommended that the application of BI in a design for the development length of reinforcement in joint core should be companied by the checking of longitudinal reinforcement ratio.
- The transverse beams and slabs are structural elements that have direct interaction with the beam-column joints which may provide significant confinement to the joint cores during bidirectional seismic loading. The major design codes such as NZS 3010 and ACI 318 allow the reduction of joint hoops area with the presence of transverse beam

7.3 Design Recommendations

Based on test results some relaxation of the bond requirements in beam-column joints is possible as improvement of bond strength was noticed. The congestion of reinforcement in a HSC beam-column joint can be improved when larger bars are allowed to be used. This relaxation should be possible because the bond strength increases with the increase in concrete compressive strength as shown in test results. Thus, to incorporate the effect of concrete grade, ratio of total area of bottom beam bars top beam bars and axial compressive load in the bond condition of larger bar in HSC beam-column joint, a modified equations on bond development of beam reinforcement was proposed to the current NZS 3101. In the modified equation, the overstrength factor in NSZ 3101 was proposed to change from 1.25 to 1.30. The design equations on bond development of beam reinforcement were verified by test data which agreed well the findings. With the proposed change in overstrength factor, the shear design equations in NSZ 3101 were reviewed too where parametric studies on eighty three (83) interior beam-column joints from test data were performed. The ultimate shear strength of these interior beam-column joints were computed using modified equation in NSZ3101 and compared with the test results. The analysis revealed that marginal improvement was found in the calculated ultimate shear strength with modified equation in NSZ3101. The limit of joint shear stress was also modified based on test findings so that it is applicable to both NSC and HSC beam-column joints.

7.4 Recommendations for Future Work

The long-term purpose of this research program is to provide guidelines for practicing structural engineers in evaluating existing reinforced concrete moment resisting frame structures, mitigating seismic hazards, and reducing the risk level to building occupants and owners in Singapore. Up till now, the research data on HSC beam-column joints is insufficient to provide a better understanding of the performance of such kind of structures. Therefore, it is necessary to conduct more investigations through both experimental and analytical approaches. From the test programme, the following recommendations for future work are proposed:

- In this study, test was carried out with applied column axial loads of $0.3A_cf_c'$. A threshold value for beneficial confinement from axial compressive load was concluded based on finite element analysis. Future studies should be carried out to investigate the seismic performance of beam-column joints with various level of column axial load to ascertain the threshold of axial compressive load that gives beneficial confinement.
- Further studies are required for the use of either deep transverse beams or very deep columns, which will influence the transfer of forces from the transverse beam to the column.
- Lap splices effect was not investigated in this study. As a typical reinforcing technology in the early design and construction practice, this should be a concern in further research.
- Due to a lack of confinement, the bond between the reinforcement and the surrounding concrete is very important for a beam-column joint. It was shown in this study that the ACI 318 [A1] provisions may not be adequate in preventing the bond deterioration occurring. Using NZS 3101 [N1] recommendation in the design of beam-column joints was suggested but this needs verification through further investigations.
- The finite element analyses in this research were conducted based on the current modelling criteria and analytical technology, which could not precisely evaluate the performance of RC frame buildings and components. More efforts have to be made to enhance the finite element analysis technology. To achieve this purpose, extensive experimental investigations are required in the future.
- To evaluate the beam-column joints in three dimension (3D). To ease the analysis process all models were modelled in two dimension. For beam-column joints with special arrangement for example, flashed beam at one column face, the presence of transverse beam or flanged beam-column joints, the current finite element simulation will have limitation to model the configuration correctly.
- To study the bond failure mechanism in HSC especially the brittle bond failure mode of HSC due to the engagement of only few deformations.

REFERENCES

[A1] ACI Committee 318, "Building Code Requirements for Structural Concrete (ACI 318-08) and Commentary", American Concrete Institute, Farmington Hills, Miami, USA, 2008, 465pp.

[A2] ACI-ASCE Committee 352, "Recommendations for Design of Beam-Column Joints in Monolithic Reinforced Concrete Structures", ACI Manual of Concrete Practice 1996, part 3, ACI 352R-91, pp.352R-1,21.

[A3] Alavi-Fard, M. & Marzouk, H., "Bond of High-Strength Concrete under Monotonic Pull-out Loading", Magazine of Concrete Research, Vol. 56, Issue: 9 November 2004, pp. 545-557.

[A4] Alavi-Fard M.& Marzouk H., "Bond Behavior of High Strength Concrete under Reversed Pull-out Cyclic Loading", Canadian Journal of Civil Engineering, Vol. 29, No. 2, April 2002 , pp. 191-200.

[A5] Architectural Institute of Japan (AIJ), "Design Guidelines for Earthquake Resistant Reinforced Concrete Buildings Based on Ultimate Strength Concept (Drift) and Commentary", Oct. 1998.

[A6] Attaalla, S.A., "Performance of Interior Beam-Column Joints Cast from High Strength Concrete Under Seismic Loads", Civil Engineering Department, University of Southern California, California, USA, Aug 1997, 300pp.

[A7] Attaalla, S.A. & Agbabian M.S., "Performance of Interior Beam-Column Joints Cast from High Strength Concrete Under Seismic Loads", Advances in Structural Engineering, Vol. 7, No. 2, 1 April 2004, pp. 147-157.

[B1] Bakir, P. G. & Boduroglu, M. H., "Parametric Studies on Cyclically Loaded Exterior Beam-Column Joints", Proceedings of The Sixth Conference on Computational Structures Technology, 2002 , pp 279 – 280.

[B2] Blaikie E.L., (1988), "Behavior of Unreinforced and Lightly Reinforced Concrete Beam-Column Joints". Proceedings of Pacific Concrete Conference, Vol. 1, Auckland, pp. 181-193.

[B3] Briss, G. R., "The Elastic Behaviour of Earthquake-Resistance Reinforced Concrete Beam-Column Joints," Research Report 78-13, Department of Civil Engineering, University of Canterbury, Christchurch, New Zealand, 1978, 105 pp.

[B4] Brooke, Nicholas J., "Bond Performance of Interior Beam-Column Joints with High-Strength Reinforcement", ACI Structural Journal, Jul/Aug 2006.

[B5] BS 8110, Structural Use of Concrete, Part 1. Code of Practice for Design and Construction, British Standard, 1997.

[C1] CEP-FIP, 'Model Code for Concrete Structures', 3rd Edition, Comite-Euro-International du Beton/Federation Internationale de la Precontrainte, Paris, 1978.

[C2] CEB-FIP Model Code 2010, Design Code (Draft). (2010). Thomas Telford, Lausanne, Switzerland.

[C3] Cheung, P.C., Paulay, T. and Park, R., "Behavior of Beam-Column Joints in Seismically-Loaded RC Frames", Structural Engineer, V.71, n8, April 1993, pp.129-137

[D1] DIANA Finite Element Analysis User's Manual- Release 9.3, "Finite Element Analysis User's Manual-Nonlinear Analysis", TNO Building and Construction Research, Delft, The Netherlands; 2008.

[D2] Durani, A. J., and Wight, J. K., "Behaviour of Interior Beam-to-Column Connections under Earthquake Type Loading," ACI Journal Proceeding, V. 82, No.3, May-June, 1985, pp. 343-349.

[E1] Eurocode 2: Design of Concrete Structures. Part 1-1, General Rules and Rules for Buildings, British Standard Institution, London, 2004.

[E2] EC8/1/1-3 (1998), "Design Provisions for Earthquake Resistance of Structures - General and Buildings. ENV 1998-1", CEN, Brussels.

[E3] El-Nabawy Atta, S. El-Din Fahmy Taher, A.-H A. Khalil & S. El-Din El-Metwally, "Behaviour of Reinforced High Strength Concrete Beam-Column Joint Part 1: Experimental Investigation", Structural Concrete, Vol 4, UK, 2003, pp 175-183

[E4] El-Nabawy Atta, S. El-Din Fahmy Taher, A.-H A. Khalil & S. El-Din El-Metwally, "Behaviour of Reinforced High Strength Concrete Beam-Column Joint Part 2: Numerical Simulation", Structural Concrete, Vol 5, UK, 2003, pp 101-112

[F1] FEMA 356, "Prestandard and Commentary for the Seismic Rehabilitation of Buildings", Federal Emergency Management Agency, 2000.

[F2] Fenwick, R. C., and Irwine, H. M., "Reinforced Concrete Beam-Column Joints for Seismic Loading", School of Engineering Report No. 142, Department of Civil Engineering, University of Auckland, New Zealand, Mar. 1992, 50pp.

[F3] Fu, J.; Chen, T.; Wang, Z.; and Bai, S., "Effect of Axial compressive load Ratio on Seismic Behavior of Interior Beam-Column Joints," *Paper* No. 2707, 12th World Conference on Earthquake Engineering, 2000.??

[H1] Hajime, O., and Kohichi, M., "Nonlinear Analysis and Constitutive Models of Reinforced Concrete" Gihodo, Tokyo, 1991, 182 pp.

[H2] Hakuto S., Park R. and Tanaka H., "Retrofitting of Reinforced Concrete Moment Resisting Frames", Department of Civil Engineering, University of Canterbury, Research Report 95-4, Christchurch, New Zealand, 390 pp.

[H3] Hanson N. W. and Conner H. W., "Seismic Resistance of Reinforced Concrete Beam-Column Joints", Am. Soc. Civ. Engrs, J. Struct. Div., 93, 5, Oct., pp. 533-560.

[I1] Ishibashi, K., "Bond Strength and Failure Mechanism within Beam-Column Joints", Reports on Earthquake Resistance of Reinforced Concrete Structures, De Dept. of Architecture, University of Tokyo, Japan, Nov. 25 1993 pp 287-.296.

[K1] Kitayama, K., Otani, S., and Aoyama, H., "Development of Design Criteria for RC Interior Beam-Column In Design of Beam-Column Joints for Seismic Resistance, ACI Special Publication, SP-123, Editor Jirsa, J.O., 1991, 97-123.

[K2] Kurose Y. (1987), "Recent Studies on Reinforced Concrete Beam Column Joints in Japan", Phil M. Ferguson Structural Engineering Laboratory, Dept. of Civil Engineering, The University of Texas at Austin, TX, Rep. 87-8, 164 pp.

[K3] Kurose Y., Guimaraes G.N., Liu Z., Kreger M.E., and Jirsa J.O., "Study of Reinforced Concrete Beam-Column Joints under Uniaxial and Biaxial

Loading". PMFSEL Report No. 88-2, Department of Civil Engineering, University of Texas at Austin, December 1988, 146 pp.

[L1] Leon, R. T., "Shear Strength and Hysteric Behaviour of Beam-Column Joints", ACI Structural Journal, V. 87, No.1, January-February 1990, pp. 3-11.

[L2] Li, B.; Pan, T.-C., "Assessment of Reinforced Concrete Interior Beam-Wide Column Joints for Seismic Performance," Research Report, Nanyang Technological University, Singapore, 2006.

[L3] Li, B.; Wu, Y.N.; Pan, T.-C., "Seismic Behavior of Nonseismically Detailed Interior Beam-Wide Column Joints-Part I: Experimental Results and Observed Behavior", ACI Structural Journal, V. 99, No.6, November-December 2002, pp791-802.

[L4] Li, B.; Wu, Y.N.; Pan, T.-C., "Seismic Behavior of Nonseismically Detailed Interior Beam-Wide Column Joints-Part II: Theoretical Comparisons and Analytical Studies", ACI Structural Journal, V. 100, No.1, January-February 2003, pp56-65.

[L5] Lin, C. M., "Seismic Behavior and Design of Reinforced Concrete Interior Beam-Column Joints," *Research Report* 2000-1, Department of Civil Engineering, University of Canterbury, Christchurch, New Zealand, 2000, 471 pp.

[L6] Liu, A. and Park, R., "Seismic Behavior and Retrofit of Pre-1970's As-BuiltExterior Beam-Column Joints Reinforced by Plain Round Bars", Bulletin of theNew Zealand Society for Earthquake Engineering, Vol.34, No.1, March 2001.

[L7] Liu, A. and Park, R., "Seismic Load Test on Two Concrete Interior Beam-Column Joints Reinforced by Plain Round Bars Designed to Pre-1970s

Codes", Bulletin of The New Zealand Society for Earthquake Engineering, Vol.31, No.3, September 1998.

[M1] Maekawa, K.; Pimanmas, A. and Okamura, H., "Nonlinear Mechanics of Reinforced Concrete", Spoon Press, London, 2002

[M2] Magnusson, Jonas, "Bond and Anchorage of Ribbed Bars in High-Strength Concrete", Chalmers University of Technology, 2000

[M3] Meinheit D.F. and Jirsa J.O., "Shear Strength of R.C. Beam-Column Connections", Am. Soc. Civ. Engrs, J. Struct. Div., 107, 11, pp. 2227-2244.

[M4] Meinheit D.F. and Jirsa J.O., "The Shear Strength of Reinforced Concrete Beam-Column Joints", CESRL Report No 77-1, The University of Texas at Austin, USA, Jan 1977, 271 pp.

[M5] Mendis, P. A. and French, C. W., "Bond Strength of Reinforcement in High-strength Concrete", Advances in Structural Engineering Journal 3 (3), 2000, pp245-253

[M6] Mo Y. L.; Tsai S. P. & Lee I. S., "Seismic Performance Behavior of Beam-Column Connections in Prestressed Concrete Bridges", Materials and Structures, Vol. 31, No. 6, July 1998, pp 411-417

[N1] New Zealand Standard NZS 3101, "Concrete Structures Standard: Part 1-The Design of Concrete Structure", Wellington, New Zealand, 2006.

[N2] New Zealand Standard NZS 3101, "Concrete Structures Standard: Part 2-Commentary on Design Concrete Structures", Wellington, New Zealand, 2006.

[O1] Otani, S., Kobayashi, Y. and Aoyama, O., "Reinforced Concrete Beam-Column Joints under Simulated Earthquake Loading", 1st U.S.-N.Z.-Japan Seminar, Monterey, July-Aug, 1984.

[P1] Pan, T.-C. and Sun, J., "Historical Earthquakes Felt in Singapore", Bulletin, Seismological Society of America, Volume 86, 1996,

[P2] Pantazopoulou, S.J. and Bonacci, J.F., "Consideration of Questions about Beam-Column Joints", ACI Structural Journal, V.89, No.1, January-February, 1992, pp.27-36.

[P3] Park, R., and Paulay, T., "Reinforced Concrete Structures", John Willey & Sons, N.Y., 1975, 744 pp.

[P4] Paulay T., "Reinforced Concrete Beam-Column Joints under Seismic Actions". ACI Journal, V. 75, 11, Nov., 1978, pp. 585-593.

[P5] Paulay, T. and Park, R., "Joints in Reinforced Concrete Frames Designed for Earthquake Resistance", Research Report 84-9, Department of Civil Engineering, University of Canterbury, Christchurch, New Zealand, 1984, pp. 71.

[P6] Paulay, T., Park, R. and Priestley, M.J.N., "Reinforced Concrete Beam-Column Joints under Seismic Actions", ACI Structural Journal, November 1978.

[P7] Paulay, T., and Priestley, M. J. N., "Seismic Design of Reinforced Concrete Masonry Buildings", John Willey & Sons, N.Y., 1992, 744 pp.

[P8] Pendyala, R., Mendis, P.A. and Patnaikuni, I., "Full-range Behaviour of High Strength Flexural Members: Comparison of Ductility Parameters of

High and Normal Strength Concrete Members", ACI Structural Journal, Vol. 93, No.1, January-February 1996, pp 30-35

[P9] Pessiki, S. P.; Conley, C. H.; Gergely, P.; and White, R. N.; "Seismic Behavior of Lightly Reinforced Concrete Column and Beam-Column Joint Details," NCEER Technical Report No. 90-0014, State University of New York at Buffalo.

[P10] Prakash, V., Powell, G. H. and Campbell, S., "Drain-2DX – Base Program Description and User Guide (Version 1.10)," Report No. UCB/SEMM-93/17, Department of Civil Engineering, University of California, Berkeley, CA, 1993.

[P11] Priestley, M. J. N., and Calvi, G., M., "Toward a Capacity-Design Assessment Procedure for Reinforced Concrete Frames," Earthquake Spectra, V.7, No. 3, 1991, pp.413-437.

[S1] Sayed A. Attaalla, "General Analytical Model for Nominal Shear Stress of Type 2 Normal- and High-Strength Concrete Beam-Column Joints," ACI Structural Journal, V. 101, No.1, Jan-Feb 2004, 65-75.

[T1] Tan, H. Y., "Experimental and Analytical Study on Lightly Reinforced Concrete Frames and Beam-Column Joints", Ph. D Thesis, School of Civil & Environmental Engineering, Nanyang Technological University, 2006

[T2] To, N. H. T., Ingham, J. M. and Sritharan, S. (2002), "Cyclic Strut & Tie Modeling of Simple Reinforced Concrete Structures," Proceedings of the 12th World Conference on Earthquake Engineering, Auckland, New Zealand, Paper No. 1249, New Zealand Earthquake Commission.

[T3] Townsend, W.H. and Hanson, R.D., "Reinforced Concrete Connection Hysteresis Loops in Reinforced Concrete Structures in Seismic Zones", ACI SpecialPublication, SP 53-13, 1977, pp. 351-370.

[V1] Vecchio, F.J. and Emara, M.B., "Shear Deformations in Reinforced Concrete Frames", ACI Structural Journal, V. 89, No. 1, 1992, pp. 46-56.

[V2] Vollum, R.L., "Design and Analysis of Exterior Beam-Column Connections", PhD thesis, Imperial College of Science Technology and Medicine-University of London, 1998.

[W1] WCOMD-2D, "Beginners Guide to WCOMD-2D".

[W2] Wong, K.C., Priestley, M.J.N. and Park, R., "Seismic Resistance of Frames with Vertically Distributed Longitudinal Reinforcement in Beams", ACI Structural Journal, V.87, July-August, 1990.

[W3] Wu, Y.M., "Experimental and Analytical Study of Reinforced Concrete Interior Beam-Wide Column Joints for Seismic Performance", Master of Engineering Thesis, School of Civil & Environmental Engineering, Nanyang Technological University, 2002.

[X1] Xin, X. Z., "Behaviour of Reinforced Concrete Interior Beam-Column Joints Designed using High Strength Concrete and Steel," Master of Engineering Thesis, University of Canterbury, New Zealand, 1992.

[Y1] Yin, H., "Behaviour of Lightly Reinforced Concrete Interior Beam-Column Joints under Reversed Cyclic Loading", Master of Engineering Thesis, School of Civil & Environmental Engineering, Nanyang Technological University, 2001, pp.110.

[Z1] Zhang L. and Jirsa, J. O., "A Study of Shear Behaviour of Reinforced Concrete Beam- Column Joints", PMFSEL Report No 82-1, Department of Civil Engineering, The University of Texas at Austin, USA, 1982.

Appendix A: Summary of Cracking Pattern of Specimens NS1 to NS4 & AS1 to AS4

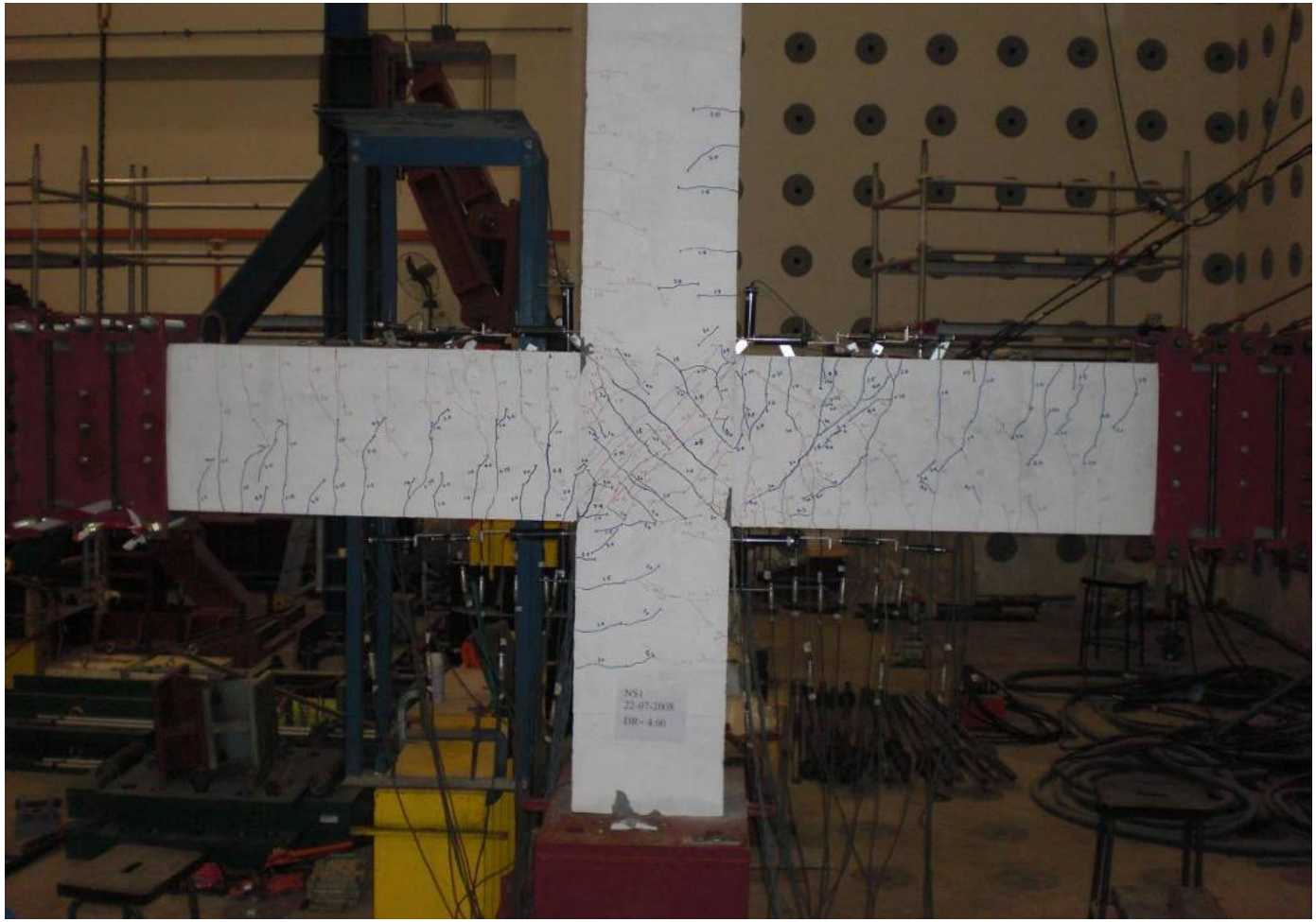

Figure A1: Final Crack Pattern of NS1

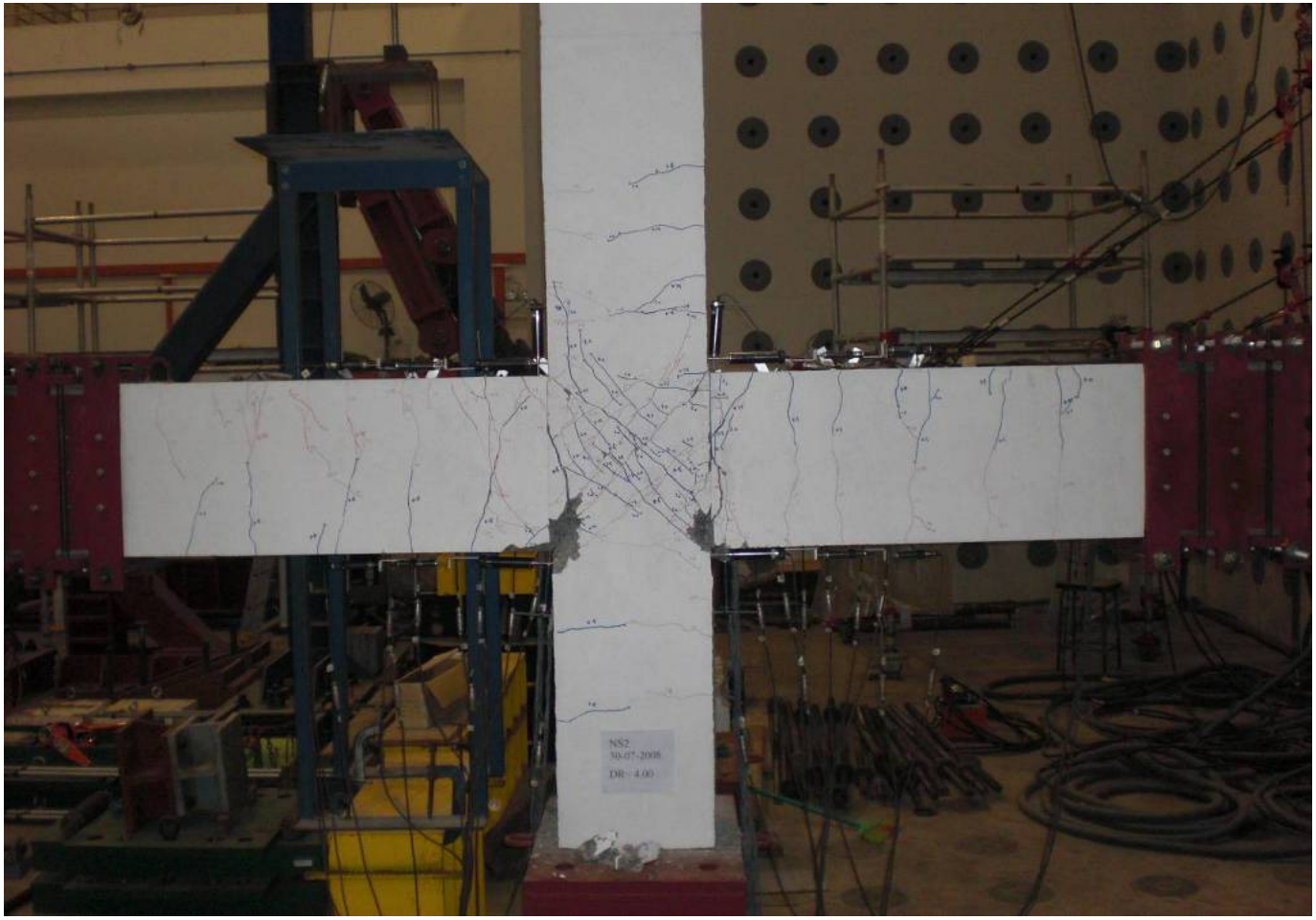

Figure A2: Final Crack Pattern of NS2

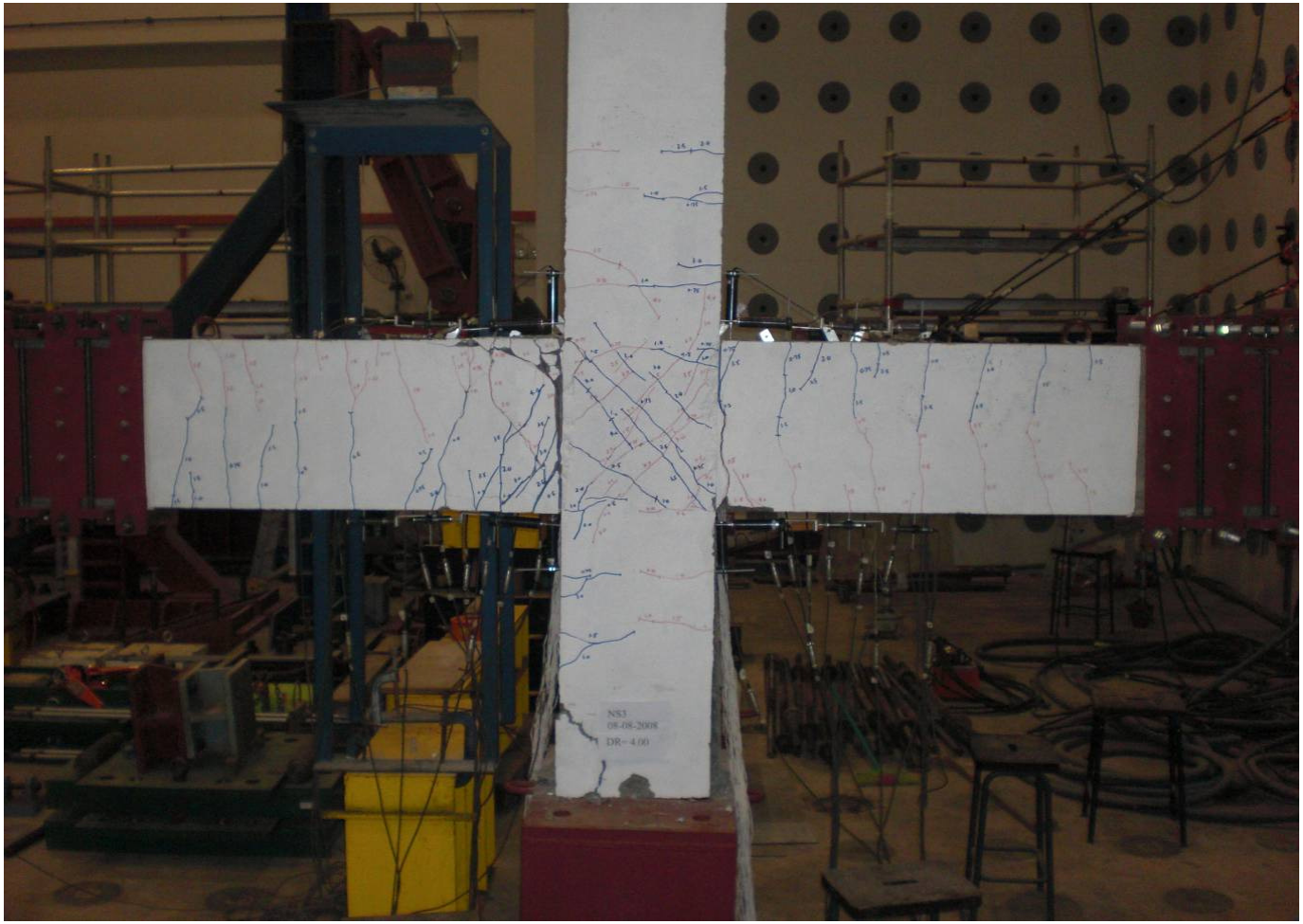

Figure A3: Final Crack Pattern of NS3

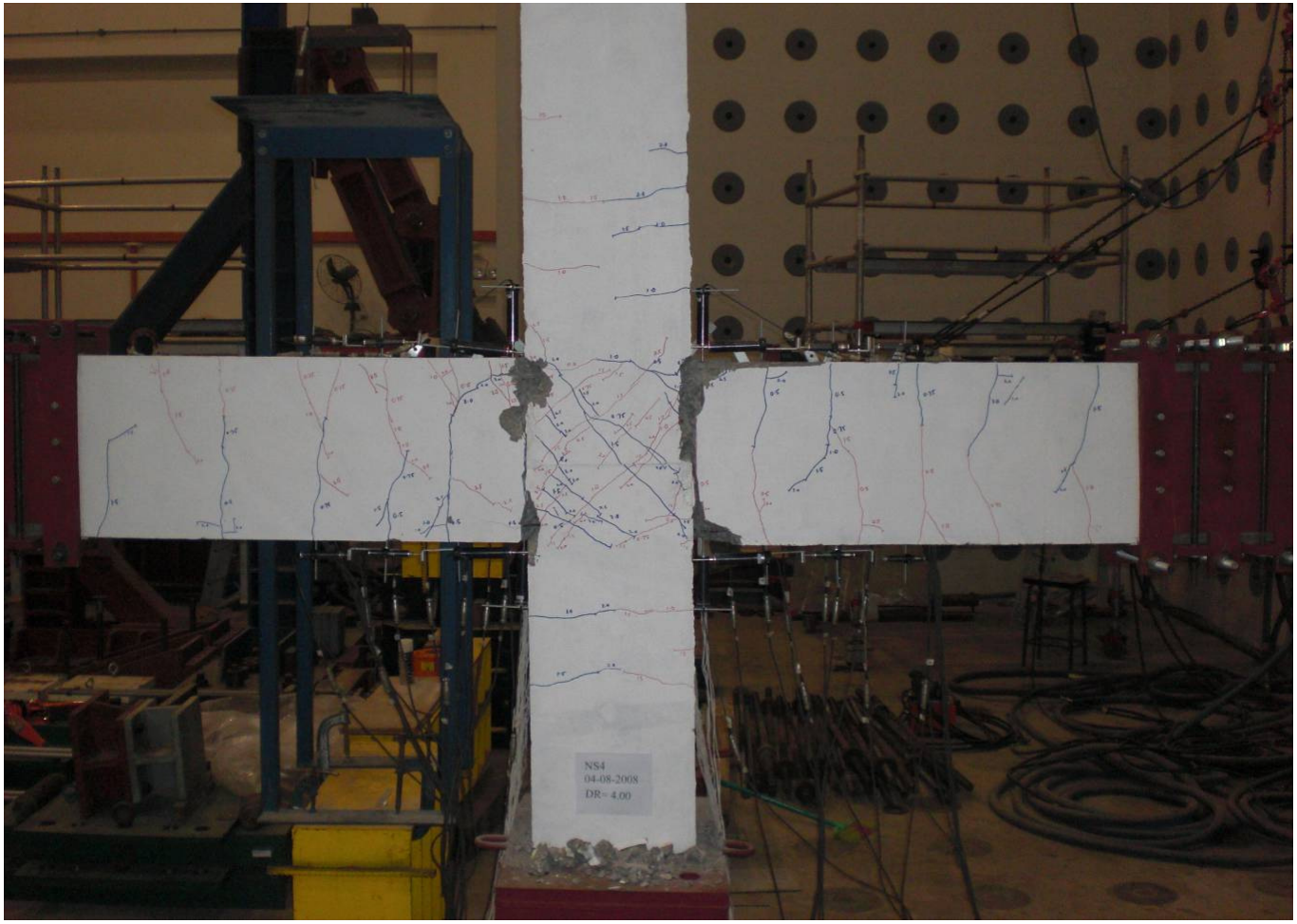

Figure A4: Final Crack Pattern of NS4

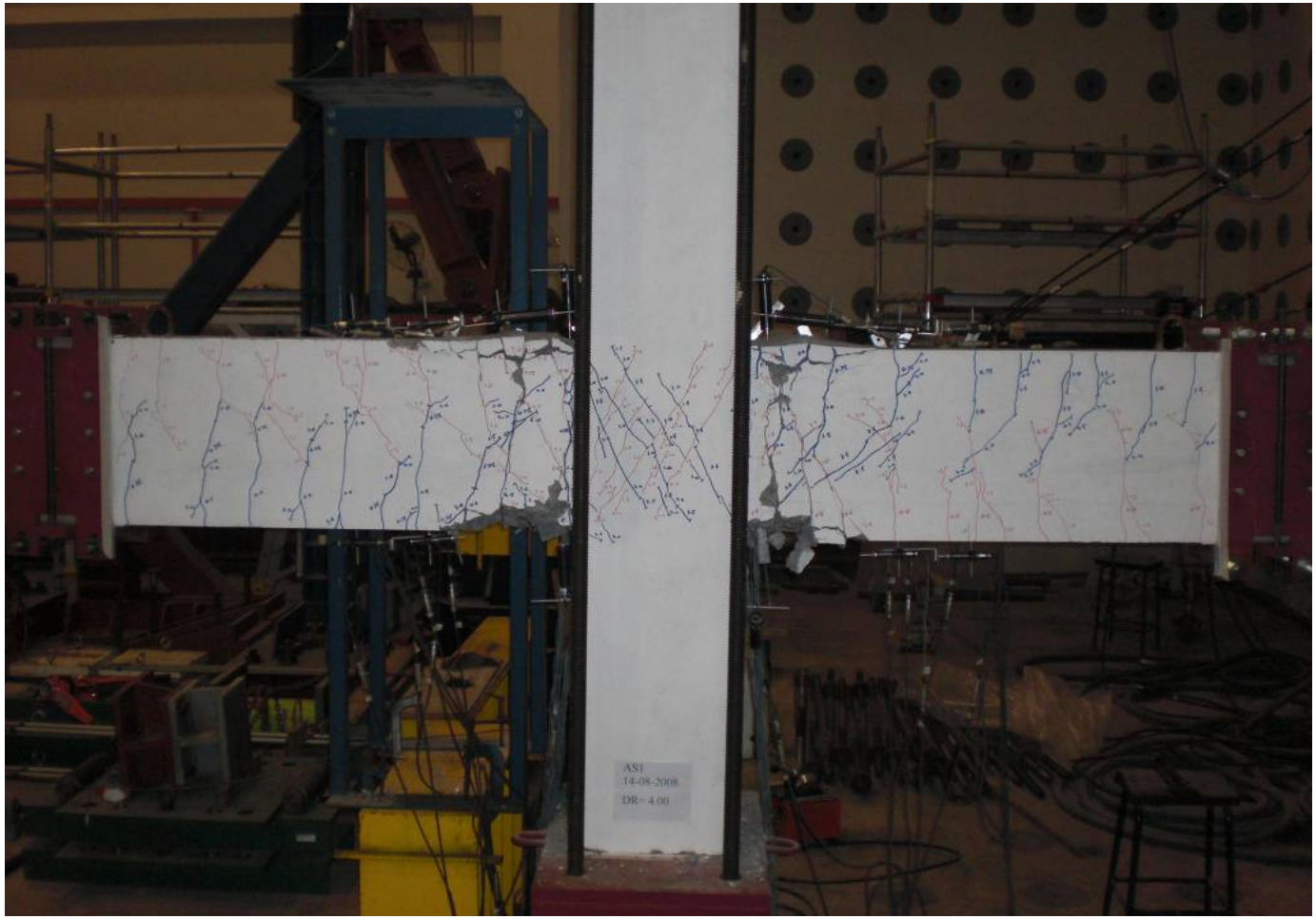

Figure A5: Final Crack Pattern of AS1

Figure A6: Final Crack Pattern of AS2

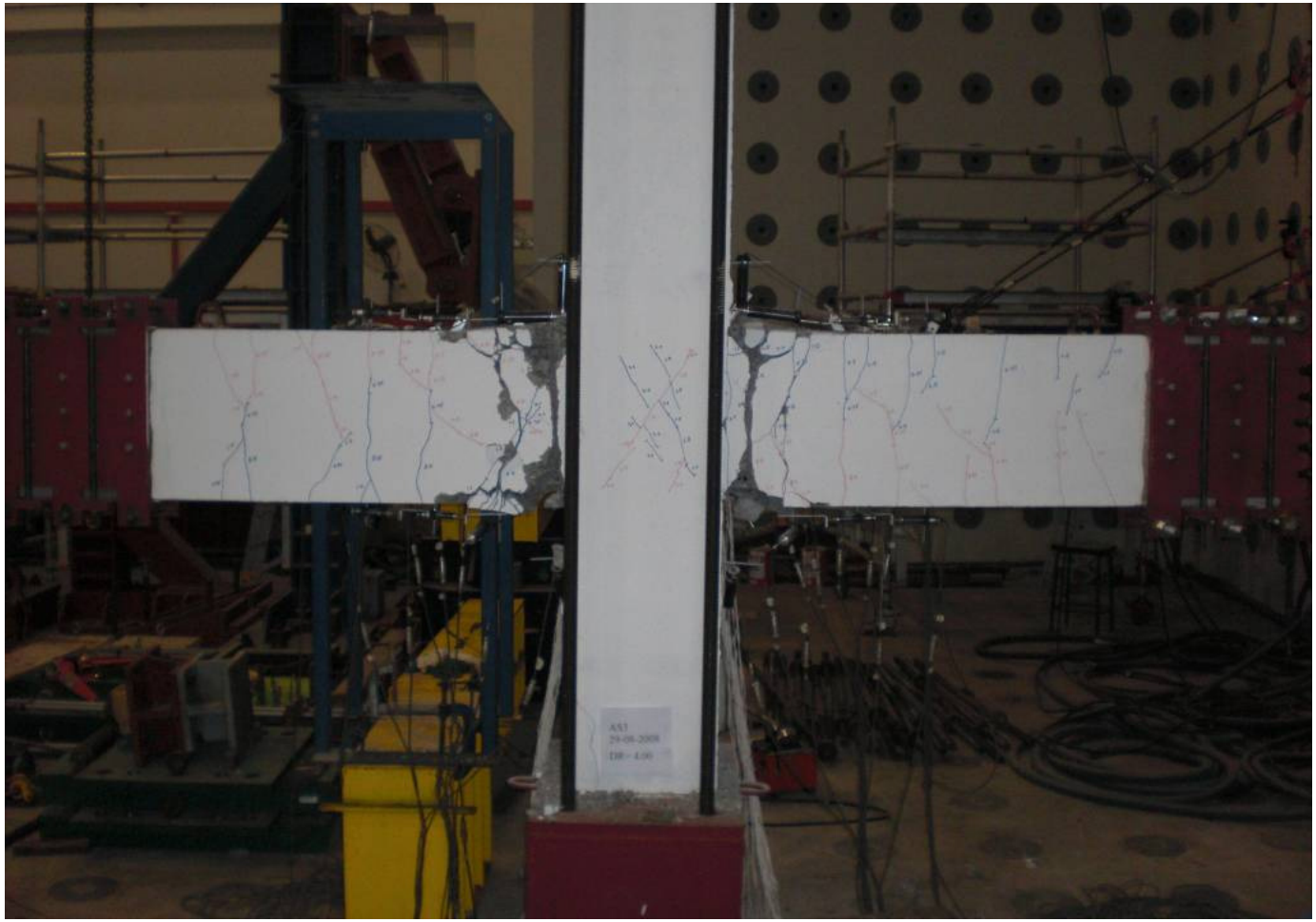

Figure A7: Final Crack Pattern of AS3

Figure A8: Final Crack Pattern of AS4